Study of the Term Neonatal Brain Injury with combined
Diffuse Optical Tomography and Electroencephalography
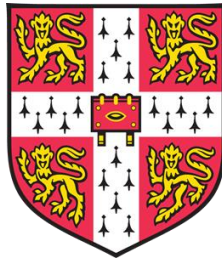
Maria Chalia

MD 2018

Study of the Term Neonatal Brain Injury with combined
Diffuse Optical Tomography and Electroencephalography

Maria Chalia
Department of Paediatrics

UNIVERSITY OF
CAMBRIDGE

DARWIN COLLEGE

9 February 2018

Supervisors: Professor Topun Austin
Dr Robert Cooper

This thesis is submitted for the degree of Doctor of Medicine (M.D.) at University of Cambridge.

Study of the Term Neonatal Brain Injury with combined Diffuse Optical Tomography and Electroencephalography

Dr Maria Chalia

This thesis describes the application of combined diffuse optical tomography (DOT) and electroencephalography (EEG) in the investigation of neonatal term brain injury. With hypoxic ischaemic encephalopathy (HIE) and perinatal stroke being the most frequent contributors to brain injury in the term neonatal population, the first part of the thesis focuses on the description and ongoing requirement for their further investigation. In continuation to that, the characteristics and unique properties of both DOT and EEG are described and explored.

The combination of these two modalities was utilised in elucidating the relationship between neuronal activity and cerebral haemodynamics both in physiological processes as well as in disease, by the infant's cot side. This work differs to previous studies using near-infrared technologies and EEG, as a denser whole head array was used, offering the potential of 3-dimensional image reconstruction of the cortical haemodynamic events in relation to electro-cortical activity. These methods were applied in the study of critically ill infants presenting with seizures in the first few days of life.

The relevant results are presented in three separate chapters of the thesis. Distinct neurophysiological phenomena such as seizures and burst suppression were detected and studied in association to underlying HIE. On the grounds of a pre-existing pilot study of our research group, distinct prolonged de-oxygenated cortical areas were identified following electrical seizure activity. Further exploration of infants with seizures provided limited supporting evidence. The investigation of burst suppression in HIE led to the first ever identification of repeated, waveform, cortical haemodynamic events in response to bursts of electrical activity with some spatial correlation to regions of brain injury. Further analysis of the low frequencies within the diffuse optical signal in cases of perinatal stroke, showed a consistent interhemispheric difference between the healthy and stroke-affected brain regions.

The limitations, prospects and conclusions are presented in the final chapter. The use of simultaneous DOT and EEG offers a unique neuro-monitoring and neuro-investigating tool in the neonatal intensive care environment, which is safe, portable, and cost-effective, Ongoing research is required for the exploration and development of the methodology and its potential diagnostic properties.

The only true wisdom is in knowing you know nothing

Socrates

I hereby declare that the work presented in this thesis is the result of my own and includes nothing which is the outcome of work done in collaboration except as declared in the Preface and specified in the text.

It is not substantially the same as any that I have submitted, or, is being concurrently submitted for a degree or diploma or other qualification at the University of Cambridge or any other University or similar institution except as declared in the Preface and specified in the text. I further state that no substantial part of my dissertation has already been submitted, or, is being concurrently submitted for any such degree, diploma or other qualification at the University of Cambridge or any other University or similar institution except as declared in the Preface and specified in the text.

In this thesis, I studied preterm and term infants using combined electroencephalogram and diffuse optical tomography (DOT-EEG) continuing a programme of work looking at the relationship between cerebral oxygenation and electrical brain activity (neurovascular coupling). As well as studying infants with seizures, I conceived the idea of studying burst suppression with the same methodology and later expanded this to the study of perinatal stroke. After my involvement in the project, following the initial pilot study, I recruited and studied the infants independently. I conducted the pre-processing and part of the processing steps in the analysis of the DOT data. I conducted the image reconstruction where necessary using pre-existing MATLAB based algorithms developed by the group (primarily by Dr Robert J Cooper).

Dr Andy Michell, consultant neurophysiologist, conducted the clinical interpretation of the EEGs and I continued with further analysis where warranted (such as EEG analysis and burst identification in chapter 4). Particularly, for chapter 5 for inter-observant variability, a PhD student, Dr Chuen Wai Lee also reviewed one third of the EEG data.

The analysis of the DOT data in chapters 4 and 5 were based on algorithms (in MATLAB) originally developed by Dr Robert Cooper. Dr Robert Cooper and I initially developed the analysis of the DOT data in chapter 6. The methodology was further explored and developed by a PhD student, Laura Dempsey.

The MRI images, used and mentioned in this thesis, were reported by Professor Mary Rutherford, at Kings College London.

This thesis does not exceed the prescribed word limit of 60,000 as specified by the Degree Committee of the Faculties of Clinical Medicine and Veterinary Medicine.

Maria Chalia

Abstract

This thesis describes the application of combined diffuse optical tomography (DOT) and electroencephalography (EEG) in the investigation of neonatal term brain injury. With hypoxic ischaemic encephalopathy (HIE) and perinatal stroke being the most frequent contributors to brain injury in the term neonatal population, the first part of the thesis focuses on the description and ongoing requirement for their further investigation. In continuation to that, the characteristics and unique properties of both DOT and EEG are described and explored.

The combination of these two modalities was utilised in elucidating the relationship between neuronal activity and cerebral haemodynamics both in physiological processes as well as in disease, by the infant's cot side. This work differs to previous studies using near-infrared technologies and EEG, as a denser whole head array was used, offering the potential of 3-dimensional image reconstruction of the cortical haemodynamic events in relation to electro-cortical activity. These methods were applied in the study of critically ill infants presenting with seizures in the first few days of life.

The relevant results are presented in three separate chapters of the thesis. Distinct neurophysiological phenomena such as seizures and burst suppression were detected and studied in association to underlying HIE. On the grounds of a pre-existing pilot study of our research group, distinct prolonged de-oxygenated cortical areas were identified following electrical seizure activity. Further exploration of infants with seizures provided limited supporting evidence. The investigation of burst suppression in HIE led to the first ever identification of repeated, waveform, cortical haemodynamic events in response to bursts of electrical activity with some spatial correlation to regions of brain injury. Further analysis of the low frequencies within the diffuse optical signal in cases of perinatal stroke, showed a consistent interhemispheric difference between the healthy and stroke-affected brain regions.

The limitations, prospects and conclusions are presented in the final chapter. The use of simultaneous DOT and EEG offers a unique neuro-monitoring and neuro-investigating tool in the neonatal intensive care environment, which is safe, portable, and cost-effective, Ongoing research is required for the exploration and development of the methodology and its potential diagnostic properties.

Acknowledgements

The nature of this research requires a strong collaboration between clinicians, physicists, and engineers. I was fortunate enough to work as part of the neoLAB group, a collaboration between the Cambridge Centre for Perinatal Neuroscience and the Biomedical Optics Research Laboratory at University College London (UCL-BORL). Under the leadership of Professor Topun Austin and Dr Robert Cooper the group has developed an international reputation in the field of optical imaging of the developing brain.

I am particularly grateful to the Evelyn Trust, a Cambridge based charitable trust, for awarding me a 2-year senior clinical research fellowship, which primarily funded my research work. I am honoured to have been a member of the Department of Paediatrics of the University of Cambridge. I would also like to thank the Cambridge Perinatal Group for funding my university tuition fees towards my MD.

Most of all, I would like to thank my supervisors, Professor Topun Austin and Dr Robert Cooper for their continuous support and guidance. They have both been inspirational mentors sharing their knowledge and wisdom. They have encouraged me and supported me along the way towards the completion of my MD.

A special thank you also goes to our research nurse Andrea Edwards and neurocritical care nurse Kelly Spike for their unconditional support and friendship throughout this time.

This project could not have taken place without the support of the nurses and doctors on the neonatal unit at the Rosie Hospital, in Cambridge University Hospitals. I am also particularly grateful to the parents who consented and allowed me to study their newborn infants, and some of them had to make such decisions during possibly the most stressful time of their lives.

Finally, I am forever grateful to my family for their unconditional love and understanding, Dimitrios and our daughter Lefkianna. This thesis is dedicated to them.

Publications resulting from this work

Peer reviewed journal papers

Chalia M, Austin T. **Practice guide to neonatal seizures**. Paediatrics and Child Health (2018), https://doi.org/10.1016/j.paed.2018.08.005

Chalia M, Lee C W, Dempsey L A, Edwards A D, Singh H, Michell A W, Everdell N L, Hill R W, Hebden J C, Austin T, Cooper R J. **Hemodynamic response to burst-suppressed and discontinuous electroencephalography activity in infants with hypoxic ischemic encephalopathy**. **Neurophoton. 3(3), 031408 (May 02, 2016).** doi:10.1117/1. NPh.3.3.031408
History: Received December 30, 2015; Accepted March 23, 2016

Conference proceedings

Chalia M, Cooper R J, Lee C W, Dempsey L, Edwards A D, Michell A W, Brigadoi S, Everdell N L, Hebden J, Austin T. '**Investigating the cortical haemodynamic response of burst suppressed or discontinuous electroencephalographic activity in infants with hypoxic ischaemic encephalopathy**'. **Neonatal Society Scientific Meeting**, London, United Kingdom, November 2015.

Chalia M, Cooper R J, Lee C W, Dempsey L, Hebden J C, Austin T. '**Can diffuse optical tomography provide early detection of perinatal arterial ischaemic stroke?**' **Meeting of the Anglo-French Neonatal Societies**, Cambridge, United Kingdom, June 2016.

Conference posters

Chalia M, Cooper R J, Dempsey L, Lee C W, Edwards A D, Michell A W, Brigadoi S, Everdell N L, Hebden J, Austin T. '**Investigating the Neurovascular Coupling of Burst suppression in Infants with Hypoxic Ischaemic Encephalopathy**'. **5th Cambridge Neuroscience Symposium, Imaging the Nervous system**, Cambridge, United Kingdom, September 2015

Chalia M, Cooper R J, Dempsey L, Edwards A D, Lee C W, Michell A W, Brigadoi S, Everdell N L, Hebden J, Austin T. '**Prospective Study of the Cerebral Haemodynamic Correlate of Burst Suppressed or Discontinuous Electroencephalographic Activity in Hypoxic Ischaemic Encephalopathic Infants'.** 1st Congress of joint European Neonatal Societies, 56th ESPR (European Societies of Paediatric Research) Annual Meeting, **jENS 2015**, Budapest, Hungary, September 2015.

Chalia M, Cooper R J, Lee C W, Edwards A D, Michell A W, Dempsey L, Brigadoi S, Everdell N L, Hebden J, Austin T. '**Prospective Study of the Cerebral Haemodynamic Response of Burst Suppressed or Discontinuous Electroencephalographic Activity in Infants with Hypoxic Ischaemic Encephalopathy**'. **9th International Conference of Brain Monitoring & Neuroprotection in the Newborn** (BMN 2015), Cork, Ireland, October 2015.

Chalia M, Cooper R J, Lee C W, Dempsey L, Hebden J, Austin T. '**Can diffuse optical tomography provide early detection of perinatal arterial ischaemic stroke (PAIS) at the cot side?**' **Functional Near Infrared Spectroscopy conference** (fNIRS 2016), Paris, France, October 2016.

Dempsey L, Chalia M, Cooper R J, Lee C W, Gibson P, Austin T, Hebden J. '**Assessing neonatal stroke lateralisation with time-resolved and continuous-wave DOT**'. **European Conferences on Biomedical Optics** (ECBO), Messe Munich, Munich, Germany, June 2017.

Table of Contents

Table of Figures and Tables

Chapter 3

Chapter 4

Chapter 5

Chapter 6

Project Rationale and Aims

The combination of multi-channel near-infrared diffuse optical tomography (DOT) and electroencephalography (EEG) offers the ability to study the vascular changes of the surface of the brain (cortex) and electrical brain activity. This makes it possible to study the relationship between cortical haemodynamics and electrical activity known as neurovascular coupling.

A previous pilot study examining the neurovascular coupling of neonatal seizures, conducted by the group, demonstrated the significance of combining DOT and EEG in detecting cortico-vascular changes in a newborn infant with hypoxic ischaemic encephalopathy (HIE). Distinct cortical haemodynamic changes were identified in relation to recurrent electroencephalographic seizures.

Therefore, this MD project is based on the use of combined DOT and EEG in the investigation of brain injury in the term neonatal population, with focus on the two, commonest such clinical entities, hypoxic ischaemic encephalopathy (HIE), and cerebral infarction.

The principal two aims of this project were to continue to investigate term newborn infants presenting with seizures and to demonstrate the practicality and readily available use of combined DOT-EEG at the cot side in the neonatal intensive care unit.

The objectives of the project as presented in chapters 4, 5 and 6 were the following:

- To investigate and improve the understanding of the potential cortical haemodynamic changes measured by DOT during neonatal seizures as detected by EEG.
- To investigate the cortical haemodynamic changes in relation to other neurophysiological phenomena seen in cases of HIE and neonatal encephalopathy, such as discontinuous cortico-electrical activity and/or burst suppression.
- To explore the potential of DOT-EEG in the detection of uni-hemispheric perinatal stroke.

Chapter 1: Neonatal Brain Injury in the Term Infant

1.1 Neonatal Encephalopathy and Seizures

A wide range of pathologies comes under the umbrella of brain injury in the term, neonatal population. Neonatal encephalopathy is a clinical expression of deranged brain function in the term infant manifesting in the early postnatal phase. It is characterised by a decreased level of consciousness and/or seizures and may be associated with respiratory distress or depression, abnormal tone, and reflexes (1). It may be the consequence of a hypoxic-ischaemic insult. However, there are other conditions which can be attributed to an infant being encephalopathic in the neonatal period, such as metabolic conditions, maternal drug abuse, and cerebral infarction. The conditions associated with neonatal encephalopathy are also associated with neonatal seizures; however, one needs to make the distinction that not all infants with encephalopathy present with seizures and not all infants presenting with seizures are encephalopathic.

Seizures are one of the commonest neurological presentations in the neonatal period with varied evolution of clinical semiology and symptoms. Therefore, their aetiology has almost become synonymous to the aetiology of term, neonatal brain injury (see Table 1.1). In term and near-term infants, the dominant causes are hypoxic ischaemic encephalopathy (HIE) and cerebral infarction. Their incidence does vary slightly depending on access to maternal and neonatal services amongst low, middle, and high-income countries.

The incidence of neonatal seizures has been reported between 0.5 to 5 per 1,000 live births (2-4), predominantly occurring in the first few days of postnatal life. Older studies were purely based on clinical observation with a mixed population of different gestational age (GA) and postconceptional age. Other studies were based on prolonged amplitude-integrated electroencephalography (aEEG) recordings with variation in the GA of infants and underlying clinical pathologies. Using this methodology, the number reported is approximately 2 in 1,000 live born infants diagnosed with seizures with this figure increasing in the instance of prematurity (5, 6). In preterm infants, who were later found to have developed intraventricular haemorrhage (IVH), aEEG studies have shown occurrence of subclinical seizures in up to 75% (7, 8).

The principal aetiological factor of neonatal seizures in both preterm and term infants is HIE, accounting for almost 60% of reported cases (2, 9-11). Cerebral infarction follows HIE in frequency in term infants. Another main factor is intracranial

haemorrhage, which includes cases of subarachnoid, germinal matrix, intraventricular and subdural haemorrhage. Intracranial infection (i.e. meningitis, encephalitis) and developmental defects (i.e., lissencephaly, pachygyria) account for 5-10% of cases respectively. Metabolic disturbances such as hypoglycaemia, hypocalcaemia, hypomagnesaemia, other metabolic conditions and drug withdrawal in cases of maternal substance abuse need to be highly considered in the differential diagnosis. There is also a group of miscellaneous neonatal seizure syndromes, such as benign familial neonatal seizures, benign idiopathic neonatal seizures, early myoclonic encephalopathy, and early infantile epileptic encephalopathy and others which are rarer but should be considered in the absence of any other aetiology and persistence of seizure activity. These aetiological factors are summarised in table 1.1. (please also refer to section 2.1.7 of chapter 2 for further details on neonatal seizures).

Causes of Neonatal Seizures	Incidence	Examples
Hypoxic ischaemic encephalopathy	37-57.5%	Grade I to III
Ischaemic infarction or cerebral sinus venous thrombosis	7-18%	Middle cerebral artery infarct
Intracranial haemorrhage	4,8-17%	Subdural, subarachnoid
Intracranial infections	3-20%	Group B Streptococcal meningitis
Metabolic or electrolyte disorders	3-19%	Hypoglycaemia, Hypocalcaemia, Hypo- or Hypernatraemia, Kernicterus
Inborn errors of metabolism	1-11.3%	Pyridoxine-dependent seizures, Glycine encephalopathy
Congenital anomalies or developmental defects	3.2-11.3%	Lissencephaly, Schizencephaly
Idiopathic	0.5-14%	Benign familial neonatal seizures
Intoxication	0.5%	Local anaesthesia

Table 1.1: Causes of neonatal seizures in the term neonatal population. This table has been adapted and modified based on reference (12). The incidence of the possible aetiological conditions for neonatal seizures was adapted from references (2, 11, 13, 14).

Although the incidence of neonatal seizures varies depending on its cause, investigatory tools, and healthcare system, its importance lies in prevention, early diagnosis and prompt, disease specific management. The aim is to improve long term prognosis, as there is increasing evidence over the years that neonatal seizures adversely affect neurodevelopmental outcome (15-19). In that perspective, there is an increasing interest within neuroscience in the recognition of neonatal brain injury as a life-long

disease, which can potentially be managed more effectively by understanding its predisposing factors and mechanisms and by developing tools for early detection, specific diagnosis, and differentiation of disease severity.

1.2 Hypoxic Ischaemic Encephalopathy

Hypoxic ischaemic encephalopathy is the result of decreased or lack of oxygen supply (hypoxia) and decreased blood perfusion (ischaemia) leading to disruption of cerebral energy metabolism (20). Hypoxia and ischaemia can occur acutely or chronically and can be associated with maternal factors (i.e. hypotension), cord factors (obstruction, prolapse), placental factors (placental insufficiency, abruption) and uterine factors (rupture) (21). Events in the first 28 days of postnatal life such as respiratory or cardiac arrest can also lead to HIE. It is interesting to note that HIE is often confused or used instead of the term neonatal encephalopathy which is a more descriptive term of deranged neurological status without assumptions on its pathogenetic mechanisms. Neonatal encephalopathy is called HIE if there is clear evidence of intrapartum asphyxia as the cause of neonatal neurological depression and/or seizures. Table 1.2 encompasses a range of clinical conditions which mimic intrapartum asphyxia and infants may present as depressed or encephalopathic (21).

Condition	Examples
Neonatal Sepsis	Group B Streptococcal septicaemia
Congenital infections	Viral, toxoplasmosis
Neuronal migration disorders	
Congenital myotonic disorders	Prader-Willi syndrome, congenital and transient myasthenia gravis
Lung or airway disorders	Pneumothorax, congenital diaphragmatic hernia
Metabolic conditions	Non-ketotic hyperglycinaemia
Extracranial trauma	Subgaleal haemorrhage, subdural haematomas
Genetic disorders associated with thrombotic or thrombophilic abnormalities	Protein C and S deficiencies, factor V Leiden deficiency

Table 1.2: Conditions causing neonatal depression and/or neonatal encephalopathy that mimic intrapartum asphyxia. This table was adapted from reference (21).

The difference in population demographics, healthcare availability and a lack of a unified, global use of terminology and definition in reporting and investigating HIE leads to a wide range in incidence from 1 to 8 per 1,000 live births (22), with more recent population studies reporting an incidence of 1.5 per 1,000 live births (23). Global estimations on birth asphyxia related deaths vary from 0.7 to 1.2 million per year (24). A history of perinatal asphyxia is strongly associated with life-long sensorineural impairment and neuro-disability (25, 26). HIE remains the leading cause of acquired brain

injury and neuro-disability in the term neonatal population in both the developed and developing world (27).

An understanding of the pathophysiology of HIE comes from a combination of clinical observations and animal studies. Based on animal work (28), the initial response to hypoxia in the foetus results in redistribution of the blood circulation to vital organs such as the heart and the brain. The heart rate decreases to minimise myocardial work but at the same time, maintaining circulation in the vital organs. Further hypoxia leads to metabolic acidosis and finally cessation of circulation to all organs including heart and brain.
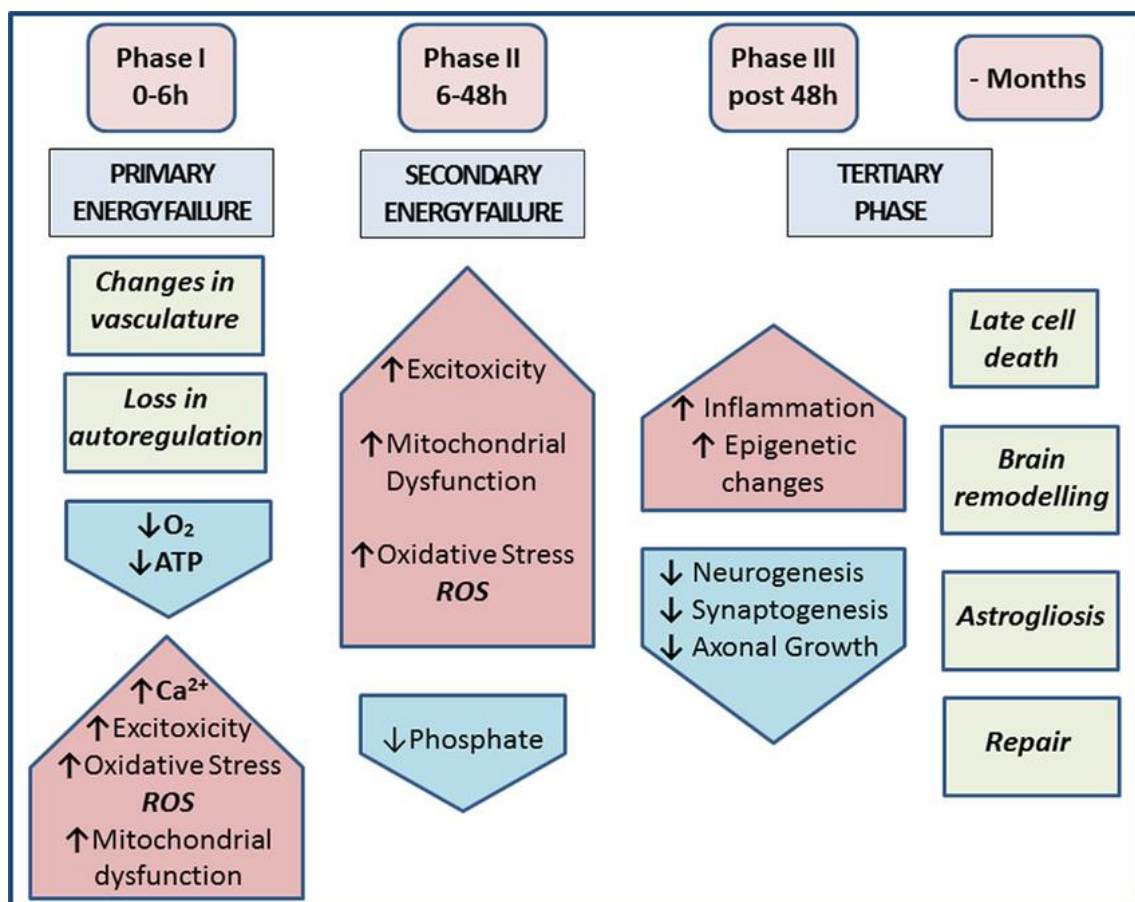
Figure 1.1: Schematic representation of the cascade of events following hypoxia-ischaemia hours to days post initial insult. Note the progressiveness of the insult months after the initial event (ROS stands for reactive oxygen species). Adapted from reference (29).

The pathophysiological mechanisms of brain injury following hypoxia-ischaemia are based on a cascade of events following the primary hypoxic episode, known as primary energy failure; lack of oxygen translates into cessation of oxidative metabolism leading to accumulation of lactate and depletion of energy supply, which at a cellular

level translates into depletion of adenosine triphosphate (ATP). This leads to failure of the ATP dependent Na^+/K^+ pump. In the very severe cases there is influx of Na^+ and water in the cell and subsequent necrosis. In the less severe cases, there is depolarisation of the membrane with increased extracellular accumulation of excitatory amino acids (glutamate) and increased intracellular Ca^{2+} with a subsequent gradual cascade of events leading to cellular apoptosis (see Fig. 1.1). The initial metabolic acidosis and increase in lactate results in increase in cerebral blood flow and production of ATP from phosphor-creatinine (PCr). While acidosis progresses ATP production diminishes and autoregulation is lost with ultimate neuronal injury and necrosis (20).

Classically there are two main types of brain injury following hypoxia-ischaemia affecting different brain regions such as the cortex and the deeper nuclear structures, basal ganglia and thalamus (30) (see Fig.1.2). The basal ganglia and thalamus (BGT) type of injury pattern is the one most frequently seen following an acute insult (31). These deep structures are particularly susceptible due to their high metabolic rate and rich concentration in N-methyl-D-aspartate (NMDA) glutamate receptors (the main excitatory receptor in neuronal synapses). BGT lesions vary in extent form focal to widespread abnormal signal intensity seen on MRI. A marker of the severity of the lesions is associated injury to the posterior limb of the internal capsule, an area which is actively myelinating at term and is highly susceptible to hypoxia-ischaemia (32). A normal appearance of the internal capsule is a good prognostic sign for normal motor function after hypoxic–ischaemic insults (see Fig. 1.3 and 1.4).
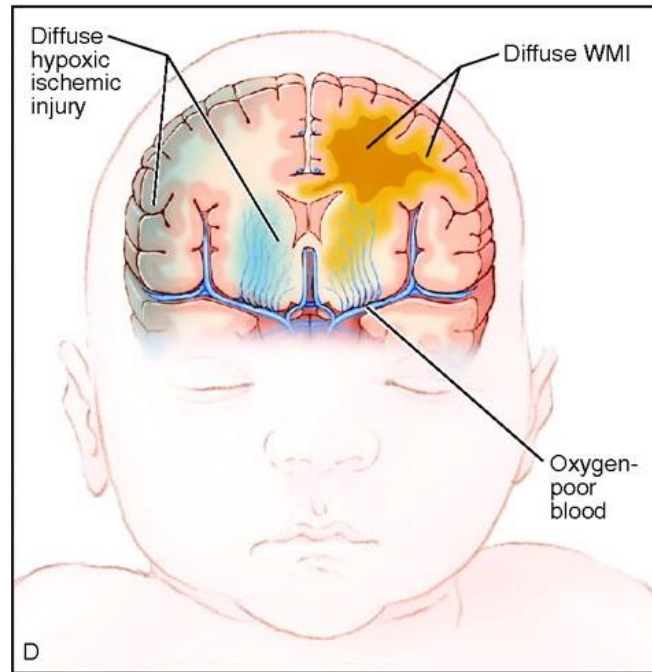
Figure 1.2: Susceptible brain regions to hypoxia-ischaemia. HIE results in global injury, affecting neurons of the cortical plate and basal ganglia as well as white matter tracts. Image adapted by reference (30).
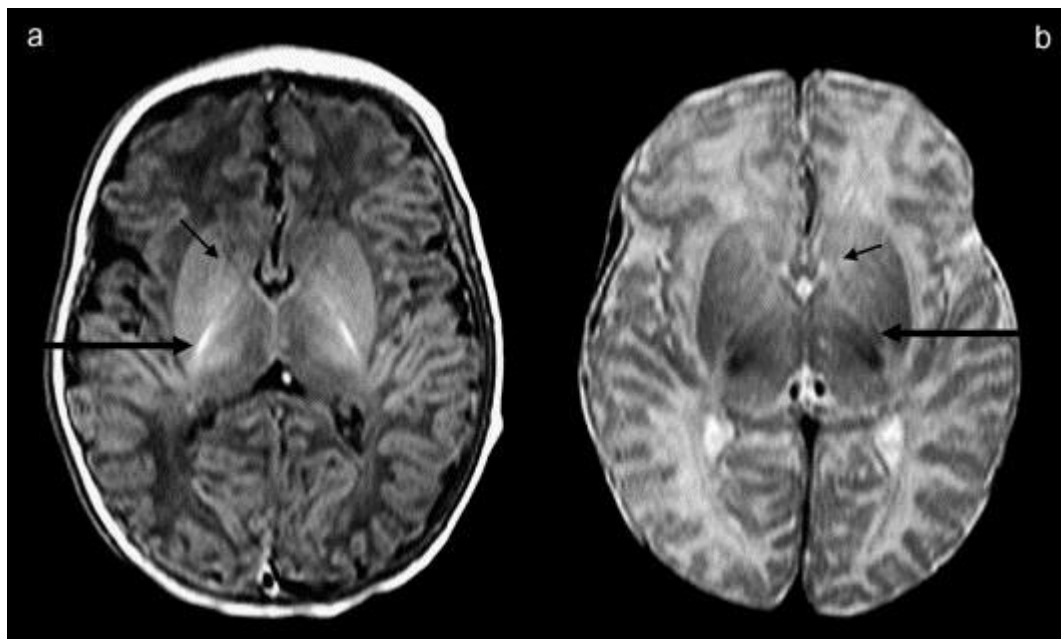
Figure 1.3: Normal axial MR images at the level of the basal ganglia of term infant brain: (a) a T1-weighted inversion recovery and (b) a T2-weighted sequence. The myelin in the posterior limb of the internal capsule (long arrows) is visualised as high signal intensity for about half its length in T1-weighted image (a) but is not as advanced on the T2-weighted image (b) where it is of low signal intensity. The short black arrows indicate the anterior limb of the internal capsule. Image adapted from reference (32).
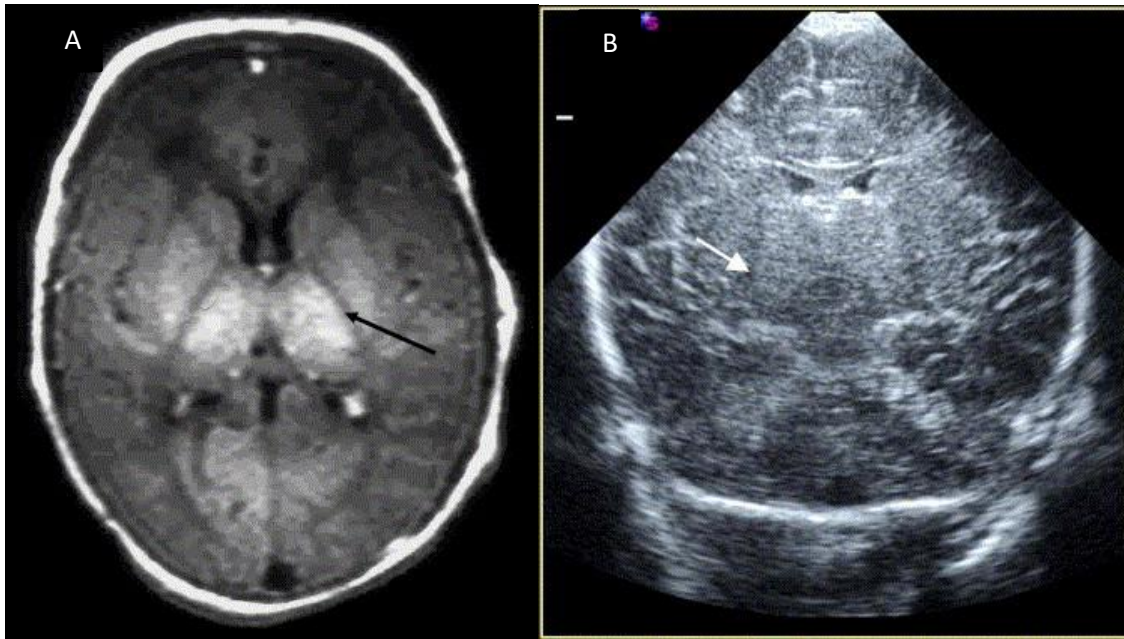
Figure 1.4: Posterior limb of the internal capsule (PLIC) in severe HIE in axial T1-weighted image (A) and cranial ultrasound (B). (A) Note the loss of the normal high signal from myelin (black arrow) with abnormal signal in the thalami and the lentiform nuclei. (B) Note the linear strip of low echogenicity (white arrow) in the basal ganglia between the lentiform nucleus and the thalami indicating the line of the internal capsule with abnormally high echogenicity in the basal ganglia and thalami in this infant with severe HIE (B). Adapted from reference (32).

The brainstem may be involved and affected in the presence of BGT injury. It tends to be present in the most severe end of the spectrum of HIE. Recent studies have shown that up to 50% of infants with brainstem lesions died in the neonatal period or within the first year of life (31). Survivors with BGT injury face a range of disabilities with cerebral palsy (CP), feeding difficulties, speech and language problems, visual and hearing impairment, seizures, and cognitive impairment. Martinez-Biarge et al., have developed flow charts of developmental outcome based on the severity of BGT injury (see Fig. 1.5). It appears that the severity of BGT injury dictates the severity of motor involvement/impairment in the manifestation of CP with the signal intensity of the PLIC on MRI being the best predictor of CP severity (31).
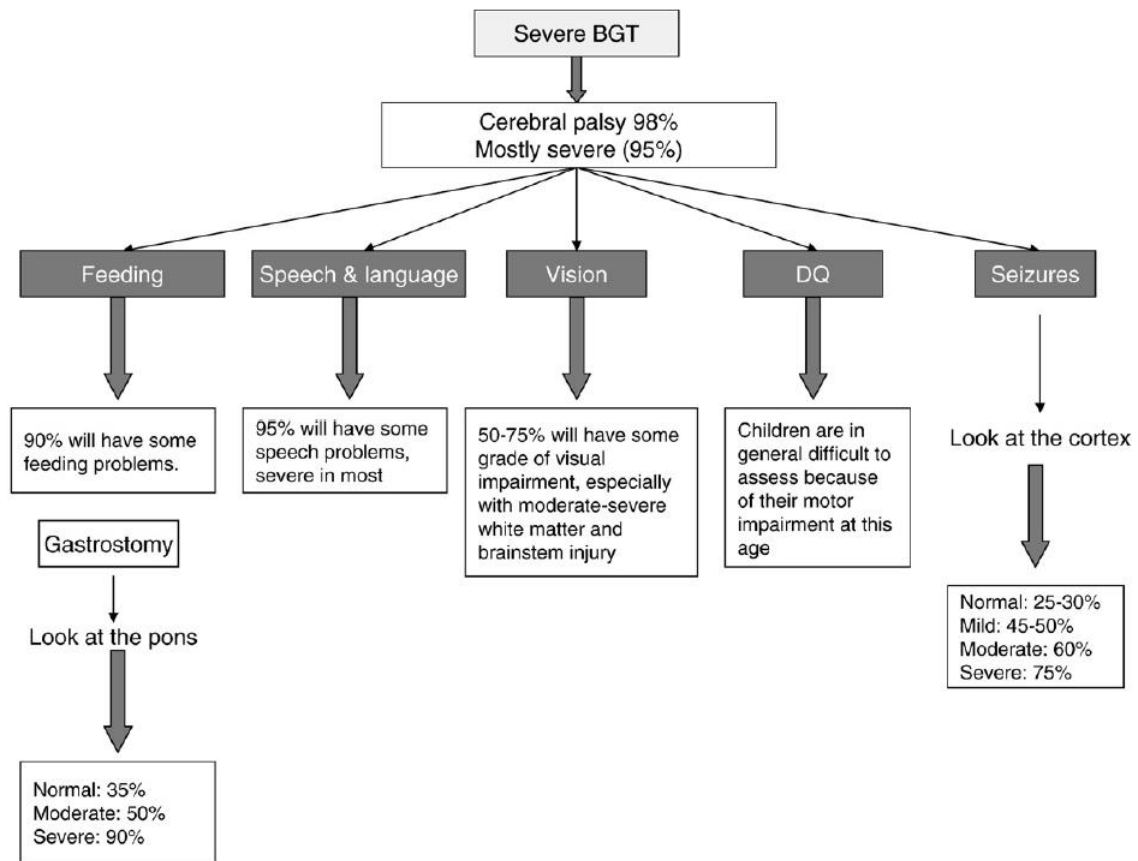
Figure 1.5: Flow chart showing the developmental outcome for infants with severe BGT injury (DQ stands for developmental quotient). Adapted from reference (31).

The cortical watershed pattern of injury tends to be associated with forms of chronic hypoxia where maternal factors such as hypotension have been shown to be related. This injury consists of cortical necrosis with involvement of the subjacent white matter. It tends to affect the parasagittal and supra-medial regions of the convexities bilaterally with distribution mostly over the parieto-occipital areas than the anterior ones (see Fig.1.6).
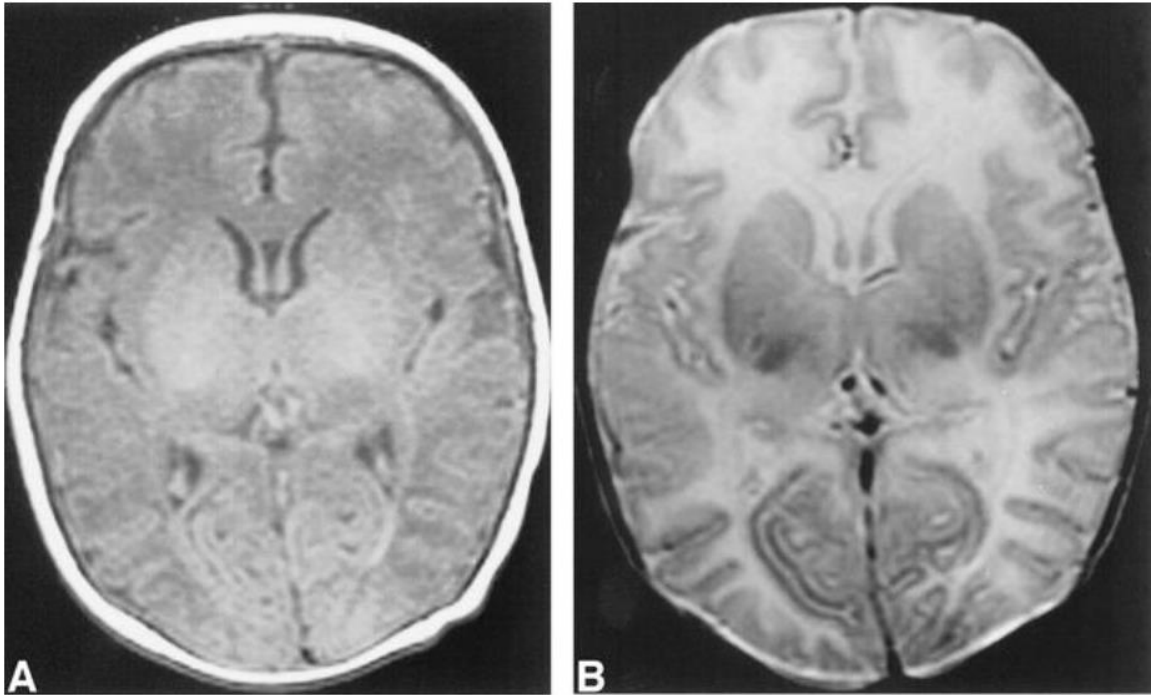
Figure 1.6: Cortical watershed ischaemic injury. (A) Axial T1-weighted image showing low signal intensity bilaterally in the anterior and posterior watershed areas. (B) Axial T2-weighted image showing increased signal intensity in the same areas, suggesting oedema. Adapted from reference (33).

Infants with watershed type of injury predominantly have cognitive impairment with motor development being spared. As the cognitive deficit presents after 12 months of age and sometimes only when schooling begins, long term follow up is crucial.

There is a global type of injury where both cortical grey and subcortical white matter are involved. These cases are the most severe ones and often fatal. In surviving infants, the injury evolves in multi-cystic encephalomalacia with global developmental delay. It is interesting to note here that infants respond differently to different degrees of acute and chronic hypoxia ischaemia and that the pattern of injury is not easily reproducible. Factors such as the primary cause, the degree of hypoxia and ischaemia, the maturational stage of the brain prior to the insult, regional cerebral blood flow (CBF), and the general health of the infant collectively play a role in the clinical course and final neurodevelopmental outcome (21).

Clinically, HIE is categorised into three stages or grades from I to III based on the Sarnat modified classification (34). However, in all grades there is a common background of perinatal asphyxia, abnormal neurological status, and varied organ dysfunction. The grading of HIE is based on a daily clinical assessment of the infant using the Sarnat

modified classification (see Table 1.3). Other scoring tools, such as the Thompson score (also known as the HIE score) have been developed and are based on the Sarnat scale (35). The Thompson score is a clinical tool assessing a range of signs associated to neurological dysfunction in infants with evidence of perinatal asphyxia (see Table 1.4). The score ranges from 0 (normal) to 22 (severe). Infants with a score of 1-10 are considered to have mild HIE, infants with a score of 11-14 are considered to have moderate HIE and infants with a score of 15-22 are considered to have severe HIE. It has been reported that a consistent score of >10 in the first 7 days of life predicts an adverse outcome with a 100% sensitivity and 61% specificity (35).

Neurologically the infant may appear hyperalert and irritable (mild), lethargic and hypotonic or utterly comatose with weak or absent respiratory effort and either no response to stimuli or exhibition of spinal reflex to painful stimuli. Seizures are present in stage II and III of HIE and commonly present within the first 24 hours of life. In stage II, there can be an overall reduced electro-encephalographic activity with loss of cyclicity between sleep and awake states. In stage III the electro-encephalographic activity can be completely flat (see Fig. 1.7) or may have the appearance of burst suppression (see Fig. 1.8) (please refer to chapters 2 and 5). Similarly, seizures may be evident (see Fig. 1.8).

Modified Sarnat			
STAGE	**Stage 1**	**Stage 2**	**Stage 3**
Level of consciousness	Hyperalert	Lethargic or obtunded	Stupor or coma
Activity	Normal	Decreased	Absent
Neuromuscular Control			
Muscle Tone	Normal	Mild Hypotonia	Flaccid
Posture	Mild distal flexion	Strong distal flexion	Intermittent decerebration (extension)
Stretch reflexes	Overactive	Overactive	Decreased or absent
Complex/Primitive reflexes			
Suck	Weak	Weak or absent	Absent
Moro (startle)	Strong; low threshold	Weak; incomplete; high threshold	Absent
Tonic Neck	Slight	Strong	Absent
Autonomic function			
Pupils	Mydriasis	Miosis	Variable; often unequal; poor light reflex; fixed; dilated
Heart rate	Tachycardia	Bradycardia	Variable
Seizures	None	Common; focal or multifocal	Uncommon (excluding decerebration)

Table 1.3: Sarnat modified classification criteria of HIE. Adapted from reference (34).

In terms of other clinical manifestations, there can be a varied involvement or dysfunction of other organs or systems. Hypoxia-ischaemia activates the diving reflex which diverts the blood circulation from the skin and the splanchnic area to the most vital organs; heart, adrenals, and brain. It was thought until recently, that all infants with HIE would at some point have developed some degree of organ or system dysfunction.

However, a recent study has shown that multiorgan dysfunction is not related to outcome in HIE cases, with renal, hepatic, cardiovascular, and respiratory involvement in 58-88% of cases with good outcome and 64-86% of infants with adverse outcome (36). Table 1.5 shows the clinical criteria for single or multiorgan dysfunction.

Sign	0	1	2	3
Tone	Normal	Hyper	Hypo	Flaccid
Level of consciousness	Normal	Hyperalert/stare	Lethargic	Comatose
Fits	None	< 3 per day	>2 per day	
Posture	Normal	Fisting, cycling	Strong distal flexion	Decerebrate
Moro	Normal	Partial	Absent	
Grasp	Normal	Poor	Absent	
Suck	Normal	Poor	Absent, bites	
Respiration	Normal	Hyperventilation	Brief apnoea	IPPV (apnoea)
Fontanel	Normal	Full, not tense	Tense	

Table 1.4: Thompson scoring system of HIE. This is a modification of the original Sarnat criteria and is based on 9 clinical signs and gives a score ranging from 0 to 22. Adapted from reference (37).
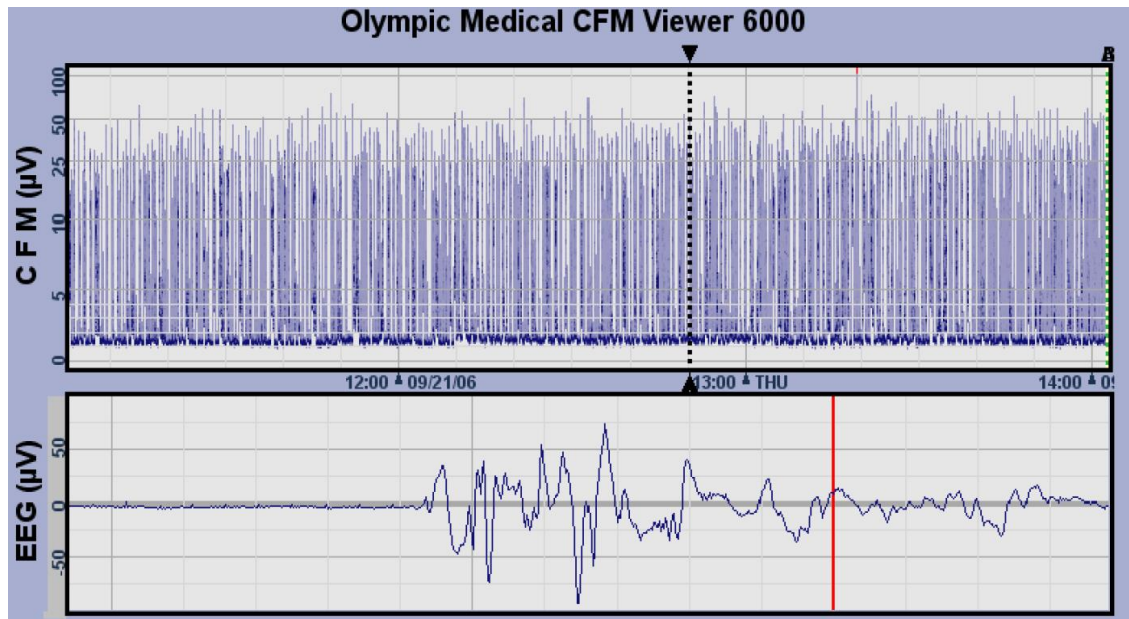
Figure 1.7: Burst suppressed trace on an aEEG monitoring device. The top part of the figure is indicating the aEEG trace from the cerebral function monitor (CFM), and the bottom part is indicating the EEG trace (please refer to section 2.1.3 of chapter 2 for further details). Image adapted from website http://www.neoweb.org.uk/CFM/Quiz.htm.
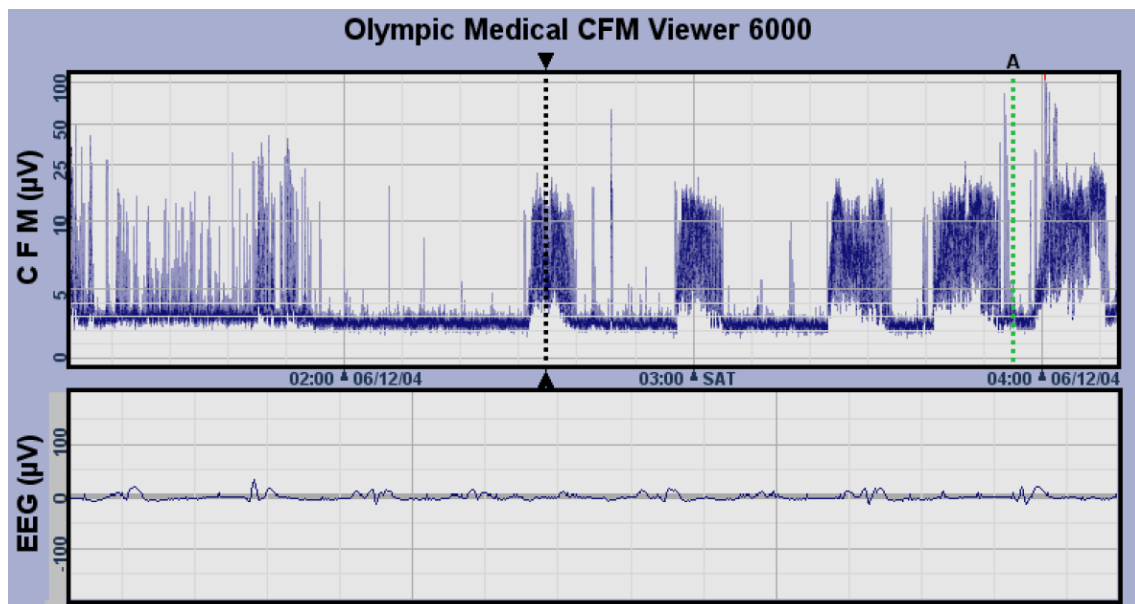
Figure 1.8: Seizure activity with a flat, isoelectric background on an aEEG monitoring device. The top part of the figure is indicating the aEEG trace from the cerebral function monitor (CFM), and the bottom part is indicating the EEG trace (please refer to section 2.1.3 of chapter 2 for further details). Image adapted from website http://www.neoweb.org.uk/CFM/Quiz.htm.

SYSTEM	CRITERIA
Renal	Anuria or oliguria (<1 ml/kg/h) for 24 hours or more, and a serum creatinine concentration >100 mmol/l; or anuria/oliguria for >36 hours; or any serum creatinine >125 mmol/l; or serial serum creatinine values that increased postnatally
Cardiovascular	Hypotension treated with an inotrope for >24 hours to maintain blood pressure within the normal range, or electrocardiographic evidence of transient myocardial ischaemia
Respiratory	Need for ventilator support with oxygen requirement >40% for at least the first 4 hours after birth
Hepatic	Aspartate aminotransferase >100 IU/l or alanine aminotransferase >100 IU/l at any time during the first week after birth

Table 1.5: Criteria for organ dysfunction in HIE. This was modified and based on a retrospective cohort study which showed that there was no association between organ dysfunction and outcome (36). Adapted by reference (36).

Historically treatment of HIE was provision of symptomatic support for all organs. However, in recent years there has been a drive towards implementing specific neuroprotective measures for the prevention of ongoing brain injury. As described earlier and as shown schematically (see Fig. 1.1) HIE is a progressive disease which does not stop once the hypoxic insult stops. Improving the peripheral circulation and supporting all the systems in maintaining homeostasis does not stop the cascade of biochemical events triggered by the initial hypoxic-ischaemic insult. A revolutionary treatment with the aim to cease the cascade of these biochemical changes is now offered to all infants with HIE in the form of therapeutic hypothermia (TH) in high income countries (38, 39). This followed the results of the TOBY (TOtal BodY, whole body therapeutic hypothermia for perinatal asphyxia) and several other randomised controlled trials and their beneficial results (40-42). Following a clinical assessment based on the TOBY clinical criteria (see Table 1.6), the infant with suspected HIE receives a 72-hour course

of whole-body TH with target core body temperature between 33 to 34 °C, and parallel continuous aEEG or EEG monitoring (depending on the facilities of the centre delivering the care). As evident form table 1.6, the treatment is offered to the moderate to severe end of the HIE clinical spectrum (stage II and III). The studies have shown that the numbers to treat for one infant to be saved, free of neurodevelopmental sequelae is 8 (43).

Criteria	Condition
Criteria A: **Infants ≥36 weeks of gestation admitted to the neonatal unit with at least one of the following:**	Apgar score of ≤5 at 10 minutes after birth
	Continued need for resuscitation, including endotracheal or mask ventilation, at 10 minutes after birth
	Acidosis within 60 minutes of birth (defined as any occurrence of umbilical cord, arterial or capillary pH <7.00)
	Base Deficit ≥ 16 mmol/L in umbilical cord or any blood sample (arterial, venous or capillary) within 60 minutes of birth
Criteria B: **Infants that meet criteria A should be assessed whether they meet the following neurological abnormality entry criteria of moderate to severe encephalopathy or seizures:**	Altered state of consciousness (reduced response to stimulation or absent response to stimulation) **and**
	Abnormal tone (focal or general hypotonia, or flaccid) **and**
	Abnormal primitive reflexes (weak or absent suck or Moro response)

Table 1.6: TOBY cooling criteria for initiation of TH on infants with suspected HIE. Note that at least one of criteria A and all of criteria B need to be fulfilled for TH to be considered as a therapeutic strategy. Adapted by the UK TOBY Cooling Register Clinician's Handbook.

Overall, it has been shown that mild to moderate induced hypothermia in HIE cases reduces the risk of death and disability in infants with less severe EEG abnormalities, reduces death and moderate to severe disability, and increases the number of disability-free survivors (40-42, 44). There is ongoing research in the identification of adjacent neuroprotective measures or agents which could be used in addition to TH for further improvement of clinical outcome.

The TOBY Xe randomised control trial explored the efficacy of TH plus xenon within 6 hours of birth versus TH alone perinatal asphyxia. This trial proved the feasibility of xenon administration but did not show any added neuroprotective effect in clinical outcome (45) despite promising animal studies (46, 47). Potential reasons for his could be the timing of Xe administration of the dosage delivered. There is an ongoing clinical trial (CoolXenon2), further exploring the efficacy of TH combined with Xe for infants born in poor condition (https://clinicaltrials.gov/ct2/show/NCT01545271).

A recent systematic review summarises the neuroprotective effects of melatonin in perinatal hypoxia-ischaemia in animal studies (48) and presents its encouraging positive neuroprotective effects, as shown so far by experimental research (49-52). This, however, has not yet translated into a clinical trial or standardised clinical approach. Researchers are also exploring the use of erythropoietin in combination with TH as an added neuroprotective agent with some variable results coming from the experimental field (53-56) and randomised controlled trial (57). A more recent randomised control trial has shown that when erythropoietin is administered in high doses with TH in infants with HIE, it potentially leads to a decrease in MRI brain insult and a better motor outcome at 1 year of life (58). Another research group is undertaking a clinical trial on the effectiveness of allopurinol as an adjacent neuroprotective agent in combination with TH (http://www.albino-study.eu/).

1.3 Perinatal Stroke

Perinatal stroke is defined as a region of damaged brain tissue secondary to focal disruption in the cerebral blood circulation due to arterial (perinatal arterial ischaemic stroke, PAIS) or cerebral sinus venous thrombosis (CSVT) or embolization as confirmed on neuroradiological or neuropathological findings (59). The exact timing of injury can be difficult to determine and has been defined as occurring anywhere between the second trimester of pregnancy (20 weeks of gestation onwards) and the first 28 days of life (59, 60). Perinatal stroke is an important clinical entity frequently underdiagnosed or under-reported in the literature. Depending on the age of presentation perinatal stroke can be classified into foetal ischaemic stroke (diagnosed antenatally or on autopsy of a stillbirth foetus), neonatal ischaemic stroke (diagnosed in the neonatal period; first 28 days of life), presumed perinatal ischaemic stroke (diagnosed after the neonatal period in infants, where the ischaemic insult is thought to have occurred in the perinatal period) or CSVT (59).

Perinatal arterial ischaemic stroke is a frequent neonatal condition affecting 1 in 2,300 infants (61) not including cases recognised outside the neonatal period. It is secondary to the occlusion of a large cerebral vessel and is ischaemic in nature (see Fig. 1.9). Approximately 75% of cases are unilateral in which nearly all are in the MCA territory. In almost 65% of those cases, there is involvement of the left rather than right MCA (62).
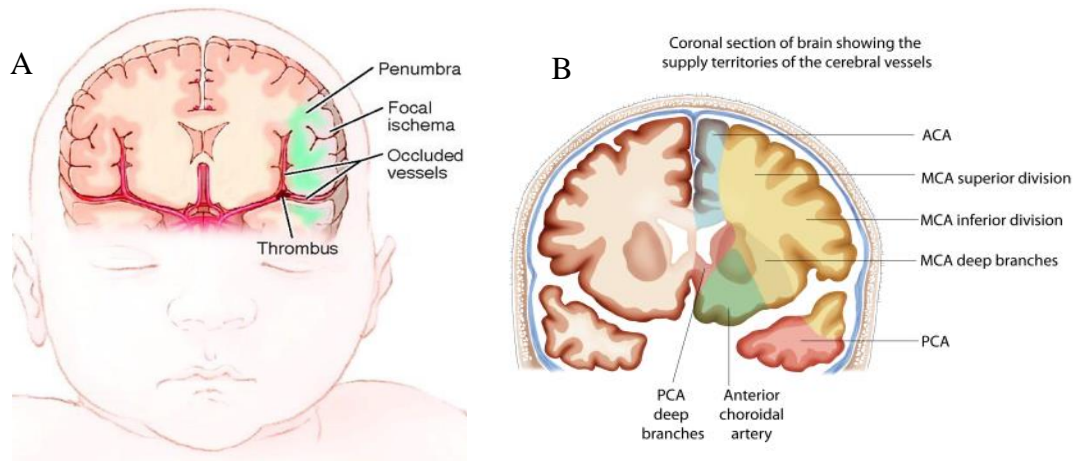
Figure 1.9: Brain susceptibility to PAIS. (A) Image showing the brain regions most susceptible to PAIS. (B) Image showing the supply regions of the large cerebral vessels. (ACA: Anterior cerebral artery; MCA: Middle cerebral artery; PCA: Posterior cerebral artery). Image (A) was adapted from reference (30) and image (B) from neuro4students.wordpress.com.

The aetiology of PAIS is uncertain in most cases. There is a variety of maternal, intrapartum, and neonatal factors considered to predispose to PAIS (see Table 1.7). The commonest hypothesis is that of a placental embolus travelling into the foetal circulation, because of the patency of the foramen ovale and the frequency at which the left MCA is involved. Other direct aetiological mechanisms have been reported, such as meningitis, presumably secondary to endothelial injury and inflammation of arteries and veins (63).

It is also associated with congenital heart disease, especially if intravascular catheters, extracorporeal membrane oxygenation (ECMO) or surgery is required (64). PAIS has been reported to coexist with NE in up to 5% of cases (65). More recent studies have shown that although infants with PAIS might have a complicated perinatal history (66), co-presenting with NE is rare, and the incidence presented in older studies may be influenced by the misclassification of neonatal seizures under the generic umbrella of NE.

Maternal Risk Factors
Primigravida
Infertility
Chorioamnionitis
Prolonged rupture of membranes (PROM)
Pre-eclampsia
Intrauterine growth restriction (IUGR)
Drugs (i.e. cocaine)
Twin to twin transfusion (TTTS)
Gestational diabetes mellitus (GDM)
Intrapartum Risk Factors
Prolonged second stage of labour
Occiput posterior presentation
Neonatal Risk Factors
Polycythaemia
Congenital heart disease
Diagnostic procedures and surgery for cardiac disease
Intravascular catheters
Exchange transfusion
Persistent pulmonary hypertension (PPHN)
Extracorporeal membrane oxygenation (ECMO)
Meningitis
Arterial dissection in the neck **(67)**

Table 1.7: Risk factors of PAIS. Modified and adapted by reference (68).

There is a male predominance and most infants present as low risk until the acute onset of symptoms. The main clinical presentation is related to seizures, with a predominance of focal seizures manifesting in the first 72 hours of life. PAIS is the second most frequent cause of neonatal seizures in the term neonatal population (69). Presentation with encephalopathy or with asymmetry of neonatal reflexes (i.e. Moro reflex, atonic symmetrical reflex) is less frequently observed early on in the course of PAIS (70). Infants or children diagnosed outside of the neonatal period commonly present with signs of hemiparesis, i.e. abnormal hand preference. Slight asymmetry in the development of the affected limb may also be apparent.

Based on older studies PAIS appears to be more frequent in the term neonatal population compared to the preterm (71). More recent work by Benders et al. looking in a cohort of infants between 27 to 36 weeks of gestation showed that PAIS also occurred

in preterm infants and was again more common on the left side and in the MCA territory. It appeared that infarct of the MCA in gestations of over 32 weeks mainly involved its main branch (72). The underestimation of its prevalence in the preterm population was highlighted and the requirement for more frequent neuroimaging was stressed (72, 73).

Several models have been developed to understand the pathophysiological mechanisms of HIE and focal arterial stroke at term (74). A hypoxic-ischemic insult was reproduced by unilateral ligation of the common carotid artery (CCA) followed by a variable duration of exposure to 8% oxygen postnatally in rats (75) and mice. Focal arterial stroke was reproduced by a transient MCA occlusion model in rats on day 7 (76) or day 10 of life (77), and mice (78), and a combined permanent MCA occlusion and transient CCA occlusion in rats (79). It was shown that the hypoxic-ischaemic insult is associated with increased cerebral blood flow (CBF) during systemic hypoxia, whereas CBF is disrupted after MCA occlusion. Lack of flow may be evident in the affected artery for hours post initial infarct (80). Reperfusion occurs either through the affected artery or via anastomotic arteries and the biochemical cascade in the reperfusion phase is very much like the one seen in HIE, with macrophages, glial cells, excitotoxic agents (such as glutamate), and oxidative stress being responsible for the ongoing injury process in the core of the infarct and its penumbra.

After the first 3 days and up to 6 weeks following the insult, the infarct organises and this may consist of gliosis, cyst formation, myelin breakdown, and neovascularisation (81). Eventually, after the second month, an infarct involving a major cerebral artery will evolve in an area of cortical and subcortical tissue loss, which appears open towards the subarachnoid space (see Fig. 1.10(B)).

The management of PAIS is supportive and consists of adequate hydration, and anticonvulsant treatment as clinically indicated. There is not enough evidence to support thrombolytic measures in the neonatal period and there is concern over the risk of intracranial haemorrhage with thrombolysis. In the instance of a clearly identified, ongoing cardio-embolic source the use of low molecular weight heparin (LMWH) may be justified but proper evidence deriving form randomised controlled trials is lacking (82).

Alternative methods of treatment are being explored in the adult population. Hypothermia preserves cerebral autoregulation (CA) and reduces cytotoxic oedema around clot formatting in the stroke affected region (83) and could play a role in the treatment of acute stroke. In a systematic review of animal studies, therapeutic hypothermia reduced infarct size by 44% (95% confidence interval 40 to 47%) with the best results being obtained at lower temperatures (≤ 31 °C). A reduction in infarct volume was also observed by approximately one third with temperature reduction to 35 °C, with initiation of treatment between 90 and 180 minutes, and in permanent ischemia models (84). Randomised trials of surface or endovascular hypothermia initiation in the treatment of acute ischaemic stroke (Cooling for acute ischaemic brain damage - COOL-AID, (85), Intravascular cooling in the treatment of stroke - ICTus, (86)) have not shown any significant difference in outcome between the cohort of patients receiving hypothermia and those who were not. However, the second COOL-AID trial, with a larger number of patients (10 in the initial, 40 in the second one), showed a trend of decreased lesion growth on diffusion weighted images (DWI-MR) in the group treated with both thrombolysis and hypothermia, although the results in clinical outcome were similar between the two groups (87). In a single-centre study it was shown that out of 15 infants diagnosed with focal stroke on MRI, 5 of them who also underwent hypothermia did not have any seizure activity manifestation, thus providing some promise in the neuroprotective role of TH in perinatal stroke (88).

The outcome of PAIS includes the development of epilepsy later in childhood, cognitive impairment, and behaviour problems (89). Language delay may be evident in up to 25% (90). PAIS in the MCA territory may lead to hemiplegia in up to 50% of cases. In cases where there is additional involvement of the basal ganglia and PLIC, the risk of developing contralateral hemiplegia is higher regardless of the extent of the infarct (91). Examples of perinatal stroke and its potential extent in preterm and term infants can be seen in figures 1.10-13.
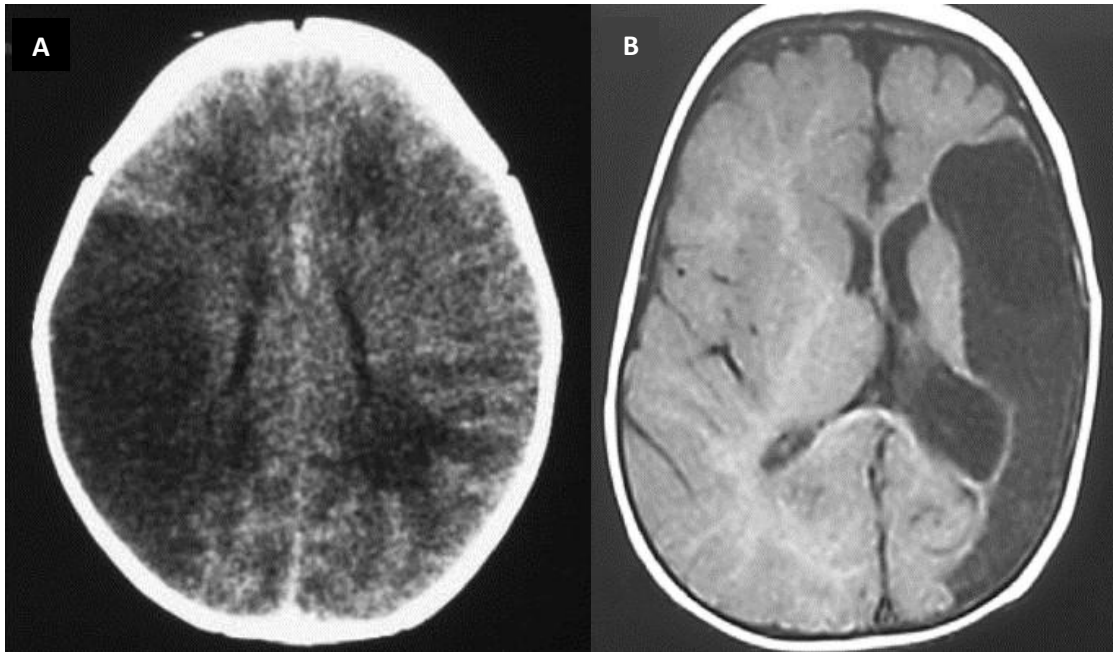
Figure 1.10: CT and MRI examples of perinatal stroke: (A) CT image of 1-day-old infant with right MCA stroke. (B) Axial T2 weighted MR image of 9-month-old child with evidence of perinatal stroke, which has led to skull asymmetry and large porencephalic cyst. Adapted from reference (92).
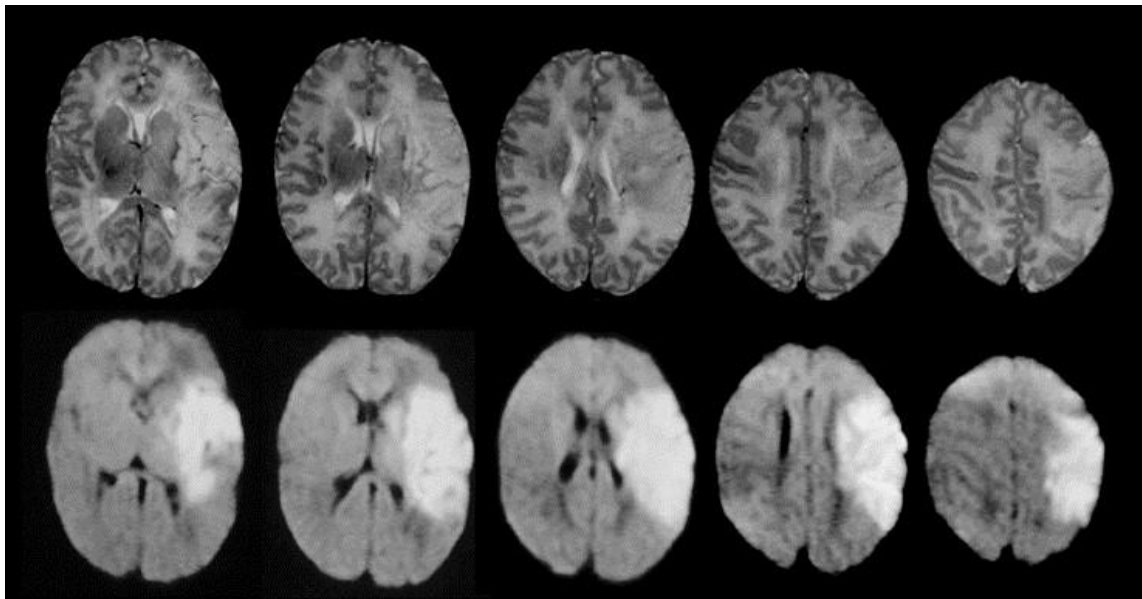
Figure 1.11: MRI of perinatal left MCA stroke: Axial T2 (top) and diffusion-weighted MRI (bottom) images of 5-day-old infant with left MCA stroke. Adapted from reference (92).
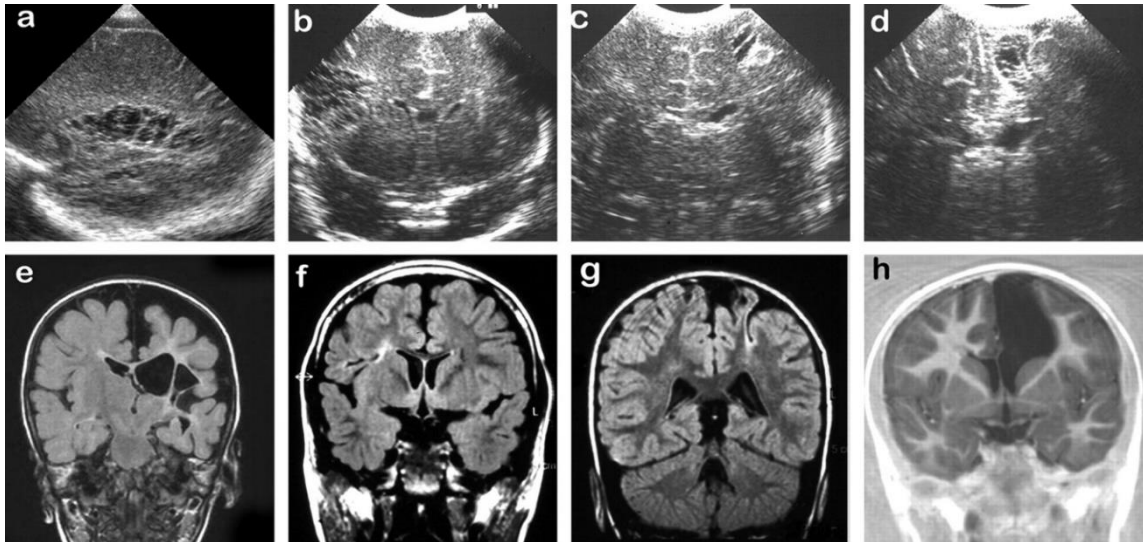
Figure 1.12: Ultrasound and MRI examples of stroke: (a) Parasagittal view on ultrasound, showing a large left MCA infarction in a 27-week infant with history of TTTS. (e) corresponding MRI, fluid-attenuated inversion recovery sequence of the same child at 18/12 showing gliosis and extensive cavitation adjacent to the left ventricle. (b) Coronal view on ultrasound, showing right anterior MCA infarction in a 29-week infant (f) corresponding MRI, at 8 years, showing gliosis adjacent to the right ventricle and cavitation. (c) Coronal view on ultrasound, showing a left-sided large MCA/ACA watershed infarction in a 30-week infant, (g) corresponding MRI, at 8 years, showing a gliotic cleft and atrophy of the area involved. (d) Coronal view on ultrasound, showing a left-sided ACA infarction in a 36-week infant, (h) corresponding MRI, at 7 years. (TTTS: twin to twin transfusion, ACA: anterior cerebral artery) Adapted from reference (72).
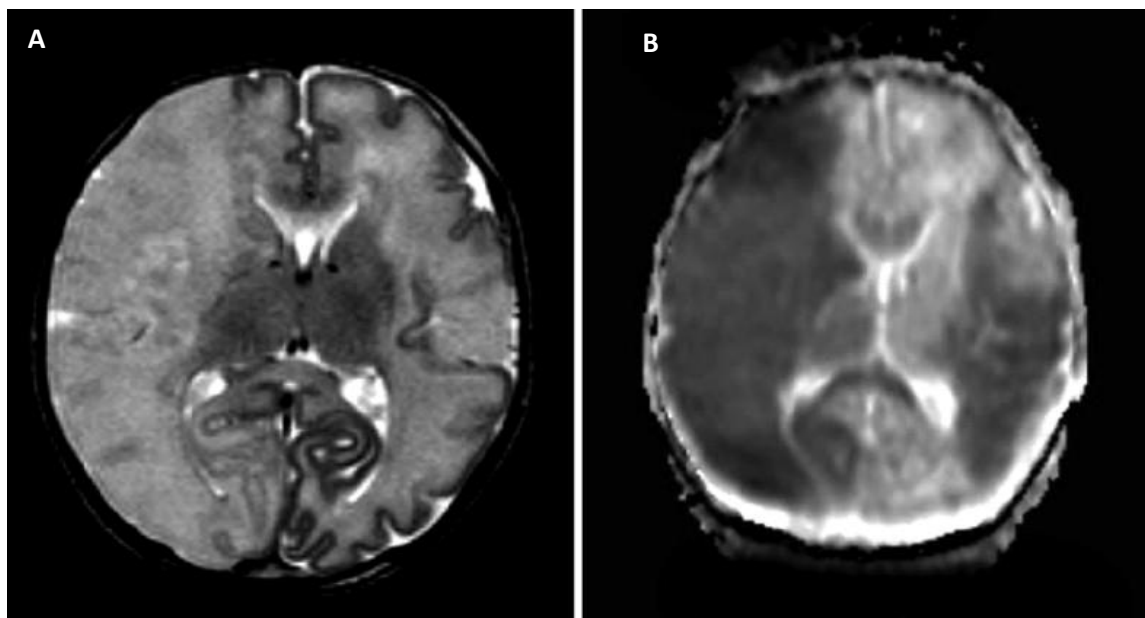
Figure 1.13: MRI example of perinatal stroke: (A) MRI, T2-weighted showing bilateral MCA infarct in an infant born at 34/40 weeks of gestation. (B) The corresponding diffusion weighted image. The MRI was performed on day 4 after birth. Adapted by reference (73).

Cerebral sinus venous thrombosis (CSVT) is another type of perinatal stroke, less prevalent compared to PAIS. It occurs in 2.6 in 100,000 live births (93), a rate most likely underestimated mostly due to under-diagnosis and lack of sophisticated neuroimaging techniques in many centres. The commonest sinus affected is the superior sagittal, often with involvement of the straight and transverse sinus (see Fig. 1.14). More than one sinus is commonly affected (94). The mechanism of injury is thought to be associated to venous occlusion and haemorrhagic infarction in the brain region drained by the sinus post CSVT. Venous engorgement, oedema, and increased capillary hydrostatic pressure lead to brain injury (95), which can vary from venous congestion to ischaemic infarction of the surrounding cortex, subcortical white matter and deep nuclear structures (see Figures 1.15, 1.16). The natural progression is haemorrhagic transformation of the infarcted brain tissue.

Cerebral sinus venous thrombosis has also been associated with secondary intraventricular, intraparenchymal haemorrhage as well as haemorrhage within the basal ganglia and thalamus due to distal draining veins. A multicentre, retrospective study in the Netherlands, has shown that amongst the 52 patients identified with CSVT, approximately 50% had thalamic haemorrhage, 50% had IVH and up to 80% had intraparenchymal haemorrhage (96).

Figure 1.14: The cerebral venous draining system. CSVT is usually located in the major dural sinuses; superior sagittal sinus, transverse, straight and sigmoid sinuses. Adapted from reference (97).
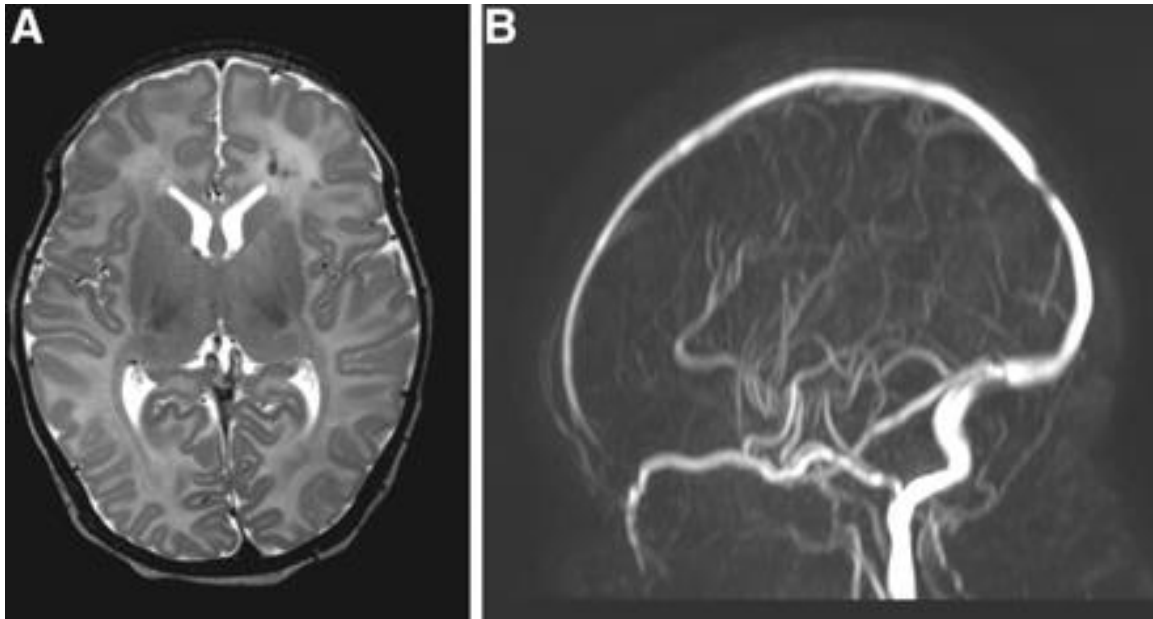
Figure 1.15: Examples of CSVT: (A) Axial T2-weighted MR image showing left-sided punctate white matter lesions. (B) Time-of-flight MR venogram image showing absent flow in the straight sinus. Adapted from reference (96)
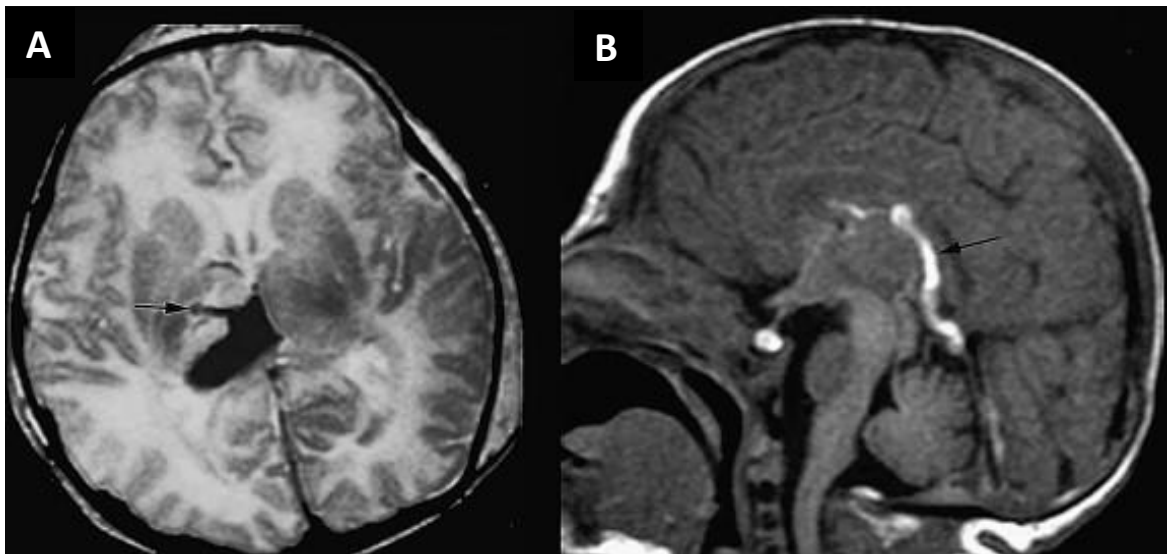
Figure 1.16: Further examples of CSVT: (A) Axial T2-weighted MR image showing right thalamic haemorrhage with a thrombosed vein (arrow) in thalamus. (B) Sagittal T1-weighted MR image showing high intensity signal in a thrombosed internal cerebral vein (arrow). Adapted from reference (93).

The risk factors predisposing to CSVT are like the ones of PAIS with polycythaemia and dehydration being the commonest clinical association. There also seems to be a consistent male predominance. It can present with seizures but sometimes the symptoms are subtle, such as hypotonia or apnoea. In the same study, as the one

mentioned above, the initial symptoms were seizures in almost 80% of the 52 cases reported (96). It may coexist with HIE, meningitis, or meconium aspiration syndrome.

The management in CSVT is once again supportive, maintaining good hydration, normocapnia and normoglycaemia with administration of anticonvulsants as required. Similarly, there is no evidence regarding the use of thrombolysis. The use of LMWH is variable and awaits formal evaluation.

Overall, PAIS is the commonest cause of unilateral spastic cerebral palsy (98), and up to 50% of cases with CSVT have been reported to possibly have some motor deficit from 20 to 80% (99, 100). PAIS is associated with minimal mortality rates with its occurrence being rare on the same patient or siblings. There is, however, a high chance of recurrence of seizures later in life up to 50% and especially in children who have developed unilateral spastic cerebral palsy (101). Seizures are usually easily controlled with standard antiepileptic agents. There are few cases where development of hypsarrhythmia is noted with later epilepsy and possible requirement for surgical resection of the epileptogenic brain region (101). Mortality rates are low in CSVT, up to 2-5% but higher than in cases of PAIS (99, 100). There are some studies that have reported higher mortality rates of CSVT in up to 19% and 25% possibly due to earlier diagnosis and different criteria for withdrawal of intensive care (96, 102). Up to 15-40% of infants with CSVT are reported to develop epilepsy in childhood (94, 99, 103). Infants with associated thalamic lesions are at higher risk of developing epilepsy which may be difficult to treat and is related to poor cognitive outcome (104). Mercuri et al., have described high association of PAIS (105). Berfelo et al., have described uncoordinated ocular movements in cases of CSVT (96).

The effect of PAIS on cognitive outcome is to yet to be determined, however, studies with serial follow ups have shown that cognition deteriorates with age and most likely due to the development of epilepsy (106-108). It also appears that learning difficulties and behavioural problems are more frequently seen in cases of PAIS who have developed unilateral spastic cerebral palsy (89). There is a wide range of occurrence of poor cognitive outcome associated to CSVT from 25% up to 73% amongst different studies (99, 109, 110).

1.4 Neuro-monitoring and Neuro-imaging tools

The above sections focused on the epidemiology, clinical course, management, and outcome of the two most frequent causes of encephalopathy and seizures in the term neonatal population. This section presents the mainstay of tools for neurological monitoring and neuroimaging in such cases. There are slight variations in practice amongst different hospitals across the United Kingdom, mainly due to different expertise in neuroradiology and access to advanced neuroimaging techniques. However, there is a general approach followed in most tertiary level neonatal intensive care units in monitoring and imaging infants with suspected HIE or perinatal stroke. In the following paragraphs, these different tools are described.

In Hypoxic Ischaemic Encephalopathy

In cases of HIE, the commonest neuromonitoring tool is a device best known as the cerebral function monitor (CFM). This is an aEEG device which provides cot side baseline monitoring of cerebral electrical activity. It is easily applicable, and both clinicians and nurses can be trained on its interpretation. It does show changes in the background electrical activity over time and following various clinical interventions. It can detect seizures but does have limitations; it is either a single or a two-channel system, thus limiting the detection of electro-cortical activity to specific scalp areas. Additionally, it does not detect low frequency activity, which is highly significant as some of the neonatal seizures can be of low frequency. Numerous studies especially from the Netherlands have shown that its correct use and knowledge of its limitations can be of immense value in clinical practice (111-115).

Continuous EEG monitoring with the option of an aEEG display is superior as it allows multichannel coverage of the brain electrical activity and thus increases the possibilities of capturing electro-cortical events of clinical interest. Few tertiary centres have access to the equipment, resources and clinical neurophysiology support required. Provision of expert neurophysiological interpretation on a 24-hour basis is costly and unsustainable as in most tertiary hospitals there is only one or two clinical neurophysiologists with expertise in paediatric and neonatal EEG. (For further details on EEG please refer to chapter 2).

In terms of neuroimaging, cranial ultrasonography (CrUS) is readily available and portable to the cot side. It is a convenient tool that allows visualisation of the neonatal

brain through the anterior fontanelle serially without having to move or disturb the infant. Depending on local practice, it is either performed by neonatologists or paediatric radiologists.

In HIE, the ultrasound findings in the first 48 hours tend to be nonspecific, as the biochemical and microvascular changes post the original hypoxic ischaemic insult are evolving (116). It is, however, useful in detecting structural abnormalities, possibly associated with metabolic or other conditions, calcifications, or cysts, suggestive of infection; atrophy, suggestive of a long-standing (intrapartum) insult or cerebral haemorrhage. Evidence of brain oedema in the context of HIE is a known association, however, it is not always apparent and the common comment on slit-like appearance of the lateral ventricles on coronal views can also be a normal appearance in healthy term infants. The presence of co-existing loss of differentiation between the different anatomical structures, and especially the presence of obscured Sylvian fissures and closure of the interhemispheric fissure, that reinforces the appearance of brain swelling. The BGT can appear bright in 24 to 48 hours post the initial hypoxic-ischaemic insult (see Fig. 1.17). The PLIC can also be visualised in the coronal ultrasound views, as a stripe of normal or even hypo-echogenic tissue between the thalami and the lentiform nuclei (of the basal ganglia), which may appear abnormally hyper-echogenic post a hypoxic ischaemic insult (117).

Ultrasound Doppler studies to assess cerebral perfusion may also inform the severity of the injury. In cases of perinatal asphyxia, low resistance index (RI) values (RI<0.55) in the anterior cerebral artery were shown to be associated with adverse neurodevelopmental outcome (118). The RI is the fraction of systolic (S) flow minus diastolic (D) flow over the systolic flow (S-D/S) within the ACA and is an indicator of cerebrovascular perfusion. It is thought that the decrease of the RI in ACA in HIE is secondary to increased diastolic flow caused by brain oedema, direct vessel injury and release of vasodilating factors in the ischaemic regions. This so called luxury perfusion has been associated with moderate to severe HIE with deep grey matter rather than cortical injury (118). However, it has been shown that although predictive in normothermia, it is significantly less predictive in hypothermia, and where infants with low RI measurement would have a poor outcome in normothermia, are more likely to

have a better outcome when cooled (119). The predictive value of RI regarding 18 months outcome during therapeutic hypothermia for HIE improves after 48 hours.
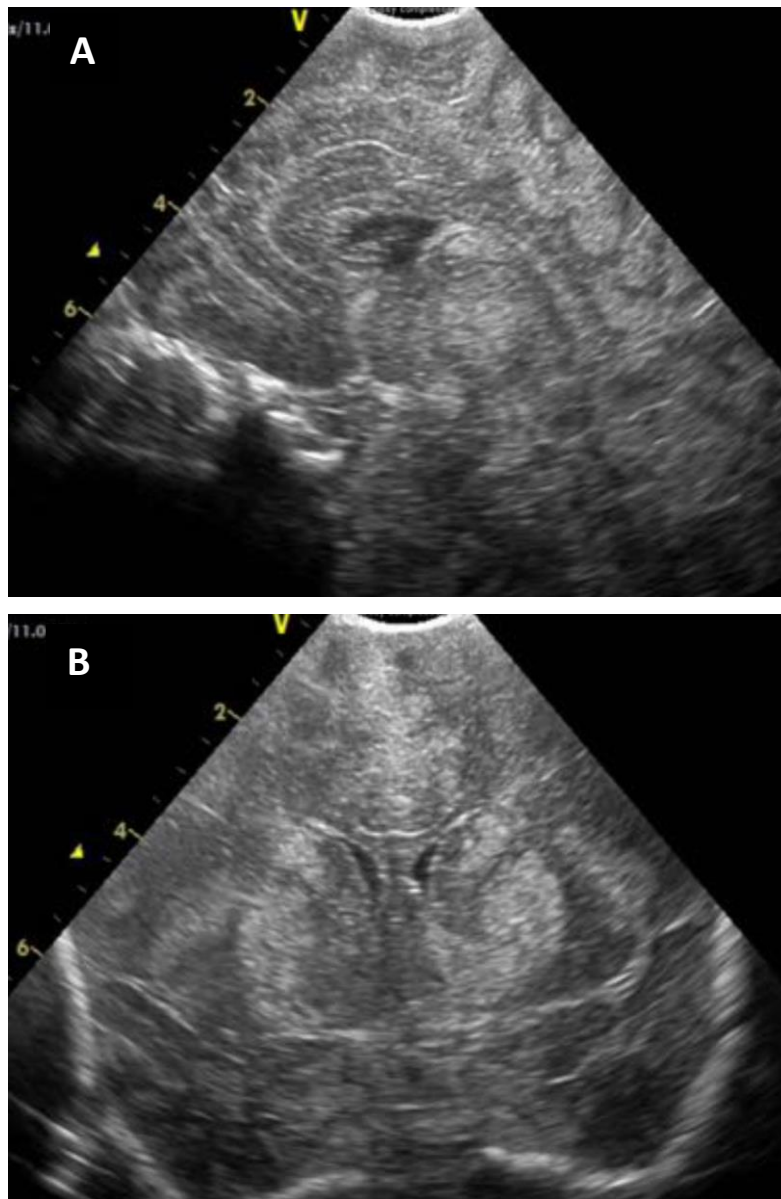
Figure 1.17: Coronal and sagittal ultrasound views in severe HIE. (A) Coronal ultrasound view of midline structures, where the corpus callosum and lateral ventricles are depicted. Note the abnormal bright appearance of the basal ganglia and thalami structures, suggesting severe hypoxic-ischaemic insult. (B) Sagittal midline view of the same case. Note the marked cortical highlighting and well defined echogenic structure of the brainstem again suggestive of severe HIE. Images from author's personal file.

Computed tomography (CT) is only used in acute situations and mainly to determine whether there is a space-occupying subdural haematoma or extradural trauma/haemorrhage (i.e. subgaleal haemorrhage), which may require neurosurgical intervention. The advantage of CT head is that is a much faster approach to obtain brain

images, the exposure of the infant to ionising radiation though must be considered. In this respect, CT should only be used in a potential neurosurgical emergency and if further neuroimaging is required MRI should be recommended.

The gold standard neuro-imaging tool for HIE is MRI (120). It allows early identification of brain injury secondary to hypoxic-ischaemic insult and assessment of treatment efficacy (121). The pattern of injury associated to the deeper grey matter structures (BGT-predominant injury) or the cortex (watershed-predominant injury) or severe global, may be more evident and specific after the first 4 to 7 days on standardised conventional MRI, but may be apparent on diffusion-weighted MR imaging (DWI) much earlier (122). Several studies have shown that MRI aids the prediction of outcome in HIE (123-126).

It is worth noting here that MRI is also the imaging technique of choice in diagnosing underlying causes of neonatal seizures (127). One study using clinical information in combination with CT or MRI identified the cause of neonatal seizures in almost 80% of a large cohort of infants (11). A more recent study showed an even higher rate, up to 95%, in identifying the aetiology of neonatal seizures and assisting the prediction of neurodevelopmental outcome by using MRI (128).

Studies on cerebral oxygen delivery and consumption have provided more information on the pathophysiology of brain injury in HIE and perinatal stroke. The use of oxygen-15 positron emission tomography (PET) and xenon-enhanced CT (Xe CT) in studies assessing brain haemodynamics are invasive and hence not applicable in the neonatal population. However, more specialised MRI techniques allow the investigation of different aspects of the brain metabolism; the phase contrast MR angiography (PC-MRA) and the arterial spin T_2-based measurements allow the estimation of oxygen saturation (SaO_2), with oxygen extraction fraction (OEF) and the cerebral metabolic rate of oxygen ($CMRO_2$), being indirectly calculated from the previously mentioned parameters (129).

Such techniques have been applied to demonstrate an increase in CBF with postconceptional age (130-132) and to study HIE and perinatal stroke (see Figures 1.18 and 1.19). For example, De Vis et al., showed significant correlation between increased perfusion in deep grey matter, as assessed by pulsed arterial spin labelling (PASL), in

infants with poor neurodevelopmental outcome at 9 and 18 months of age following HIE (133). Shi et al., showed association between higher signal intensity in deep grey matter structures in infants with HIE, thus indirectly implying association with hyper-perfusion in the areas of injury (134). However, a study evaluating brain perfusion in the second week following HIE, showed hyper-perfusion locally and globally but lower perfusion in the thalami, thus implying a regional low metabolic demand post irreversible injury (135). This supports a later study which evaluated the progression of brain perfusion in the first week following HIE, which identified low perfusion on day one followed by hyper-perfusion in affected regions (136).

Studies based on magnetic resonance spectroscopy (MRS) can also aid prognostication in cases of HIE (137, 138). Phosphorus MRS studies have shown the primary and secondary energy failure in hypoxia-ischaemia (as described in section 1.2 of chapter 1) (139, 140). Proton MRS based studies have shown that cerebral lactate increases in hypoxia-ischaemia, which resolves following effective resuscitation, only to be followed by a secondary rise 12 to 24 hours post primary insult (141-143) due to intrinsic production (144). Changes detected by MRS have been shown to provide earlier indication markers of disease severity in HIE than conventional MRI. Markers such as lactate to creatinine, lactate to N-acetyl-aspartate (NAA), lactate to choline peak-area ratios aid prognosis of disease severity and later neurodevelopmental outcome in brain injury accurately (140, 141, 145-147).
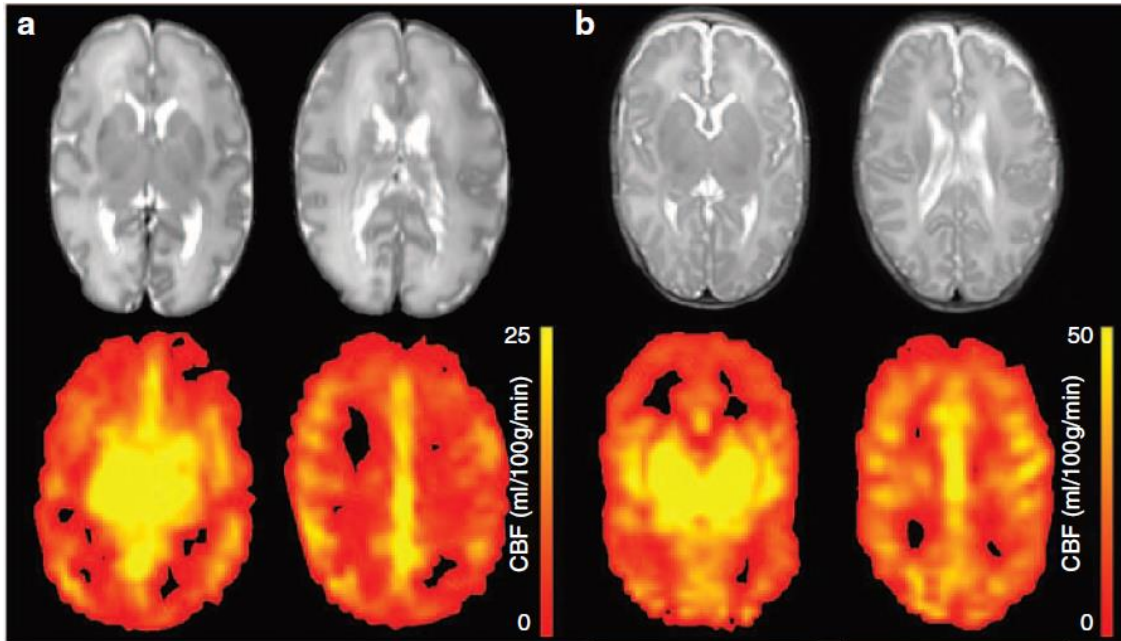
Figure 1.18: Brain maturation based on tissue perfusion of an infant born at 30 weeks of gestational age: (a) T2-weighted images and PASL images at 31 weeks of postconceptional age, (b) T2-weighted images and PASL images at 38 weeks of postconceptional age. Brain perfusion is expressed as cerebral blood flow (CBF) in ml/100grams/minute (PASL stands for pulsed arterial spin labelling). Image adapted from reference (129).
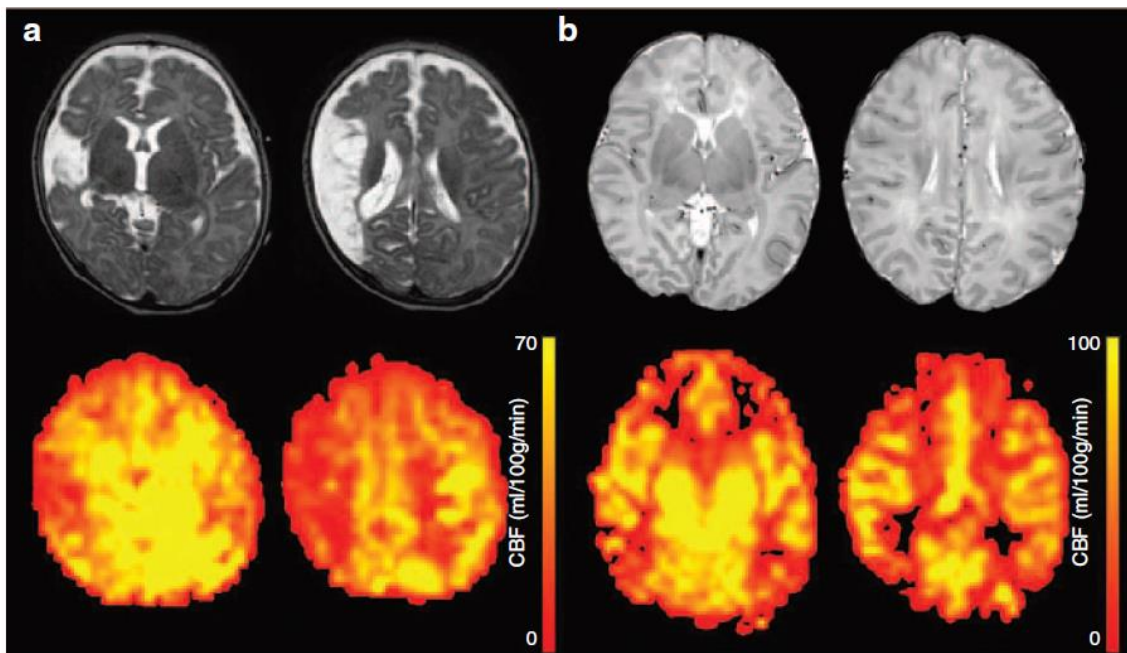
Figure 1.19: MRIs and PASL images of PAIS and HIE: (a) T2-weighted images and PASL images of an infant with PAIS in the right MCA. Note the loss of tissue in the T2 images and the associated lower perfusion seen in the PASL images. (b) T2-weighted images and PASL images of an infant with HIE. Note the global hypo-perfusion (see colour bar). Brain perfusion is expressed as CBF in ml/100grams/minute. (PASL: pulsed arterial spin labelling). Image adapted from reference (129).

In Perinatal Stroke

In cases of perinatal stroke, the current available diagnostic tools by the cot side on an NICU are CrUS, aEEG and EEG. Both CrUS and aEEG are readily available, while the access to multichannel EEG is more variable and dependent upon local practice and expertise.

Studies have shown that aEEG can significantly contribute to the diagnosis of perinatal stroke (148). It can, however, be less effective in detecting seizures and provides limited information regarding their origin, location, and nature. Early multichannel EEG has been shown to aid in the differential diagnosis of between seizures secondary to perinatal stroke and seizures secondary to HIE based on the background electrographic activity and the focal nature of seizures in stroke (149). Multichannel continuous EEG monitoring is a valuable tool in early diagnosis of perinatal stroke in terms of lateralisation of seizures and certain electroencephalographic features associated with stroke (150). Asymmetry or attenuation of the background activity tend to depend on the extent of the infarction (150).

Approximately 70-80% of perinatal stroke cases can be visualised with ultrasound performed by experienced professionals, except for small cortical infarcts in areas away from the transducer (i.e. posterior fossa lesions) (151-153) (see Fig. 1.20a). However, the lesion may take hours to days to organise in the hyperechoic appearance which can be characterised as stroke; therefore ultrasound is a less sensitive tool in detecting stroke early (154). Following the infarct there is reperfusion either through the affected or anastomotic arteries. The macrophages and glial cells that invade the affected region make the lesion hyperechoic and visible to scanning (81).

Ultrasound Doppler studies can also be utilised in the detection of perinatal stroke. This is infrequently used, and it is entirely dependent on expertise. The idea is that during reperfusion of the ischaemic region, high flow velocities may be recorded with low values of the RI on the affected area compared to the healthy side (155, 156).

The gold standard for detection of perinatal stroke is MRI (157) (see Figures 1.20a and 1.20b). Among specific MRI techniques, DWI may detect the infarct prior to standardised conventional T1 and T2 weighted MR images (158). From a pathophysiological aspect, immediately after the infarct, there is localised oedema which

increases the water content of the affected brain region. Any change in water content is detected by DWI; although this is not entirely specific and can also be secondary to encephalitis or venous ischaemia (81).

As with HIE, different MRI techniques such as PC-MRA and ASL have been used to assess perfusion in cases of perinatal arterial stroke. The findings appear to be variable between hyper- and hypo-perfusion between the infants studied depending upon time of study compared to time of injury and region of interest (159-161).
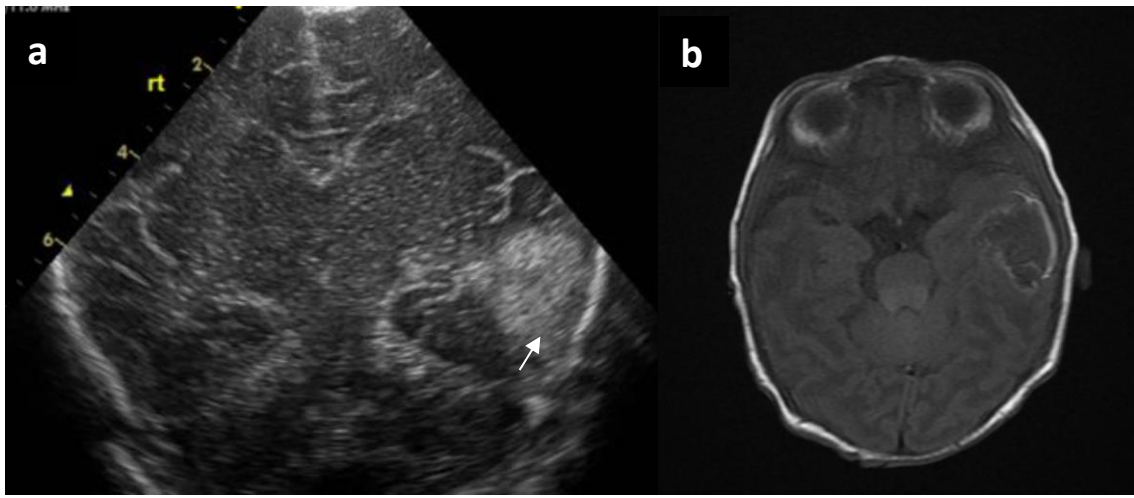
Figure 1.20: Example of perinatal stroke: (a) Coronal midline ultrasound view of perinatal stroke noticed on admission scan. Note the bright echogenic circular region on the left temporal region (white arrow) in proximity to the Sylvian fissure. (b) Axial T1 weighted image of the same case depicting the area of infarction in keeping with the ultrasound imaging findings. Images from author's personal file.

Alternative neuro-investigating tools

Magnetic resonance imaging (MRI) remains the gold standard in the diagnosis of both HIE (120) and perinatal stroke (157), and overall neonatal seizures (127). However, this is a non-portable, expensive technique requiring transport of infants away from the acute clinical area in most institutions and is rarely available out of hours.

In addition to this, there are very few institutions with expertise to apply more advanced MRI techniques, as the above mentioned and/or MRS. The proximity to the scanner, the long duration of the scan, and the requirement for transportation decrease the possibility of serial and follow up scans. This has an impact on serial scans of preterm infants where not only transport but also equipment to maintain homeostasis and temperature during the scan is challenging. There are neonatal incubators specifically designed and built for MRI scanners, but these are not available universally. Expertise in

neonatal neuroimaging is required for the interpretation of the acquired MR images. Although most tertiary hospitals have neuroradiology support on site there are few with specific neonatal neuroradiology experience support, and therefore, external advice is often sought.

There is an ongoing requirement for the development of cost-effective automated cot-side brain monitoring and imaging tools which will ultimately improve clinical care and facilitate application of precision medicine. Near infrared spectroscopy (NIRS) and different NIR modalities can provide this alternative option as they permit non-invasive and continuous monitoring of cerebral haemodynamics and oxygenation at the cot side, by measuring changes in the concentration of oxy- and deoxy-haemoglobin (162-164). NIRS can augment monitoring of physiological parameters to inform perfusion status in cases of neonatal brain injury and may be highly valuable in clinical conditions such as HIE, where there is constant dynamic changes of brain oxygenation and metabolism over the course of the illness.

Near-infrared techniques have been utilised in the study of infants with HIE and brain injury since the early eighties and in the next chapter a new approach of NIR methodology, diffuse optical tomography (DOT) combined with electroencephalography is presented. By combining DOT and EEG in monitoring and imaging infants with HIE or stroke, who originally presented with seizures, one may evaluate and begin to understand the constant dynamic changes in cerebral circulation. The aim of this study is to prove the feasibility of this imaging modality on a neonatal intensive care environment and to utilise this in the deeper understanding of the physiology of these morbidities from a combined neurophysiological and cerebrovascular perspective.

Chapter 2: Electroencephalogram and Diffuse Optical Tomography

2.1 Electroencephalogram

2.1.1 Origin of the EEG signal

The mystery of brain electrical activity has for long been the focus of investigation for the world of physiology and neuroscience. The foundation of EEG is attributed to an English physiologist Richard Caton in 1875. He was the first to record the electrical activity from dog and rabbit brains with a primitive device (165). There follows numerous studies and descriptions of brain electrical response to electrical stimuli and seizure like activity in the 1800s and early 1900s (166-168). However, the first to describe the human EEG was Hans Berger with his report of human EEG recordings dating back to 1929 (169). Since then, EEG has been widely used for the study of behaviour, wakefulness, and sleep states in research as well as for monitoring and detection of abnormal or epileptiform activity in clinical practice.

The EEG measures the difference in electrical potential in the scalp. The human cerebral cortex contains billions of pyramidal neurons (nerve cells), which are electrically charged, forming complex connections and networks. This continuous neural electrochemical signalling gives rise to electric fields, which is what is detected via EEG. This activity, however, has a long distance to travel through different structural layers of non-neuronal tissue, such as the meninges, cerebrospinal fluid, skull, and skin, to reach the EEG electrodes. Hence many activated and synchronised neurons are required for the EEG signal to be produced, transmitted, and measured. For instance, it has been described that in cases of epileptiform discharges, up to 6 cm^2 of neuron surface is required to exhibit synchronous neural activity in order for it to be detected by scalp EEG (170).

Each neuron consists of axons, dendrites, and cell bodies (soma), (see Fig. 2.1.1). The nerve cells respond to stimuli and transmit information down the axons. The dendrites are either connected to axons or dendrites of other cells and are the recipients or transmitters of impulses between nerve cells. Neural activities in the central nervous system (CNS) are based on the synaptic currents travelling along these connections between dendrites and axons, called synapses (see Fig.2.1.2).
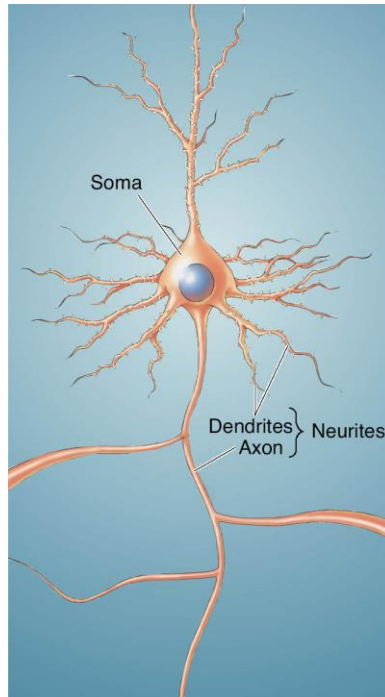
Figure 2.1.1: A neuron and its main parts. Adapted from reference (171).
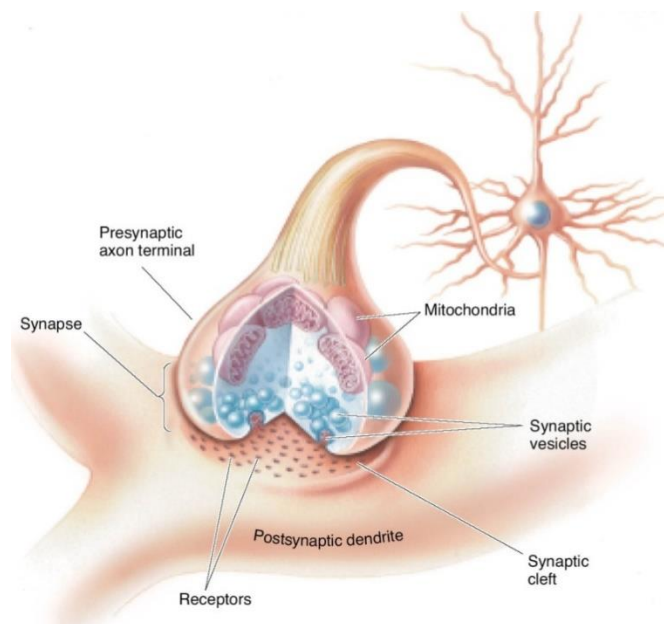
Figure 2.1.2: An electrical synapse and its components. Adapted from reference (171).

The nerve cell membrane is usually negatively polarised at 60-70 mV, which is termed the resting potential. This potential differs in accordance to changes in synaptic activity. If a neuron is stimulated above a certain threshold (see Fig. 2.1.3) the polarity of its membrane potential is briefly reversed, and this is called an action potential. If an action potential reaches an excitatory synapse, an excitatory postsynaptic potential

(EPSP) will occur and depolarise the following neuron. If an action potential reaches an inhibitory synapse, an inhibitory postsynaptic potential (IPSP) will occur and hyperpolarise the postsynaptic neuron accordingly. Essentially both EPSPs and IPSPs cause current to flow across the neurons but also amongst the neighbouring extracellular space.
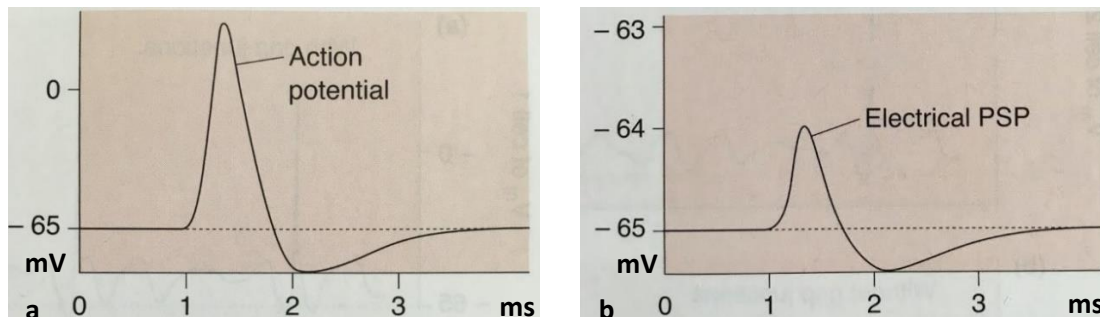
Figure 2.1.3: Action potential and electrical postsynaptic potential (PSP). The x axis in both graphs represents time in milliseconds (ms) and the y axis potential in millivolts (mV). The dotted line represents the negatively polarised threshold of the membrane (resting potential) beyond which the membrane of a neuron can be electrically stimulated (a) An action potential generated at one neuron causes an ionic current to flow into a second neuron (b) causing an electrical post synaptic current. Adapted from reference (171).

It is the synchronisation of these electric fields generated by post-synaptic potentials (EPSPs and IPSPs) in pyramidal neurons which is thought to produce most of the actual EEG signal (172, 173). The EEG measures the difference in electrical potential between different locations over the scalp. The action potentials travelling along the neurons are higher in amplitude than post-synaptic potentials. However, the latter are longer in duration and occupy a larger surface of the membrane. This allows both temporal and spatial accumulation. Action potentials occupy a very small surface and are up to 30 times shorter in duration than synaptic potentials, factors which prevent their synchronisation on a neuronal basis. Thus, the electric fields resulting from asynchronous action potentials are not significant at the scalp. The duration of potentials in relation to their synchronisation also explains the association of frequency and wave amplitude seen on EEG. High frequencies produce lower amplitude EEG waves with a typical such example being the alpha frequency (α) (8-13 Hz), mostly associated with awake state in adults. On the other hand, low frequencies produce higher amplitude signal, with such an example being the delta waves (δ) with frequencies from 0.5 to <4 Hz.

The pyramidal neuron resembles the behaviour of an electrical dipole (174), with either ends positively or negatively charged based on the type of input being applied. The

theory that best describes the conduction of the potential through the extra-cellular spaces and the association between the recordings and the distance from the source is one of volume conduction. The best mathematical approach to describing this is the solid angle theorem of volume conduction (173). The theorem provides a basic understanding of how the cortical pyramidal dipoles generate the waves seen on EEG, it states that the potential generated at an electrode (relative to a reference) will be proportional to the solid angle subtended by the poles of the dipole generator (173).

In terms of size, shape and duration of EEG potentials, there are certain factors which play a crucial role. These are: (1) the distance of the recoding electrode from the source of the potential, (2) the duration of post-synaptic potentials (PSPs), (3) the number of simultaneously activated PSPs and (4) the anatomical orientation of the pyramidal neurons generating the potential (173). The electrical field produced by the pyramidal neurons is termed an open field. The potential of an open field decreases inversely to the distance from each source. The architectural structure of neurons in other regions of the brain does not resemble the alignment of neuronal dipoles of the cortex. Therefore, the field potentials generated from the regions of the thalamus and the brain stem are called closed potentials and are not large enough to be detected on the scalp (173).

It is often presumed that if an electrode is placed deeper than the scalp, more information will be gained. As briefly mentioned above, the potentials in an open field decrease in amplitude with the square of the distance from the generator. Due to this, when an electrode is placed near to one source over the cortex, it will be less sensitive to more distant regions because of the size of the signal at that location. Whereas if the electrode is sampling from further away (the scalp) the signal strengths from the close and distant sources are both smaller, but closer to each other in amplitude and thus more likely to sample both. Therefore, deeper electrodes detect higher potentials from a small surface-source and scalp electrodes detect from a large surface-source at a greater distance (175).

The signal produced at an extracellular level has a certain distance to travel amongst different anatomical structures to be measured by scalp EEG. This distance (and the fact that these layers are semi-conductive) decreases the amplitude of the electric field and leads to loss of spatial information. Therefore, the EEG signal requires amplification

by a factor of approximately 10^6 for it to be effectively measured. This makes it vulnerable to noise interference and artefact.

2.1.2 EEG in clinical practice

To perform EEG, one requires the following: (i) electrodes to detect the electrical activity placed over the scalp, (ii) an amplifier that magnifies the signal (as mentioned in section 2.1.1, page 17), (iii) filters, (iv) a device to record the captured activity and (v) a video recorder to capture any simultaneous physical activity of the subject.

In clinical practice, the EEG electrodes used are constructed from highly conductive, non-reactive metal such as gold or silver chloride coated. They are usually cup shaped and attached to insulated wires (see Fig. 2.1.4), which can be connected into the amplifier, which is then connected to the EEG recording device (see Fig. 2.1.5). In parallel with the EEG electrodes, other electrodes are often used to monitor cardiac rhythm, respiratory rate, and eye movements. These parameters, in association with video monitoring, allow the informed interpretation of the EEG trace and the distinction of various behavioural states as well as the identification of normal or abnormal activity.

Fig. 2.1.4: A silver cup EEG electrode with a 10-mm diameter. Image adapted from www.cephalon.dk.

Figure 2.1.5: Example of a complete video-EEG system. Image adapted from ww.micromed.eu.

The arrangement of the electrodes over the scalp (array) is standardised according to the 10-20 international system of electrode placement (176). Each one of the electrodes is placed 10 or 20 per cent of the total nasion-inion (front–back) or right auricular to left auricular (right–left) distance of the skull, away from a neighbouring electrode (see Fig. 2.1.6). Each electrode is identifiable by one to two initials and a number which represent the location on the scalp and the hemisphere they are placed on, respectively; for instance, F stands for frontal, C for central, T for temporal, P for parietal, O for occipital. The electrodes over the right hemisphere are represented by even numbers and the ones over the left with odd numbers.
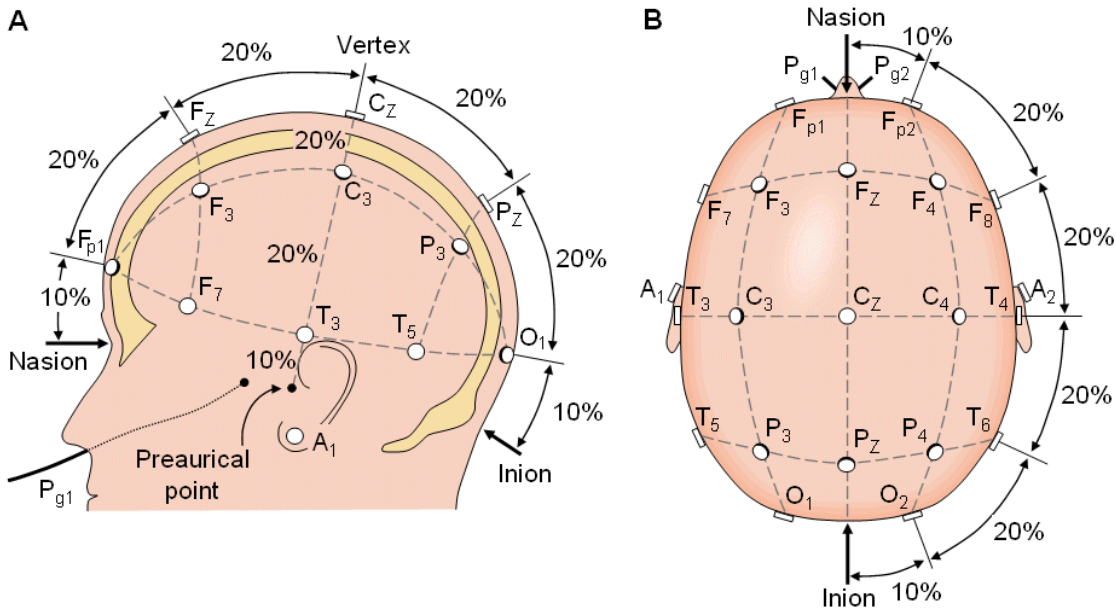
Figure 2.1.6: The standardised 10-20 system for scalp-EEG application. Each one of the electrodes is placed 10 or 20 per cent of the total nasion-inion (front–back) or right auricular to left auricular (right–left) distance of the skull, away from a neighbouring electrode (see Fig. 2.1.6). Each electrode has identifiable one to two initials and a number which represent the location on the scalp and the hemisphere they are on. Even numbers represent the right hemisphere and odd numbers the left one. Adapted from reference from www.BCI2000.org.

For infants, the standardised array of the EEG electrodes on the scalp follows a modification of the 10-20 system (177, 178), to accommodate for the infant's immature frontal lobes which do not extend as anteriorly to the skull as in older children and adults (179). The recommended and widely accepted number of EEG electrodes for sufficient representation of the whole scalp activity is 21. One may create as sparse or dense of an array required as per clinical or research purposes. The minimum recommended electrode number for infant EEG is 11 with locations situated at Fp_1, Fz, Fp_2, T_3, C_3, Cz, C_4, T_4, Pz, O_1, O_2 (see Fig. 2.1.7). A carefully conducted study comparing the full 10/20 array and a reduced (9-electrode) array showed that 90% of 187 seizures detected by the full montage were also identified by the reduced version (178).
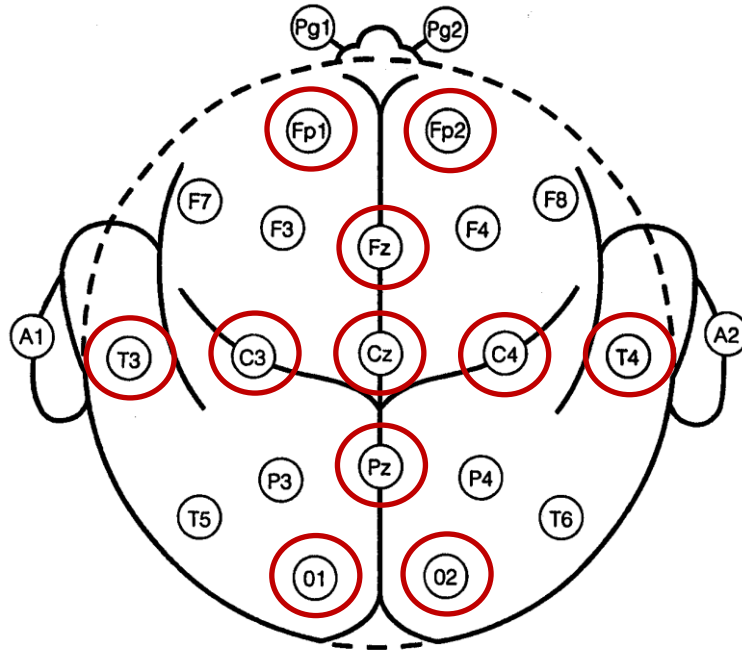
Figure 2.1.7: Example of the proposed reduced montage for neonatal EEG. Image from author's personal file.

In addition to the electrodes capturing the cortical electrical activity, the position of a reference electrode is important as all the variations in electrical potential difference are recorded relative to it. The reference electrode can be placed on the scalp or away from the scalp (i.e. shoulder, chest). If the reference is placed too close to a sensing electrode, the signal recorded across that channel will be reduced as the electrical potential difference between the two electrodes will tend to zero. However, if the reference is placed away from the scalp, more noise components will be introduced.

Another important factor during EEG recording is the impedance. This is the measure of the resistance of a circuit to an alternating current when a certain voltage is applied. The use of abrasive gel and conductive paste prior to the application of the sensing electrodes aids the reduction of the impedance. A good contact impedance is usually defined as one lower than 5 kΩ. However, it is possible to obtain a good signal-to-noise ratio with contact impedances higher than 5 kΩ and similarly to have a noisy EEG trace with good contact impedances. Electrical interference in the recording environment may affect the EEG signal, especially in an acute clinical environment with electrical infusion pumps or mechanical ventilators.

The amplification of the EEG signal is essential for the recording and visualisation of the EEG trace. The EEG amplifiers are multi-channel differential devices arranged in

such a way that the signal at each active electrode is amplified relative to the reference electrode. The sampling rate is usually between 250 and 2000 Hz. Certain filters can be applied across a range of ~0.01 to 100 Hz to minimise noise effects. Most EEG systems have a 50 Hz notch filter to eliminate interference at mains frequency.

The ways in which EEG electrodes are positioned and referenced is known as an EEG montage. Common forms include the referential and the bipolar montages. The referential montage measures EEG signals between each sensing scalp electrode and a single reference electrode, while the bipolar montage records the difference between neighbouring pairs of sensing scalp electrodes. The bipolar montages can be arranged in an orderly way in chains; front to back or side to side (see Fig. 2.1.8).
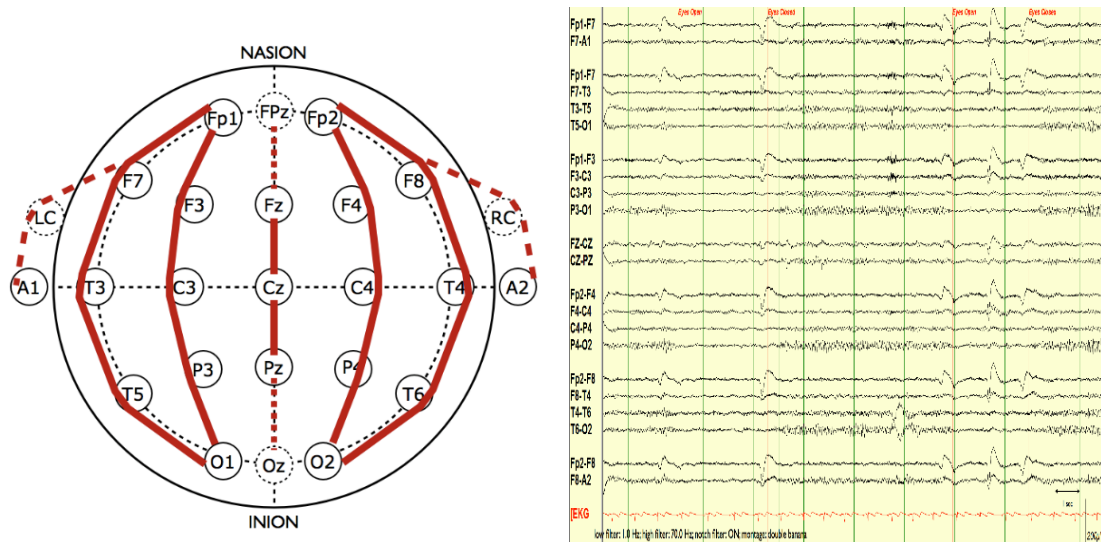
Figure 2.1.8: Example of a typical bipolar montage (double banana). Image adapted by www.eegatlas-online.com.

The EEG signal consists of a combination of transient waveforms and oscillatory features. The latter are categorised based on their frequency, measured as cycles per second (Hz) in four main frequency bands; delta, δ (<4 Hz), theta, θ (4-<8 Hz), alpha, α (8-13 Hz), and beta, β (>13 Hz). These rhythms are found in different ages and under different conditions. Most commonly there is a dominant frequency throughout the recording which is referred to background rhythm. In the awake state, the delta and theta activity are more characteristic of neonatal EEG, the theta more dominant in childhood and alpha in adulthood. Additionally, in adults, the predominant rhythm in REM sleep is theta activity, and delta activity in the non-REM sleep.

Neonatal EEG recordings can be challenging. The basic clinical EEG requires a minimum of 20 minutes recording. Longer sampling periods (of at least one hour long)

can be more informative, in capturing a wide variability of different states which differ with gestational age and postconceptional age (180). However, in the instance of abnormal or suspected seizure activity continuous recordings will aid and inform clinical management (181).

During recordings that take place in the clinical area, and particularly in a neonatal intensive care unit (NICU), there are certain precautions and considerations to be considered. The EEG device should be placed as close to the infant possible in a way that does not interfere with other devices and monitors (i.e. ventilators, intravenous pumps, other monitors). The electrodes should be placed onto the infant's scalp appropriately and not interfering with any clinical care that the infant may be receiving (e.g. hats used to apply continuous positive airway pressure-CPAP mode of ventilation). The infant should be positioned ideally supine with head, face, trunk and both upper and lower limbs visible. Depending on the clinical circumstances and management this might not be possible and EEG recording should continue and be optimised based on the clinical requirements and not vice versa.

Simultaneous video monitoring should be performed to capture any abnormal or seizure-like movement of the infant. The camera should be positioned in a way that captures the best possible view of the infant. It should capture any interventions (i.e. suctioning of the ventilated infant), but it should not video the personnel or conversations around the infant. Its purpose is exclusively to provide information for remote EEG interpretation. Most modern cameras will have a low light capability to record in ambient or dim light which is sometimes necessary in the NICU.

2.1.3 Amplitude integrated EEG in clinical practice

In a neonatal intensive care environment, amplitude integrated EEG (aEEG) is frequently used as a simplified continuous monitoring system of the electrical cortical activity. This method was developed by Maynard in the 1960s for adult intensive care units in response to a requirement for ongoing neuro-monitoring (182) and evolved further in association with Prior (183, 184). This method consists of a single or dual channel EEG recording which is filtered and time compressed (see Fig. 2.1.9) with the aim to monitor trends of the background electrocortical activity. The monitor is widely known in clinical practice as a 'cerebral function monitor' (CFM).

Figure 2.1.9: A comercially available single channel aEEG-CFM system. The electrodes are applied onto the infant's scalp and connected to the aEEG recording system via insulated wires. The aEEG monitor demonstrates the live continuous single channel EEG trace at the bottom of the screen and the amplified, time compressed aEEG signal at the top of the screen (adapted from the natus.com website).

The single or dual-channel aEEG signals are derived from electrodes placed on the centro-parietal and parietal regions of the scalp. The recommended positions of the electrodes for the single channel is the bi-parietal placement (P3 and P4, see Fig. 2.1.10a) and for the dual channel, C3, P3, C4, P4 (see Fig. 2.1.10b) with the neutral electrode placed along the midline and away from the open anterior fontanelle. The bi-parietal region is the least likely to be affected by scalp muscle activity and eye movements.
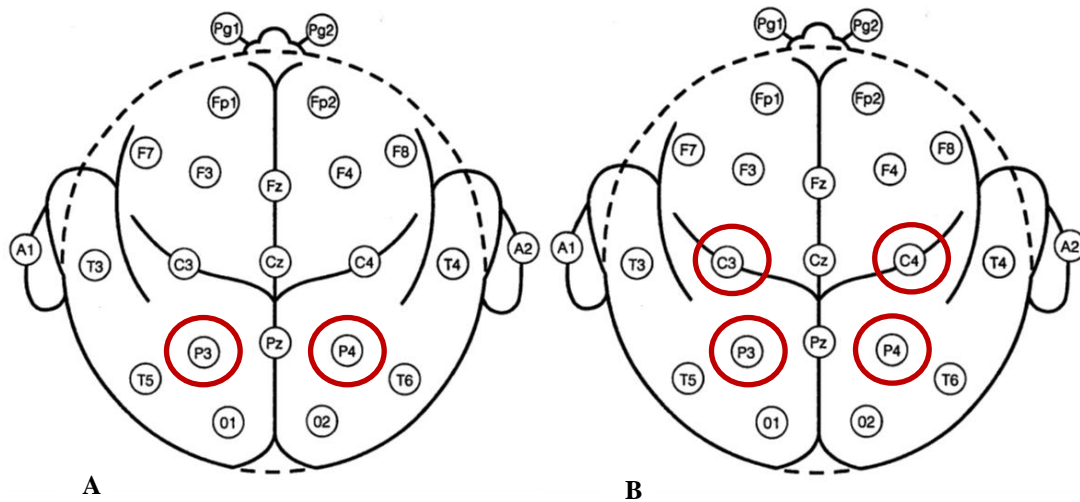
Figure 2.1.10: Single and double-channel aEEG electrode placement: A) biparietal placement of electrodes in a single aEEG recording. This region is least likely to be affected by sweat, scalp muscle or eye movements, B) Electrode placement in double channel aEEG recording. Similarly this part of the scalp is less likely to produce artefacts deriving from eye movements or muscle. A neutral electrode completes the application of the aEEG, which is placed in the midline anteriorly or posteriorly to the anterior fontanelle. Image adapted from personal file.

The aEEG monitor captures the background electro-cortical activity in real time for extended periods. The signal is amplified and passed through a pass band (with high pass band at 2 Hz and low pass band at 15 Hz). This essentially minimises interference from artefacts related to sweat, muscle activity, movements or surrounding electrically powered equipment. It also means that any normal EEG activity of slow frequency (<2 Hz) is attenuated and not detected by aEEG. The second important component of aEEG processing is amplitude compression in a semi logarithmic manner (0-100 µV) and time compression (6 cm of trace are equivalent to one-hour recording) (185). This means that normal, variable activity will result in a narrow high amplitude signal (>10 µV), whereas minimal activity (i.e. discontinuous trace, low amplitude activity) will result in a broad signal of low amplitude.

The interpretation of the signal is simple and does not require expert neurophysiology support. Any member of the attending team including; physicians, nurse practitioners and nurses can be trained in applying the aEEG leads and interpreting the signal accordingly to clinical practice and management. There are different aEEG signal classifications with main components being the morphology of the background activity, cycling between sleep and awake state and the amplitudes of the upper and lower margins of the trace (185-187). Any sudden brief or prolonged elevation above the bandwidth

should raise clinical suspicion. This should be inspected carefully in association with the underlying live single or dual channel EEG recording, the overall clinical context and nursing observations as to whether it is related to artefact or seizure activity.

Overall aEEG is a useful monitoring tool in the NICU. However, low frequency activity may not be captured. Similarly, low frequency or short-lived seizure activity may not be detected. The restriction to single or dual channel offers very limited scalp coverage, which risks not detecting frontal or occipital abnormal activity. The differentiation between seizures and artefacts may also be difficult to decipher and requires careful overall monitoring of the infant and information input related to drug administration or other medical intervention. In any instance of uncertainty or possible seizure activity, the investigations should be completed by performing a formal EEG, which remains the gold standard for monitoring of the electrocortical activity.

2.1.4 Principles of neonatal EEG

The human EEG goes through certain developmental trajectories, the features, and characteristics of which are best seen throughout the neonatal period. This makes interpretation of neonatal EEG dependent on the gestational age (GA) but also post-conceptional age. Features which may be classified as pathological in older infants or children may classify as normal, age appropriate EEG features in the preterm and term infants.

This section attempts to explain some of these features as it is essential for the understanding of the description and interpretation of pathological traces and EEG states in the neonatal period. The main EEG aspects covered below, as described by numerous studies (188-192), are the following: (i) states of sleep and wakefulness, (ii) background activity, (iii) synchrony, (iv) EEG provoked reactivity, and (v) other special EEG features.

The evaluation of different behavioural states is a multifactorial process and various physiological and EEG components should be taken into consideration (193). In the normal term neonate, based on observation (i.e. open eyes, spontaneous movements), physiological parameters (eye movements, heart rate, respiratory rate) and EEG features, the following behavioural states can be identified: (i) wakefulness where the infant appears awake, vigorous with eyes open (active wakefulness, AW) or quiet without agitation (quiet wakefulness, QW), (ii) active sleep (AS), where the infant appears asleep with the presence of rapid eye movements (REM-also known as REM sleep) (iii) quiet sleep (QS) or non-REM sleep, where the infant appears asleep with the absence of REM (188, 194). A period between two discrete sleep states where the infant appears asleep, but the rest of the expected parameters are equivocal, is referred to as transitional sleep state. If this period is not between two distinct sleep states it is simply termed as indeterminate (195, 196) (see Fig. 2.1.11). The emergence of discrete sleep states occurs as early as 26-27 weeks of gestation. However, at this stage the EEG may still appear inconsistent with the infants' behavioural state. It becomes clearer at gestations 28-29 weeks where one may see distinct AS and QS with the presence of REM (190).
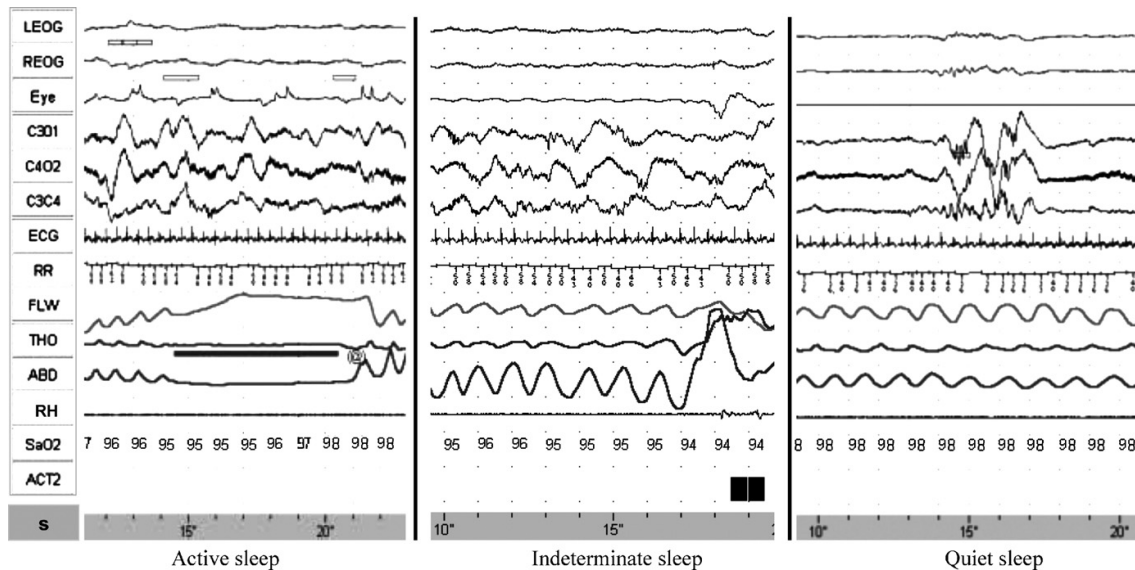
Figure 2.1.11: Example of polysomnographic digitized recording in a 34/40 weeks healthy premature baby. (LEOG: left electro-oculogram; REOG: right electro-oculogram; Eye: eye movements recorded using a piezo transducer; C3O1, C4O2 and C3C4: EEG recordings; ECG: electrocardiogram; RR: respiratory rate interval measurement; FLW: naso-buccal airflow (thermistor); THO and ABD: thoracic and abdominal respiratory movements (strain gauges); RH and ACT2: right hand (piezo transducer) and left leg (actimetry) movements; SaO2: oxygen saturation; s: seconds). Image adapted from reference (190).

The background activity of the typical preterm neonatal EEG is characterised by discontinuity, and is known as discontinuous trace or tracé discontinu (TD) (197). In this state, the EEG consists of epochs of activity (short bursts of slow and fast rhythm) followed by epochs of inactivity (inter-burst intervals, IBIs). The amplitude of the signal during the inactive periods is <25 µV, where the trace appears as almost or on occasions completely flat (see Fig. 2.1.12). The duration of the inter-burst intervals classified as normal varies with gestational age from 46-60 seconds for extremely premature infants born at 24 weeks (198, 199), to 6-10 seconds for term infants (198, 200) (see Figures 2.1.13 & 14).

As the infant matures the IBIs shorten and the trace becomes more continuous (191, 200, 201). Specifically, at the gestation of 30 weeks the background EEG activity becomes continuous only during AS and progressively by 34 weeks this is also maintained during wakefulness. At this stage the continuous trace is characterised by the term activité moyenne (192). This is a poly-frequency state of low amplitude with mixed frequencies. Continuity is gradually established during QS by 36-37 weeks. However, at the same time a characteristic trace appears during quiet sleep of semi-periodic features of voltage attenuation (< 50 µV) up to 15 seconds, termed trace alternant (TA) (202). This

has been observed to emerge as early as 34 weeks of GA (198) and may persist up until 45-46 weeks of CA.
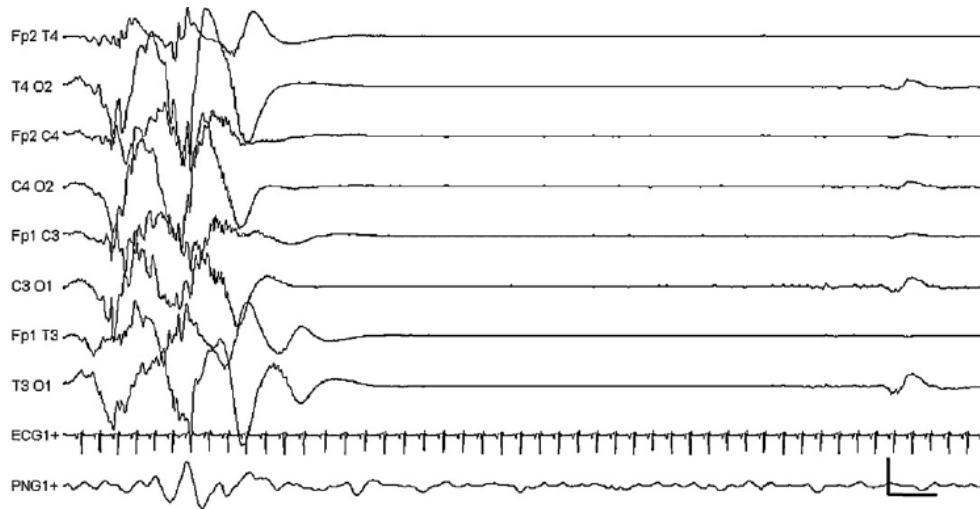
Figure 2.1.12: EEG of a 24/40 weeks infant. Discontinuous trace with no variability between sleep and awake state. Prominent burst like activity of slow δ frequency with intermixed higher frequencies (SATs). Adapted from reference (190).
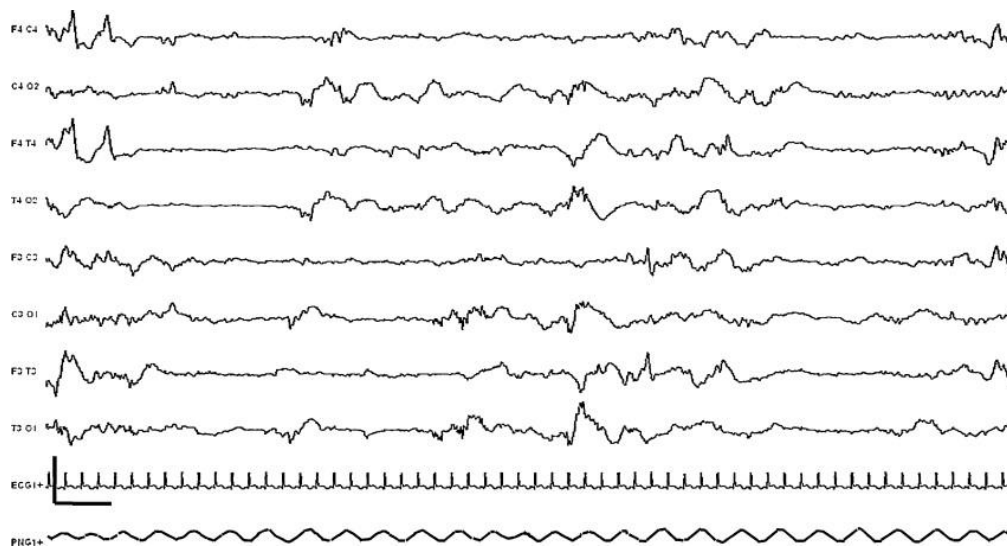
Figure 2.1.13: EEG of a 39/40 weeks infant. Quiet sleep with tracé alternant and slightly discontinuous background. Adapted from reference (190).
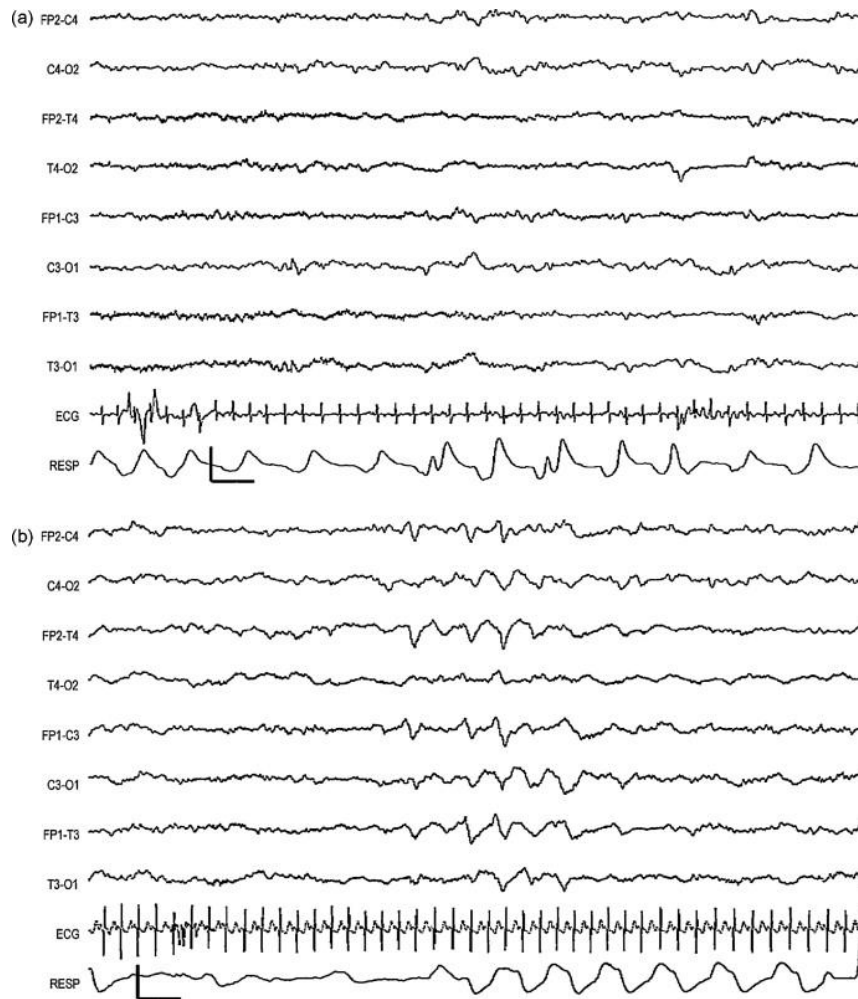
Figure 2.1.14: EEG of a 40/40 weeks infant: a) Quiet wakefulness. Polyfrequency activity (activite moyennne). b) Active sleep. Continuous activity with mixed frequencies. Low amplitude. Bilateral anterior dysrhytmia (normal developmental EEG feature). Adapted from reference (190).

The extremely preterm infant EEG appears, paradoxically hypersynchronous with an observed absolute synchronisation of the bursts and IBIs. At the stage of 27-28 weeks of GA the EEG becomes asynchronous with the general rule of thumb that the greater the distance of the activity from the midline the greater the asynchrony between the two hemispheres (179). The maturity of the synchrony of the two hemispheres, likewise continuity of the background activity, first emerges in active sleep and then progresses in all states coming up to term CA.

Another feature of the EEG examined during neurophysiological studies is the provoked EEG activity, otherwise known as the EEG reactivity to stimulation. Although one may observe some reactivity as early as 26-27 weeks (190) this is not always in

accordance with behavioural states and is quite inconsistent. It emerges more clearly at 33-34 weeks of GA with consistency between clinical and neurophysiological state.

The overall pattern of infant EEG is undergoing constant temporal and spatial reorganisation as functional connectivity between the two hemispheres is evolving. It changes from discontinuous to continuous and from asynchronous to synchronous. As the different behavioural states are established, more mature waveforms and frequencies replace the primitive features (see Fig. 2.1.15). The most important factor in EEG interpretation is the knowledge of the infant's GA and/or postconceptional age.
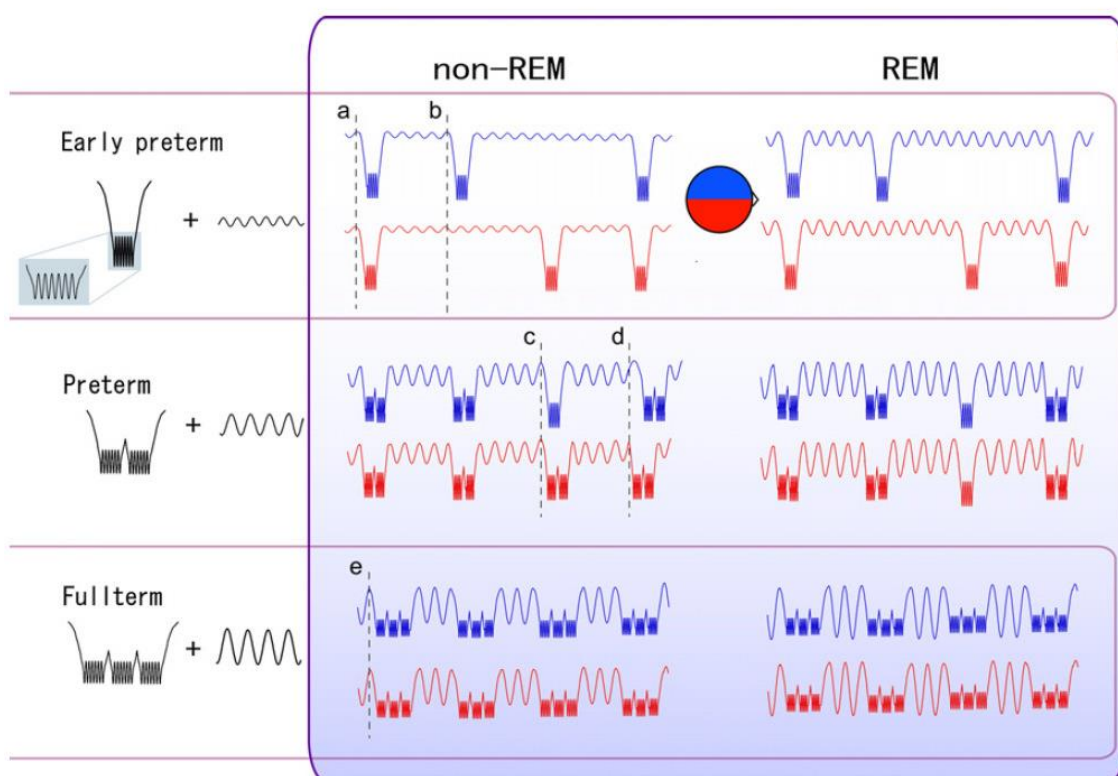
Figure 2.1.15: A simplified schematic representation for neonatal EEG intrepretation. This framework demonstrates how two prinicpal components of neonatal EEG; background cortical activity and SATs evolve in association with REM and non-REM sleep sates, from preterm to term GA. Adapted from reference (203).

2.1.5 Frequent EEG Artefacts

In an intensive care environment, electrical interference from surrounding devices is very common. However, some of the most frequent artefacts seen in an EEG recording usually derive from the infant themselves.

One of the most common EEG artefacts is the electrode-pop artefact (see Fig. 2.1.16). This is a result from a sudden decrease in electrode contact (increase in impedance). It appears as a sharp feature, isolated to one electrode, which in a bipolar montage will lead to a mirror image across two or more channels. The recognition of this artefact is significant as it might be mistaken as a spike or epileptic-form activity.
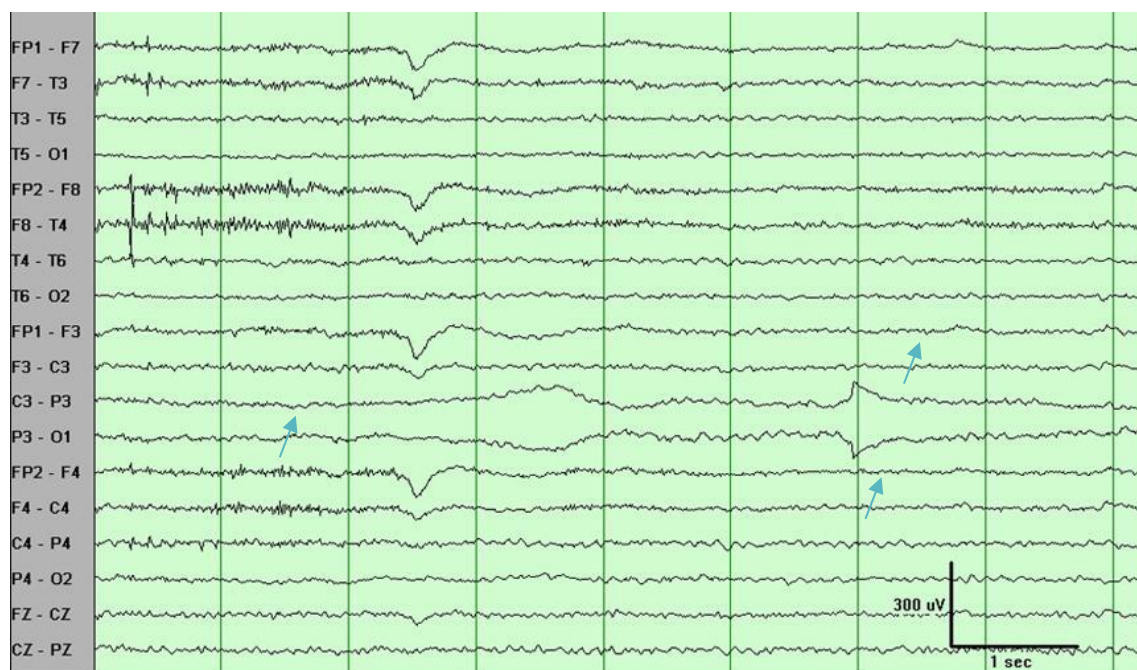
Figure 2.1.16: Example of the electrode-pop artefact related to the P3 electrode. Note that in the beginning of the trace over the fronto-temporal region there is also EMG artefact. (adapted by emedicine.medscape.com).

Another frequently seen artefact is the one arising from muscle activity also known as the electro-myogram (EMG) artefact (see Fig. 2.1.17). Muscle contraction produces high frequency (20-100 Hz) and high amplitude (up to 100 µV) potentials which appear as sudden onset of activity with no equivalent to any meaningful cortical waveform. This can typically derive from muscle contraction from and around the head with frontalis and temporalis muscles being the principal contributors.
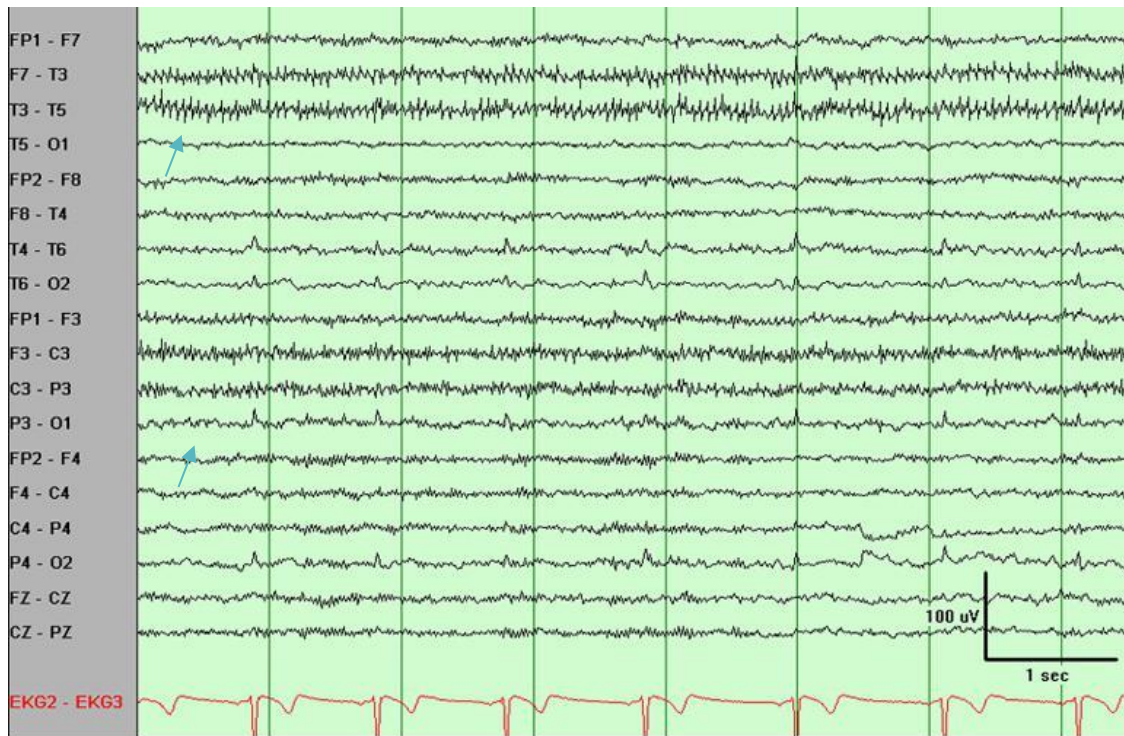
Figure 2.1.17: Example of an electromyogram (muscle) artefact mostly pronounced over the left temporal region. ECG artefact also is present, best observed in the posterior region (adapted by emedicine.medscape.com).

The electro-cardiographic (ECG-cardiac) artefact is also invariably seen in EEG recordings (see Fig. 2.1.17). The heart beat produces a high amplitude electrophysiological signal, which can appear in the EEG recording. The key feature is that its frequency is identical to that of the patient's heart rate. A single channel ECG alongside the EEG recording facilitates the identification and rejection of the ECG artefact.

The eye movement artefact (see Fig. 2.1.18) occurs because the eyeball acts as an electrical dipole with the retina negatively charged and the cornea positively charged. This electrical potential can infiltrate the EEG recording. Lateral, vertical, and blinking eye movements can be identified based on the polarity and symmetry of the changes in electrical potential difference as detected by the frontal EEG electrodes. They are rarely apparent posterior to the mid-temporal region. This artefact is quite common in EEG recordings but can be difficult to identify in the absence of recorded eye movements. In this respect an electro-oculogram (EOG, where additional electrodes are placed in the outer canthus of the eyes) can facilitate the identification of eye movement artefact (204), as well as REM sleep state.
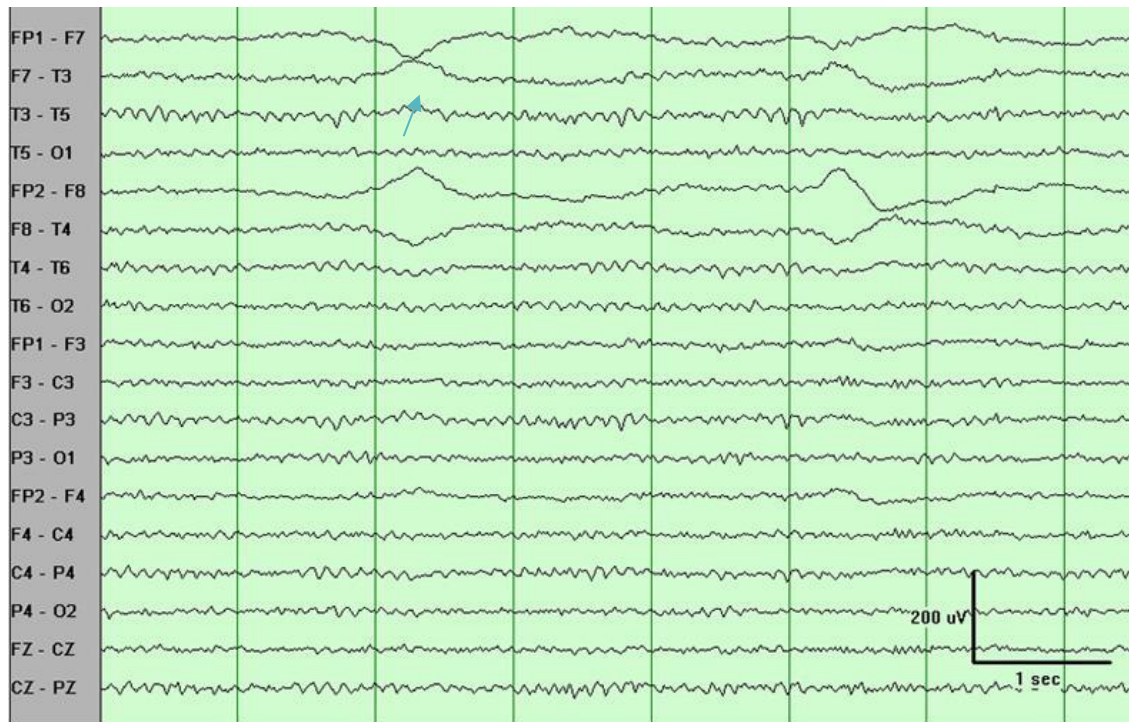
Figure 2.1.18: Example of an eye movement artefact mainly observed in frontal electrodes and not further posteriorly than the mid-temporal region (adapted by emedicine.medscape.com).

Normal respiration can produce two types of artefacts; slow, rhythmic waves in synchrony with body movements during respiration, which typically affects the impedance of one electrode or slow or sharp waves in synchrony either with inspiration or expiration, which affect the electrodes upon which the infant is lying. Many commercially available devices couple the respiration monitoring with ECG and EEG. This is performed with a band over the infant's abdomen and a sensor detecting the movements in inspiration and expiration.

Other significant artefacts include those due to movement of the mouth and tongue, and artefacts due to equipment such as intravenous pumps, mechanical ventilators.

2.1.6 Abnormal EEG features and rhythms

The interpretation of EEG requires the expertise of a clinical neurophysiologist. Pattern recognition and detection of abnormalities in a neonatal EEG can only be achieved with good understanding of the developmental features in different GA and postconceptional age, which have been described previously. For monitoring and prognostic purposes, the first EEG in at risk infants should be performed within the first 24 hours of life or after a significant event such as a brain insult (179). Similar electroencephalographic abnormalities are seen in both preterm and term neonatal EEG. In this section, the main aim is to briefly describe some of these patterns but not to exhaust the wide range of variations seen in neonatal EEG.

One of the things that one may comment on whilst reviewing an infant's EEG is the maturity of the trace compared to the infant's GA and postconceptional age. However, in cases where the EEG does not contain the expected developmental features for the equivalent GA or postconceptional age, the EEG is characterised as dyschronous. If the features are absent in all states then there is external dyschronism, whereas if appropriate features are seen in the awake state but not in the quiet sleep state, that is termed internal dyschronism.

Some maturational abnormalities observed may be transient, especially in clinical situations such as HIE. At a later stage, as the infant is recovering from the initial hypoxic-ischaemic insult, the observed EEG activity may normalise completely. It is therefore always important to repeat an EEG study in the recovery or even healthy state as it may appear that these abnormalities are no longer present. Similarly, an EEG feature which may be affected by a cerebral insult but may also reflect the use of sedative medications (205) is the prolongation of IBIs. In the acute phase of HIE faster frequencies in the electrocortical activity tend to be depressed or absent. It is as if the cortex regresses to a more primitive low energy activity, the trace becomes less variable or more discontinuous.

Another finding of abnormal cortical function is the recurrence of either generalised or localised amplitude attenuation. Along the same lines, depression, or lack of differentiation in the cortical activity may be a sign of cortical dysfunction in cases such as HIE, where there is partial or complete absence of the normally expected poly-frequency activity (206). Therapeutic hypothermia (TH) applied to infants with HIE may

also have an added effect on the EEG activity. As the infant recovers and TH is gradually discontinued these features may persist or may be replaced by the emergence of continuous trace, poly-frequencies, and multifocal sharp waves or even seizures (207, 208). However, if the EEG remains undifferentiated and depressed in the recovery phase, this is a sign of poor prognosis.

Burst suppression (BS) is a pathological EEG trace that may be seen in the neonatal period. This electroencephalographic pattern is defined as a constant alternation between high-voltage slow, occasionally sharp waves (bursts) and depressed or suppressed low-voltage activity (IBIs) (209) (see Fig.2.1.19). This abnormal EEG pattern is described in more detail in section 2.1.8.
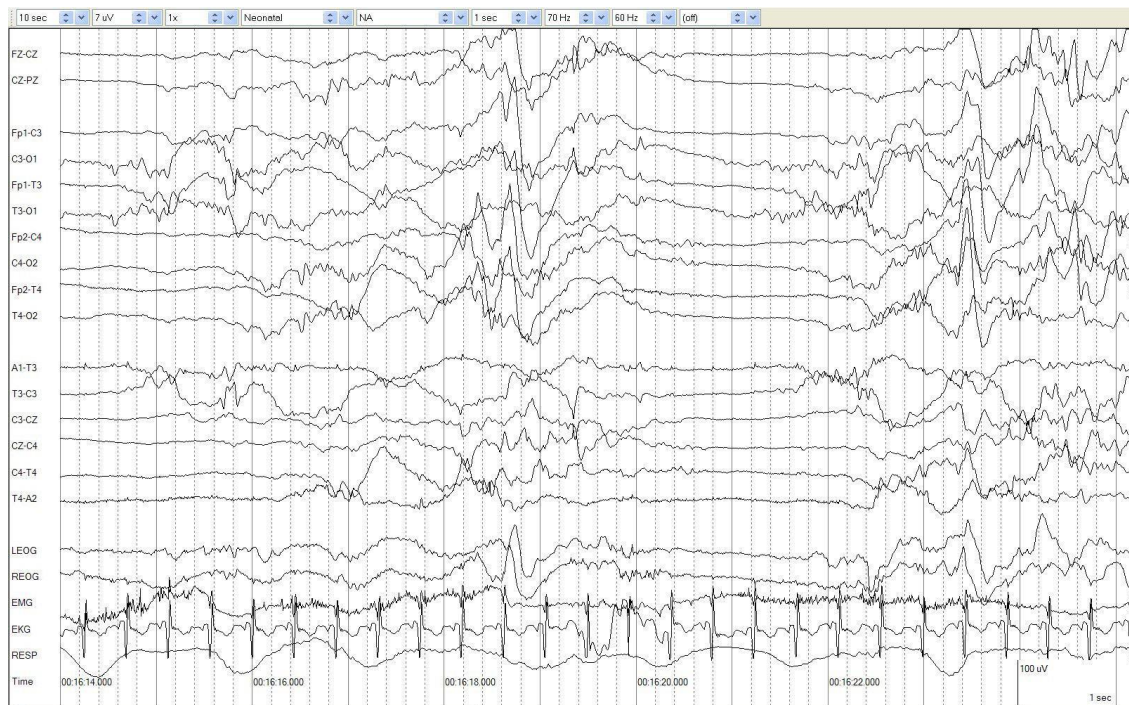
Figure 2.1.19: Burst-suppressed pattern of a 42/40 weeks post-term infant with HIE. Image adapted from www.emedicine.medscape.com.

A more severe form of cerebral dysfunction is electrocortical silence (see Fig.2.1.20). It is important to note that an isoelectric EEG trace represents absence of activity over the cortex but does not exclude activity in deeper brain structures such as the brainstem, which may sustain vital functions for prolonged periods in the absence of higher cerebral function.

There are certain generalised EEG patterns typical of certain syndromes or clinical entities. Gibbs and Gibbs described the pattern of hypsarrhythmia, which is closely

associated to the condition of infantile spasms and is characterised by high amplitude and irregular waves and spikes in a background of chaotic and disorganized activity (210) (see figure 2.1.21). Another example is that of holoprosencephaly, a congenital developmental defect, where the EEG appearance consists of multiple features occurring randomly with abrupt changes from one pattern to another, and consist of multifocal spike and polyspike activity, monorrhytmic activity, asynchrony, iso-electric or low frequency activity, and overall lack of normal organisation (179, 211).
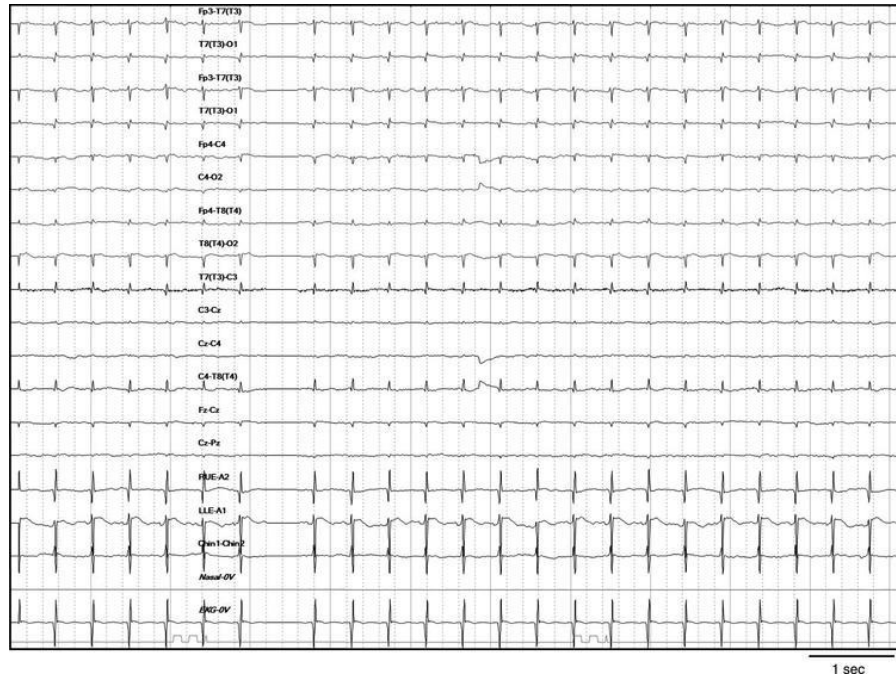
Figure 2.1.20: EEG showing electrocortical silence. Note the presence of regular electrocardiographic cardiac rhythm. Image adapted from reference (212).

In other cases of abnormal EEG patterns there can be focal or generalised features. For instance, there can be sustained rhythmic alpha and theta activity, or sustained rhythmic delta activity especially in the bifrontal regions, which are all considered pathological. Other focal abnormalities consist of periodic complexes, which are closely associated with neonatal herpes simplex encephalopathy (213, 214). The presence of central positive sharp waves in an infant's EEG recording has also been associated with neonatal brain injury. These are not epileptiform discharges, but their natural progress and physiological process is not well understood. The rate of their occurrence (more than 2 per second) has been proven to be associated with poor outcome (215, 216). Central positive sharp waves have been linked to severe intraventricular haemorrhage, periventricular leukomalacia, haemorrhagic parenchymal infarct and periventricular

echodensities, and are considered more specific to white matter necrotic lesions than to intraventricular haemorrhage (217). Temporal sharp waves may also be noted in an infant's EEG, and it is often difficult to differentiate whether they are normal or abnormal. Overall, random sharp waves with infrequent recurrence (less than 2-3 per hour), with negative polarity of their initial component and arising from any location of the scalp without specific focality are considered normal with unclear clinical significance.

Focal slow activity that is persistent over a certain brain region is suggestive of a focal lesion such as infarction, haemorrhage, or even specific congenital anomalies. Similarly, unilateral attenuation of the background activity can be associated with focal intraparenchymal lesions such as cerebral infarction. A certain degree of asymmetry of the background activity between the two hemispheres is expected in the neonatal EEG, particularly during non-REM sleep.
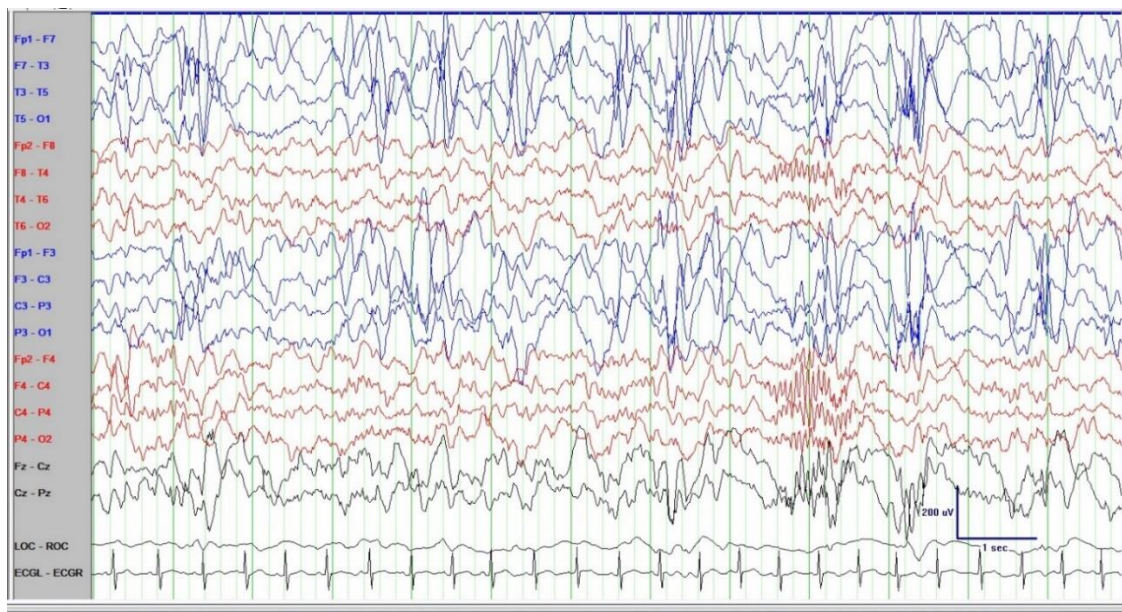
Figure 2.1.21: Hypsarrhythmic EEG pattern. Note the characteristic high-voltage, disorganized, chaotic, and asynchronous slow waves with superimposed multifocal spikes or sharp waves. Periods of generalized electro- decrement are seen throughout the recording and may be associated with clinical spasms. The above pattern is often more pronounced during non-REM sleep with the background activity during wakefulness even being normal. Image adapted from www.acns.com.

2.1.7. Neonatal Seizures

Seizures occur secondary to an excessive synchronous depolarisation of neurons within the central nervous system (218-220). Clinically, a seizure is defined as a sudden, stereotypical and repetitive episode of abnormal electro-cortical activity with a peak-to-peak amplitude of at least 2 µV, a minimum duration of 10 seconds, and dynamic evolution over time with clear beginning, middle, and end (221).

A series of studies have explored the potential pathophysiological trajectories behind the genesis of neonatal seizures. It is fair to say though that neonatal seizures are still not clearly well understood. As described and summarised by Volpe, neonatal seizures can be secondary to: i) disruption in energy production, affecting the energy based Na^+-K^+-pump, ii) excess of excitatory versus inhibitory neurotransmitters, iii) deficiency of inhibitory versus excitatory neurotransmitters; the latter two both resulting in excessive rate of depolarisation, and deficiency of calcium and/or magnesium which play a significant role in the balance of the neuronal membrane permeability to Na^+ (222).

Neonatal seizures are a separate clinical entity compared to those of older children and adults and may also vary when comparing preterm with term infants. This is primarily due to a series of neuroanatomical and neurophysiological maturing processes of the developing brain. From an anatomical perspective, the main developmental features are the migration, orientation, and alignment of cortical neurons, the development of axonal and dendritic ramifications and creation of synapses. From a neurophysiological perspective, the most crucial role is played by the neurotransmitters: gamma-aminobutyric acid (GABA) and glutamate in terms of their levels, activation or inactivation (223).

Neonatal seizures, more recently reported as occurring in 0.5 to 3 infants per 1,000 live births, with their incidence increasing in preterm infants (4). This might appear as a relatively rare occurrence, but when centres deal with up to 6,000 births a year and regions up to 80,000 births a year, it translates to a relatively frequent clinical problem. Additionally, most of the epidemiological studies include only clinical seizures with the incidence of purely electroencephalographical seizures not yet known. The requirement for early identification, diagnosis and effective treatment lies in the significant association of neonatal seizures with disability in life. In up to 50% of cases, there will be some form

of neurological sequelae, such as epilepsy, cerebral palsy, and/or intellectual disability (224, 225).

Variations in reported incidence of neonatal seizures can be explained by different diagnostic definitions and methods used. Most neonatal seizures occur on the first day, and 70% of all cases eventually recognised have been diagnosed by the fourth day. Humans are more likely to present with a seizure in the neonatal period than any other point in their lifetime. Subtleties, such as equivocal clinical manifestation, electroclinical dissociation with ongoing epileptiform electrical activity without any clinical association, and the lack of equipment and trained staff for 24-hour service in EEG readings, make the diagnosis of seizures challenging. In a recent study in which members of a clinical team were shown 20 video recordings of infants with seizure or seizure-like activity, only 50% were correctly identified, with poor inter-observer agreement and no difference between medical and non-medical staff in the interpretation of the videos (226).

Seizures are clinically subdivided into clonic, tonic and myoclonic. They can also be focal or generalised. Generalised tonic-clonic seizures are rare in the neonatal period. They can be very difficult to differentiate from spontaneous normal movements, with variable EEG correlation and associated autonomic phenomena (226). An additional type of neonatal seizures, where the described paroxysmal movements and changes in the behaviour of the infant are neither of the above, nor normal (see Table 2.1). These are termed as subtle seizures, and are associated with a variety of abnormal movements, such as eye flickering, staring, chewing, lip smacking, cycling movements of the lower extremities with autonomic phenomena (most usually referring to increase of systemic blood pressure) (227). Their correlation to electroencephalographic activity is variable (227). They are more frequent in premature infants (228), but can also be noted in term infants with variable EEG correlation (229).

Clonic seizures are most frequently associated with time-synchronised EEG seizure activity (229, 230). They are rhythmic and rather slow compared to other seizure types. They can be focal, multifocal, or generalised. Focal clonic seizures are most frequently associated with cerebral infarction but can also occur in the background of metabolic encephalopathies. Tonic and myoclonic seizures are less likely associated with time-synchronised abnormal electrical activity (229). Tonic seizures are usually focal or generalised and involve sustained posturing of limbs or trunk and neck. Horizontal

deviation of the eyes has been described as a type of focal tonic seizure (229). Myoclonic seizures are differentiated from the rest and especially clonic seizures by the fact that they are more rapid and preferably involve flexor muscle groups. They can be focal, multifocal, or generalised. Knowledge of the different types of seizures is crucial in determining underlying pathologies and strategic approach in their management.

TYPE	**CLINICAL MANIFESTATION**	**FREQUENCY AND EEG CORRELATE**
Subtle	Eye flickering, eye deviation, stare, blinking. Apnoea. Cycling, boxing, stepping, swimming movements of the limbs. Mouthing, chewing, lip smacking, smiling.	~50% of neonatal seizures; EEG correlation is variable; EEG changes occur most likely with ocular movements.
Tonic	Stiffening, decerebrate posturing	~5% of neonatal seizures; EEG correlation is variable.
Clonic	Repetitive jerking, distinct from jitteriness. May be uni- or multifocal.	25-30% of neonatal seizures; EEG correlation highly likely especially if focal.
Myoclonic	Myoclonic jerks; sleep myoclonus can be benign.	15-20% of neonatal seizures. EEG normal if focal or if sleep myoclonus.

Table 2.1: Types of neonatal seizures. Table adapted from reference (231).

Neonatal seizures tend to occur during active sleep, if sleep-wake cycle is preserved (232). The average seizure duration is from 1 to 5 minutes (221, 233, 234). However, more recent studies with the added benefit of continuous EEG monitoring have shown a high incidence of seizure activity lasting up to 30-40 minutes (235-237). For seizures to be considered as distinct phenomena there needs to be at least a 10 second inter-ictal interval between one seizure to the next (238).

Neonatal seizures have been categorised as local, lateral, diffuse or unifocal, multifocal, and bilaterally independent (239). This categorisation is done based on the location, the focal point of seizure onset and the region involved during the maximal spread of the seizure activity as observed on EEG recordings. Most commonly neonatal seizures are initially focal and then spread to become generalised. It is very rare that they are originally diffuse or generalised (240). What is of great interest is that the focus of seizure activity can shift from one hemisphere to the other, known as the flip-flop phenomenon (241). Identifying the focal onset of seizures is of utmost importance in

aiding clinical diagnosis as focal seizures can be associated with focal injury, while generalised events are more often associated with widespread injury, such as infection (242). However, it is important to note that in the neonatal period, generalised injury can also present as focal seizures (243).

Diagnosis of neonatal seizures is further complicated by the fact that infants may present with stereotypical, rhythmic movements with no EEG correlate. It is unclear as to whether these events arise from subcortical structures (i.e., brainstem, hippocampus) impossible to capture with conventional EEG and as to whether one should treat with anticonvulsant medications (5). On the other hand, what is frequently seen especially in immature infants or infants who have already received anticonvulsant treatment, is the presence of electrographic seizures in the absence of clinical seizure activity. This is widely known as electroclinical dissociation, a phenomenon well described in the literature (10, 244-246). One hypothesis supports that the electro-clinical dissociation could be due to the excitatory as opposed to inhibitory role of the GABA neurotransmitter in the neonatal period. This is mediated by the efflux of chloride ions (Cl^-) (secondary to expression of two membrane co-transporters of Cl^- at the perinatal period), which eventually depolarises the neuronal membrane causing excitation (247-249). Frequently used anticonvulsant agents such as benzodiazepines and phenobarbital act as GABA agonists which may be an explanation for the fact that despite cessation of the clinically observed seizure there is ongoing electrographic seizure activity.

Another challenge in managing neonatal seizures is the clinical significance of electrical seizures with no clinical manifestation, termed subclinical seizures. Previous studies assessing continuous video-EEG monitoring amongst children admitted in intensive care units have identified subclinical seizures in up to 46% and status epilepticus in as many as 23% (250-252). Similar results have been shown in studies of critically ill neonates with subclinical seizures (18, 210). Most of these seizures would go undetected without the presence of continuous video-EEG recordings. Their effect on ongoing brain injury has long been debatable (252), with increasing evidence to support an association between subclinical seizures and poor neurodevelopmental outcome (19, 253).

The question that naturally arises is why is it important to monitor these events if we do not yet fully comprehend their clinical relevance? Furthermore, should we only treat clinically obvious seizures and not EEG-only seizures? Such questions have

tormented clinical neurophysiologists and neonatologists for years and clear answers are yet to be established. However, continuous EEG monitoring increasingly reveals that exclusive clinical judgement on seizure detection is a poor and incomplete approach which can lead to over or underestimation of the seizure incidence, morphology, and evolution.

There are extensive animal-based research studies showing the direct effect of seizures on brain injury. Recurrent seizures in infants may affect their ventilation and lead to periods of prolonged hypoxia and hypercapnia that precipitate brain injury, especially in an already insulted cerebral region. However, there are clinical ways to support and improve ventilation and oxygenation. Studies in paralysed adult animals showed that the recurrence of seizures results in a point where the increase in energy supply can no longer maintain the decrease in energy reserves. It was shown that failure in energy supply leads to further prolongation of the seizures with irreparable injury to the brain tissue (254-256). Other studies have shown that severe seizures result in excessive secretion of excitatory amino acids, such as glutamate; a principal excitatory neurotransmitter in the central nervous system. This appears to occur preferentially in areas involving the hippocampus and limbic structures leading to neurotransmitter mediated post-synaptic damage and eventually neuronal death (254-258). Although, most studies suggest that the neonatal brain is more resilient to seizure mediated neuronal necrosis than that of the adults (259), it is worthwhile noting that critically-ill infants will most likely present with EEG-only seizures rather than clinical seizures (243, 260). Therefore, close, continuous monitoring and a careful clinical approach is required for the neonatal groups most at risk of seizures and brain injury. Examples of neonatal seizure patterns may be seen in the following figures (2.1.22-24).

Timebase = 30 mm/s; sensitivity = 10 μV/mm; high cut = 70 Hz and low cut = 1 Hz
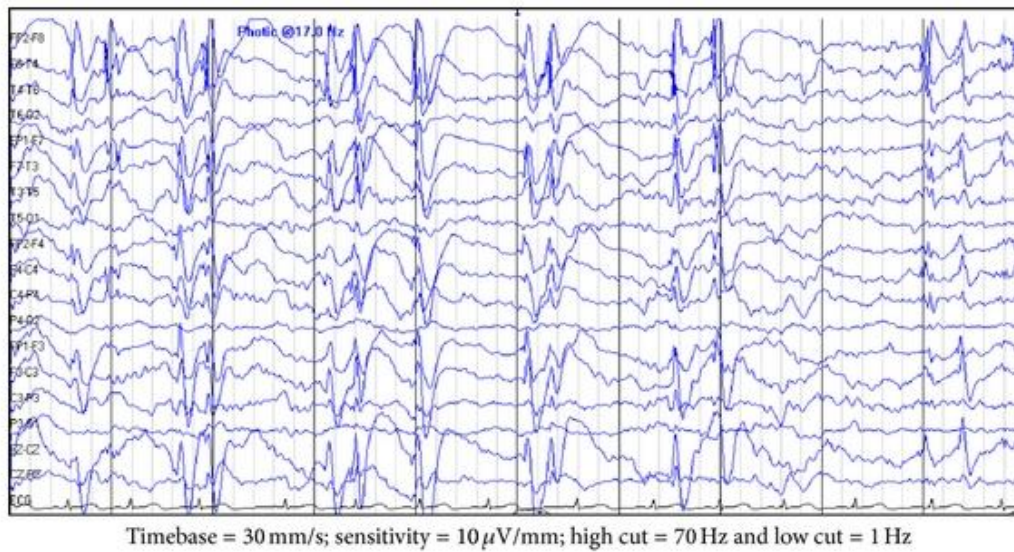
Figure 2.1.22: EEG trace in epileptic encephalopathy with continuous spike-and-wave appearance during sleep. Adapted from reference (261).
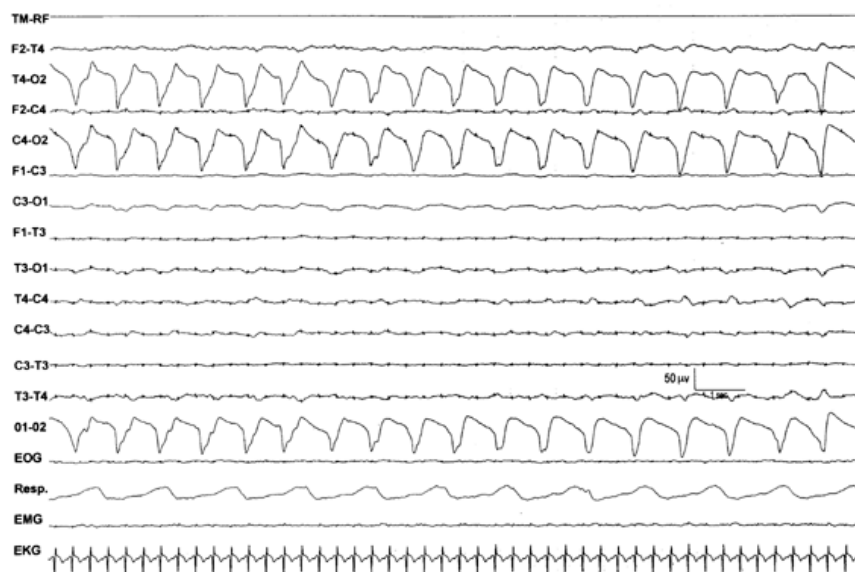
Figure 2.1.23: Example of rhythmic right delta occipital epileptiform discharge at a suppressed electrical background. This trace was not associated with any clinical seizures. Image adapted from reference (262).
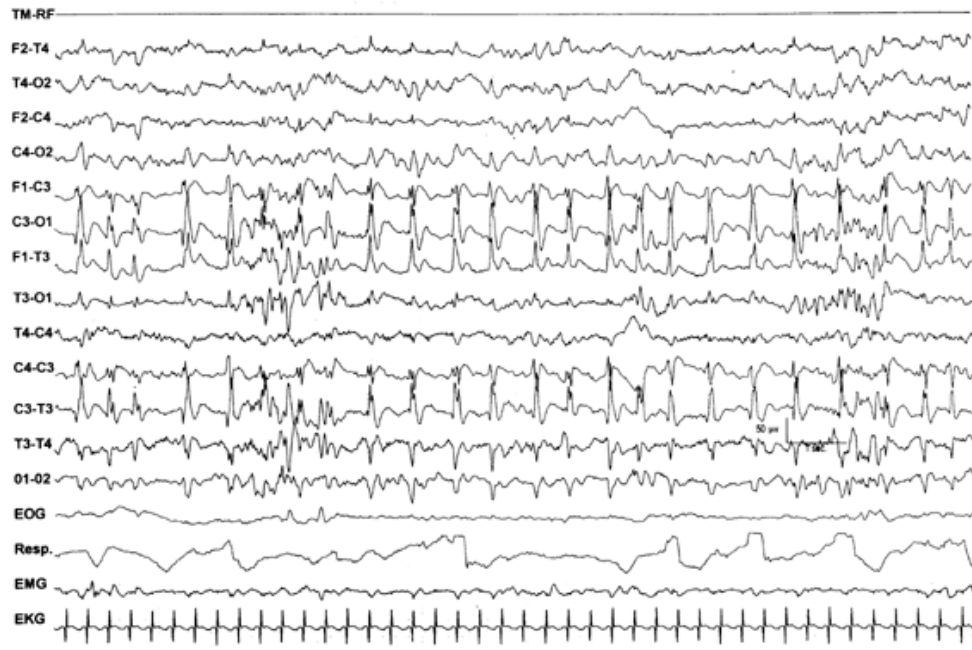
Figure 2.1.24: Example of rhythmic sharp wave activity over the left hemisphere. This was clinically associated with clonic jerking of the right arm and of the leg. Adapted from reference (262).

2.1.8 Burst Suppression

Burst suppression (BS) is a pathological EEG trace defined as the periodic alternation between high amplitude waves (bursts, 150 -350 µV) and depressed or suppressed cortical activity (inter-burst intervals, IBIs, <25 µV). It is considered as a state of profound brain inactivation (263) (for example see Fig. 2.1.19). It is an indication of global brain dysfunction and inactivation. Many studies have shown an association between the recovery rate from a burst-suppressed to a continuous EEG trace and long-term prognosis, and outcome post HIE in the neonatal period (113, 264). The presence and persistence of such electrocortical activity (or inactivity) is therefore associated with poor prognosis and adverse neurodevelopmental outcome (111, 265, 266).

In stricter neurophysiological terms, though, the IBI activity seen on a BS pattern is minimal to non-existent with amplitudes of less than 5 µV. When the IBI amplitude ranges above that threshold but remains less than 25 µV it is referred to as a discontinuous trace. There are other sources, that have used different upper thresholds of IBI amplitude to define BS, including 10 µV (267), 20 µV (180) or 25 µV (268). The BS pattern in the neonatal EEG is associated with poor outcome. However, this serious abnormal pattern constitutes only a small proportion of discontinuous neonatal EEGs (264).

The term discontinuous EEG is invariably used to describe the preterm EEG of different postconceptional ages as well as different sleep states (see section 2.1.4). Conversely, a discontinuous EEG pattern in the term-age infant, with no variability over the sleep-wake cycle is representative of neuropathology. In this instance, we are referring to the pathological discontinuous pattern which shows no variability between the awake and sleep state and is characterised by the quiescence of bursts; high voltage waves with intermixed, disorganised frequencies and IBI periods of suppressed activity (with amplitude of <25 µV).

Burst suppression can be secondary to a variety of conditions, such as hypoxia and ischaemia (269), coma (269), specific encephalopathies with neonatal presentation, such as Ohtahara syndrome (270), anti-epileptic medications, deep anaesthesia (271), and hypothermia (272, 273) and is observed across all age groups. Chapter 5 focuses on these EEG states of infants, secondary to HIE. This clinical entity is characteristic of the term infant who has experienced a severe perinatal deficit in the cerebral oxygen delivery leading to the disruption of the cerebral energy metabolism (222) (see section 1.1.2).

In infants with HIE, the severity and persistence of such abnormal EEG changes has traditionally been one of the markers directly related to the severity of the insult, the risk of ongoing neuronal damage and poor long-term prognosis. Several studies have shown that the rate of recovery of the electro-cortical activity is closely related to outcome and that the longer the EEG remains abnormal the higher the risk of an adverse neurodevelopmental outcome (111, 113, 114, 265, 274). In a study looking at aEEG background tracings in the first 6 postnatal hours in infants with HIE, it was shown that 80% of the infants presenting with BS either died or had severe disability at follow up (111). Another study looking at term infants with excessively discontinuous EEGs, showed that when infant's EEG contains a predominant IBI duration of more than 30 s there is 100% probability of severe neuro-disability or death and an 86% chance of developing epilepsy (264).

More recent EEG work has focused on developing more objective mathematical metrics for prediction of outcome in HIE infants. This has demonstrated that certain parameters of the BS trace such as the distributions of burst area (area under the curve) and burst duration predict later clinical outcome comparable to structural neuroimaging and neurodevelopmental assessment (267). Japaridze et al., identified different neuronal networks in the burst and suppression phases in human infants with BS, by applying dynamic imaging of coherent sources (DICS) on EEG segments (268).

Despite the extensive EEG work, certain aspects of the BS pathophysiology, its behaviour and characteristics remain unclear. Its unified appearance and presentation in different age groups and under different conditions suggest a common pathophysiological process. It appears as the brain becomes inactive, entering a low energy phase in response to brain injury in the same way that a chemical agent (such as an anaesthetic agent) would induce BS.

2.2 Near-Infrared Diffuse Optical Imaging

2.2.1 Basic Principles of Biomedical Optics

Biomedical optics is a broad term which incorporates the various approaches and methods of using light to study biological tissue. Diffuse Optical Imaging (DOI) is one of these methods, which have evolved from near-infrared (NIR) spectroscopy, originally described in the 1970's (275). The description of the properties of NIR light and the physical principles of tissue spectroscopy is therefore essential to the understanding of DOI.

Visible light exists at wavelengths in range of 450 to approximately 700 nm and is strongly attenuated by biological tissue. As a result, it is difficult to transmit visible light more than a few millimetres through tissue. However, biological tissue is relatively transparent to NIR wavelengths of light, whose spectrum is just beyond the visible, ranging from approximately 700 to 1000 nm. Near infrared spectroscopy (NIRS) therefore, uses variations in the intensity of back-scattered NIR light through a region of tissue to determine the changes in the optical properties of that tissue. These changes or variations in tissue optical properties are dependent upon changes in concentration of tissue chromophores. Chromophores (optical absorbers) are compounds within biological tissue that absorb light in the NIR spectrum. The most important such chromophores are the oxygenated and deoxygenated forms of haemoglobin, referred to as oxy-haemoglobin (HbO_2) and deoxy-haemoglobin (HHb). Haemoglobin carries oxygen to tissue via the circulatory system. Changes in the levels of haemoglobin indirectly suggest changes in oxygen supply to and consumption by the tissue. By using simple models with regards to how NIR light is absorbed and scattered through tissue one can calculate changes in the tissue concentration of HbO_2 and HHb.

Absorption of light

Understanding the principles of how light is absorbed by the chromophores and scattered within the tissue, and how it provides a way of measuring the changes in oxy- and deoxy-haemoglobin concentrations is complex. However, the description of what happens when light is transmitted through a simple, one-dimensional medium aids in the understanding of the basics of light interactions.

If we assume that NIR light is transmitted through a non-scattering medium that contains an absorbing compound of concentration (c), the intensity of that light will fall

exponentially with distance through this medium. Each absorbing compound has specific absorbing properties, described by its absorption coefficient, μ_a, which is related to the probability of a photon being absorbed per unit length of travel through a medium containing that compound alone. The mathematical description of this fall in light intensity, is expressed by the **Lambert-Bouguer Law**:

$$I/I_0 = e^{-\mu a.d}$$ **Equation 2.1**

In the above equation, I is the transmitted light intensity, I_0 the incident light intensity and d, the optical pathlength, which is the distance traversed through the medium, μ_a expresses the absorption coefficient of the absorbing compound at a given wavelength (See Fig. 2.2.10).

Equation 2.1 originates from Bouguer (276), and was adopted by Lambert who stated that when light travels through a layer of a substance, the fraction of the radiation absorbed is only dependent on the thickness of the layer (pathlength) (277). Beer was the first to describe the relationship between the absorption coefficient and the concentration of the absorber. He stated that: *'for an absorbing substance dissolved in a non-absorbing medium, the optical density is proportional to the concentration of the absorber.'* (278). The following equation mathematically expresses this:

$$\mu_a = \alpha.c$$ **Equation 2.2**

Where α is the specific absorption coefficient for that compound, and c is the molar concentration of the specific compound. The specific absorption coefficient represents the level of absorption per mole of absorber per litre of solution per unit distance of optical pathlength. It is related to the probability of a photon being absorbed per unit length. This was adapted and expressed as the **Beer-Lambert Law**:

$$I/I_0 = e^{-a.c.d}$$ **Equation 2.3**

The negative logarithm of the intensity ratio on the left-hand side of Eq. 2.3 is known as optical attenuation and is measured in the units of optical density. The higher the attenuation, the lower the ratio of transmitted light to incident intensity, i.e. the higher the absorption of light by the medium. Essentially attenuation is the decrease in light

intensity whilst light is travelling through an absorbing, non-scattering medium, and is expressed by the following equation:

$$A=ln[I/I_0] = a.c.d$$ **Equation 2.4**

The transmitted light intensity, *I* is dependent on both the absorbing properties of the absorbing compound (given here by the specific extinction coefficient) and upon the wavelength of the light that is incident upon it; the absorption spectrum of the compound describes this wavelength dependent absorption.

Absorbers in tissue

The principal medium of interrogation in biomedical optics is the human tissue, within which the main compound of interest is haemoglobin. However, it is also important to have a basic understanding of the optical properties of other chromophores within human tissue, such as water, lipids, melanin, and cytochrome oxidase.

Water

Water is one of the principal components of human tissue, with 80% of the adult brain tissue mainly comprising water (279). The light absorption by water is higher at wavelengths above 900 nm (see Fig. 2.2.1). Between wavelengths of 200 to 900 nm, water exhibits a window of transparency (280) within which human tissue can be investigated.
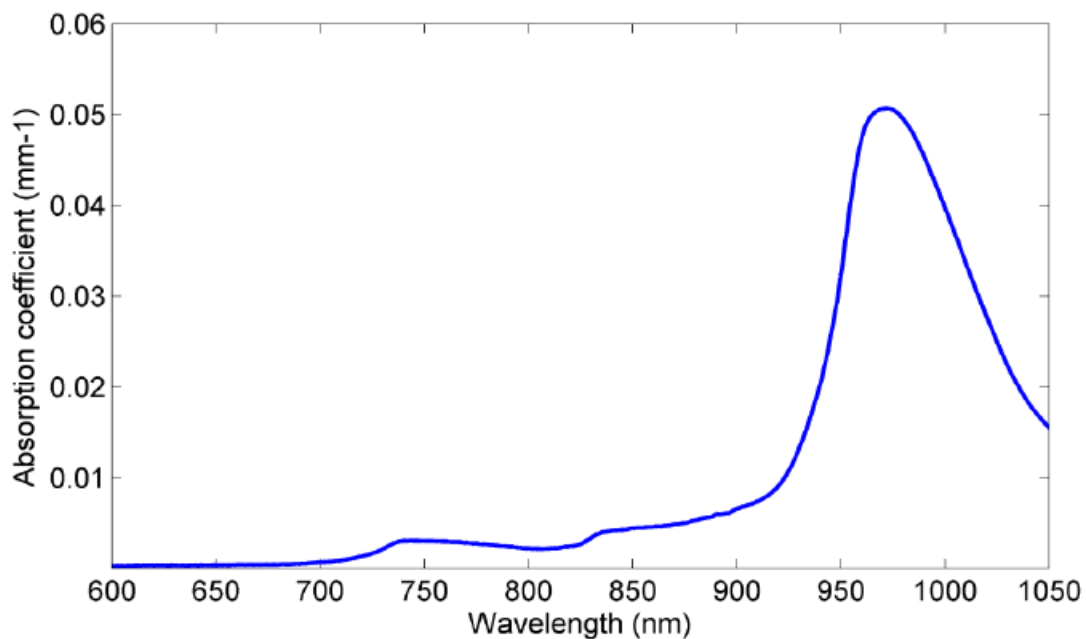
Figure 2.2.1: Representation of the absorption coefficient of water. Adapted from reference (280).

Haemoglobin

Within this window of transparency, haemoglobin is the chromophore which is absorbed in the NIR spectrum, between 600 and 900 nm. It is worth noting that there is a differentiation in absorption properties between HbO_2 and HHb. The difference in the absorption levels between these two compounds in the visible part of the spectrum explains the appearance of blood; where oxygenated blood (arterial) appears bright red, and deoxygenated blood (venous) appears more purple or blue (see Fig. 2.2.2). Similarly, light at 850nm will be absorbed more by HbO_2 and less by HHb; conversely light of 750nm will be absorbed predominantly by HHb (see Fig. 2.2.2 & 2.2.3). An isosbestic point, where the specific extinction coefficients of both haemoglobin compounds are equal exists at 800 nm. Before and after this point the absorption of the spectra differs for HbO_2 and HHb. This difference allows spectroscopic separation of the two compounds by only using a few sample wavelengths. By illuminating tissue with two or more wavelengths, the changes in the absorption of those two wavelengths of light can be used to calculate the relative concentration changes of both HbO_2 and HHb.
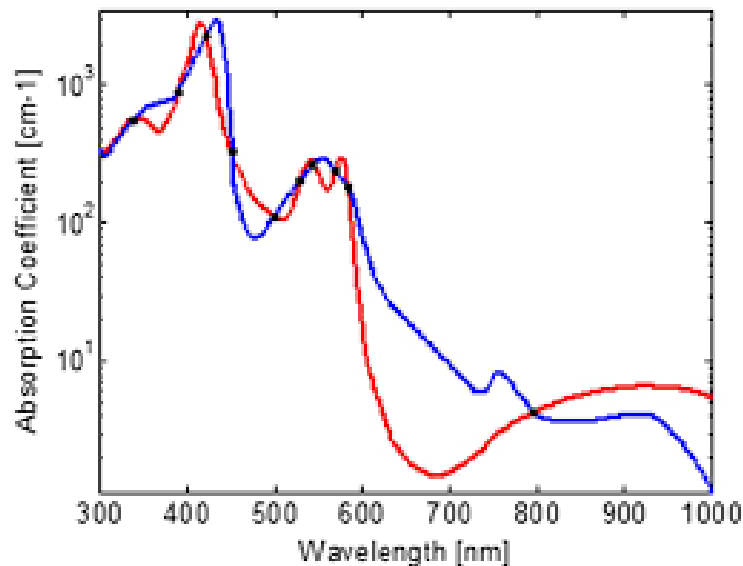
Figure 2.2.2: Representation of the absorption (molar extinction) coefficients of HbO2 (blue line) and HHb (pink line) for different wavelengths between 400 to 1000 nm. The spectrum of visible light is overlaid on the x axis. The black square indicates light in the NIR range with the isosbestic point of HbO_2 and HHb. Adapted from reference (281).
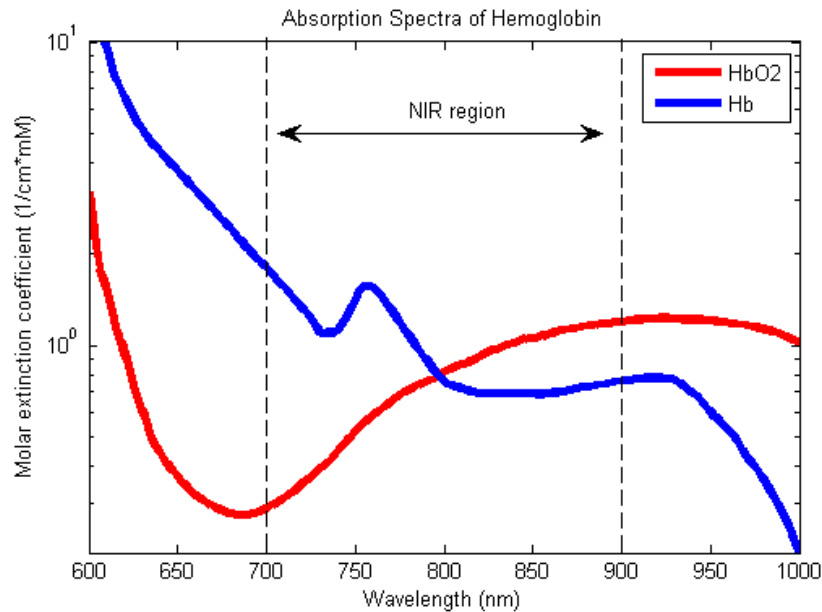
Figure 2.2.3: Representation of the absorption spectra for HbO$_2$ and HHb in the NIR range. Note the significant differentiation in absorption before and after 800nm, where the specific absorption coefficient is equal for both compounds. This is the isosbestic point at which the concentration of the two chromophores can be estimated independent of the oxygen saturation. Before and after this point the differences in absorption of the spectra are significant and consistent. Therefore, the changes in the absorption of two wavelengths of light on either side of the isosbestic point can be used to calculate the relative concentration changes of both oxy- and deoxy-haemoglobin. Adapted from reference (281).

Lipids

Although the distribution of lipid in tissue may vary based on different types of tissue, it can also be considered as a constant absorber, the concentration of which is unlikely to change during an experiment. The absorption spectrum of lipid is like the one of water.

Cytochrome c

Cytochrome c oxidase (CtOx) is the last enzyme of the cellular respiratory electron transport chain, within the mitochondrial membrane. It receives an electron from each of four cytochrome c molecules, and transfers them to one oxygen molecule, converting molecular oxygen to two molecules of water. The concentration of CtOx in tissue is approximately a tenth of that of haemoglobin and consequently has a relatively small effect on the total absorption coefficient of tissue. It is worth mentioning that the relative amount of CtOx in a reduced or oxidised state can provide an indirect measure of the metabolic demand of a region of tissue. As the total concentration of cytochrome oxidase is a constant which does not vary, it is the difference in the absorption coefficient of reduced and oxidised CtOx which is relevant to spectroscopic measurement. Its

concentration, however, is relatively low compared to haemoglobin and unless using specific broadband spectrophotometers it is difficult to measure (282).

Scattering of light

Scattering is the other main way in which light interacts with tissue. The term scattering includes a variety of light-matter interactions which maintain the existence of the incoming photon but may alter its direction of travel (elastic scattering) or degrade the photon's kinetic energy (inelastic scattering). Scattering is the dominant light-matter interaction in biological tissue at visible and NIR wavelengths. In most cases, when a photon travels within a scattering medium, the different compounds will change its direction of travel but not its kinetic energy. Inelastic scattering is generally neglected in biomedical optics. In the same way that the absorption coefficient (μ_a) describes the absorption properties of a certain compound, the scattering coefficient (μ_s) describes its scattering properties.

Because of the effect of scattering and unlike the controlled example above, light does not travel in a straight line through biological tissue. The biological tissue per se is a scattering medium with its compounds constantly changing the direction of light (see Fig. 2.2.4), forcing to follow a random path. This is where the term, diffuse, often used to describe imaging methods (see section 2.2.4), derives from. The direction in which the scattered photon will travel is dependent on the size of the scattering compound, the light wavelength, and the refractive indices of the scattering medium.
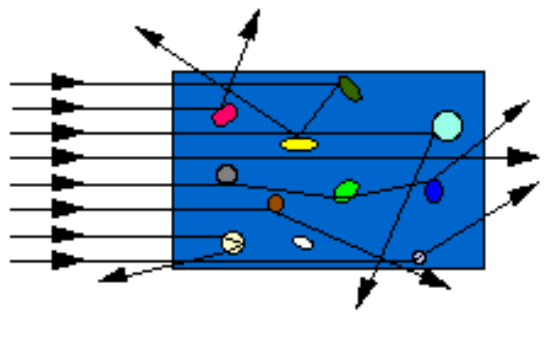
Figure 2.2.4: The effect of light scattering through a medium containing a scattering component.

The probability of any given photon being absorbed will no longer be a simple function of the thickness of the medium as originally described by Bouguer. As a photon is undergoing a great number of scattering events, it must travel a greater distance to

traverse the medium, thus increasing the probability being absorbed. The revision of the model for the attenuation of light intensity whilst travelling through biological tissue, is known as the **modified Beer Lambert law**:

$$A = log_{10}[I/I_0] = a.c.d.B+G$$

Equation 2.5

A stands for attenuation of light intensity, I_o for intensity of light incident upon an absorbing and scattering medium, *I* intensity of light transmitted through the medium, *a* for the specific extinction coefficient of the absorbing compound measured, *c* for concentration of the absorbing compound in the solution, *d* geometrical distance that the light travels, *B* for differential pathlength factor (DPF) and *G* as the additive term to account for scattering losses (i.e. photons that are scattered away from the detector). The DPF accounts for the expected increase in average pathlength due to scattering events (283), and is dependent upon the reduced scattering coefficient, the absorption coefficient and the geometry of source and detector.

2.2.2 Measurements using near-infrared light

The modified Beer-Lambert law is the most important equation in biomedical optics and it allows us to calculate several physiologically important characteristics. However, in the same manner the original Beer-Lambert law did not account for the scattering effect, there are certain limitations within the modified version of the law regarding these measurements.

The factor which is the most difficult to calculate is the geometrical loss due to scattering events, G, as this is dependent upon the geometry of the tissue, as well as the scattering coefficient of the tissue under investigation. Without knowledge of G, the calculation of the absolute concentration of a compound, c, becomes impossible. However, if one assumes that the factor G, remains constant and does not change between two, it then becomes possible to calculate the changes of concentration of a compound from the measured change in attenuation between the experiments.

Imagine light of intensity I_o, illuminating a highly scattering medium that contains an absorber (chromophore) with a concentration c_1. The light attenuation is measured as A_1, but c_1 is not possible to determine due to the unknown contribution of scattering losses, G. Similarly, if we repeat the experiment with the exact same medium and incident light intensity, I_o, but change the concentration of the absorber within the medium to c_2, we will be able to measure the light attenuation, A_2.

$$A_1 = c_1.a.d.B + G \qquad \text{Equation 2.6}$$

$$A_2 = c_2.a.d.B + G \qquad \text{Equation 2.7}$$

Note that in both equations 2.6 and 2.7, and following certain assumptions, we can calculate the absolute *changes* in chromophore concentration based on the absolute measurements of light attenuation as shown in equation 2.2.8.

$$\Delta A = A_2 - A_1 = (c_2 - c_1).a.d.B \qquad \text{Equation 2.8}$$

As noted above, factor G is eliminated in Eq. 2.8. Therefore, based on measurements of the change in attenuation one could determine the changes in absorption

coefficient. However, prior to that, there remain the DPF and optical pathlength (*B* and *d* respectively) to be calculated. These two values together represent the average time taken by photons to travel through a medium. By calculating the mean time in which photons travel through a medium and knowing the optical properties of the medium, one may determine the DPF. The latter can also be approximated based on the optical properties of the medium (284, 285). In NIRS applications, the DPF is often taken as a fixed, constant value, based on previous measurements according to type of tissue and subject being interrogated.

As mentioned in section 2.2.1, there are many chromophores in biological tissue, but only those which vary in concentration over the timescale of an experiment, as well as absorb light in the NIR spectrum, will contribute to the absorption coefficient. Therefore, the ones of most physiological interest are the changes in concentration of HbO_2, HHb and CtOx to provide any measured variation in absorption coefficient.

Combining the above knowledge with the basis of Eq. 2.8, by measuring at two different wavelengths simultaneously it is possible to calculate the concentration changes in HbO_2 and that of HHb, as shown in Eq. 2.9 and Eq. 2.10. The standard approach to performing NIRS is by measuring the changes in attenuation at two light wavelengths over the same volume of tissue. The concentration changes of the chromophores are subsequently calculated by solving equations 2.9 and 2.10. By adding a third wavelength it becomes possible to measure another chromophore, i.e. CtOx.

$$\Delta\mu_{a\,(\lambda1)} = \varepsilon_{HbO2(\lambda1)}.\Delta C_{HbO2} + \varepsilon_{HHb(\lambda1)}.\Delta C_{HHb} \qquad \textbf{Equation 2.9}$$

$$\Delta\mu_{a\,(\lambda2)} = \varepsilon_{HbO2(\lambda2)}.\Delta C_{HbO2} + \varepsilon_{HHb(\lambda2)}.\Delta C_{HHb} \qquad \textbf{Equation 2.10}$$

$\Delta\mu a_{(\lambda1)}$ and $\Delta\mu_{a\,(\lambda2)}$ represent changes in absorption coefficient, whereas $\varepsilon_{HbO2(\lambda1)}$ and $\varepsilon_{HbO2(\lambda2)}$ represent the specific extinction coefficient for HbO2 at the relevant wavelengths λ_1 and λ_2 (and similarly for HHb - $\varepsilon_{HHb(\lambda1)}$ and $\varepsilon_{HHb(\lambda2)}$).

2.2.3 Neurovascular coupling

NIRS is an ideal tool for measurements of *changes* in the chromophore concentration of a given medium, and it is thus mostly applied to experiments where a stimulus invokes a change in the chromophore concentration. An ideal such medium is the human cortex, which is rich in both neuronal and vascular activity.

During a purposeful movement or a cognitive task there is a natural increase in electro-cortical activity which leads to increased metabolic demands and energy supply at a cellular level (286, 287). The principal molecule in energy production or consumption on a cellular level is adenosine tri-phosphatase (ATP), which is the end-product of cellular respiration. Repeated neuronal activation results in a constant re-polarisation of the neuronal membrane back to its resting potential state, a highly energy consumptive process. The ion transporters across the neuronal membrane are fuelled by ATP and their increased activity leads to high ATP requirements and therefore, increase in cellular respiration. The latter process is driven by both O_2 and glucose supply, which is provided by the flow of regional vasculature (see Fig. 2.2.5).

Cerebral blood flow (CBF) is vital to the brain, and there is a constant baseline flow for maintaining all basic functions (288). Within the cerebrovascular system there are heterogenous mechanisms which maintain cerebral blood flow at a level which meets the energy requirements and prevents sudden fluctuations due to changes in systemic arterial blood pressure. The control of blood supply to the brain is tightly regulated at both a global and regional level. Global cerebral autoregulation, which maintains CBF over a range of perfusion pressures is regulated by smooth muscle cells in the cerebral arterioles (289). Local supply of blood to meet metabolic demand of neuronal tissue is regulated both by smooth muscle cell activation as well as local metabolic factors. In this way, a constant supply of oxygen and glucose is provided to the neuronal tissues in an activity-dependent manner.
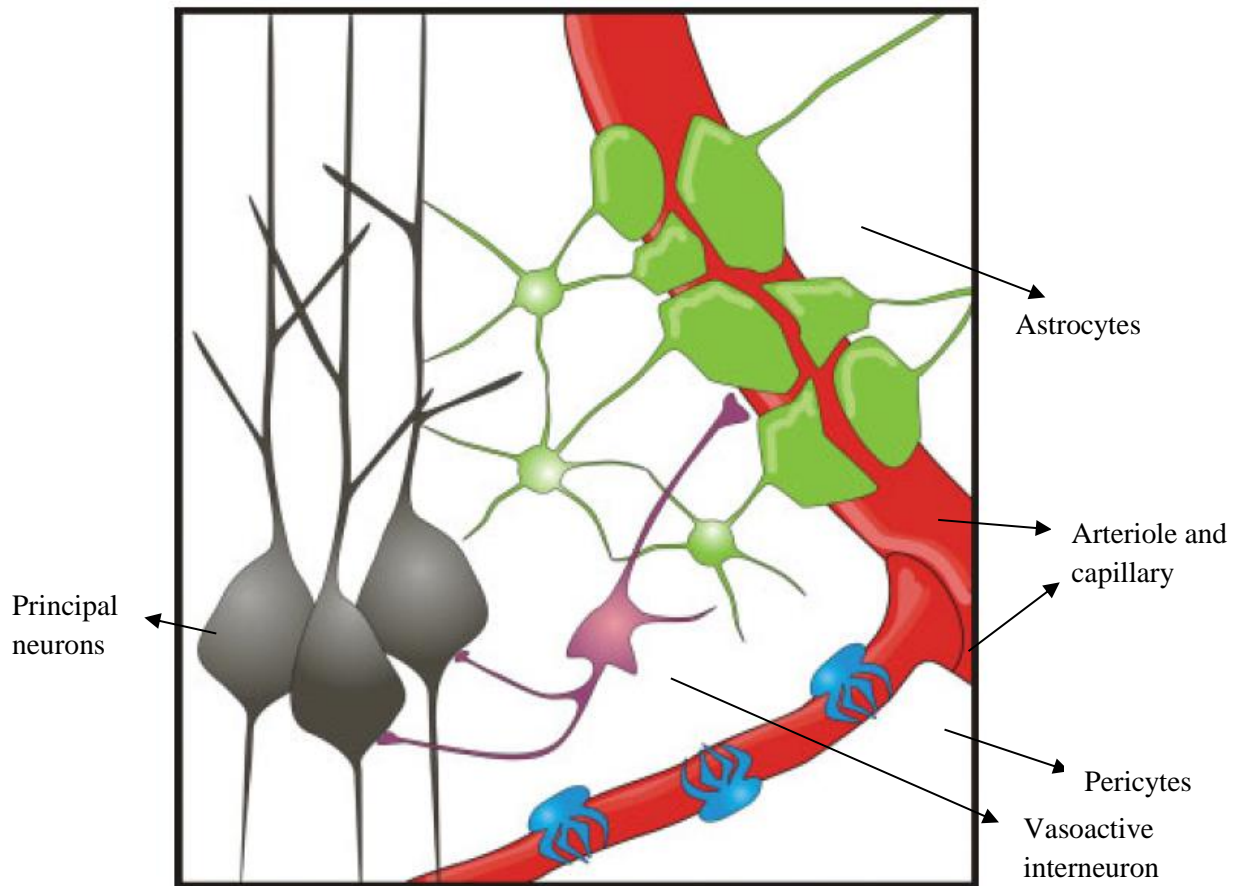
Figure 2.2.5: Representation of the interactions between neuronal and vascular activity. The above shown cell types are thought to contribute primarily in the cerebro-vascular control with vasoactive interneuron and astrocyte processes being transmitted to both the principal neurons (in grey) and the arterioles (in red). Image adapted from reference (286).

This link between transient neuronal activity and the corresponding increase in cerebral blood flow (CBF) is called neurovascular coupling (NVC). It was initially thought that this increase in CBF, described as functional hyperaemia, was a result of a regional decrease in oxygen concentration (290). However, more recent studies have indicated that NVC is mediated by a combination of vasoactive agents (291, 292).

Studies have also shown that mediated by the release of glutamate (an excitatory neurotransmitter), astrocytes directly affect local CBF (293). Under the effect of glutamate substances such as nitric oxide (NO) and arachidonic acid (AA) are released and play a significant vasomotor role in the cerebral microvasculature, with NO being a primarily vasodilating substance, while AA is vaso-constricting. Further studies have shown that the final effect of these agents depends on local oxygen concentration and may differ between brain regions (292, 294).

As previously discussed NIRS can measure fluctuations in the concentrations of HbO_2 and HHb. Hence, the NIRS signal reflects the balance between the oxygenated CBF and the rate at which O_2 is consumed (known as the cerebral metabolic rate of oxygen, $CMRO_2$). Logically, one would anticipate that increased localised neuronal activity would lead to a localised decrease in HbO_2 and increase in HHb secondary to increased $CMRO_2$. However, the classical anticipated NIRS response is the result of a decrease in HHb and an increase in HbO_2 concentration.

The change in $CMRO_2$ and the corresponding change in CBF are poorly balanced. With CBF being an indirect measure of oxygen supply, it has been shown that CBF may increase 6 times more for a given increase in $CMRO_2$ following a somatosensory stimulus (295). However, although the actual figure remains debatable through the literature, similar studies have shown that stimulation of changes in the neuronal activity does lead in CBF over-compensation (296, 297). It is this signal that forms the foundation of research in the field of investigating the functional cortical activation using NIR optical techniques and MRI, known as functional NIRS (fNIRS) and blood oxygen level dependent (BOLD) fMRI.

The classic NIRS functional response in the adult brain is represented by an increase in HbO_2 concentration, accompanied by a decrease in HHb concentration on a micro-molar scale (see Fig. 2.2.6). This has consistently been demonstrated by adult NIRS based studies (298-303). As discussed above, it is thought that the decrease in HHb is secondary to oxygen delivery in excess of oxygen consumption in response to functional activation of the brain (295). This activity-induced vascular response is known as the haemodynamic response function (HRF). Normally the HRF to a stimulus is typically quite slow; it begins at approximately 3 seconds post stimulation and reaches its crescendo within 20 seconds (304). The shape of the HRF and its time-course will naturally differ depending upon the type of stimulus (different amplitudes in the signal have been noted to brief or long-lasting stimuli) (305), the subject, age group, the region of the brain interrogated and the underlying neuronal activity.

Research studies in adults suggest that the observed haemodynamic response measured by NIRS is comparable to the BOLD response observed in functional MRI. The superiority of NIRS is that it is based on the intrinsic blood light absorption and therefore provides separate measurements of changes in HbO_2, HHb, and HbT concentrations.

Functional MRI is based on the paramagnetic properties of HHb and therefore the BOLD signal derives from local changes in the HHb concentration (306, 307). In that respect, studies that have compared the two techniques in experiments of functional activation have shown better correlation of the BOLD signal to the changes in HHb concentration (308-311). However, Yamamoto and Kato, and Strangman et al. showed a better correlation of the BOLD signal to the changes of the HbO_2 concentration, as measured by NIRS (312, 313), whereas Punwani et al., and Chen et al., showed that the BOLD signal is similar to the NIRS one without specifying for which type of haemoglobin that was (314, 315). Huppert et al., tried to overcome some of the challenges of previous experiments, by using BOLD fMRI and NIRS with a high signal to noise ratio, to investigate the haemodynamic changes in a short-lived motor task. They reported that the obtained BOLD signal correlated to the NIRS measured changes of the HHb concentration and not those of the HbO_2 (316).
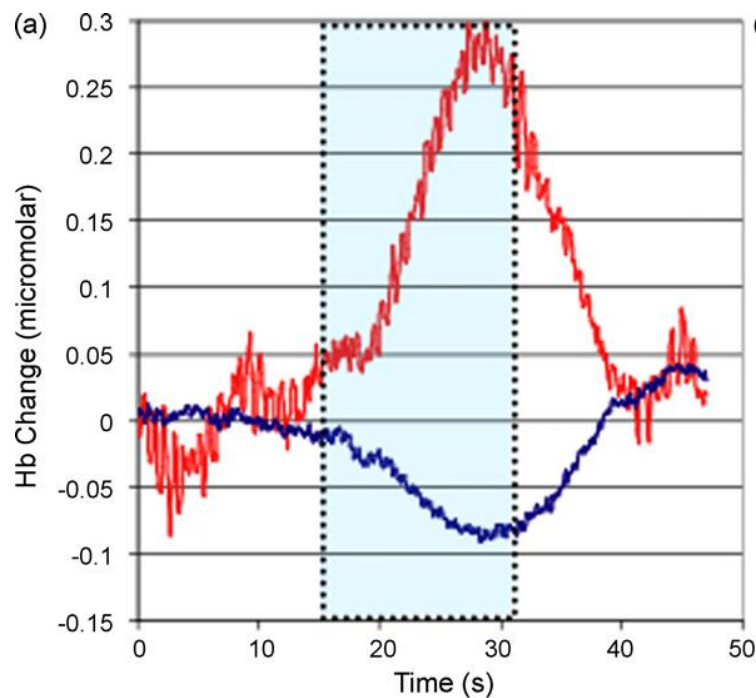
Figure 2.2.6: A typical HRF to cortical activation by showing an increase in HbO₂ and decrease in HHb (blue)along the y axis over time, along the x axis. Graph adapted from reference (317).

In infants the haemodynamic response to stimuli appears to have a less consistent pattern in comparison to adult studies. Functional NIRS studies in infants have shown an increase in HbT and HbO_2 with a simultaneous, smaller amplitude increase in HHb, which contradicts the anticipated decrease (318-323). Figures 2.2.7 and 2.2.8 are typical

examples from two different studies showing this pattern in the HHb signal during functional NIRS studies on infants. Hoshi et al., have suggested that the observed increase in HHb following the increase in HbT and HbO$_2$ over the investigated area of the neonatal cortex, may be attributed to venous dilatation, and that this may vary with different developmental stages (319). Age or developmental stage could be a factor influencing the balance between oxygen supply and demand, in addition to other factors such as region of interest, sleep states, level of anaesthesia (324-327). Similarly, studies using BOLD fMRI have shown the variable scale of the HRF to somatosensory stimuli between adults, term, and preterm infants (see Fig. 2.2.9), with the response to functional activation becoming more brisk and greater in scale with maturation (328).

Finally, most infant fNIRS studies employ HbO$_2$ as the preferred measure of cortical activation. This is most likely because HbO$_2$ has the highest signal to noise ratio. Generally, the direction of its change is consistent amongst different subjects and different paradigms. However, HbO$_2$ signals are more heavily influenced by systemic physiological changes (such as the cardiac cycle, and blood pressure etc.).
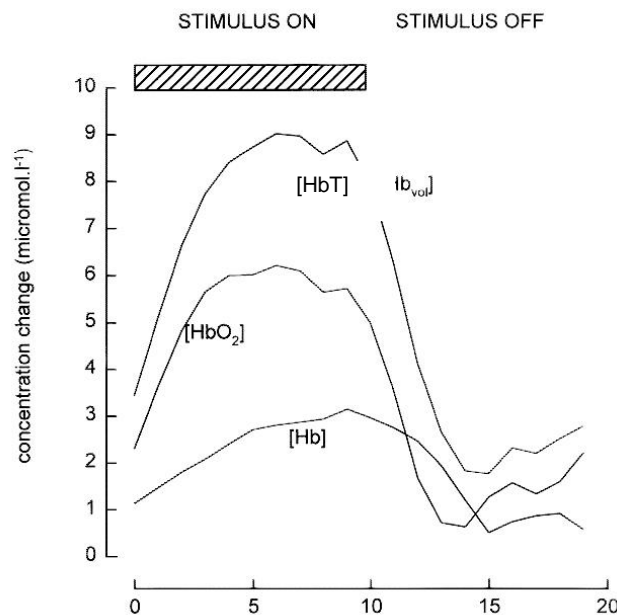
Figure 2.2.7: Changes in the HbT, HbO$_2$, and HHb with visual stimulation of the occipital cortex averaged and smoothed over nine cycles in the same infant. Note the increase and subsequent decrease in all the parameters at a different scale and over a slightly different time. Image adapted from reference (320).
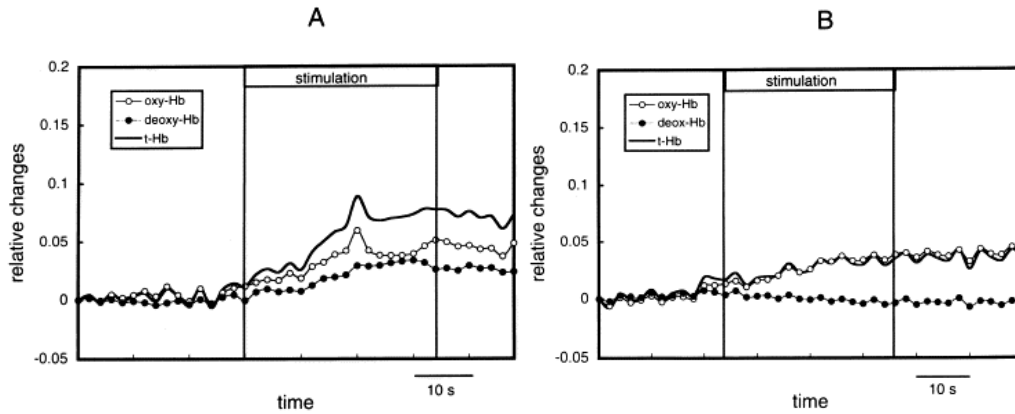
Figure 2.2.8: Example of functional activation. Changes in oxygenated haemoglobin (oxy-Hb), deoxygenated haemoglobin (deoxy-Hb), and total haemoglobin (t-Hb) over one channel in one infant during the (A) first and (B) second stimulation. Note the increase in deoxy-Hb in Figure A and its decrease in Figure B. Image adapted from reference (319).
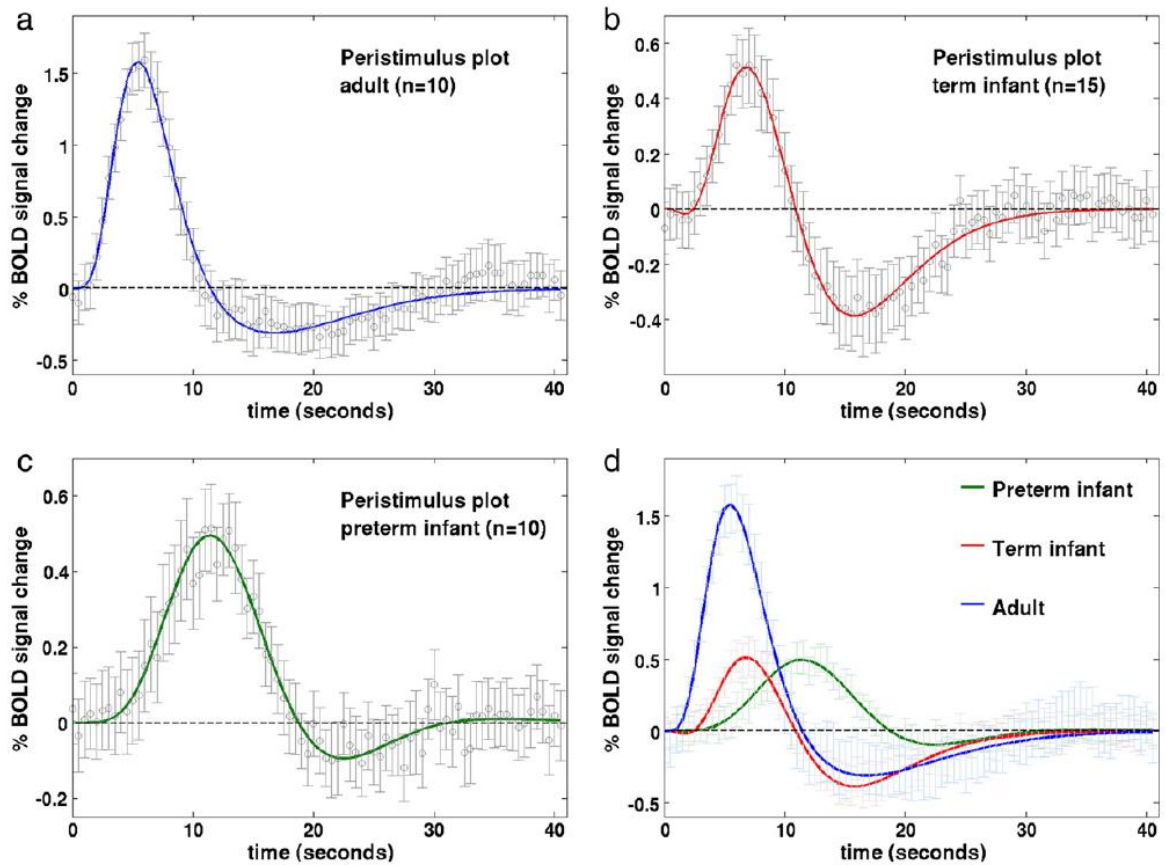
Figure 2.2.9: Time-series plots of the BOLD signal change post somatosensory stimulus for different age groups: the (a) adult; (b) term equivalent infant; (c) preterm infant groups. (d) Note the decrease in the time to peak of the HRF, and the increase in peak amplitude with increasing age. Graphs adapted from reference (328).

2.2.4 Types of near-infrared techniques

NIR techniques are classified in three main categories: continuous wavelength, time domain and frequency domain modalities. This classification mainly derives from the type of instrumentation, type of tissue illumination and type of information acquired at the end of each recording. Figure 2.2.10 provides an idea of the different measurements obtained by these three fundamental NIR techniques.
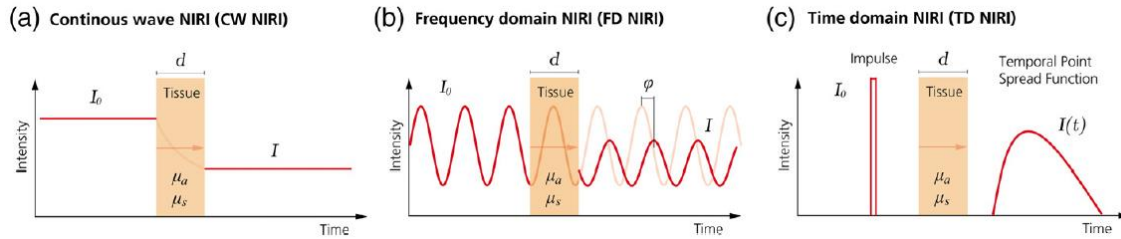
Figure 2.2.10: Demonstration of the three different NIR techniques. (a) CW emits light at a constant intensity and then only measures the changes in the intensity of the light travelling through tissue. (b) The frequency domain technique modulates the emitted light intensity and subsequently measures the intensity of the detected light and the phase shift, equivalent to the time of flight. (c) The time domain technique emits a short pulse of light (in picoseconds) into the tissue and calculates the time of arrival of each emerging through tissue pulse of photons. (I_0: incident light signal, I: transmitted light signal, d: thickness of the medium, μ_a: absorption coefficient, μ_s: scattering coefficient, φ: phase delay, and I(t): temporal point spread function of the transmitted light signa). Image adapted from reference (329).

Continuous Wavelength

The term 'continuous wavelength' (CW) essentially means that the device is exclusively based upon a light intensity measurement. For example, NIR light illuminates tissue and the intensity of the re-emerging light is measured. Continuous wavelength systems measure back-scattered light and are characterised by light emission at a constant intensity, allowing detection of variations in attenuation from different regions of tissue. These fluctuations in attenuation provide information on the chromophore concentration changes, which are calculated either based on the modified Beer-Lambert law or more advanced models of light transports (see section 2.2.5). These constitute most of the commercially available NIRS systems and can be single or multi-channel systems (see Fig. 2.2.11). They are overall inexpensive, safe, wearable, and portable (305, 330).
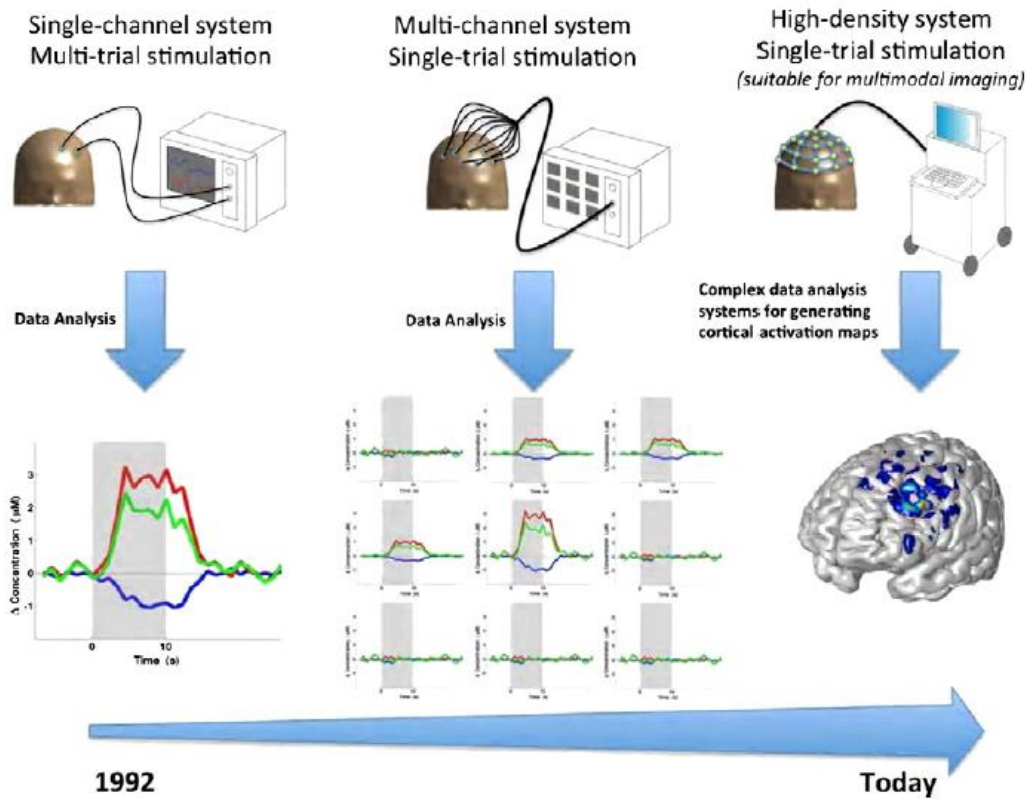
Figure 2.2.11: Different end-products using CW NIR systems. This is dependent on the number of channels and the arrangements of the sources and detectors across the scalp. Adapted from reference (331).

Continuous wavelength, single channel NIRS systems utilise one source location and one detector location to investigate a chosen region of tissue. The source and detector are typically coupled to the body via optical fibres. However, single-channel NIRS systems can only sample and provide information for a small volume of tissue.

Multi-channel CW NIR systems employ an array of multiple sources and detectors to investigate the haemodynamics of a broader area of tissue. The use of multiple sources creates an engineering challenge, because it is critical that the origin of any detected light is known. There are several methods that allow sources to be distinguished including time multiplexing (i.e. you turn them on one at a time) and frequency multiplexing (where each source is modulated at a known frequency) (332). However, still, simple multi-channel, CW NIRS only provides a series of spectroscopic measurements across different areas of the tissue investigated.

Continuous wavelength, diffuse optical imaging (DOI) systems have been widely used in the investigation of the haemodynamic changes of the cortical surface of the brain. Mainly dependent upon the arrangement of channels used, they offer the possibility of

reconstructing 2-dimensional (2D) and 3-dimensional (3D) images of the observed haemodynamic changes of the interrogated tissue. In the literature 2D imaging systems are called diffuse optical topography or mapping or imaging and similarly 3D imaging systems are called diffuse optical tomography or mapping or imaging. The term diffuse optical imaging in this thesis is used to describe both these techniques. The device used in the study is a diffuse optical tomography device, which will be described in detail in chapter 3.

Optical topography is also a multi-channel CW NIRS method. As mentioned above, it produces two-dimensional (2D) maps of the captured cortical haemodynamic changes (see Fig. 2.2.12). This is achieved by interpolating the signal measured from different channels across the area of investigation (333). This approach has aided the study of cortical activation to visual stimulation, sound, and speech through the different neurodevelopmental stages of infancy (334-339).
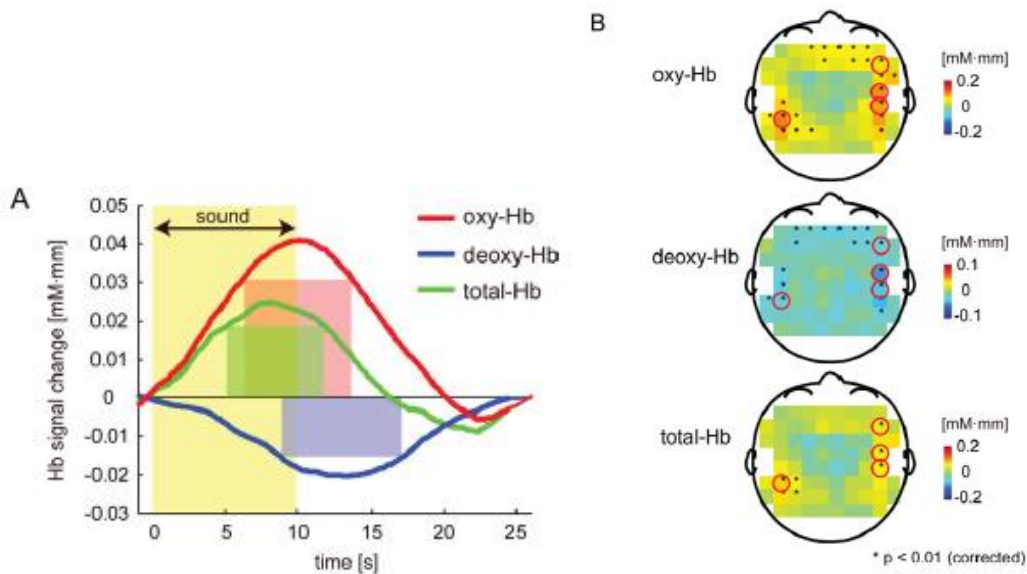
Figure 2.2.12: Optical topography of the cortical haemodynamic response to sound stimuli. 17 Japanese infants were studied with a 72-channel whole head NIR device whilst four different types of language were played (maternal and foreign language, both forward and backward played). (A) Graph showing the grand average for all channels and all infants of haemoglobin signals in response to sound. (B) Topographic maps of the grand average activation with common activation channels amongst the infants over the posterior part of the left temporal cortex and anterior part of the right temporal cortex (indicated with red circles). Image adapted from reference (340).

However, optical topography has limitations regarding the anatomical registration of the channels and critically provides no depth information. Diffuse optical tomography (DOT) can allow for increased spatial resolution and provides full three-dimensional (3D)

images (341). Diffuse optical tomography uses multiple overlapping channels with multiple source-detector distances (usually ranging from 1.5 to 4 cm) to increase spatial resolution and improve haemodynamic information deriving from different layers of depth within the cortex (342, 343) and essentially enables the acquisition of 3D images (344).

The source-emitted NIR light penetrates tissue in a banana-shaped fashion and the transmitted light is measured by a neighbouring detector (see Fig.2.2.13). The intensity of light travelling from a source to a detector through tissue decreases exponentially with source-detector distance. The source-detector distance is significant as it determines the sampling depth and the spatial resolution of the final image acquired. A large distance allows greater sampling depth into the cortex, whereas a short distance provides better spatial resolution. In infants, a separation of 3 cm typically penetrates 1–1.5 centimetres into the cortex (281), reported as 0.5 to 2 cm in human adults (345).
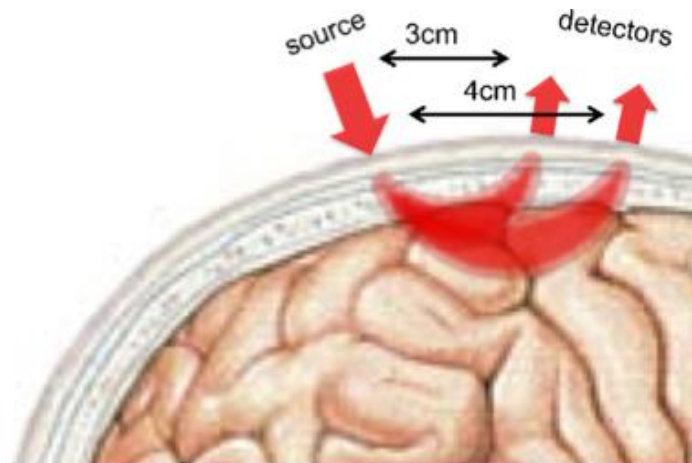
Figure 2.2.13: The banana shaped trajectory of NIR light at different source-detector separations in DOI. The sensitivity distribution of light has a banana shape. The areas proximal to the source and the detector have the greatest effect on the captured light. Depending on the depth of the tissue, the spatial sensitivity varies. Hence, by using multi-distances between sources and detectors, the depth spatial sensitivity increases. Image adapted from reference (281).

The quality of the images is dependent upon the number of channels, which in practice is modulated by the weight and number of available optical fibres, as well as the age of the subject under investigation. Most commercial systems provide 10-20 sources and 10-20 detectors respectively. Users must choose to cover a wide area sparsely at the expense of lower resolution, patchy sensitivity, less depth discrimination, or a small area densely with better resolution and better 3D images, but small field of view (346).

Frequency Domain

In contrast to CW NIR systems that only provide intensity measurements, frequency, and time domain NIR techniques provide additional information about the transmission of photons through tissue.

The frequency domain system, in addition to light attenuation, also measure the phase shift by using a sinusoidally modulated input intensity. By comparison of the phase of the modulated signal going in to the tissue and that coming out, it is possible to measure the phase shift caused by the tissue. The principal advantage of this method is that from phase shift, one can calculate the mean optical pathlength. As a result, it is no longer necessary to estimate the DPF, significantly reducing errors in the measurement of absorption coefficient. It also allows the effects of absorption and scattering to be studied separately, something which cannot be achieved by CW NIR systems. Frequency domain systems have been designed to perform spectroscopic measurements, optical topography, and optical tomography (333, 347, 348).

Time Domain

The time domain systems are the most sophisticated amongst the NIR techniques as they measure the time that individual photons take to travel across a volume of tissue. Time domain systems employ sources that emit very short duration pulses (a few picoseconds), and extremely sensitive detectors that can pick up the difference between the time of the pulse, and the arrival time of a photon at the detector. Because of scattering effects, the input pulse of light is stretched in time: some photons travel in a near straight line to the detector and thus have a short time of flight, while others experience many scattering events and take a longer time to reach the detector. The distribution of photon flight times is called a temporal point spread function (TPSF), which typically has a width of several nanoseconds. The TPSF represents a histogram of the time of flight of pulses of photons between source and detector (349). The information within this histogram includes measurement of the intensity of detected light (like a CW system would). Additionally, the Fourier transform of the TPSF provides measures of phase shift at every frequency. Time domain systems provide the same information as both the CW and frequency domain systems as well as absolute measurements of changes in HbO_2 and HHb concentrations, and the potential to study the separate effects of absorption and scattering.

Time domain systems, therefore, offer the richest dataset of all forms of NIR imaging (see Fig. 2.2.14).

In summary, CW NIR systems cannot fully describe the optical properties of the biological tissue being investigated. They can, however, provide measurements of the relative changes in HbO_2, HHb and HbT. On the other hand, time resolved systems can provide both qualitative and quantitative measurements. However, the latter are much more expensive systems, with a lower overall temporal resolution. Furthermore, time of flight can be a noisier parameter to measure as opposed to intensity. Nevertheless, what appears to be more important in neuroscience is the demonstration of a qualitative, statistically significant change in brain activity, rather than one that is necessarily a quantitative one. These measures can be obtained by CW NIR systems (329).
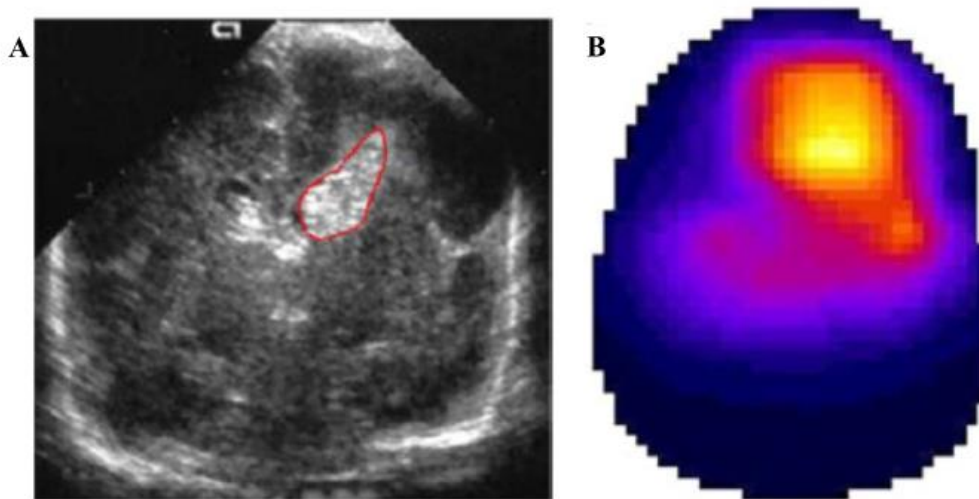
Figure 2.2.14: A time domain image. (a) coronal cranial ultrasound section of a preterm infant showing a left intraventricular haemorrhage with corresponding haemorrhagic parenchymal infarct. (B) A coronal section of the same preterm infant of regional blood volume. Note the increase in regional haemoglobin concentration over the corresponding pathological lesion outlined in the cranial ultrasound view. Image adapted from reference (350).

2.2.5 Image reconstruction

As mentioned in section 2.2.4 multi-channel CW NIR systems that employ multi-distance overlapping channels can measure haemodynamic changes in the cortical area monitored, which can be reconstructed into images. Therefore, this section focuses on the process of image reconstruction.

Diffuse optical image reconstruction requires three main components; an anatomical head model, a mathematical model of light transport in tissue and the data which contain the haemodynamic changes. With these components, it is possible to produce 4-dimensional (three spatial dimensions plus time) structurally registered images of changes in HbO_2 and HHb concentration.

Near-infrared light is highly scattered in tissue and does not travel in a straight line (see section 2.2.1, fig. 2.2.4). Therefore, the first stage of image reconstruction is to provide a mathematical model of light travelling through cerebral tissue. The most widely used model of light transport in DOI is based on the diffusion equation, which derives from the radiative transport equation (that models the transport of a variety of particles through a variety of media). The diffusion equation is used to estimate where light travels in a head model and thus identify which areas of this head model are sensitive to light. From this, it is possible to determine the spatial distribution of light that leaves a given source and reaches a given detector (332), and calculate the sensitivity matrix (J).

The sensitivity matrix is then used to solve the forward problem as seen in Eq. 3.1 below:

$$\Delta y = J * \Delta x \qquad \textbf{Equation 3.1}$$

where:

J = a sensitivity matrix

Δy = changes in measurements of light intensity

Δx = changes in the optical properties of a volume of tissue

The changes in light intensity (Δy) represent the obtained optical signal in a given volume of tissue with changes in optical properties (Δx) for a given arrangement of sources and detectors. However, numerical modelling techniques such as the finite element method (FEM) are needed to model the diffuse transmission of light within

complex geometries such as the brain (341). The FEM approach involves producing a mesh to separate the volume of brain tissue into a finite number of tetrahedral elements labelled by tissue type (i.e. skin, bone, CSF, etc). Solving the diffusion equation within the FEM will provide an estimate of the photon density within each finite element for a given source. Using this information results in a sensitivity matrix, which relates the changes in optical properties of brain tissue (Δx-image) to the changes in light intensity (Δy) at a given channel. It therefore provides a solution to what is known as the forward problem.

The changes in optical properties within a given head model represents the desired image. For the reconstruction of an image (i.e. the calculation of Δx), the sensitivity matrix (J) must be inverted. This is described as the inverse problem and is defined in Eq. 3.2 below. The inverse problem is described as the process of calculating from a given set of measurements the elements that produced them.

$$\Delta x = J^{-1} * (\Delta y) \qquad \textbf{Equation 3.2}$$

where:

J^{-1} = the inverse of the sensitivity matrix

Δx = the desired image (changes in the optical properties of tissue)

Δy = the measurements of change in light intensity

A software package, "time-resolved optical absorption and scatter tomography" (TOAST++) (351), developed by the Centre for Medical Imaging Computing at University College London. This software package uses FEM approaches to solve the diffusion equation for a given mesh geometry, which can be used to calculate J (thus solving the forward problem, as mentioned above-see Eq. 3.1).

2.3 Diffuse Optical Imaging and EEG

In this section, the use of the terms diffuse optical topography and tomography are used interchangeably according to the different studies. Therefore, the term DOI is used as a generic term characterising both topographic and tomographic methodologies.

The unique properties of DOI have been employed in the investigation of the human cortex. In 1993 different research groups demonstrated the possibility of non-invasive investigation of the brain with functional NIRS (162, 301, 352-354). In 1998, Chance et al., produced the first diffuse optical images of haemodynamic changes in response to sensorimotor stimuli in premature infants (see Fig. 2.3.1) (352).

Continuous wave DOI systems cannot fully determine a tissue's optical properties or provide absolute measurements, but with certain assumptions, it can quantify *changes* in HbO_2 and HHb concentration. Depending on the allocation of NIR light sources and detectors these systems can provide good spatial resolution (~1cm) in combination with a good temporal resolution (~10Hz) and measuring haemodynamic fluctuations across different cortical regions. This, along with their low cost and the ability to position these systems at the patient's bedside allows their application in the investigation of a variety of neurological conditions.
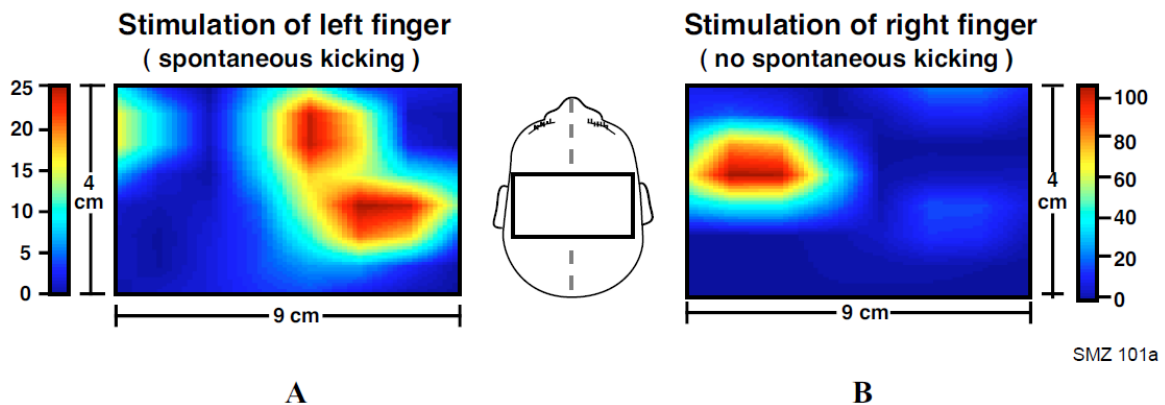
Figure 2.3.1: Diffuse optical topographic illustration of the increase in phase shift following sensorimotor stimulation of the brain. Whilst stroking the left and subsequently right finger of a preterm infant born at 26 weeks of GA, studied at CGA of 30 weeks, there is significant haemodynamic response in the contralateral parietal region (A for left finger stimulation and B for right finger stimulation respectively) lasting up to 30 seconds. Image acquired from reference (352).

Liao et al., employed a continuous wavelength, high-density system to study the haemodynamic response to visual stimuli of the neonatal occipital cortex (346). Eleven term newborn infants were studied between day one to two of life, postprandially and whilst resting or asleep for up to two hours. A screen at 20 cm distance from the infant's face would alternate a repetitive 10s visual stimuli, from a checkerboard to a flat pattern of different luminance. Since the infants had their eyes closed during the study, the visual-evoked response obtained was secondary to the variation in the luminance. A consistent distinct increase in the HbO_2 concentration, peaking between 10 to 14s post stimuli over the visual cortex was noted in 7 out of the 11 infants (see Fig.2.3.2) (346). Sato et al. produced diffuse optical images demonstrating the cortical spatiotemporal haemodynamic changes in 17 Japanese newborn infants to the sound of their native language (Japanese) played forward and backwards as opposed to a foreign language (English) similarly played forward and backwards. A whole-head array was used and overall 72 channels were representing cortico-vascular changes over the neonatal cortex. There was significant haemodynamic response to all the sound stimuli over both temporal and frontal regions with significantly more pronounced response to forward-played Japanese language as opposed to backwards-played Japanese, forward-played or backwards-played English (340).

Another group investigating the functional organisation of the brain and its intrinsic activity by using a highly dense continuous wave DOI technique, produced the first diffuse optical images of bilateral occipital resting state connectivity in newborn infants (355). The existence of resting state connectivity networks in adults (356) and in infants (357-359) has previously been demonstrated with BOLD fMRI.
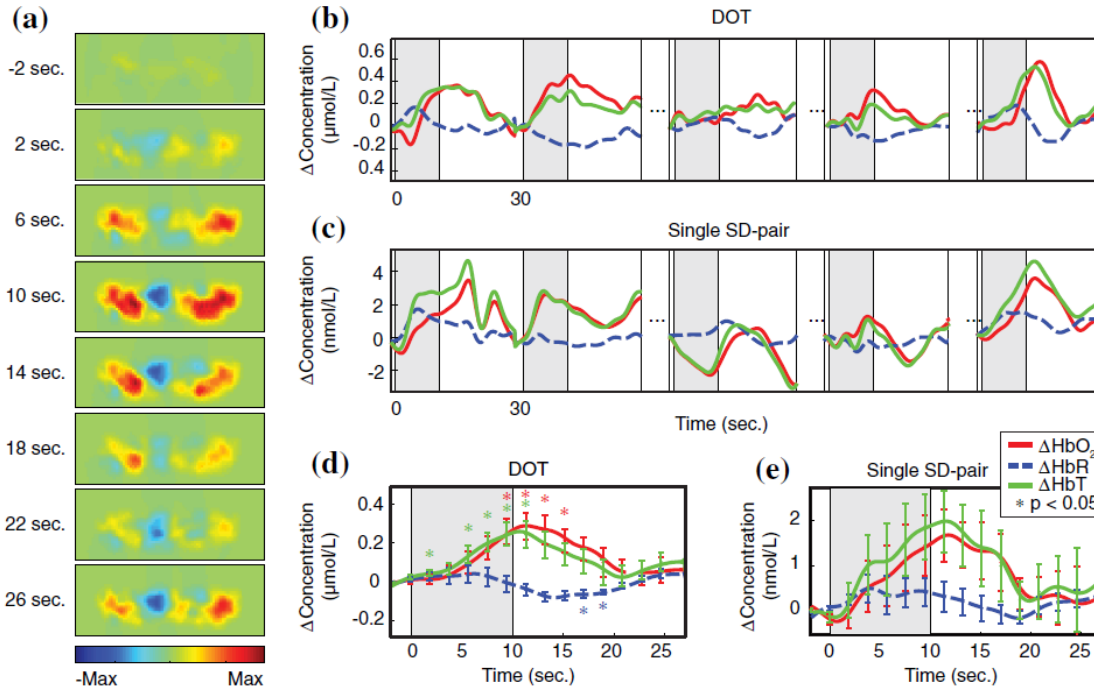
Figure 2.3.2: Diffuse optical topographic illustration of visual stimulation in infants: (a) images showing the spatiotemporal haemodynamic response for HbO₂ to 10s long visual stimulus on a single infant. Note the marked bilateral increase in HbO₂. (b) and (c) average traces for the cortical region with the maximum response to stimulus versus single channel measurement over five stimulus blocks. (d) and (e) block average time trace of the peak region of interest versus single channel measurement. Image adapted from reference (346).

The EEG has an excellent temporal resolution in monitoring changes of the electro-cortical activity (sub-millisecond), monitoring the continuous electrophysiological cortical activity and detecting distinct phenomena (e.g. seizures). It does, however, lack in spatial resolution compared to imaging. It is thought that main components contributing to this are the various layers the electrical cortical activity needs to go through to reach the EEG scalp electrodes (360) with the skull being the main one (361). Therefore, any scalp electrode detects the activity from the underlying brain layers including the cortical activity (362). The use of a reference electrode in EEG recordings also contributes negatively in the degree of spatial resolution.

Combining DOI and EEG facilitates the study of functional activation, and neurovascular coupling of either spontaneous oscillations (363), evoked potentials (364), or abnormal electrical activity such as seizures (365). These two modalities of brain monitoring complement each other in a fashion that maximises the overall temporal and spatial resolution; thus, making simultaneous DOI-EEG a unique tool for functional imaging. For example, during the study of functional activation (e.g. associated with the

movement of an arm), one may obtain parallel information via event related potentials across time (EEG) and the haemodynamic response (DOI) to the event (stimulus). The signals from the two techniques can provide a map of what the haemodynamic changes look like in different cortical regions in response to neuronal activation (see Fig. 2.3.3).
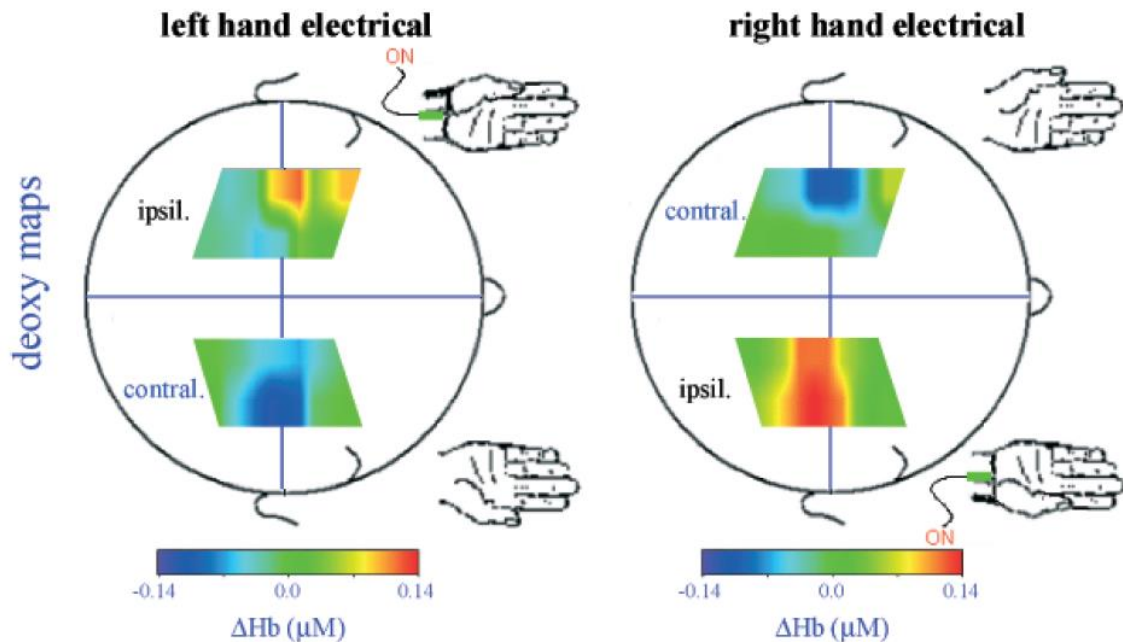
Figure 2.3.3: Diffuse optical topographic illustration of functional activation in adults. Representation of the block average cortical haemodynamic response of HHb 10s after the onset of left and right hand electrical stimulation on an adult patient. The study showed a consistent increase in HbO_2 and decrease in HHb (as shown in the image above) over the contralateral cortical side compared to the stimulation. Image adapted from reference (364).

Diffuse optical imaging can similarly offer information on changes of cortical haemodynamics in cases of neonatal brain injury. There are however, very few studies exploring this field. In the study of newborn infants presenting with seizures in the neonatal period using EEG and DOI, transient haemodynamic events of small increase followed by profound sustained decrease in HbO_2 concentration were identified. This was consistent amongst the subjects and not seen in the healthy controls, suggesting altered cortico-vascular activity associated with affected brain tissue (366). For further details of this work please see section 6.1.

A case study of a term infant with severe HIE and electrophysiological seizures by Singh et al., using simultaneous EEG and DOI (as described in section 3.2.1), showed significant changes in HbO_2 following seizures (see Fig. 4.1.3 in chapter 4) (365). Seven

distinct seizures were detected lasting from 30 to 90s. Although there was a degree of variability during the separate episodes, the reconstructed diffuse optical images revealed a consistent increase in HbT and HbO_2 concentrations related to the seizure activity. The diffuse optical images revealed an initial small increase in the HbO_2 concentration followed by its dramatic decrease. The latter persisted for several minutes after the end of the seizure activity (see Fig. 4.1.3 in chapter 4).

This work by Singh et al., constitutes the initial pilot study that gave rise to this to this MD research project and lays the ground for the investigation of acquired neonatal brain injury with video-EEG and DOT. The improved spatial resolution provided by DOT enhances the information obtained during interesting neurological phenomena as captured by EEG, in situations of neonatal brain injury. The principal aim of the MD project presented in my thesis was to understand the physiological haemodynamic changes of the neonatal brain in response to pathological events (evident in the EEG) in the context of acquired brain injury.

The main pathological events studied included seizures and burst suppression in the context of HIE, and perinatal stroke. The results of each topic are presented in chapters 4 to 6. The following chapter broadly describes the study designs, recruitment, data acquisition, and methodologies. As each condition explored is different, additional methodological details are provided in each of chapters 4 to 6.

Chapter 3: Patients and Methods

3.1 Patients

3.1.1 Ethics

The National Research Ethics Service Committee East of England (REC reference 09/H0308/125) approved the conduction of this study and allowed patient recruitment under the regulations of the Declaration of Helsinki (DoH) as developed by the World Medical Association (WMA) (367).

3.1.2 Recruitment

Following informed parental consent, infants were recruited to the study upon their admission to the Neonatal Intensive Care Unit (NICU) at the Rosie Hospital of Cambridge University Hospitals NHS Foundation Trust.

The patients recruited in the study are divided in three categories; the healthy term, the preterm and the infants presenting with seizures. The data selected during the conduction of the pilot study, prior to the commencement of my project, have been included in the analyses of this thesis.

The number of patients recruited during the conduction of the pilot study from January 2013 until August 2014 was 28:

- Healthy term infants: 9
- Preterm infants: 6
- Infants presenting with seizures: 13 (with data acquired from 12)

During the conduction of the pilot study, the research nurse, Andrea D. Edwards (ADE) was responsible for patient recruitment. In the beginning of the study she was supported by Dr Chuen Wai Lee (CWL), clinical research fellow at the time. The data acquisition was performed by Dr Harsimrat Singh, a post-doctoral research associate in medical physics with the clinical support of ADE. During that period a total of 51 patients with presentation of suspected or confirmed seizures were screened. A total of 18 patients were approached, out of which 13 were consented in the study (see Table 3.1).

My study was completed over a course of two years from September 2014 until August 2016. Having received training to perform the EEG-DOT scans independently, I actively started recruiting patients in December 2014. The number of patients recruited from December 2014 until August 2016 was 34:

- Healthy term infants: 1
- Preterm infants: 17 (data acquired from 14)
- Infants presenting with seizures: 16

During this period, a total number of 34 patients with presentation of suspected or confirmed seizures were screened. 5 of these patients were deemed inappropriate for recruitment due to co-existing neurosurgical entities, and one due to redirection of cares

being considered and discussed. Eventually 19 patients were approached, out of which 16 were consented and recruited in the study (see Table 3.1). The total number of infants (both controls and patients) recruited in conjunction with the preliminary pilot study was 62. The clinical details of all 62 infants are presented later in this chapter, in tables 3.2, 3.3 and 3.4.

Healthy term and preterm infants

The eligibility of the healthy term and preterm infants was determined upon clinical evaluation and discussion with the medical team. The infants had to be either with their mothers on the postnatal ward or on the NICU receiving minimal clinical input (mainly requiring help with establishing feeds). Exclusion criteria for the recruitment of healthy infants were the existence of antenatally diagnosed congenital anomalies or obvious postnatal dysmorphic features and/or other anomalies. The presence of skull trauma, such as a cephalohaematoma, caput and/or a skull fracture, and/or abnormal findings on cranial ultrasound scan (if clinically indicated during their stay) were also considered as exclusion criteria for the healthy control population. Amongst the preterm population recruited by me, 7 patients had significant abnormal findings on serial cranial ultrasound scans. These were recruited and enrolled in the study at a later stage and not in the first week of life.

Infants presenting with seizures

The infants presenting with seizures and/or HIE were recruited as soon as possible after their admission to the unit. Most of these patients were transferred in by the neonatal transport service from other district hospitals, rather than from the Rosie Maternity and Delivery Unit in Cambridge. This meant that occasionally the parents were still in the referring hospital. On other occasions, the father would accompany the infant but depending on their marital status with the mother, consenting the infant was not an option. This posed significant difficulty in recruiting these patients during their most acute phase, when they were most likely to seize.

The eligibility for recruitment of seizure/HIE patients was again evaluated based on the patients' clinical presentation and the severity of their condition. Following discussion with the medical team, I would approach the parents for consent and participating to the study. In situations where consent was granted, but an acute clinical procedure was required (e.g. insertion of percutaneous long line, transfer to MRI), the

study would be deferred for much later in the day or the following day. Infants with an antenatal diagnosis of congenital anomalies, or those with a strong clinical suspicion of skull fracture and/or a neurosurgical diagnosis (e.g. subgaleal haemorrhage, subdural haemorrhage) were excluded from the study.
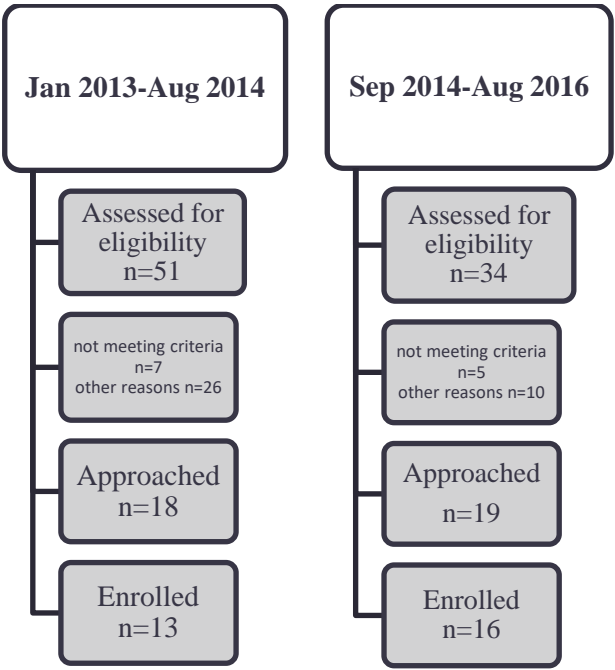
Table 3.1: Consort diagram demonstrating the recruitment of the patients presenting with seizures in the intensive care unit at the Rosie Hospital. As it appears on the diagram, the occurred between January 2013 and August 2014 by a research nurse and a postdoc researcher prior to my involvement in the project as part of a pilot study. After my involvement in the project, the recruitment continued between September 2014 and August 2016. The main reasons for patients not being approached for recruitment were the following: not meeting eligibility criteria (i.e. neurosurgical co-morbidities); clinical team not happy for recruitment into studies; redirection of cares; not available research staff.

3.1.3 Clinical details

The healthy term infants were recruited in the study in the first few days of postnatal life and required minimal clinical input. The study was conducted in the postprandial phase to minimise motion-related artefact.

The preterm infants recruited in the study likewise were receiving low dependency care. Few of them were receiving non-invasive ventilatory support in the form of high flow nasal cannula oxygen. The rest of the infants were breathing in air unaided and were enterally fed. The scans were again performed in the postprandial phase.

The near term or term infants with seizures were recruited in the acute phase of their presentation to the unit. This meant that they were receiving intensive neonatal care in the form of mechanical ventilation, potential inotropic support, multiple intravenous infusions, intravenous antibiotics, and potentially anticonvulsant treatment. The nature of these admissions limited the timing of the study. Apart from gaining parental consent, the fact that most infants were transferred in from another hospital, meant that the infants had already received one or more anticonvulsant medications in the referring hospital.

Most of the infants presenting with seizures had a suspected primary diagnosis of HIE, based on their condition at birth, neurological examination, and clinical examination as described by the Sarnat classification (34). In the instance of strong clinical suspicion of HIE the infants would be reviewed as to whether they were eligible for total body therapeutic hypothermia (TH) with target core body temperatures between 33-34 ºC. This clinical evaluation is based upon the TOBY (TOtal BodY, whole body hypothermia for the treatment of perinatal asphyxial encephalopathy) cooling criteria (43, 368). These clinical criteria reflect the condition of the infant at birth and their neurological presentation/examination; if fulfilled, therapeutic hypothermia can be commenced within the first 6 hours of postnatal life. In the cases of infants delivered elsewhere and transferred in, passive cooling was commenced from the referring hospital within 6 hours and active cooling was initiated by the transport services and continued upon arrival to the NICU at the Rosie Hospital. Most of the patients, 23 out of 29, had a diagnosis of HIE, 19 of which received a 72-hour course of TH. The other three (patients 1, 12, and 28) presented with seizures at a later stage outside the window of the first 6 hours of life. Their condition and clinical evaluation at birth and in the first few postnatal hours did not

warrant initiation of TH. In one patient (patient 20), TH was discontinued, although cooling criteria were fulfilled as there was co-existing group B streptococcal meningitis which was felt to be the main contributing factor in the clinical condition of the infant and that it would not benefit further from TH.

Within the cohort of patients recruited, however, some presented with seizures in the first 48 hours of life without any clinical indication or suspicion of a hypoxic-ischaemic insult in the perinatal period. These patients numbered 5 in total. Patients 16, 25 and 29 had a primary diagnosis of perinatal stroke and presented as previously asymptomatic, low risk infants with seizures. Patient 23 presented with seizures with suspected sepsis on the background of maternal varicella infection close to the delivery. The CSF tested negative for the Varicella-Zoster virus and the MRI showed a mild to moderate dilatation of the ventricles with a small co-existing intraventricular haemorrhage (IVH) and mild changes in the cortical appearance of unclear clinical significance. Patient 27 had poor perinatal adaptation and a seizure at 30 minutes of life, which was attributed to co-existing hypoglycaemia. The MRI showed small foci of restricted diffusion in the posterior periventricular white matter and otherwise a normally formed brain.

All the infants presenting with seizures had an MRI of the head within the first 10 days of life. This was part of their standard clinical care. The local neuro-radiologist reported the MRI scans. They were also reviewed and reported by Professor Mary Rutherford, expert in perinatal neuroimaging at Kings College London. All the MRI reports mentioned in this thesis are the official reports given by Professor Rutherford.

The clinical details of all the infants recruited in the study can be seen in the following tables 3.2-4. Additional clinical details are also provided in the separate chapters 4, 5 and 6.

Subject ID	GA	Day of Life at Scan	Mode of Delivery	Mode of Ventilation	Background activity of EEG	Clinical Background
Patient 1	38+1	10	Vaginal Ventouse	SVIA	Continuous	HIE II, TH, seizures, phenobarbitone
Patient 2	40+1	5	SVD	SVIA	Continuous	HIE I, TH, self-limiting seizures
Patient 3	-	-	-	-	Discontinuous	Not scanned
Patient 4	40+4	5	SVD	HFOV	Discontinuous with seizures	HIE III, TH, seizures, phenobarbitone, clonazepam, phenytoin
Patient 5	40+4	6	SVD	SVIA	Discontinuous	HIE II, TH, seizures, phenobarbitone
Patient 6	40+4	5	EmLSCS	SVIA	Discontinuous	HIE II, TH, seizures
Patient 7	39+3	4	SVD	HFOV	Discontinuous	HIE III, TH, seizures, phenobarbitone
Patient 8	41+6	5	Ventouse	SVIA	Continuous	HIE III, TH, seizures, phenobarbitone
Patient 9	35+6	2	EmLSCS	SVIA	Continuous	HIE II, TH
Patient 10	41+3	3	SVD	SIMV Vg	Continuous	HIE III, TH, seizures, phenobarbitone, clonazepam, phenytoin
Patient 11	40+5	19	SVD	HFNC	Continuous	HIE II, TH
Patient 12	34+5	1	EmLSCS	SIMV Vg	Continuous	HIE III, TH, seizures, phenobarbitone
Patient 13	41+5	4	SVD	SVIA	Mild discontinuity	HIE III, TH, seizures, phenobarbitone, clonazepam
Patient 14	38+6	7	EmLSCS	SIMV Vg	Mild discontinuity	HIE III, TH, phenobarbitone, clonazepam
Patient 15	40+6	1	SVD	SIMV Vg	Discontinuous with seizures	HIE III, TH, phenobarbitone
Patient 16	38+4	2	SVD	HFNC	Continuous	Neonatal stroke: Lt temporal lobe infarct, seizures, phenobarbitone
Patient 17	41+6	1	EmLSCS	SIMV Vg	Continuous	HIE II, TH, phenobarbitone, midazolam
Patient 18	37+2	1	EmLSCS	SIMV Vg	Discontinuous with seizures	Feto-maternal haemorrhage, Lt MCA infarct, HIE II, TH, phenobarbitone
Patient 19	37+5	1	EmLSCS	SIMV Vg	Continuous	HIE II, TH, midazolam
Patient 20	41+3	1	SVD	SIMV Vg	Continuous with seizures	GBS meningitis, B/L stroke, HIE III, TH, phenobarbitone, midazolam
Patient 21	39	2	EmLSCS	SIMV	Limited interpretation	HIE II, TH, seizures, phenobarbitone, clonazepam
Patient 22	38+6	2	SVD	SIMV Vg	Discontinuous	HIE II, TH, seizures, phenobarbitone, phenytoin
Patient 23	37+5	3	SVD	SVIA	Continuous	Apnoea, maternal varicella, none
Patient 24	42	7	EmLSCS	HFNC	Continuous with seizures	HIE grade III, TH, seizures, phenobarbitone
Patient 25	40	3	Vaginal Forceps	SVIA	Continuous	Rt MCA, seizures, phenobarbitone
Patient 26	40+3	3	Vaginal Ventouse	SVIA	Discontinuous	HIE I, TH, seizures, phenobarbitone
Patient 27	37+5	3	EmLSCS	SVIA	Discontinuous	Neonatal Hypoglycaemia, seizures, none
Patient 28	37+4	3	EmLSCS	SVIA	Continuous	HIE I, TH, seizures, phenobarbitone, clonazepam
Patient 29	41+3	3	EmLSCS	SVIA	Continuous	Lt MCA, seizures/phenobarbitone

Table 3.2: Clinical details of recruited patients presenting with seizures. (GA: gestational age, SVD: spontaneous vaginal delivery, EmLSCS: Emergency low segment Caesarean section, SVIA: self-ventilating in air, SIMV: synchronised intermittent mandatory ventilation, Vg: volume guarantee, HFOV: high frequency oscillatory ventilation, HFNC: high flow nasal cannula, HIE: hypoxic ischaemic encephalopathy, TH: therapeutic hypothermia, Lt: left, MCA: middle cerebral artery, GBS: group B streptococcus).

Subject ID	GA	GA at scan	Mode of Delivery	Mode of Ventilation	Clinical Background
Control 1	36+1	39	EmLSCS	SVIA	Establishing feeds
Control 2	37+0	37+3	EmLSCS	SVIA	Establishing feeds
Control 3	38+0	38+4	SVD	SVIA	Establishing feeds
Control 4	37+5	38+0	Forceps	SVIA	Establishing feeds
Control 5	35+1	36+2	EmLSCS	SVIA	Establishing feeds
Control 6	41+5	42+2	EmLSCS	SVIA	Establishing feeds
Control 7	36+0	36+5	EmLSCS	SVIA	Establishing feeds
Control 8	40+1	40+2	Forceps	SVIA	Establishing feeds
Control 9	38+5	40+2	Forceps	SVIA	Establishing feeds
Control 10	37+2	37+3	SVD	SVIA	Establishing feeds

Table 3.3: Clinical details of the healthy controls recruited in the study. Abbreviations as in table 3.2. (IVH: intraventricular haemorrhage, PVL: periventricular leucomalacia)

Subject ID	GA	GA at scan	Mode of Delivery	Mode of Ventilation	Clinical Background
Preterm 1	31+5	34+3	Forceps	SVIA	Normal
Preterm 2	30+2	32+2	EmLSCS	SVIA	Normal
Preterm 3	30+6	32+3	EmLSCS	SVIA	Normal
Preterm 4	30+0	35+0	EmLSCS	HFNC	Normal
Preterm 5	30+4	32+4	EmLSCS	SVIA	Normal
Preterm 6	23+3	35+3	SVD	HFNC	Normal
Preterm 7	28+3	34	EmLSCS	HFNC	Cystic PVL
Preterm 8	28+3	34+2	EmLSCS	HFNC	Rt IVH
Preterm 9	28	32+4	SVD	HFNC	Normal
Preterm 10	27+5	29+3	SVD	HFNC	Normal
Preterm 11	27+5	29+6	SVD	HFNC	Normal
Preterm 12	29	30+4	EmLSCS	HFNC	Normal
Preterm 13	28+1	31+3	SVD	HFNC	Lt Grade II IVH
Preterm 14	24+6	Not scanned	EmLSCS	N/A	B/L IVH Grade II
Preterm 15	30	32+3	EmLSCS	HFNC	Normal
Preterm 16	29+6	30+3	EmLSCS	SVIA	Normal
Preterm 17	28+2	34+3	SVD	SVIA	Normal
Preterm 18	25+1	Not scanned	EmLSCS	N/A	Lt Grade III IVH with HPI
Preterm 19	29+6	36+2	SVD	SVIA	B/L cystic PVL
Preterm 20	32+1	38+1	SVD	SVIA	B/L cystic PVL
Preterm 21	29+4	30+4	SVD	HFNC	Normal
Preterm 22	28+3	34+2	SVD	SVIA	Normal
Preterm 23	27+1	Not scanned	SVD	HFNC	Normal

Table 3.4: Clinical details of the preterm infants in the study. Abbreviations as in able 3.2.

3.2 Equipment and Study Conduction

3.2.1 Simultaneous video-EEG & DOT

The Cambridge Centre for Perinatal Neuroscience (CCPN) has a long-term collaboration with the University College London Biomedical Optics Research Lab (UCL BORL), collectively known as neoLAB. The UCL BORL have developed their own in-house diffuse optical tomography (DOT) system, the NTS Optical Imaging System (369), which is also commercially available (see Fig. 3.2.1).

Continuous wave DOT data were acquired using the UCL NTS Optical Imaging System. This device employs 16 dual-wavelength laser diode sources operating at 780 nm and 850 nm, and 16 avalanche photodiode detectors (APDs). Each source is modulated at a different frequency between 2-4 kHz. The amount of light which can be coupled into the scalp is limited for safety reasons, and thus the device maintains an output intensity below that of the eye safety limit (10 W/m2 for NIR wavelengths in continuous operation (British Standard EN 60825-1:2007)). The sources are illuminated simultaneously, and a Fourier transform of the transmitted light recorded at each detector determines the modulation frequency and thus the origin of the detected light. The arrangement of source-detector positions on the head determines the spatial resolution of the final image. The sampling frequency rate of the device is 10 Hz.

Video-EEG data were obtained using a BrainVision V-Amp system (Brain Products GmbH, Germany). During the conduction of the pilot study, for the first few patients recruited, the Micromed SystemPlus clinical EEG system (Micromed S.p.A., Italy) was used. The sampling frequency of both systems is 250 Hz.

To allow simultaneous DOT-EEG recordings with full scalp coverage, an integrated infant head-cap was employed. The sources and detectors were coupled to the infants' heads using 32 optical fibre bundles (Loptek GmbH & Co. KG) attached to a soft, flexible head cap (EasyCap, Germany) (see Fig. 3.2.2). Caps of different sizes in circumference were manufactured by EasyCap to match the age and size of each infant's head. The range in head circumference during my study was 28-38cm, in 2cm intervals. The optical fibres were positioned within the cap at a subset of locations taken from the 10–5 system (370). These locations were chosen to maximize the density of DOT source–detector pairs (channels) with optimal separations between 20 and 40 mm while also

covering the whole scalp. This distance is large enough to sample brain tissue and small enough for enough light to be detected. A relative experimental rule-of-thumb, is that a source-detector pair separated by a distance d will only be sensitive to a depth of approximately d/2 (371). The array design, which provides a total of 58 dual-wavelength DOI channels, is shown in figure 3.2.2 and was designed by Laura Dempsey (LAD) (MPhil student in Cambridge at the time) and Dr Chuen Wai Lee (CWL) (clinical research fellow at the time) in 2012 prior to the onset of the pilot study.

For the EEG recordings, 13 ring Ag/AgCl EEG electrodes were coupled to the head cap in the initial studies and following that ring EEG electrodes were coupled to the head cap (see Fig. 3.2.2). The positions of the EEG electrodes conformed to the standard neonatal EEG montage (Fp1, Fp2, Fz, T3, T4, C3, Cz, C4, Pz, O1, O2) with reference and ground electrodes at AFpz and FC1 respectively (see Fig. 3.2.2).

As mentioned before DOT is a safe and non-invasive technique that uses light in the near-infrared spectrum relying on two principal phenomena, (i) the relative transparency of biological tissue in this region of the spectrum and (ii) the presence of compounds in tissue whose absorption of light is oxygen concentration dependent.

Figure 3.2.1: The combination of systems used for the study on a portable trolley: (A), the EEG V-Amp (B), and the UCL NTS optical imaging system (C). Image from personal file.
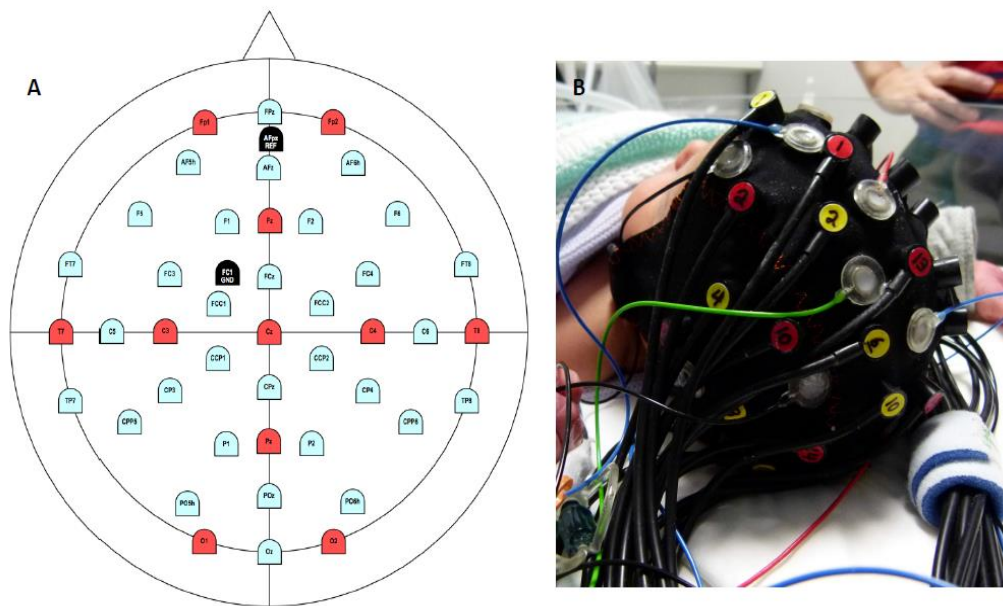
Figure 3.2.2: DOT-EEG whole head array and cap: (A) The design layout of the DOT sources and detectors (blue) and EEG electrodes (red and black) defined using the international 10-5 positions, (B) DOT-EEG flexible cap with DOT sensors (red: sources, yellow: detectors) and EEG electrodes (clear rings) on an infant control subject during a study (following parental permission). Image from personal file.

3.2.2 Data Acquisition

The data acquisition was performed in the NICU, by the infants' cot side. The only exception to this was that some of the healthy control infants in the pilot study were recruited in the postnatal ward. For dimmer lighting and a relatively noise-free environment, these infants were scanned in the baby scan room, in the Evelyn Perinatal Imaging Centre (EPIC).

Following informed parental consent, the equipment was prepped and the right size head cap per infant was selected. This was according to the occipital-frontal circumference (OFC), right to left auricular distance (AA) and the nasion to inion distance (NI). Note that prior to approaching the parents for consent, with permission by the medical team, the infant would be examined with special focus on the inspection of the head for any areas of oedema, soft tissue swelling (e.g. haematomas, caputs, etc.). The anterior and posterior fontanelle, as well as the sutures, were palpated to ensure a normal head examination without suspicion of fractures or haematomas. If the exact sized head cap was not available, the nearest smaller size would be selected; for instance, if an infant's head circumference was 33 cm, the head cap with a 32-cm head circumference rather than the 34-cm one would be used. Once the correct size head cap was selected, the optical fibres based on the whole-head array were attached onto it (see Fig. 3.2.2(A)). At the surface of the optical fibres adhesive foamy circular pads were applied to achieve a better fit over the infant's head and avoid trauma, as the surface of the optical electrode is a flat, hard disc (see Fig. 3.2.3). The EEG leads were attached last and connected to the V-Amp.

The above preparation would take place in the lab and subsequently the equipment was taken to the infant's cot side (see Fig. 3.2.1(A)). The infant's head was cleaned with sterile gauze soaked in sterile water, and then dried. The cap was applied and the NTS and EEG systems would be switched on. Soft straps attached to the head cap would be strapped underneath the infant's mandible. Abrasion gel and conductive paste were applied to ensure EEG electrode impedances were kept below 5 kΩ. ECG leads would also be applied to monitor the HR trace and to also facilitate artefact recognition in the EEG trace. Once the NTS was warmed up, checks of the source light emission would be performed and checks of the EEG electrodes impedance would be checked on the separate EEG system. The camera would be attached or stabilised at an optimum position around

or inside the infant's cot (see Fig. 3.3.3 (A)) and linked to the EEG system. Once all checks were done, the data acquisition would start with the simultaneous onset of both systems. The DOT and EEG systems were synchronised using a custom-made external trigger generator, developed by UCL BORL.

Preparation of the head gear required at least 15 minutes. Application of the head gear onto the infant's head and initiation of the study required 10 to 20 minutes. There was only one occasion where the head gear prepared was not fitting well and a different size head cap had to be prepared, causing a 20-minute delay. No adverse events were noted around or during the studies. There was great acceptance of the research study by the medical and nursing stuff showing support and facilitating its conduction. Parents had the option of being present throughout the conduction of the study with the only limitation not to stimulate (i.e. stroke) their infant during the scan. On the contrary, they were encouraged to pacify their infant in the beginning of the study if they appeared overly alert or unsettled. Approaching the infants in the postprandial phase, making a cocoon/nest, and swaddling them aided in acquiring better quality data with fewer motion-related artefacts. The latter mostly applied to the healthy term or preterm infants, whereas the patient cohort group were less active.

Throughout the conduction of the scans, clinical care continued undisturbed. The duration of the recordings varied from 45 to 240 minutes. I was present throughout the recordings, monitoring the infant, overseeing the quality of the signal, making any necessary adjustments, and noting any significant events (e.g. seizures, desaturation, cares being given by the nurse, suction).

Figure 3.2.3: Images of infants during the study conduction. (A) Preterm infant breathing in air unaided. (B) Term infant with HIE presenting with history of perinatal asphyxia and seizures, ventilated and whilst receiving therapeutic hypothermia (note the cooling blanket the infant is wrapped in). Images have been acquired following parental permission. Images from author's personal file.

3.2.3 Data Analysis

The EEG recordings were assessed by using the BrainVision Analyser (Brain Products GmbH) and EEGLAB software packages (372). Part of simple pre-processing steps were the application of a high pass filter at 0.5 Hz and a low pass filter at 70 Hz, with an added notch filter at 50 Hz. The ones with an abnormal trace or seizure-like activity were reviewed by Dr Andrew Michell (AWM), Clinical Neurophysiologist, who reported on the quality of the recording, the background state (e.g. continuous, discontinuous, or burst suppressed), the presence of any asymmetry between the two hemispheres, presence of cyclicity (between awake and sleep state) and detection of any abnormal rhythmic activity or seizures.

Using MATLAB and a synchronisation algorithm developed by RJC, the EEG and DOT datasets were synchronised, and events were marked (for instance in the presence of burst activity: burst onset and offset, seizures: seizure onset and offset). The synchronised and marked DOT data were then loaded on Homer2, a NIRS processing toolbox (www.homer-fnirs.org) for visual inspection. Homer2 is a MATLAB-based toolbox with a graphical user interface that offers a variety of options including visualisation of the NIRS signal, artefact rejection and extraction of the haemodynamic response to a specific stimulus (373). First, channels were excluded from each dataset based on a simple optical intensity threshold, and on visual inspection of their frequency content (this was necessary due to the impact of high-frequency oscillatory ventilation, in infants that required this for ventilatory support). If more than 15 (of 58) channels were excluded from any one DOT dataset, that dataset was excluded from any further analysis. The raw intensity data were then converted to optical density, and periods of motion artefact were identified using a combination of visual inspection and Homer2 motion artefact detection approaches (374). The latter was not applied in all paths of the analysis but mainly for the burst suppression analysis (see Chapter 5). The final steps of the processing differed for the different parts of the analysis. Please see the relevant chapters 4, 5, and 6 for details of the analysis in the group of infants with seizures, burst suppression, and stroke, respectively.
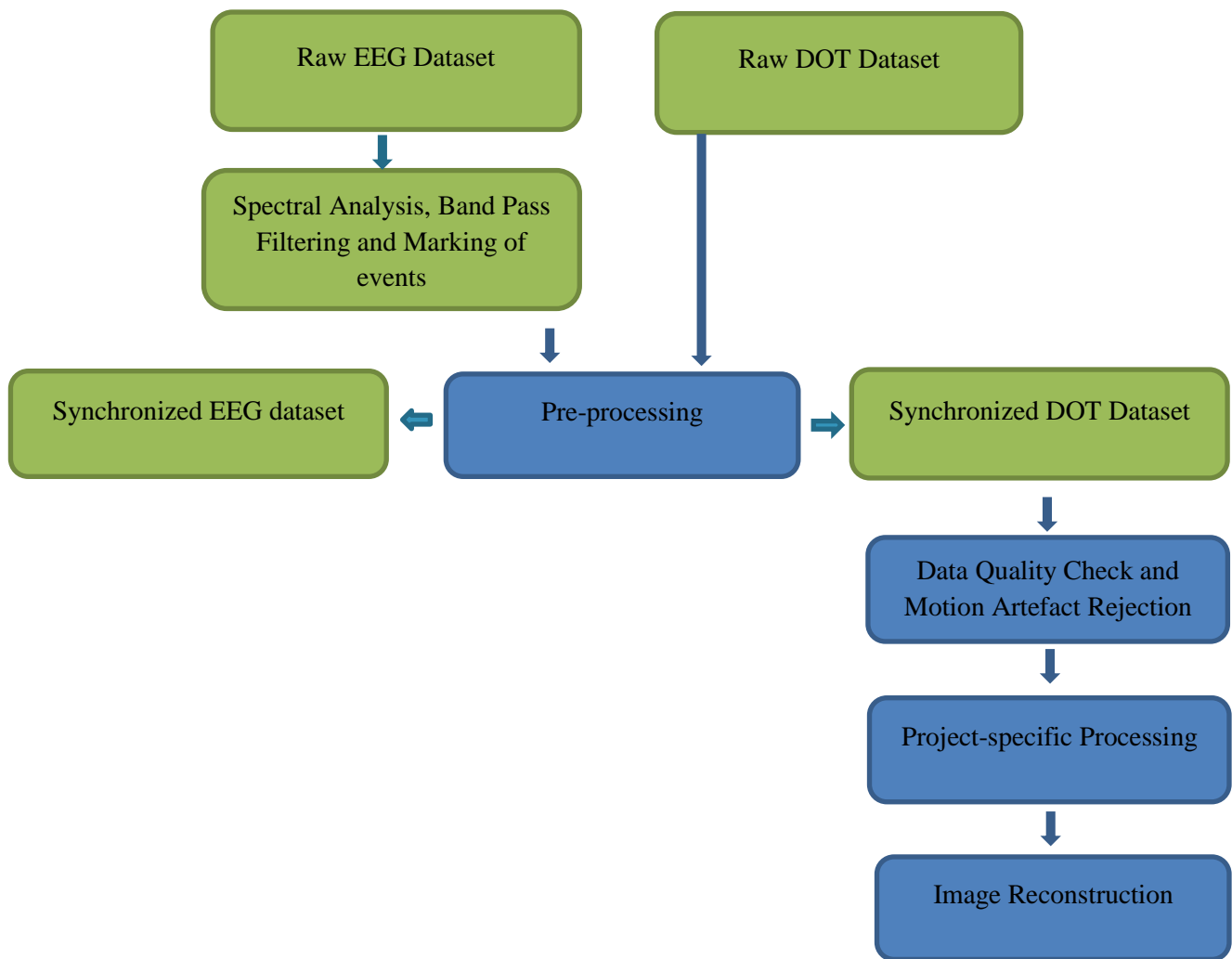
Figure 3.2.4: Graph of the different pre-processing and processing steps.

Chapter 4: Cortico-vascular Changes in Neonatal Seizures

4.1 Optical methods and EEG on neonatal seizures

Near-infrared spectroscopy (NIRS) has been used in the investigation of seizures to understand the associated haemodynamic phenomena and develop early detection tools. As mentioned previously (section 2.2.3 of chapter 2), an increase in neuronal activity leads to increase in metabolic demand, thus causing local vasodilatation, increased CBF and oxygenation, via a process known as neurovascular coupling. This mechanism is not fully understood but it is believed that vasoactive neurotransmitters, released during neural activity, trigger the contraction or dilatation of the cerebral blood vessels depending on localised energy demands (375). The combination of EEG and NIR techniques allows the study of neurovascular coupling, especially in the occurrence of overt electrical phenomena such as seizures.

Steinhoff et al., demonstrated that coupling NIRS and video-EEG in the pre-operative assessment of two patients of temporal-originating intractable focal epilepsy, can aid targeted neurosurgery. They showed marked desaturations in accordance with the seizures. These were particularly observed in the postictal phase on the ipsilateral region with inconsistent findings on the contralateral side (376). Sokol et al., showed that data from combining a single sensor NIRS and EEG could differentiate complex partial seizures from rapidly evolving secondary generalised seizures. They demonstrated that there was an increase in cerebral oxygenation during partial seizures with no change of peripheral oximetry. In contrast they observed a decrease in cerebral oxygenation during the generalised seizures with a concomitant decrease in peripheral pulse oximetry (377). This was a study based on a single probe NIRS system (Invos^{TM} system, cerebral/somatic oximeter, Covidien AG, USA) which provides a single measurement of cerebral oxygenation from the forehead.

In 2007, Zhao et al., measured intrinsic optical signals from human cortex intra-operatively during focal seizures. They showed an increase in both cerebral blood volume (CBV) and HHb concentration preceding and during seizure activity, suggesting an inadequate supply to meet the metabolic demands (378). The group used optical imaging in two wavelengths to achieve these measurements but in an alternating pattern rather than simultaneously, which introduces potential variations between measurements and artefact, ultimately affecting the calculations of Hb concentrations.

Although there is supporting literature on the neurovascular coupling in asphyxiated neonates from the early nineties (162, 379), Wallois et al., were the first to demonstrate evidence of haemodynamic changes in association with seizure-like activity in the neonatal period combining NIRS and EEG (380). The group used a device with a limited number of NIRS channels over the parietal areas emitting light simultaneously at two wavelengths (using a frequency domain spectrophotometer device) for the measurement of the haemodynamic changes in combination with EEG. They noted a paradoxical increase in HHb prior to the onset of the event followed by its decline and an increase in HbO_2 and HbT concentration during the seizure-like activity (see Fig. 4.1.1). This could be explained by a regional increased metabolic rate driving a rapid increase in CBV, which is insufficient to achieve the expected washout of HHb, as the one noted in functional activation studies (328). This haemodynamic pattern has also been demonstrated on the rat neocortex in correlation to inter-ictal activity using multi-wavelength NIR methodologies (optical recording of intrinsic signals-ORIS) (381).
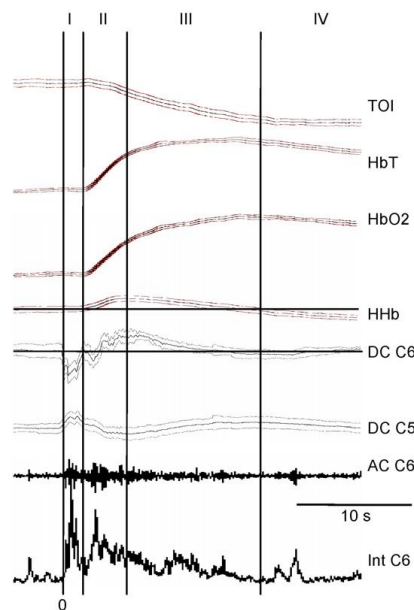
Figure 4.1.1: Representation of the changes in tissue oxygenation index (TOI), HbT, HbO_2 and HHb in response to seizure activity in the neonatal period. This graph shows the different phases in relation to seizure activity: phase (I) corresponds to no haemodynamic changes right after the seizure onset, phase (II) to the increase in HbT, HbO_2 and HHb, and decrease in TOI, (III) to a plateau of HbT, HbO_2 and HHb, and further decrease in TOI and (IV) to a plateau and gradual return to the baseline following the seizure offset. Adapted from reference (380).
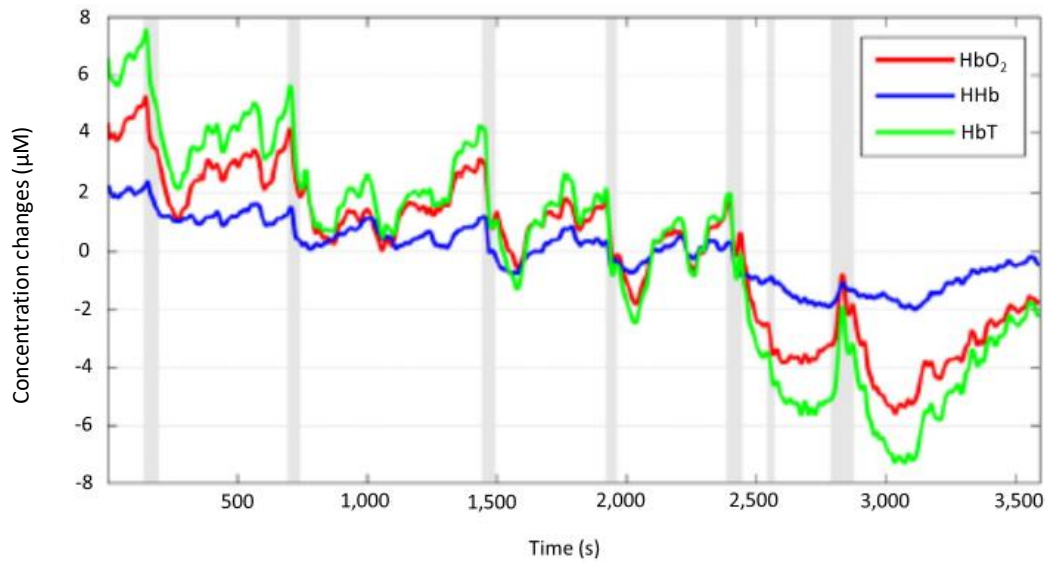
Figure 4.1.2: Graph showing the average changes relative to the changes of HbO$_2$ (red), HHb (blue) and HbT (green) concentrations (y axis) during seizure activity (grey shaded area) over time (in 3,600 s, x axis), for one-hour recording. Adapted from reference (365).

Based on the pilot study conducted prior to my MD project, the first ever diffuse optical tomographic images of the cortical haemodynamic response to neonatal seizures were reported (365). This study of an infant in the first few days of life with severe HIE used the combined EEG and DOI methodology described in chapter 3. Seven discrete seizures were identified on the EEG during the recording. The relative changes in concentration of the HbO$_2$, HHb, and HbT were calculated and utilised for the reproduction of images (see figures 4.1.2 and 3). On average, across all channels, there was a consistent increase in all three haemodynamic parameters in response to the seizure activity. There was variation in the magnitude of changes per type of haemoglobin. Clear spatial variation was also apparent across different cortical locations, and this spatial pattern remained consistent across most seizure events (365).
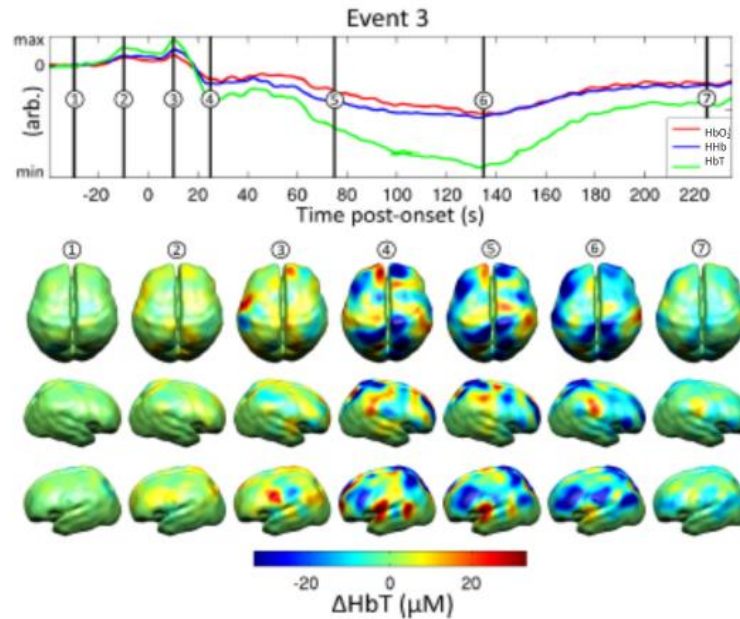
Figure 4.1.3: A series of DOT images showing the changes in HbT observed at different phases of a single neonatal seizure 50-seconds long in duration. The top of the image is showing the changes in concentration of the oxy (red), deoxy (blue) and total (green) haemoglobin before, during and after the seizure. The lower part of the image demonstrates the spatial distribution of the changes across the cortex. Note the characteristic rise in all three parameters 10 s prior to the seizure onset, the peak at 10 s into the seizure and the beginning of their decrease prior to the offset of the event. A marked decrease in HbT lasts for several minutes after the offset of the seizure. (Numbers 1 to 7 on the graph and over the DOT images signify the following: 1-30 s prior to seizure onset; 2-10 s prior to seizure onset; 3-10 s after seizure onset; 4-25 s after seizure onset; 5-25 s after seizure offset; 6-85 s after seizure offset; 7-175 s after seizure offset). Image adapted from reference (365).

The aim of this part of the project was to explore the cortical haemodynamic changes observed during electrical seizure activity in the term neonatal population.

4.2 Patients and Methods

4.2.1 Patients and Data Acquisition

Newborn infants presenting with seizures in the first 72 hours of life were recruited to the study following informed parental consent as described in section 3.1.1 of chapter 3. The video-EEG and DOI device were used in combination to scan the infants whilst receiving acute neonatal clinical care. The recording period varied from 45 to 240 minutes. Depending on the day of recruitment and their clinical status, some infants had more than one scan, performed on consecutive days. No adverse events were recorded during the study and the scans were well tolerated throughout without interfering with the clinical management and treatment being delivered.

4.2.2 EEG Data Analysis

During the conduction of the study, there was continuous monitoring of the infant and the quality of the data being recorded. Simultaneously, the EEG trace was being reviewed throughout its recording for the detection of any artefact, abnormal rhythm, or seizure-like activity. A detailed timesheet was kept, reporting all the important events during the recording from a clinical and data-quality point of view. In the instance of any abnormal EEG trace detection, the rest of the observations and physiological parameters, such as peripheral pulse oximetry, mean blood pressure, heart or respiratory rate were noted. Additionally, any abnormal or unusual infant behaviour, such as unusual breathing pattern, stereotypical movements (i.e. lip smacking, hiccups, cycling movements of lower limbs) were noted.

The EEG recordings of the infants with a pathological clinical background were routinely reviewed and reported by Dr Andrew Michell (AWM), Clinical Neurophysiologist. The EEG data containing suspected abnormal rhythms (as identified during data acquisition), were brought to his attention for reporting. In the instance of identified seizures, the duration, the onset and offset, and the change in frequency during the seizure activity were noted. The exact timings of the events were then used as markers on the DOT signal for further processing as described in the following section.

4.2.3 DOT Data Analysis

Using MATLAB, the EEG and DOT datasets were synchronized to the first point in time of parallel data acquisition and the seizure onset and offset markers were transformed to the DOI time-base. Using functions from the Homer2 NIRS processing toolbox (www.homer-fnirs.org) (373) and MATLAB, the DOT data were pre-processed prior to extracting the haemodynamic response to seizure activity. The seizure onset and offset timings were marked against the DOT signal. The DOT data were low pass filtered at 1 Hz to eliminate heart rate and high frequency interference, which could be generated by equipment in the clinical area, such as the ventilator and/or intravenous pumps. The raw optical intensity data were then converted to optical density for further visual inspection and artefact rejection processing (374). For channel-wise visual inspection and analysis, the optical density data were converted into changes in concentration of HbO_2, HHb and HbT using the modified Beer-Lambert law and a pathlength factor of 4.9 (382). The fluctuations in the haemodynamic signal were then inspected for any obvious deviation from the baseline in association with the seizure activity.

4.3 Results

4.3.1 Clinical Details

The total number of infants presenting with seizures and recruited into this study was 29. Amongst these, 5 infants were studied whilst having seizures. These were patient 4, 15, 18, 20 and 24. The clinical details and the results showing the haemodynamic response to seizures in patient 4 had already been described and published prior to this MD project, as a pilot study (please see reference (365)).

Patient 15

Patient 15 was a female infant born unexpectedly in a very poor condition, following induced vaginal delivery at 40+5 weeks of gestation in a local district hospital. Her birth weight was 3216 grams. This was a low risk pregnancy with no antenatal concerns and the first baby to this mother. She was born unresponsive with no respiratory effort or heart rate. The cord was wrapped around her neck. She was given full resuscitation including intubation, ventilation, cardio-pulmonary resuscitation with three rounds of Adrenaline, O negative blood and bicarbonate. The APGAR scores were very poor: 0 at 1 minute, 0 at 5 minutes and 2 at 10 minutes. The initial lactate was 20 and pH 6.6. She started seizing right after being resuscitated and was loaded with intravenous phenobarbitone (20 mg/kg). She was urgently transferred to the Rosie NICU and therapeutic hypothermia was commenced as a follow up of passive cooling since birth.

 On admission, she was ventilated and exhibited abnormal neurology; hypotonia, posturing, absent gag reflex and fixed, dilated pupils. Her aEEG showed burst suppressed pattern. On day 2 of life she continued to have seizures associated with profound desaturations and bradycardias, for which she received a further dose of phenobarbitone.

 In view of poor condition at birth, ongoing intractable seizures, no improvement in neurological status, fixed, dilated, non-responsive pupils, a joint decision with the family was made for re-direction of care. Following this, she was transferred to a hospice and intensive care was withdrawn. The MRI showed severe abnormalities within the basal ganglia, thalami, posterior limb of the internal capsule (PLIC), brainstem and cortex consistent with a severe acute hypoxic ischaemic insult. These imaging findings were reported to be in keeping with a likely very severe global neurodevelopmental impairment.

Patient 18

Patient 18 was a female infant born at 37+2 weeks of gestation, following an emergency low segment Caesarean section (LSCS) due to irregular foetal heart rate. Labour was induced prior to this due to gestational diabetes mellitus (GDM) and was progressing. There were otherwise no antenatal concerns and the mother was primigravida. The infant was born slightly compromised with irregular breathing and heart rate of 80 bpm (beats per minute). Ventilation support was offered, but she remained pale with the haemoglobin on the gas being extremely low, 25 gr/dl (normal value for a newborn >120 gr/dl) and the blood glucose level of 1.8 (normal value >3.5). A dextrose bolus and O negative emergency blood were administered via an umbilical venous catheter during resuscitation. In view of persistent desaturations, she was eventually intubated and ventilated and was transferred to the Rosie NICU. She required further blood transfusions for anaemia secondary to significant feto-maternal blood loss (Kleihauer test positive), and inotropic support to improve cardiac function. On her neurological examination, she was hypertonic with reduced tendon reflexes, pupils were symmetrically and equally reactive. reacting and equal. She continued to have subclinical seizures on aEEG for which she received Phenobarbitone.

The MRI showed a large stroke in the left middle cerebral artery with involvement of the basal ganglia, thalami and PLIC on the left, and abnormal diffusion in the left cerebral peduncle; findings suggestive of a possible right sided motor impairment. Her examination prior to transfer back to referring hospital revealed a weak palmar grasp and poor head control, but otherwise normal.

Patient 20

Patient 20 was a female infant born at 41+3 weeks of gestation, following a spontaneous vaginal delivery after a low risk pregnancy. There was background of maternal intrapartum pyrexia >39.0 degrees with suspicion of prolonged rupture of membranes. The maternal c-reactive protein (CRP) was markedly raised, 107 and she was commenced on antibiotics. The infant was born in poor condition and was intubated at 8 minutes of age. She made a quick recovery and was extubated shortly after. However, at 4 hours of life, she started exhibiting back arching posturing followed by clonic movements of all limbs, cycling of lower limbs and eye flickering. Each episode was associated with desaturations and on several occasions, she required bag-valve mask inflation breaths to

recover. Most episodes lasted up to 2 minutes (the longest one lasted 10 minutes) with less than 10-minute inter-ictal periods. She received Phenobarbitone and was put on a Midazolam infusion. She was intubated and ventilated for stabilisation. Subsequently, a decision was made to start passive therapeutic hypothermia and to transfer to the Rosie NICU for advanced neonatal care. A lumbar puncture performed prior to the infant's transport was suggestive of meningitis and the infant was already on appropriate antibiotic cover. She was intubated and ventilated for transfer. She continued to have seizures, detected on aEEG monitoring. The Midazolam infusion rate was increased and a further dose of Phenobarbitone and Phenytoin were administered.

In view of a positive initial blood culture for group B Streptococcus (GBS) and the positive lumbar puncture result, the principal working diagnosis was GBS sepsis and meningitis. Therapeutic hypothermia was discontinued. The MRI showed a normally formed brain with bilateral infarction of both posterior parietal, temporal and occipital white matter, and cortex. There was some sparing of the left visual cortex but involvement of both optic radiations. There was additional involvement of the body and posterior aspects of the corpus callosum and abnormal high signal intensity in the posterior thalami. The prognosis based on the MRI findings was that the affected tissue would atrophy with head growth possibly being suboptimal and at increased risk of visual impairment, and later cognitive and behavioural impairments, potentially within the autistic spectrum disorders. On discharge, her neurological examination appeared normal and she was demand breastfeeding.

Patient 24

Patient 24 was a female infant born at 42 weeks of gestation, following an emergency LSCS due to irregular foetal heart rate. She was born in good condition with APGARS of 8 at 1 minute and 10 at 5 minutes. At 3 hrs of age, however, she started having multiple apnoeic episodes with posturing and significant desaturations, highly suggestive of seizures. She was, therefore, transferred to the Rosie NICU for therapeutic hypothermia. Seizures were managed with Phenobarbitone, Phenytoin, and Midazolam.

All investigations including a metabolic screen, blood cultures, CSF cultures (cerebro-spinal fluid), TORCH screen (screen for congenital infections; Toxoplasma, Rubella, Cytomegalovirus, Herpes Simplex Virus) were negative. In view of ongoing persistent seizures, she was put on maintenance Phenobarbitone and had a trial of

Pyridoxine. The MRI revealed widespread abnormal signal intensity within the white matter (involving the PLIC, thalami and corpus callosum) and cortex with an additional focal haemorrhagic lesion over the left occipital lobe. The prognosis given, based on the MRI findings, was that the insulted brain tissue would atrophy with subsequent suboptimal head growth and likely later cognitive and probably some motor impairment. The findings were consistent with a chronic hypoxic ischaemic injury rather than typical of isolated acute hypoxic ischaemic injury. Upon discharge, there was truncal hypotonia and she was still requiring nasogastric tube feeds as unable to complete all bottle feeds.

4.3.2 Seizure detection

Patient 15 was studied on day 2 of life, whilst being ventilated, for approximately one hour. Discrete electroencephalographic seizures were noted during the recording with associated desaturations and bradycardias. They were four in total with minimum duration of 35 seconds and maximum of 76 seconds. The focus of electrographic activity appeared to be the right anterior quadrant cortical region with the seizures becoming generalised soon after their onset.

Patient 18 was recruited and studied on the day 2 of life, whilst being ventilated, for approximately 4,500 seconds. During the study, she was noted to have 5 discrete episodes of seizures which remained purely electro-graphical with no clinical correlation. She received Phenobarbitone towards the end of the study due to seizure identification on the simultaneous aEEG monitoring. The seizure activity during the recording was quite prolonged with a minimum duration of 60 seconds and a maximum of 639 seconds. In total, the infant was exhibiting electrical seizure activity for one third of the period during EEG and DOI data acquisition (1,387 seconds out of 4,500 seconds).

Patient 20 was recruited and studied on day 2 of life for approximately 7,650 seconds. The patient was mechanically ventilated during the scan. During the study, there were 5 discrete seizures in the space of 2 hours. The minimum seizure duration was 29 seconds and the maximum 1,189 seconds (equivalent to almost 20 minutes). In total, there was seizure activity (principally subclinical) for one fifth of the period of data acquisition (1,731 seconds in total out of 7,650 seconds). The ictal activity commenced either from the right hemisphere or the midline and then became generalised involving all channels and both hemispheres. All the events were subclinical with no change in any of the physiological parameters, such as heart rate or peripheral pulse oximetry. She was on a Midazolam infusion at the time. After the study, the infusion rate of Midazolam was increased and a further dose of Phenobarbitone and Phenytoin were administered. An example of the seizure activity detected in patient 20 can be seen in figure 4.3.1.
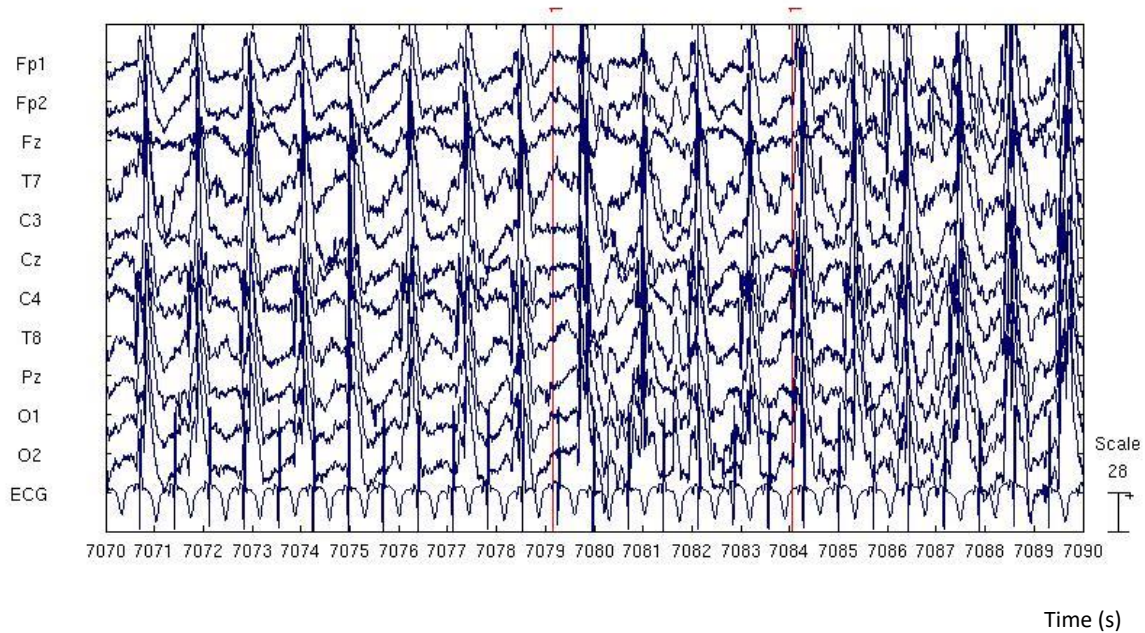
Figure 4.3.1: An EEG snapshot of patient 20. This EEG segment represents part of the 5th seizure detected whilst studying this patient. One can notice the fast, rhythmic activity across the scalp over a 20-second epoch (from the 7070 to 7090 seconds into the EEG recording).

Patient 24 was recruited and studied on day 7 of life for approximately 5,100 seconds. Prior to the onset of the study the infant was on aEEG continuous monitoring. The trace at the time was being reported as exaggerated sleep wake cycle with no clear evidence of seizure activity. No clinical concern regarding any abnormal or stereotypical movement resembling seizure activity had been raised at the time. However, during the study, 15 discrete seizures were identified on the EEG. There was no associated change in physiological parameters. However, during each episode, the infant would start grunting, which was followed by swallowing movements. Towards the end of each seizure, she would become agitated and cry. Saturations were self-maintained throughout whilst she was breathing in air unaided. The minimum seizure duration was 22 seconds and the maximum 114 seconds. There was at least a 100-second inter-ictal period with only two occasions where seizures occurred with only a 20-second recovery phase in between ictal activity. Despite the frequency of the seizure activity, most of the seizures were very short and the overall burden over one hour was 12%. Interestingly in this case the seizures were multifocal and of various frequencies, with seizures on one occasion starting over one hemisphere and a different ictal activity of different frequency starting

on the other hemisphere shortly after. An example of the seizure activity detected in patient 24 can be seen in figure 4.3.2.

Time (s)
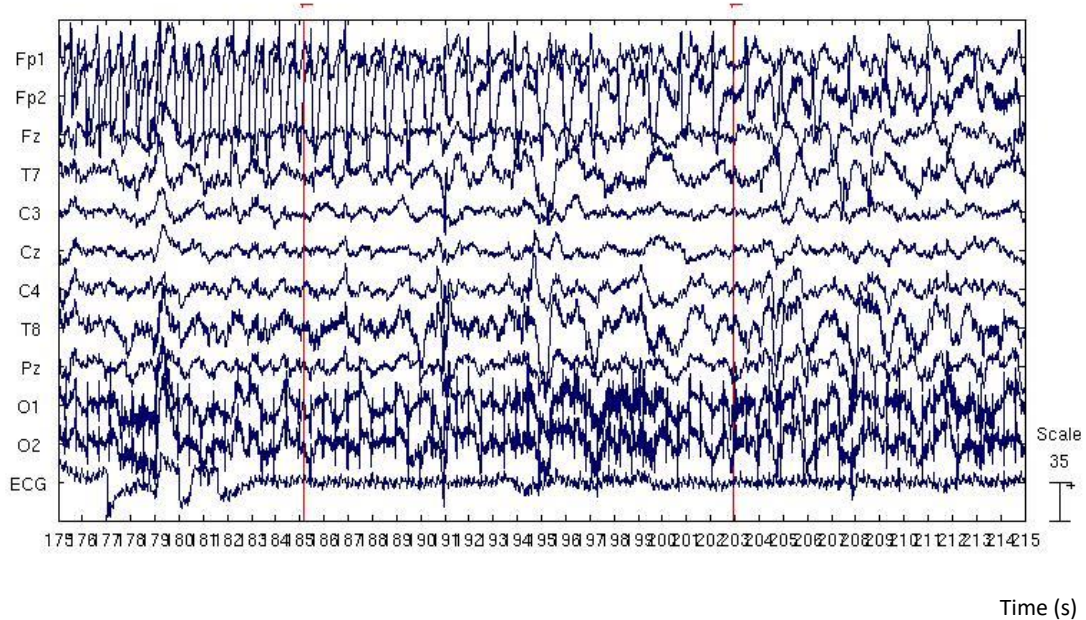
Figure 4.3.2: **An EEG snapshot of patient 24. This EEG segment represents part of the 1ˢᵗ seizure detected whilst studying this patient. There is on-going rhythmic activity over the right anterior region, demonstrated in this graph over a 40-second epoch (from 175 to 215 seconds into the EEG recording).**

A summary of some of the clinical details as well as the exact timings of the seizures for each patient can be seen in the following tables from 4.1 to 4.5.

Subject ID	Background EEG activity	No of Seizures	Focus	Medications	Underlying Clinical Condition
Patient 15	Discontinuous	4	Right anterior quadrant	Phenobarbitone	HIE III, TH
Patient 18	Discontinuous	5	Anterior midline	Phenobarbitone	Feto-maternal haemorrhage, Neonatal stroke: Lt MCA infarct, HIE, TH
Patient 20	Continuous	5	Right hemisphere/midline	Phenobarbitone, Midazolam	GBS meningitis, B/L stroke, HIE III, TH
Patient 24	Continuous	15	Multifocal	Phenobarbitone	HIE grade III, TH

Table 4.1: Clinical and EEG details for patients 15, 18, 20 and 24. Further clinical details can be seen in table 3.1, chapter 3. (HIE: hypoxic ischaemic encephalopathy, TH: therapeutic hypothermia, Lt: left, MCA: middle cerebral artery, GBS: group B streptococcus).

Patient 15			
Seizures	**Seizure onset (s)**	**Seizure offset (s)**	**Duration of event (s)**
1	27	103	76
2	925	978	53
3	1,346	1,419	73
4	2,119	2,154	35

Table 4.2: Timings and duration for each seizure event in seconds for patient 15.

Patient 18			
Seizures	**Seizure onset (s)**	**Seizure offset (s)**	**Duration of event (s)**
1	176	338	162
2	1,788	2,019	231
3	2,109	2,427	318
4	2,689	2,749	60
5	3,000	3,526	526

Table 4.3: Timings and duration for each seizure event in seconds for patient 18.

Patient 20			
Seizures	**Seizure onset (s)**	**Seizure offset (s)**	**Duration of event (s)**
1	3,527	3,572	45
2	4,233	4,262	29
3	4,927	5,055	128
4	5,582	5,922	340
5	6,360	7,549	1,189

Table 4.4: Timings and duration for each seizure event in seconds for patient 20.

Patient 24			
Seizures	**Seizure onset (s)**	**Seizure offset (s)**	**Duration of event (s)**
1	170	216	46
2	558	596	38
3	807	859	52
4	1,165	1,210	45
5	1,400	1,489	89
6	1,877	1,899	22
7	2,512	2,563	51
8	2,711	2,825	114
9	3,782	3838	56
10	3,958	3,980	22
11	4,162	4,186	24
12	4,366	4,400	34
13	4,422	4,476	54
14	4,868	4,895	27
15	4,920	5,020	100

Table 4.5: Timings and duration for each seizure event in seconds for patient 24.

4.3.3 Cortical haemodynamic changes in response to seizure activity

Patient 15

The raw optical signal obtained for patient 15 can be seen in figures 4.3.3 and 4.3.4. These present the optical intensity prior to any processing or artefact rejection steps. Any abrupt change of the signal, usually rapid rise from the baseline, is considered as artefact and not a physiological change.

Figure 4.3.3: The raw optical signals for patient 15, demonstrating the optical intensity changes in µV (y axis) over time (x axis in ms). The different colours correspond to the different optical channels. The black arrow indicates a sudden increase of the signal from the baseline, attributed to movement artefact.
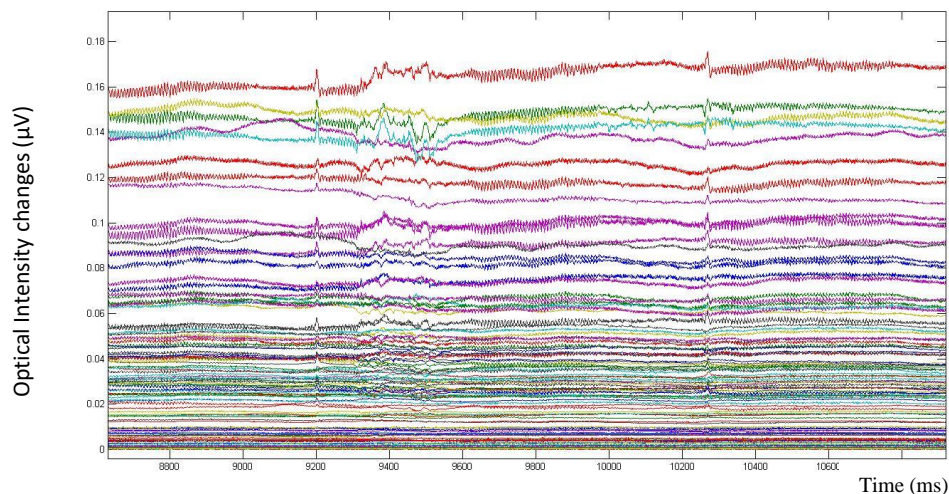
Figure 4.3.4: Close-up of the optical signal for patient 15 showing global, ongoing high frequency interference.

At a first glance, the signal appears good. However, upon closer inspection, there is ongoing high frequency interference, most likely of mechanical origin (see Fig. 4.3.3). Further inspection of the signal and a fast Fourier transform (FFT) analysis to investigate the power spectra of the data was used to assess whether the data captures the expected physiological range of frequencies. This analysis showed the same superimposed oscillation with multiple harmonic peaks in frequencies which cannot be explained physiologically (see Fig. 4.3.5).
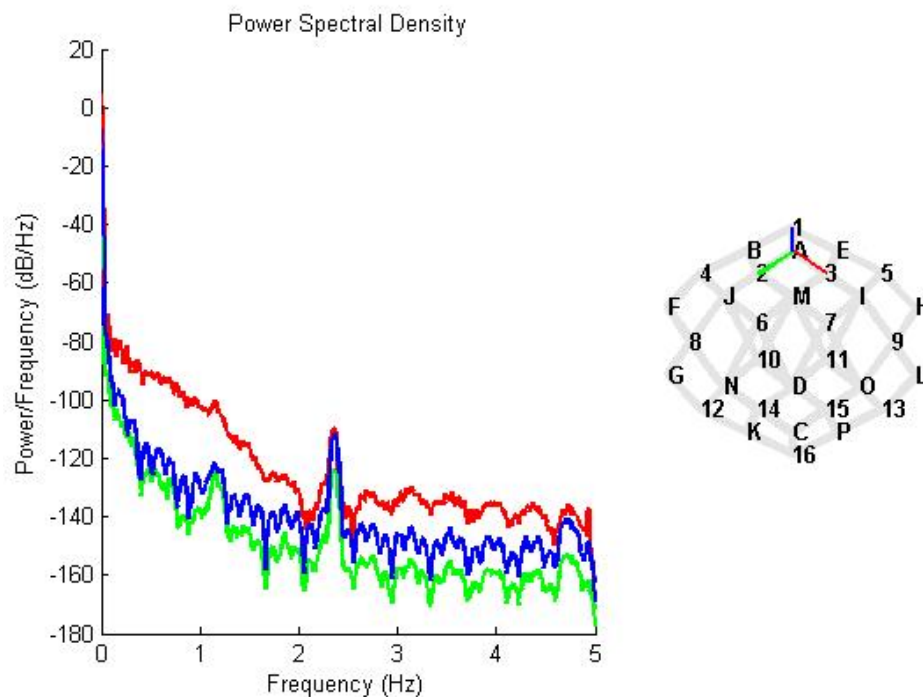
Figure 4.3.5: A sample for the power spectra plot for channels 1, 2 and 3 for patient 15. Apart from the peak in the power between 2 and 2.5 Hz which corresponds to heart rate, most of the features are not physiological and appear as repetitive and stereotypical in the power spectrum, suggesting a non-physiological origin. The graph on the right top hand side is showing the whole head array-design of 16 sources (letters A to P) and 16 detectors (numbers 1 to 16).

Following processing in Homer and MATLAB the haemodynamic response to each seizure event for patient 15 was obtained, despite the issue of high-frequency signal contamination. In total, 16 out of 58 channels were excluded due to either low optical intensity or artefact corruption throughout the recording. By using a lower pass filter of 0.5 Hz instead of the standard 1.0 Hz, the changes in the HbO_2 concentration in relation to seizure event 4 (see Table 4.2) are shown in figure 4.3.6A. These changes related to three randomly selected channels (channels number 27, 43, and 51). Across all 3 channels there is an obvious increase in HbO_2 starting almost 12 s (marked as -1 on the graph in

figure 4.3.6A) prior to the onset of seizure activity (marked as 0 on the graph in figure 4.3.6A) which lasts up to 20 s (marked as 1 on the graph in figure 4.3.6A) and is followed by a more pronounced decrease which lasts for 30 s and essentially returns to baseline in approximately 5 s after the offset of the seizure. However, figure 4.3.6B highlights the ongoing increase and decrease in HbO_2 in-keeping with the background ongoing oscillation independent of ₀˙zure activity.
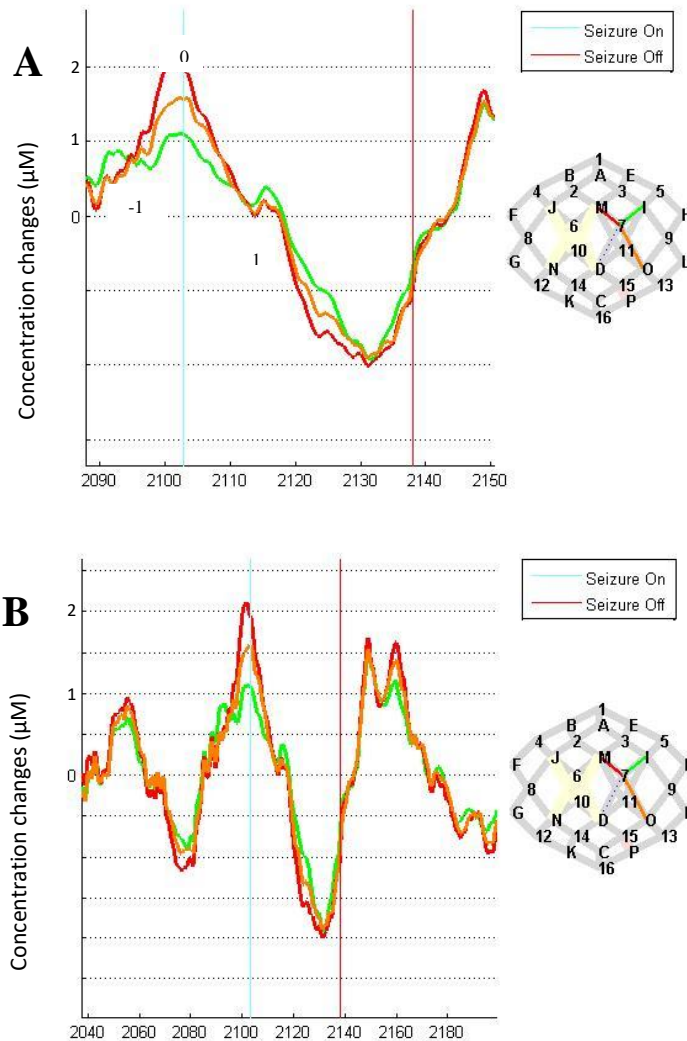
Figure 4.3.6: The relative changes of HbO_2 concentration (y axis in μM) in relation to the seizure activity over time (x axis in seconds), using a lpf of 0.5 Hz for patient 15: (A) shows the increase in HbO_2 concentration (time point -1) prior to the seizure onset (time point 0), lasting for 20 s (time point 1) followed by a decrease and return to the baseline few seconds after seizure offset seen in all randomly selected three channels (right hand side), whereas (B) shows the ongoing HbO_2 fluctuations during the recording independent to the seizure activity (light blue vertical line for seizure onset; red vertical line for seizure offset; right hand side for whole-head array 16 sources (A-P) and 16 detectors (1-16).

No meaningful results were obtained in the extraction of the haemodynamic activity in relation to the seizure episodes noted in patient 15. Overall, there was an

ongoing oscillation of the optical trace irrelevant of seizure activity throughout the recording. The extracted HRFs for each seizure event returned an almost identical pattern, heavily corrupted with artefact (as seen in Fig. 4.3.7).
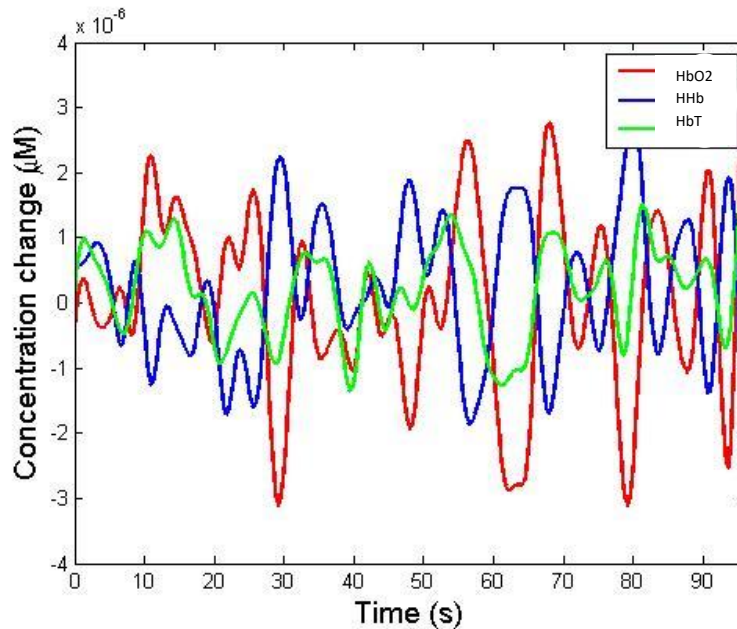
Figure 4.3.7: Graph showing the changes in HbO$_2$, (red line) HHb (blue line) and HbT (green line) concentration (over the y axis in µM) during the seizure event 1 on patient 15 over time (x axis in seconds) for all 42 channels. Time 0 signifies the seizure onset. The duration of the seizure was 35 seconds.

Patient 18

The raw optical signal acquired for patient 18 (see Fig. 4.3.8), prior to any processing or artefact rejection steps, was characterised by a rhythmic almost step-wise superimposed elevation of the trace. Its presence interfered with the onset and offset of the co-existing ongoing seizure activity. An example of the returned results for seizure event 5 which lasted approximately 9 minutes (526 s) (see Table 4.3 for details) can be seen in figure 4.3.9. The observed decrease in all HbO$_2$, HHb and HbT concentrations which become more pronounced 200 s into the seizure activity and continue until the seizure offset can only be attributed to artefact rather than any meaningful physiological change. In the analysis of this signal 16 channels were excluded either due to low intensity levels or excessive noise interference.
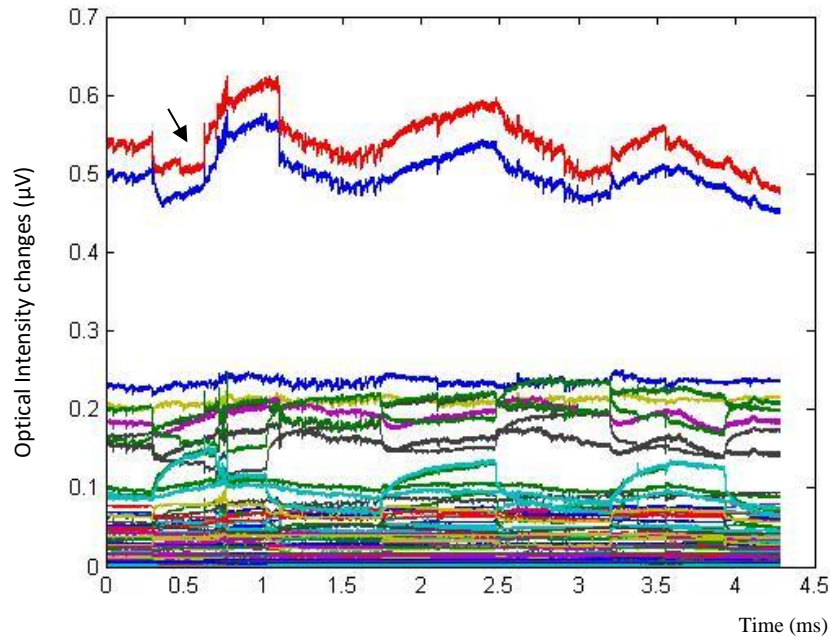
Figure 4.3.8: Graph showing the raw optical signal for patient 18, demonstrating the optical intensity changes in µV (y axis) over time (x axis in ms). The different colours correspond to the different optical channels. Note the black arrow showing the consistent rhythmic interference with the background signal.
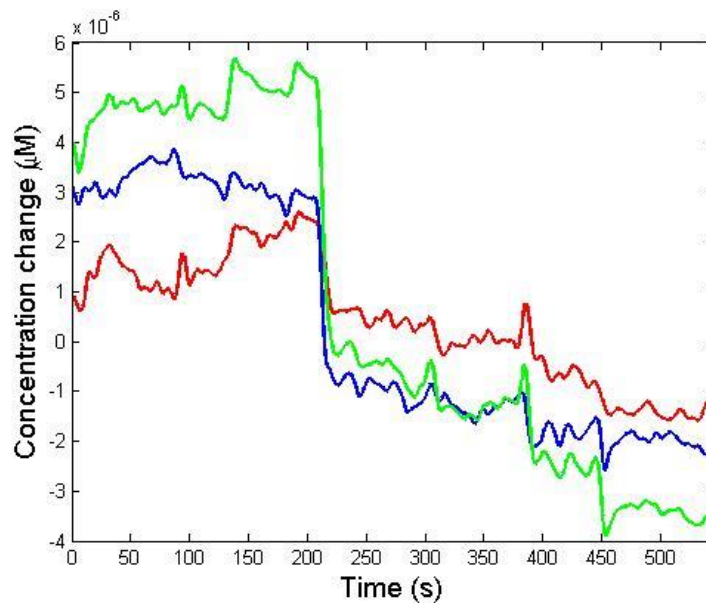
Figure 4.3.9: Graph showing the changes in concentration of all HbO$_2$, (red line) HHb (blue line) and HbT (green line) (over the y axis in µM) during the seizure event 5 on patient 18 over time (x axis in seconds) for all 36 channels. The abrupt nature of the change suggests superimposed artefact.

Patient 20

The optical signal acquired for patient 20 (see Fig. 4.3.10), prior to any processing steps, was also characterised by a rhythmic, step-wise superimposed elevation of the trace. After

further processing, 22 channels were excluded mainly due to motion related artefact. Similarly, its presence interfered with the onset and offset of the co-existing seizure activity (see also Fig. 4.3.11), and therefore no meaningful results in terms of the relative changes in any of the HbO_2, HHb and/or HbT concentrations were obtained.
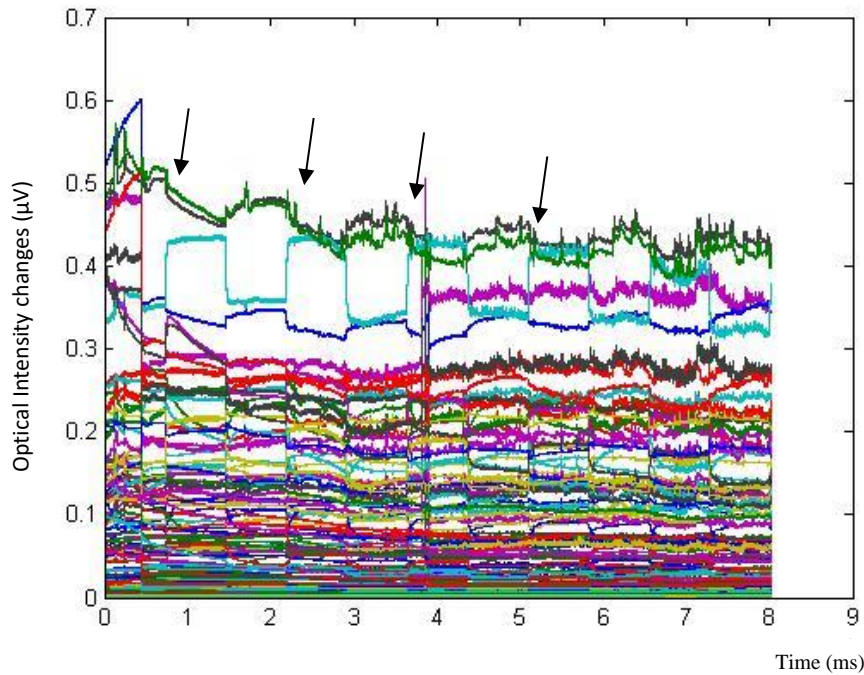
Figure 4.3.10: Graph showing the raw optical signal for patient 20, demonstrating the optical intensity changes in µV (y axis) over time (x axis in ms). The different colours correspond to the different optical channels. The black arrows point to the onset of the step-wise rhythmic elevation of the trace independent to seizure activity.

This elevation in the trace (see Fig.4.3.10, arrows) was persistent throughout the recording and as mentioned before was also present in the optical signal of patient 18. It was occurring approximately every 13 minutes and was 8 to 8.5 minutes long in duration. This was not obvious at the time of data acquisition. The elevation from the baseline is quite dramatic but one may notice that it is not as abrupt as the standard motion-associated artefact (see Fig. 4.3.11).
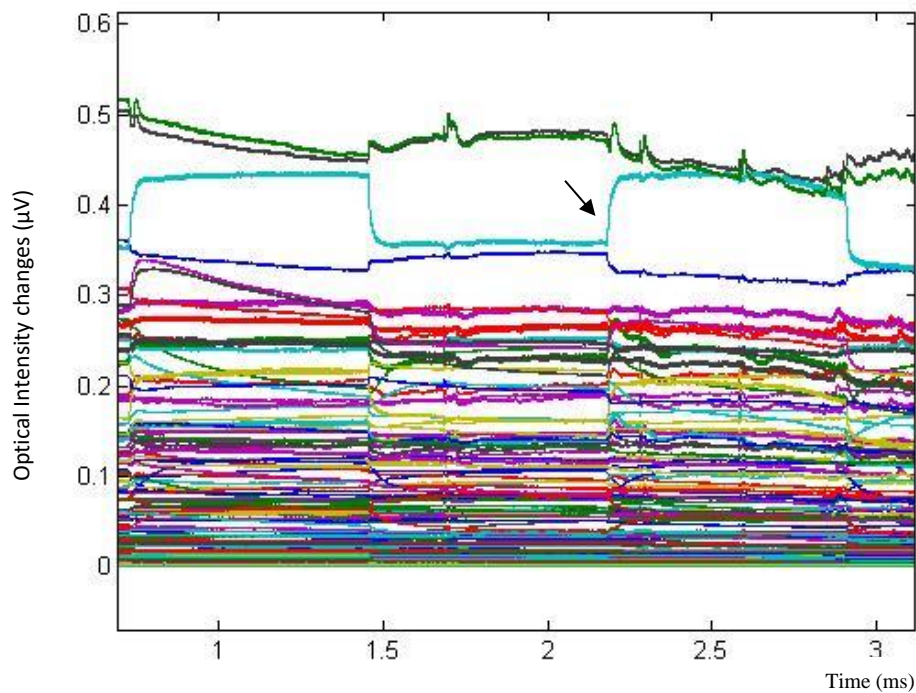
Figure 4.3.11: Close-up of the raw optical signal for patient 20. Note the changes in optical intensity in μV (y axis) over time (on the x axis, in milliseconds). The different colours correspond to the different optical channels. Note the black arrow showing the consistent rhythmic interference with the background signal.

Patient 24

The optical signal acquired for patient 24 (see Fig. 4.3.12), prior to any processing steps, was characterised by significant motion-related artefact. Following further processing steps, 6 channels were excluded due to low signal to noise ratio (SNR). During this recording, the patient had 15 seizures of variable duration (see Table 4.5 for details), all of which were both clinical and electrographic. In the onset of the seizure the infant would go quiet followed by a change in the breathing pattern with audible grunting associated with swallowing movements. Towards the end of each episode, the infant would cry and become very unsettled. This led to excessive motion artefact throughout the recording and almost invariably coinciding with the end of each seizure. Analysis of the trace was thus challenging, and all channels were affected by the excessive motion during the recording. One example of an attempt to extract the HRF during seizure event 3 can be seen in figure 4.3.13. This oscillatory pattern seen in figure 4.3.13 is secondary to excessive artefact and was present during all seizure episodes.

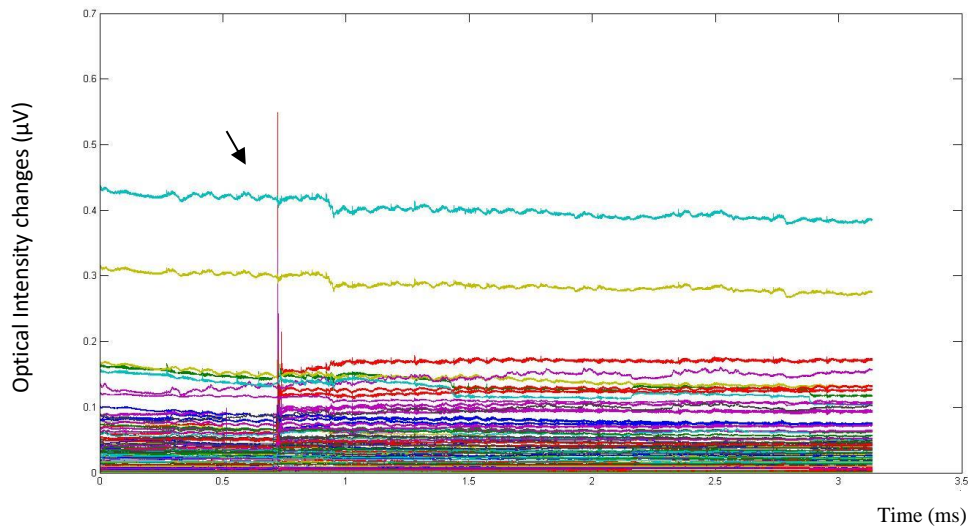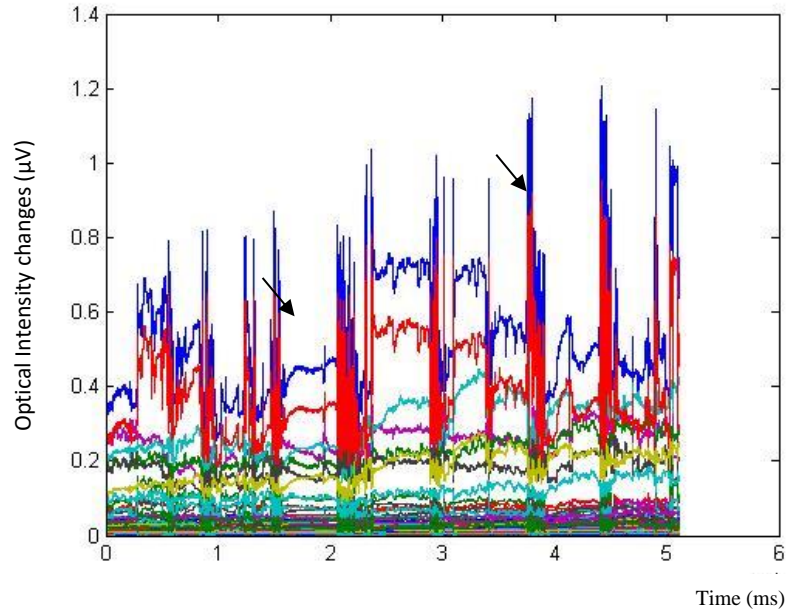**Figure 4.3.12: Graph showing the raw optical signal for patient 24, demonstrating the optical intensity changes in µV (y axis) over time (x axis in ms). The different colours correspond to the different optical channels. The black arrows are pointing to some of the significant motion artefacts in the recording.**
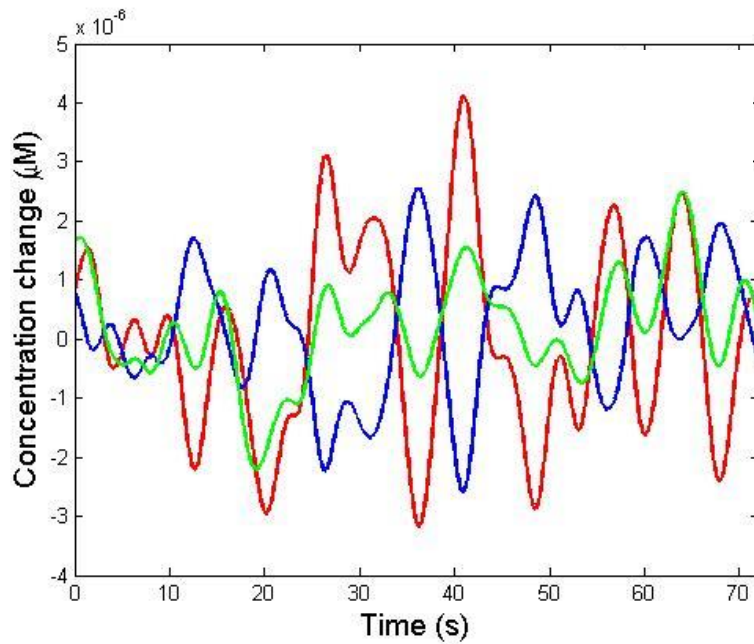
Figure 4.3.13: Graph showing the changes in concentration of all HbO_2 (red line) HHb (blue line) and HbT (green line) (over the y axis in µM) in relation to the seizure event 3 on patient 24 over time (x axis in seconds) for all 52 channels. Time 0 signifies the seizure onset. This seizure was 52 s long in duration. Note a decrease in HbO_2, HHb and HbT 7 s prior to the seizure offset.

4.4 Discussion and Conclusions

The results for this part of the study are not enough to draw any significant conclusions regarding the cortico-vascular changes in association to seizure activity. Although for some of the seizures there was a subsequent increase in the concentration of HbO_2 and HbT, followed by a decrease, this was not consistent across the patients or amongst the different seizures of the same patient. There were multiple barriers and challenges during the study which may explain why the results were not as expected or comparable to the original case study (365).

Most of the patients recruited in the study were transferred to the recruiting unit rather than being inborn. This meant that most patients already had some definite or suspected seizure activity with subsequent treatment prior to their admission to the unit and recruitment to the study. Additionally, patients transported in, often may not have travelled with the mother or guardian with parental rights, thus delaying the consenting process. In that respect, most patients were recruited and studied beyond the acute phase of their seizure activity. Most frequently, when the patients were recruited to the study, they had already received one or multiple anticonvulsant agents leading to seizure control. The EEG trace would appear as either burst suppressed, discontinuous, or normalising, depending on the severity of the initial insult and overall clinical condition.

In study populations of HIE patients receiving TH a wide range of electrographic seizure onset has been demonstrated. Wusthoff et al., studied 26 infants receiving TH and showed electrographic seizure onset of 35 hours with more than half of the patients exhibiting seizure activity in less than 24 hours (383). Glass et al., in a larger cohort across three centres (n=90) reported a median age of seizure onset at 18 hours with the latest at 62 hours (207). This makes it hard to know exactly when to study the patients in the absence of continuous multi-channel EEG monitoring. The overall aim was to study the patients in the acute phase, first 48 to 72 hours. However, the intermittent periods of 1-4 hours of data acquisition rather than continuous (as per granted ethics permission at the time) limited the detection rate of seizure activity. Furthermore, most of the HIE patients were receiving TH at the time of data acquisition, which has been reported to contribute to decreasing seizure burden and altering seizure characteristics (208, 236, 384).

Nevertheless, the patients with seizures during data acquisition, were amongst the most critically ill infants recruited in this study and approaching the parents was time-

critical. It was also challenging as there were situations, where redirection of care was being considered. The consenting process needed to not interfere with the delivery of the best clinical care and not pose any added burden to the parents. Regardless of the difficult circumstances, most families were often happy that their infant's condition could contribute to research and potentially help future patients.

On reviewing the optical signal, it becomes apparent to the naked eye as to whether there are any obvious changes in cortical Hb concentrations in response to seizure activity. One may also establish by visual inspection whether these changes appear physiological or artefact related. In the instance of co-existent electrical events on the EEG trace, multiple artefact correction processes of the optical signal may distort the presumed neurovascular coupling response. While methods for artefact correction exist (374), their application was not appropriate for this study. As the interest lies in the changes of the trace from the baseline any artefact interference leads to multiple assumptions about the change in trace on removing the artefact. This is a limitation of the system in collecting meaningful data during a seizure, especially if a patient is exhibiting physical manifestations during this, as such was the case in patient 24.

It is quite evident from section 4.3 that there were significant issues regarding artefact in the raw optical signal of all patients (see figures 4.3.3, 4.3.4, 4.3.8, 4.3.10-12). In patient 15, there was an ongoing oscillatory type of activity superimposed on the signal throughout the recording (see figures 4.3.3 and 4.3.4). This could be electrical interference from the equipment around the patient, such as the ventilator. For patient 18 and 20, apart from occasional motion related artefact there was a slow periodic rise and subsequent fall in the baseline of the optical signal throughout the recording (see figures 4.3.8, 4.3.10, and 4.3.11). This periodic feature appeared to have no temporal correlation with the seizure events, as it was present at different points during each of the identified seizures in these infants. Because this feature had a large amplitude, it was impossible to separate any haemodynamic features related to the seizures themselves.

On reviewing the traces and considering other contributing factors to these periodic features, the most logical explanation was that the observed repetitive events could be due to the periodic inflation and deflation of the cooling mattress. The cooling mattress was wrapped around the patients whilst receiving therapeutic hypothermia during data acquisition. The mattress used on the unit inflates approximately every 13

minutes and the actual inflation lasts up to 10 minutes. During the study, the cooling part of the mattress around the head was removed and the cap was applied while the rest of the trunk, upper limbs and lower limbs remained wrapped within the mattress. It is possible that the inflation of the mattress caused an elevation of the body compared to the head, which created a head-tilt or slow-motion artefact effect that was apparent in the DOT trace (see figures 4.3.8, 4.3.10, and 4.3.11).

An interesting observation was that out of 15 patients that were being cooled during data acquisition, this periodic feature was noted in only 4. One possible explanation for this phenomenon is that the inflation of the mattress constricts the limbs, causing an increase in arterial blood pressure. This would not matter in a healthy infant but in a critically ill infant with altered or absent cerebral autoregulation it may have an immediate effect on cerebral haemodynamics; increasing the cerebral arterial blood pressure; increasing the concentrations of HbO_2 and HbT in the cortical vasculature; observed as an elevation of the baseline in the raw optical trace (see figures 4.3.8, 4.3.10, and 4.3.11). To prove this, however, continuous measurement of the arterial blood pressure and an accelerometer applied on the head gear (used for scanning the patients) are required.

In retrospect, the absence of continuous recording of the patients' physiological parameters (i.e. heart rate, respiratory rate, mean blood pressure) limits further analysis of electro-cortical phenomena. As mentioned before, there was continuous observation of the patients during recording and any change or abnormal activity was noted and documented, however, subtle trends or changes may well have been missed. For continuous blood pressure measurement, invasive monitoring (via umbilical arterial or peripheral arterial catheter in situ) is required. This requirement would limit the recruitment criteria further and hence it was not pursued.

In view of the excess in noise in the optical signals obtained in patient 15, a lower lpf was also applied to extract the HRF (see Fig. 4.3.6). The standard approach was to apply no hpf and to set the lpf at 1.0 Hz. This allowed the exclusion of heart rate (usually 2-3 Hz), and respiratory rate (0.5-1.0 Hz). It also allowed the study of physiological frequencies associated with resting state (355, 356), smooth muscle cell activity and cerebral autoregulation (385-387) potentially affected by seizure activity. At a lower lpf of 0.5 Hz, a naturally smoother HRF was obtained (see Fig. 4.3.6), but that did not alter

the overall appearance of the HRF as a harmonic oscillation was still present throughout the recording.

Therapeutic hypothermia is considered to decrease cerebral perfusion (388, 389). Existing studies considering the effect of TH with NIRS and MRI have shown that the expected brain reperfusion/hyperperfusion is still occurring in infants with moderate and severe HIE whilst receiving TH (390, 391). These are small sample size studies and have primarily investigated arterial spin labelled-MRI and NIRS in the assessment of cerebral perfusion in HIE patients during TH. There are few in vivo studies on newborns to investigate how TH directly affects cerebral perfusion to understand how this may have affected the patients studied in this thesis. Existing research currently supports that the anticipated haemodynamic phenomena in HIE patients should be observed despite TH.

Due to noise interference and motion-related artefact, the results of the extracted HRFs in relation to seizure activity were inconclusive and not consistent with the results published during the conduction of this research as a pilot study; decrease in HbO_2 and HbT following onset of seizure activity lasting for several seconds after the offset of the event (365). Zhao et al., noted an associated increase rather in CBV related to seizure activity. By performing optical imaging and EEG intraoperatively in the exposed cortex of adult human subjects, an increase in CBV and HHb preceding the seizure onset was identified, indirectly suggesting inadequate tissue perfusion (378). Cortico-vascular activity preceding the neuronal activity has been repeatedly observed (392, 393).

The phenomenon of cortical spreading depression (CSD), which is characterised by disrupted cortico-electrical activity secondary to loss of ion homeostasis (394) and is associated with brain injury (395-397), could be an association to the observed sustained decreases in perfusion seen in similar studies. Most certainly the results demonstrated by Singh et al. (365), suggest that the pattern of the response to seizure activity could be associated to CSD and needs to be investigated further.

Due to the inconsistencies in the data and the excessive artefact, no meaningful HRFs were obtained. Therefore, it was not possible to reconstruct any images of the spatial variation of the observed haemodynamic phenomena. Upon reflection of improving similar studies in the future, both from observation and existing literature it appears that prolonging the study period alongside continuous multi-channel EEG and

aiming for early DOT monitoring in the first 48 hours maximises the chances of capturing seizures. NIRS-based studies have demonstrated that neurovascular coupling in different conditions is not altered under the effect of different anaesthetic drugs, amongst which phenobarbitone was also tested (398). The effect of TH on seizure activity should be encountered more carefully in the sense that the seizure burden may be lower or the electrographic semiology of the seizures different than the expected; subtle; of slower frequency; of short duration. The direct effect of TH on cerebral perfusion as assessed by NIRS methodologies is yet to be defined and should be considered in the analysis of neurovascular coupling in patients with seizures whilst receiving TH. Finally, further work is required to refine the technique of data acquisition. In that respect, collection of continuous physiological parameters, such as invasive arterial mean blood pressure, saturations, heart rate may aid the interpretation of the data in relation to cortical blood volume changes. Furthermore, a possible way to improve motion artefact correction in the future would be to adjust an accelerometer on the recording cap. Thus, by capturing the movements of the head, motion related artefact can safely be rejected from the optical signal.

Chapter 5: Neurovascular Coupling of Burst Suppression

5.1 Functional imaging of burst suppression

The actual interaction between abnormal electrical activity and the cortico-vascular circulation is under-investigated and poorly understood. There is a paucity of studies investigating cortical haemodynamics in critically ill adults, let alone infants with pathological EEG tracings. There are some animal studies which combine EEG and functional neuro-imaging techniques, such as BOLD fMRI. These studies have presented results on neurovascular coupling in burst suppression and types of epilepsy under the effect of certain anaesthetic drugs (399-401).

Other animal studies using functional neuroimaging techniques in the form of BOLD fMRI have shown the existence of spontaneous fluctuations in the BOLD signal even during BS, in the deepest forms of anaesthesia, suggesting that these may be a reflection of an inner functional brain organisation (402). One of the first studies to use EEG and fMRI on a porcine model to investigate changes in functional brain activity at different levels of thiopental-induced anaesthesia, showed that the intensity of the signal changes was more prominent in the thalamic as opposed to the cortical regions of interest (399). In 2011, Liu et al., used simultaneous epidural EEG and double channel laser Doppler to measure cerebral blood flow (CBF) at different depths of isoflurane-induced anaesthesia on the rat model. Under the same conditions of neuronal status, they performed BOLD fMRI independently. They showed strong neurovascular coupling between the EEG bursts of the BS trace and CBF 'bumps' in the Doppler trace, which varied per level of anaesthesia. These were similarly identified as BOLD 'bumps' during the fMRI, which were also dependent on the degree of anaesthesia (401). In 2014, Sutin et al., used simultaneous NIRS and EEG to investigate the haemodynamic responses associated with isoflurane-induced BS in the rat model, similarly showing the existence of neurovascular coupling between burst activity and the oxy- and deoxy-haemoglobin fluctuations (403). These studies are the closest to identifying neurovascular coupling in BS but still refer to animal models. Prior to this investigation there were no in-vivo functional neuroimaging studies of burst suppression in humans.

Multi-modality neuroimaging approaches (such as DOT-EEG) have the potential to elucidate the fundamental physiological, neurovascular, and neuro-energetic characteristics of the BS and discontinuous EEG state. One added advantage is that they allow the investigation of the spatial characteristics of these states. We conducted this

part of the study with the principle aim to investigate the haemodynamic events associated with the BS and discontinuous EEG in critically ill infants with HIE, using DOT and video-EEG.

The working hypothesis was that there are cortical haemodynamic changes in response to EEG bursts and therefore to the neuronal activity.

5.2 Patients and Methods

5.2.1 Patients and Data Acquisition

Infants selected for the burst-suppression investigation phase of this work presented with seizures and/or a clinical diagnosis of HIE. They were recruited as mentioned in section 3.1.1 and were scanned during or after having received therapeutic hypothermia. They were selected in this part of the analysis as they presented with either BS or a pathologically discontinuous EEG trace during the recording period which ranged from approximately 60 to 120 minutes. No adverse events were recorded during the study and the scans were well tolerated throughout without interfering with the clinical input or management required.

5.2.2 EEG Data Analysis

The definition used for identification of a BS trace within these datasets, was the recurrence of high amplitude, occasionally sharp burst activity alternating with inactive periods of low amplitude < 25 µV (IBIs). Another criterion for the selection of EEGs studied was that there was no variability in the trace, with no identified changes due to sleep states and no seizure activity during the recording.

Once the EEGs were identified as burst suppressed or discontinuous, the Clinical Neurophysiologist, Dr Michell (AWM, co-author to the relevant published paper) would review them for confirmation of diagnosis and identification of any other abnormal activity, such as seizures. Using the BrainVision Analyser and EEGLAB toolbox within MATLAB, I then proceeded to further spectral analysis and manual artefact rejection. Both the raw and filtered data were reviewed for artefacts. The EEG datasets were bandpass filtered with a high pass filter at 0.5 Hz and low pass filter at 70 Hz, with a notch set at 50 Hz. The last step in the EEG spectral analysis was the marking of the bursts and for this, the onset and offset of each burst were identified based on the strict criterion that prior to each burst there should be an IBI of ≥ 2 seconds in duration. Both discrete bursts and IBIs themselves were marked. As a more objective way of burst identification, a second observer, Dr Lee (CWL, PhD student and co-author to the relevant paper) independently marked the bursts in a subset of EEGs. The inter-observer comparison indicated that for every burst onset identified by me (MC), a burst onset was independently identified by CWL within an error of 1.5 seconds in 84 % of cases.

5.2.3 DOT Data Analysis

Using the MATLAB toolbox, the EEG and DOT datasets were synchronised, and the burst onset and offset markers were transformed to the DOT time-base. Using functions form the Homer2 NIRS processing toolbox (www.homer-fnirs.org), the DOT data were first pre-processed using the standard pipeline described in detail in section 3.2.3. Further project-specific processing consisted of the raw intensity data being converted to optical density. Periods of motion artefact were identified using a combination of visual inspection and Homer2 motion artefact detection approaches (374) prior to band-pass filtering in the range 0.01 to 1 Hz.

To extract the haemodynamic response to the EEG bursts in each dataset, the bursts were first sub-divided based on their duration into 2-second wide bins over the range from 0 to 30 s. Bins containing less than 5 bursts were excluded. The burst onset markers associated with each bin were then treated as separate conditions in an event-related general linear model of the DOT data (such that the model contained a 0-2 s burst condition, a 2-4 s burst condition etc.). The general linear model is a generalization of multiple linear regression model in the instance of more than one dependent variable. The general linear model was constructed using a series of Gaussian basis functions (with a standard deviation of 2 s and separated by 1s), to model the haemodynamic response function (HRF) associated with each burst duration. In this instance, the different variables are the scale of each basis function used to model the HRF to burst of different durations. The time range of the modelled HRF was set to -10 to 40 s relative to the burst onset markers. This approach resulted in an HRF for each accepted DOT channel, burst duration bin and infant.

To provide an objective representation of the morphology of the spatially-varying haemodynamic response to bursts in each infant (instead of arbitrarily selecting a channel to display or taking an average), the principal component analysis (PCA) method was used. This type of analysis entails finding the linear relationship of a set of variables that has maximum variance, removing its effect, and repeating this successively. PCA was performed across the accepted channels in each dataset. An HRF was then produced for each infant and each burst duration by combining the components required to account for 80 % of the signal variance.

To ensure that any extracted HRF was not an artefact of the data processing procedure, and was directly temporally correlated with the EEG bursts, additional HRFs were computed using 10 randomly generated dummy onset vectors in place of the burst onset markers for each dataset. These dummy vectors contained the same number of 'events' as the largest number of bursts in any one bin for each infant. A one-tailed, Bonferroni-corrected t-test was then performed to identify channels in which the haemodynamic response to EEG bursts is statistically distinguishable from a vector produced by concatenating the 10 dummy HRFs.

The algorithms for the synchronization of the DOI-EEG datasets and the HRF extraction were developed by my co-supervisor and physicist, Dr Cooper (RJC). The image and video reconstruction of the HRFs were accomplished based on the methodology described in section 3.2.5.

5.3 Results

5.3.1 Clinical Details

Between March 2013 and September 2015, 9 infants presented with either BS or a discontinuous EEG trace as defined in section 5.3.2 (patients 2, 4, 7, 10, 12, 14, 18, 19, 21). Three infants were excluded due to excessive noise or artefact within the DOT datasets (>15 DOT channels were rejected in each dataset), leaving a total of 6 datasets suitable for analysis. Further clinical information regarding the 6 infants included is provided in Table 5.1. The median gestational age at birth was 38+6 weeks (range from 34+5 to 40+1 weeks). The median age of the infants at the time of the study was 3.5 days (with a range from birth to 7 days of life). The length of the DOT-EEG recording ranged from 47 to 115 minutes with a median period of 59 minutes.

All infants presented with seizures in the first 48 hours of life and received either one or three types of anticonvulsant treatment prior to (or in one case during), the study (see Table 5.1). All infants were receiving respiratory support during the study in the form of conventional mechanical ventilation, apart from patient 7, who was receiving high frequency oscillatory ventilation and patient 2 who was breathing spontaneously in air. All infants had stable levels of carbon dioxide partial tension (PCO_2) within the normal range (4.7-6.0 kPa) 34 throughout the study. Two of the infants were receiving inotropic support during the study to maintain a stable systemic arterial blood pressure (patients 7 and 21). Each infant underwent a structural MRI between 7 to 10 days of life as per the standard clinical care protocol and all received a final diagnosis of HIE grade III, apart from patient 2 who received a final diagnosis of HIE grade I (please refer to section 1.1.2 for further details on HIE grading). The MRIs were provisionally reported locally and were further interpreted by Professor Mary Rutherford as an external expert on neonatal MRI, as part of the standard clinical care (see Table 5.1). All 6 infants survived and were either discharged back to the referring hospital or to home.

Infant	GA	CGA	Neurology	Anticonvulsant treatment (hours prior to study)	MRI findings
Patient 2	40^{+1}	40^{+6}	Self-limiting seizures	None required	Normal findings.
Patient 7	39^{+3}	40^{+2}	Clinical seizures	Phenobarbitone (40)	Diffuse multiple haemorrhagic lesions.
Patient 12	34^{+5}	34^{+6}	Clinical &electrical seizures	Phenobarbitone (24)	Abnormal signal intensity within the WM, BG, thalami & cortex. Thrombosis within the TS and SSs.
Patient 14	38^{+6}	39^{+6}	Clinical &electrical seizures	Phenytoin (4), Phenobarbitone (22)	Multiple areas of cortical highlighting Left>Right. Lesions within the BG and thalami.
Patient 19	37^{+5}	37^{+6}	Clinical seizures	Midazolam (5)	Diffuse abnormal signal intensity within the BG and thalami. Bilateral increased signal intensity along the cortex & central sulci. Bilateral swollen medial temporal cortex. Possible haemorrhagic lesion within the right parietal lobe.
Patient 21	39	39^{+2}	Clinical &electrical seizures	Midazolam (12), Phenobarbitone (2), Clonazepam (infusion)	Abnormal signal intensity within the BG, thalami, PLIC and superior cortex.

Table 5.1: Clinical details of the study subjects for the investigation of neurovascular coupling in BS. The information regarding their neurological status refers to the clinical presentation of the infants prior to the initiation of the recording. The anticonvulsant medications reported also reflect treatment which was administered prior to the recordings (as indicated in hours in the brackets) except for the ones indicated as infusions, which the infants were receiving during the study. The MRI findings refer to structural MRI, T1 and T2 weighted images obtained after day 7 of life (GA: gestational age at birth, CGA: corrected GA at time of study, WM: white matter. BG: basal ganglia. TS: transverse sinus. SSs: sagittal sinuses. PLIC: posterior limb of the internal capsule).

5.3.2 Burst Identification

The total number of bursts identified in each infant ranged from 87 to 257, with a median of 129. An example of an identified burst is shown in Fig. 5.3.1. Most bursts had a duration between 1 and 7 seconds. The single most common burst duration across the group was 4-6 seconds. A histogram of burst durations by infant, binned as per the DOT analysis, is shown in Fig. 5.3.2.
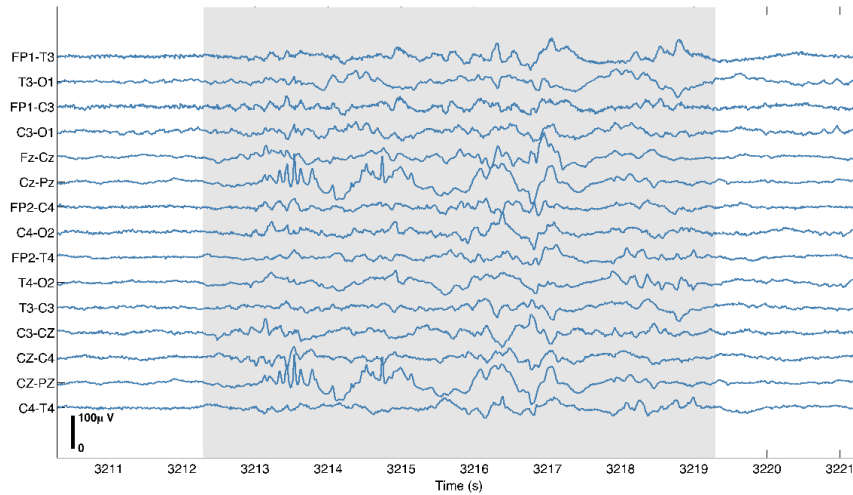
Figure 5.3.1: EEG snapshot from infant patient 19 showing a typical example of burst activity lasting approximately 6 s with low amplitude IBIs prior to burst onset and after burst offset respectively.
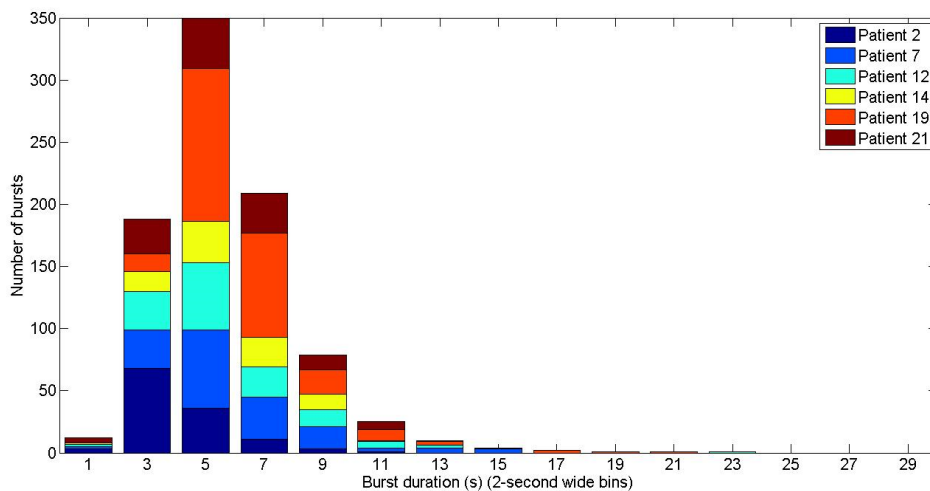
Figure 5.3.2: Burst durations binned as per DOT datasets. The x axis represents the different bin durations in seconds and the y axis the absolute number of bursts per bin duration. The different colours represent the different patients as shown in the legend on the right upper part of the figure.

5.3.3 Haemodynamic Response to Bursts

The number of DOT channels rejected across the 6 datasets ranged from 2 to 9, with median of 4 per dataset (from a total of 58 channels). HRFs were successfully extracted for burst durations in the range 2-4, 4-6, 6-8, 8-10 and 10-12 s across the group of six infants. However, only the ranges 2-4, 4-6 and 6-8 s contained enough bursts (>5) to meet our criteria for all 6 infants. The proportion of DOT channels exhibiting a statistically significant oxy-haemoglobin response to bursts with duration 4-6 s ranged from 30 % (in patient 7), to 100 % (in patient 19). In figure 5.3.3 one can see the channel-wise haemodynamic response to EEG bursts of 4-6 s durations in patient 2. A pronounced response is noticeable on most of the channels, with a clear spatial variation in amplitude and morphology.
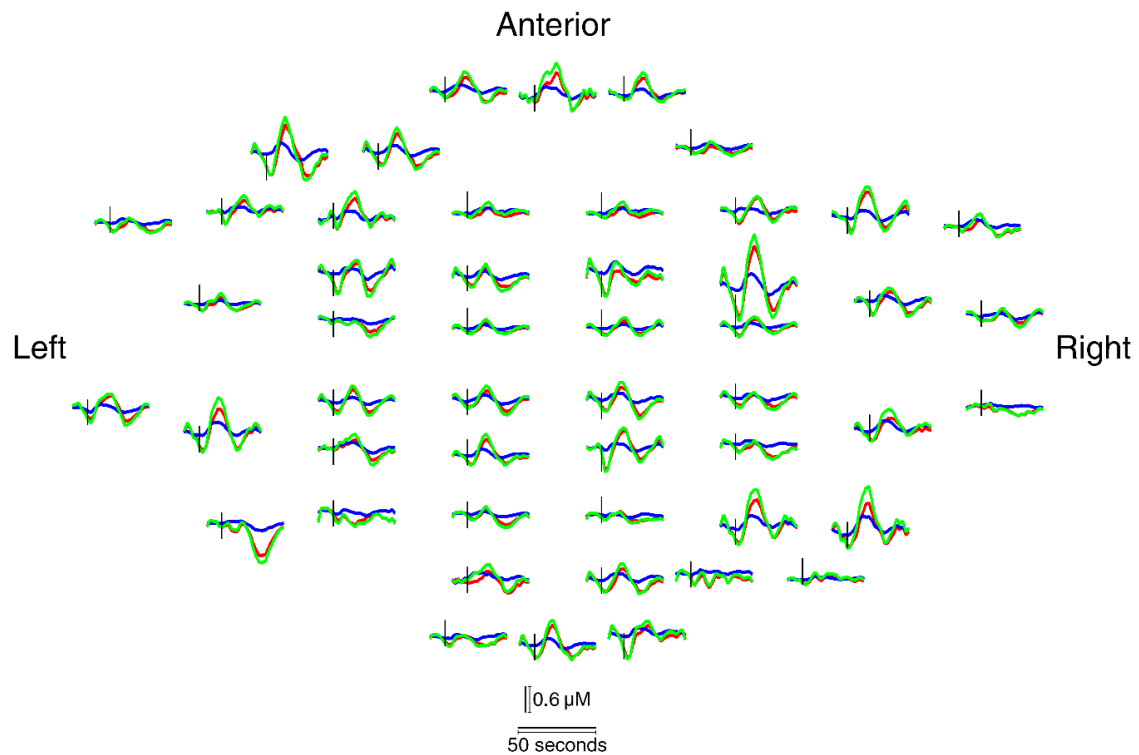
Figure 5.3.3: Representation of the HRFs to bursts lasting from 4 to 6 s in patient 2. The arrangement of the channels is mimicking the array of channels across the scalp based on the DOT channel layout (see Fig. 3.2.2). Note that some of the channels are not displayed at all due to rejection. In each graph, the black vertical line represents the burst onset, the green line the HbT, the red line the HbO$_2$ and the blue line the HHb. These results are referring to 50 out of a total of 58 channels.

The PCA-extracted HRF to 4-6s duration bursts in all 6 infants can be seen in figure 5.3.4. These provide a representation of the typical response across the cortex in each case. The number of components required to account for 80% of the channel-wise

variance ranged from 1 to 3 components. In each infant, there is a clear response to burst activity, which on closer inspection appears similar for all infants: the response consists of a marked decrease in both HbO_2 and HHb and consequently in HbT before or with the onset of burst activity. This response is identical in the first 3 infants but appears to have a slight delay in patient 14 and patient 21 (see Fig. 5.3.4). In patient 19 (see Fig. 5.3.4) it appears that this drop occurs at least 5 seconds prior to the onset of the burst activity. In all infants, however, the initial shape of the HRF is identical with slight temporal variation. This decrease is then followed by a large increase in HbO_2, HHb and HbT, which reaches a peak approximately 20 s after the burst onset before returning towards the baseline and exhibiting an undershoot. In patient 19 (see Fig. 5.3.4) the HbO_2 response shape does differ; the peak increase in HbO_2 occurs at a similar time to that of the other infants, but its increase is more gradual and commences during the actual burst activity. It is worth noting at this point that the HHb response is less pronounced in comparison to that of HbO_2. In all cases, the HHb shows a notable increase that reaches a peak between 10 and 20 s post burst onset.
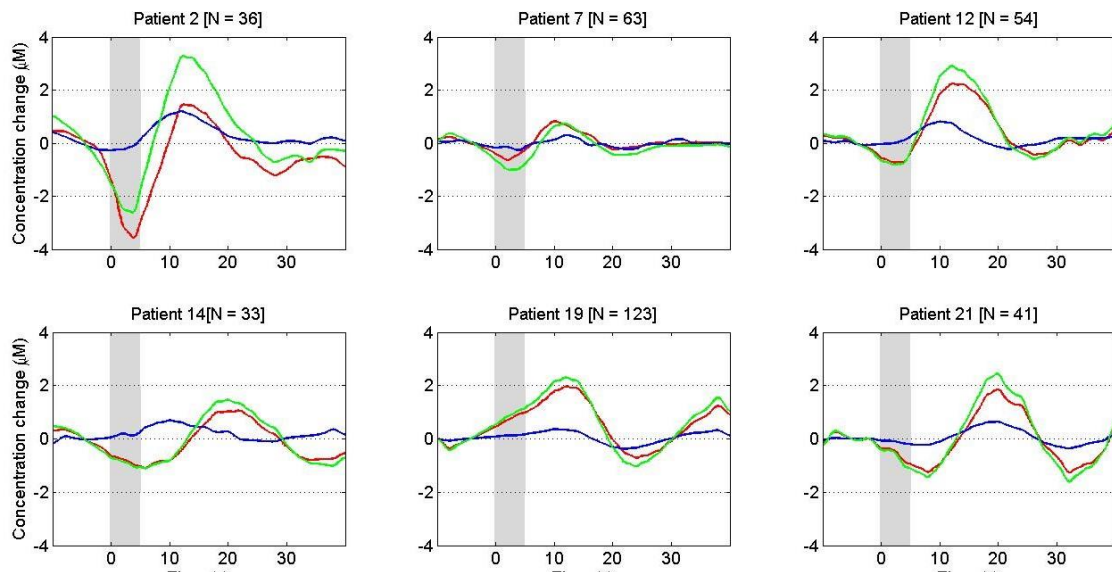
Figure 5.3.4: The PCA-extracted HRFs to bursts lasting from between 4 to 6 s in each infant. The grey shaded area indicates the period of the average duration burst. The value of 'N' in each case indicates the number of bursts between 4 and 6 s identified in each infant. The green line the HbT, the red line the HbO_2 and the blue line the HHb.

5.3.4 Imaging of the Haemodynamic Response to Bursts

The reconstructed HRFs can be visualised on an image basis across the scalp (see Figures 5.3.5-8). These were reconstructed based on a neonatal head atlas for the correct gestation per infant (404). Figure 5.3.5 shows three views of the reconstructed cortical image of changes in HbT for patient 12 at the minimum of its initial decrease (as defined from the PCA-extracted representative response, see Fig. 5.3.4). This moment in time coincides with the minimum decrease in both HbO_2 and HHb. A small decrease in HbT is apparent across the cortex, but the changes appear more pronounced in the bilateral temporal and temporal-parietal regions. Figure 5.3.6 shows data from the same infant at the peak of the increase in HbT, which occurs at approximately 12 s post burst onset. This moment in time coincides with the maximum increase in both HbO_2 and HHb. The frontal lobes, right temporal and left parietal regions exhibit the largest increases in HbT, while the occipital cortex displays a slight decrease. The combination of regions that show a pronounced increase in HbT during the peak phase (see Fig. 5.3.6) are not completely consistent with those exhibiting the largest decreases in HbT during the initial dip phase of the HRF (see Fig. 5.3.5).

Similarly, figure 5.3.7 shows the reconstructed cortical image of HbT at the peak of the post-burst increase in patient 19, which is also the point of maximum increase in both HbO_2 and HHb. The increase is broadly global, with the largest increases occurring in both temporal lobes, and an apparent lack of response over the right parietal lobe. The structural MRI of the same patient (see Fig. 5.3.9) revealed swelling of the bilateral medial temporal cortices and a possible haemorrhagic lesion over the right parietal lobe. The last figure 5.3.8, depicts the HbT image associated with the undershoot phase in patient 19, which shows the largest decreases occurring in the bilateral frontal cortices and reflects the minimum decrease in both HbO_2 and HHb.
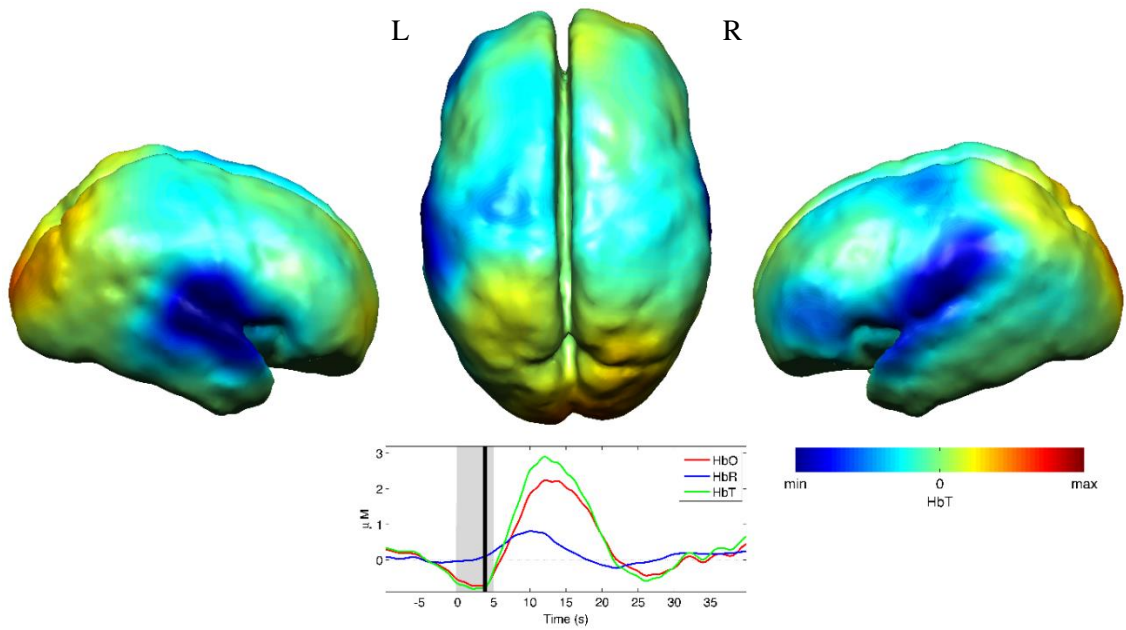
Figure 5.3.5: The reconstructed image for the HbT-HRF associated with the initial decrease in the response to 4-6 s duration EEG bursts for patient 12. These images represent the change in HbT at the time point indicated by the black vertical line in the lower panel. Note that the most significant decrease in HbT is localised to the bilateral temporal-parietal boundary (see Movie 5.1).
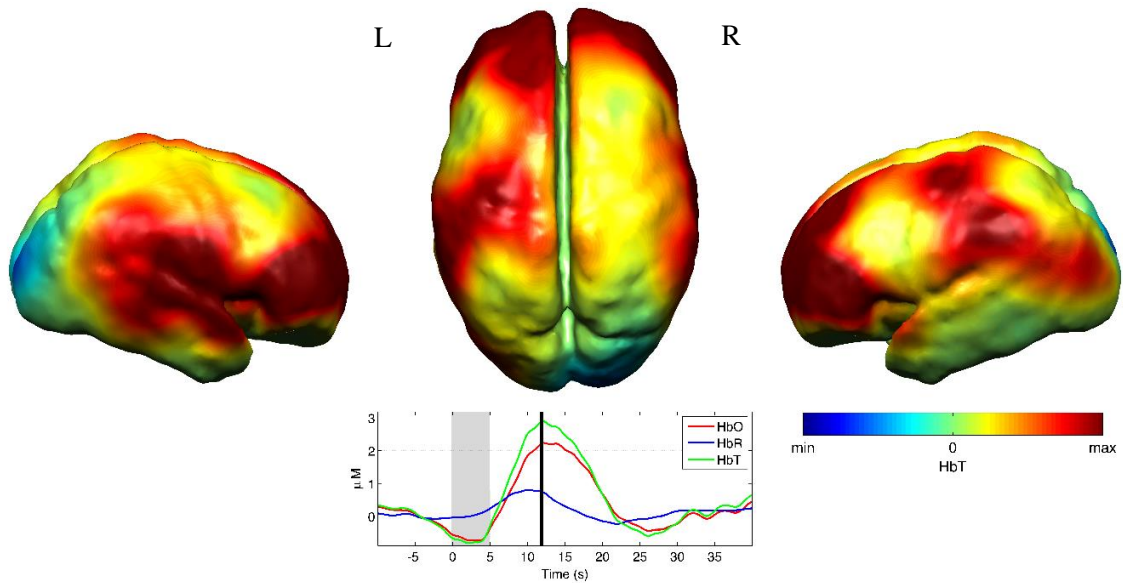
Figure 5.3.6: The reconstructed image for the HbT-HRF associated with the peak increase in the response to 4-6 s duration EEG bursts for patient 12. These images represent the change in HbT at the time point indicated by the black vertical line in the lower panel. Note the marked increase in HbT in the prefrontal cortex (see Movie 5.1).
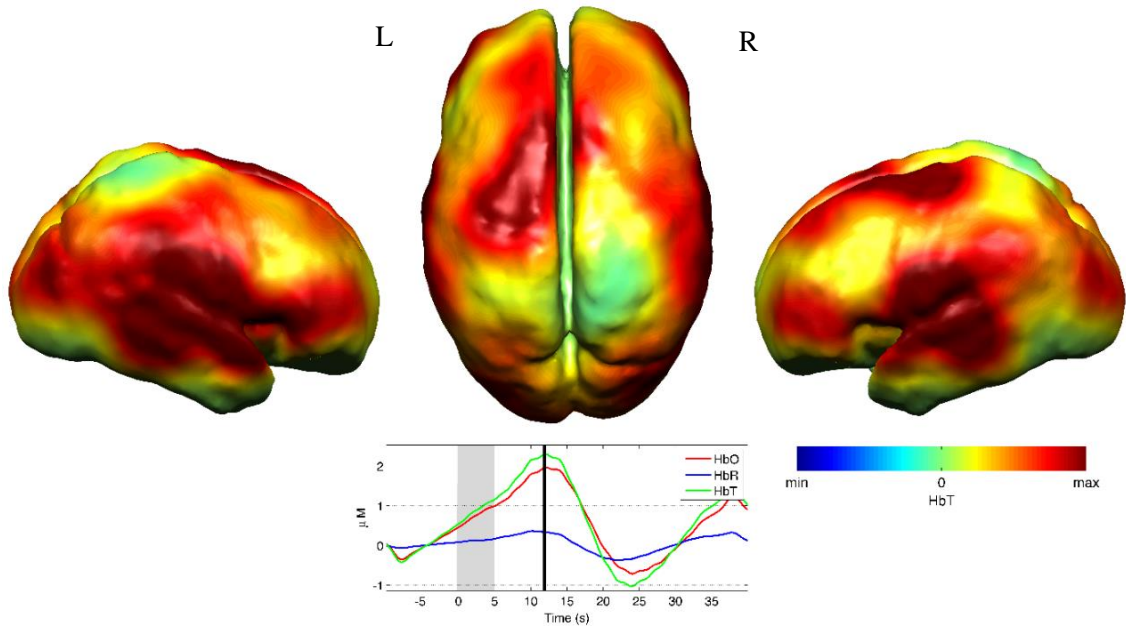
Figure 5.3.7: The reconstructed image for the HbT-HRF associated with the peak increase in the response to 4-6 s duration EEG bursts for patient 19. These images represent the change in HbT at the time point indicated by the black vertical line in the lower panel. Note the marked increases in HbT in the bilateral temporal regions and the absence over the right superior parietal area (see Movie 5.2).
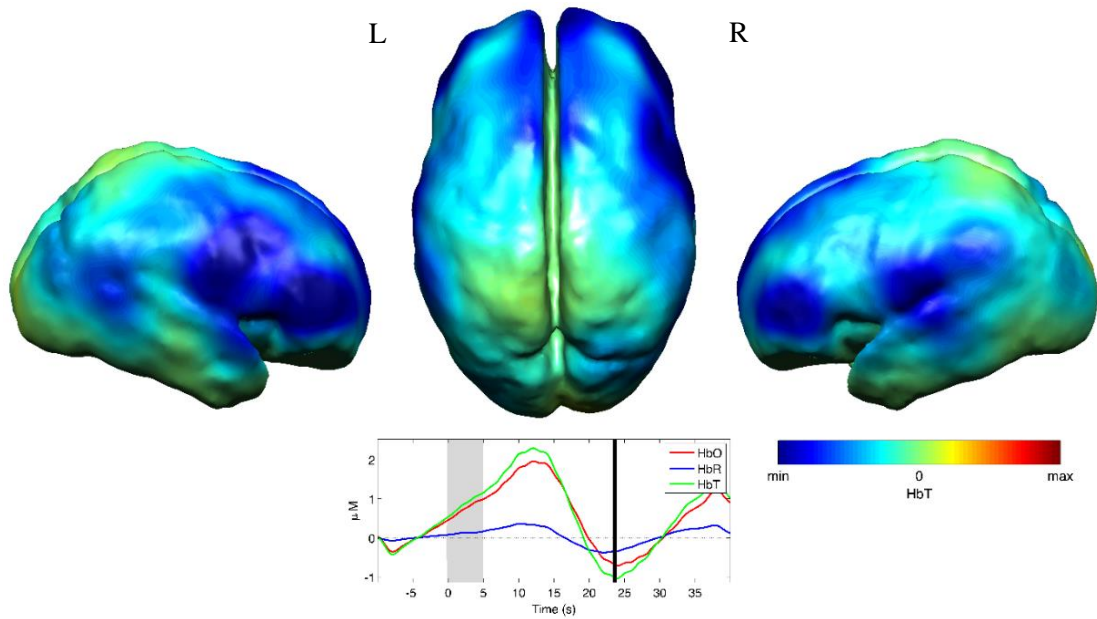
Figure 5.3.8: The reconstructed image for the HbT-HRF associated with an undershoot in the response to 4-6 s duration EEG bursts for patient 19. These images represent the change in HbT at the time point indicated by the black vertical line in the lower panel. Note that this decrease is most apparent in the frontal cortices (see Movie 5.2).
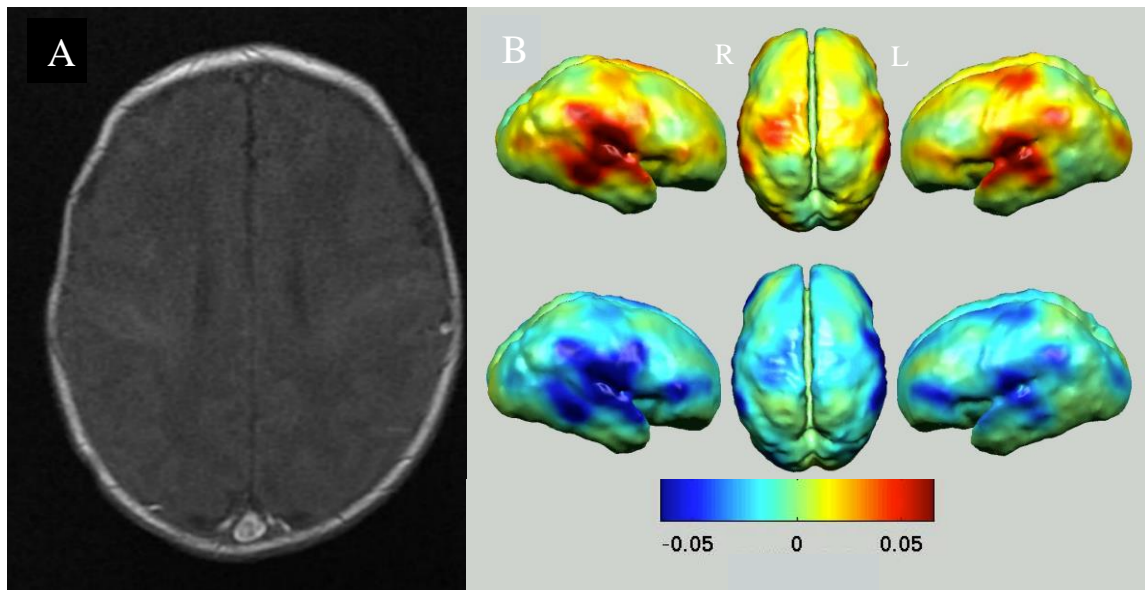
Figure 5.3.9: Comparison of MR image and DOI for patient 19: (A) T1 weighted MRI of patient 19, showing bilateral temporal oedema, and (B) DOT images of patient 19 showing the maximum increase in HbO$_2$ (top section of figure) and minimum decrease of HbO$_2$ concentration (lower section of the figure) in response to burst activity. Note the localisation of the haemodynamic changes in both temporal cortices, where the MRI has identified bilateral temporal oedema.

Movies showing the haemodynamic response to 4-6 s duration bursts in patients 12 and 19 will be provided with the presentation of this thesis.

5.4 Discussion and Conclusions

Burst suppression has traditionally been considered as a uniform, global, brain state. It appears that regardless of the causative mechanism of BS the EEG trace typically seems consistent and synchronous across the scalp. This has led to the perception that BS reflects a state of global brain inactivity and thus can be pharmacologically induced in cases of head injury (405) or status epilepticus (406), as a therapeutic means of minimising or depressing cortical activity. However, it is still unclear as to whether BS is truly a state of global suppression of brain function.

There is supporting evidence form the literature that despite the apparent cortical inactivity in BS, there can be increased activity in subcortical structures, which may trigger and signal activity in the hyper-excitable cortex. This is a possible hypothesis of the origin of the observed bursts in BS. This activity has been described as a novel neurophysiological parameter, known as 'Nu-complexes' that originate from the hippocampus at different depths of coma and therefore in BS (407). Researchers have attempted to capture more spatial information by performing high density electro-corticography as opposed to standard scalp EEG on propofol-induced comatose human adults. They demonstrated that, unlike traditional perception, BS is not a global, unified phenomenon; it can be localised to specific cortical areas, whilst other regions may exhibit continuous activity and bursts may occur asynchronously across different brain locations (263).

These findings have opened new horizons in the way we perceive cortical activity and have introduced the potentially crucial role of the subcortical structures in the observed neuronal activity. This gives rise to questions as to how the sub-cortex interacts with the cortex and as to whether there is a similar interaction between subcortical neuronal structures and the cortical vasculature, which may contribute to the observed neurovascular coupling as shown in previous studies (363) and ours (365, 408). They have also enhanced the importance of using neuroimaging techniques with increased spatial specificity than scalp EEG to investigate BS and discontinuous EEG phenomena.

Simultaneous DOT-EEG approaches have the advantage of allowing the investigation of both the temporal and spatial features of the haemodynamic correlate of BS, which facilitates the investigation of the relationship between discontinuous EEG states and cerebral function.

In this part of the study a significant haemodynamic response to burst activity in infants with HIE was shown. To date, this appears to be the first study to examine this phenomenon in this patient group. The haemodynamic component of burst activity in infants with HIE was best characterised by an initial decrease in HbO_2, which reaches a minimum during or soon after the burst, followed by a pronounced increase (see Fig. 5.3.4) peaking at 10 to 12 s after the burst onset. The changes in HHb are more variable, but follow the trend of the HbO_2 changes and it is quite clear that they are not consistent with the typical, expected HRF shown in healthy adults (409). There is ongoing debate regarding the nature of the healthy neonatal HRF. While several studies suggest the neonatal (and even early pre-term) haemodynamic response is consistent with that observed in the mature brain (328, 410), a recent study in the rat model suggests that the haemodynamic response to an external stimulus varies significantly with postnatal age (411). The latter showed that in the infant rat, the haemodynamic response consists of a small increase in HbO_2, followed by increase in deoxy-haemoglobin, while the response in the adult rat was consistent with the expected adult human response; an increase in HbO_2 with a parallel decrease in HHb.

A possible interpretation of the observed HRF shape in our data, is that burst activity induces a regional increase in perfusion and therefore blood volume. The oxygen extraction is either abnormally low or the oxygen supply exceeds the regional metabolic demands and hence, the increase in perfusion results in little change in oxygen saturation with no occurring decrease in HHb. It may, nevertheless, be part of a physiological process based on most recent literature and a normal variant of haemodynamic response observed in infancy (411). Another possible explanation to the observed result is considering the pathophysiological mechanisms of HIE in the following hours post injury, and specifically the biochemical changes associated with reperfusion injury (412-414).

There are additional confounding factors which may affect the neurovascular coupling and subsequently the observed HRF, such as therapeutic hypothermia, anticonvulsant treatment, inotropic support. Anticonvulsant treatment is known to depress the EEG background activity and its effects are dependent on the type of medication, the dosage and the timing of administration, and the gestational age of the infant (415). Standard phenobarbitone loading doses (10-20 mg/kg) only moderately affect the EEG background activity in full term infants. However, evidence suggests that

the more severe the hypoxic ischaemic insult, the more discontinuous and suppressed the EEG may become post phenobarbitone administration (416). Midazolam is another medication frequently used in cases of HIE, for its anticonvulsant effects and occasionally for its sedative effects during mechanical ventilation. It appears that its administration has limited if none effect on the EEG background appearance (416). The effect of anticonvulsant treatment on the background electro-cortical activity is decreased over time as the drugs are metabolised with a median time-to-recovery of 2.5 hours, ranging from 2 to 15 hours (417). A recent study looking at the effect of anaesthetic drugs on neurovascular coupling concluded that there is no actual variation across different agents (398). A recent study on the influence of therapeutic hypothermia on cortico-vascular activity in infants with HIE, using frequency domain NIRS and diffuse correlation spectroscopy, showed that compared to the post-hypothermic phase, cerebral oxygen metabolism and CBF were lower and CBV was higher during hypothermia (418).

While all six infants included in this study were diagnosed with HIE and were receiving therapeutic hypothermia, the severity of their clinical situation varied. They had also received a range of anticonvulsants at different times relative to the period of recording (see Table 5.1). Despite these many confounding factors, the shape of the principal haemodynamic response to burst events is remarkably consistent across our cohort (see Fig. 5.3.4).

In 4 out of 6 infants, the peak increase in total haemoglobin occurs between 11 and 12.5 s after the onset of burst activity. A possible explanation for this could be their common EEG state acts as a control for the many other experimental variables: i.e. the haemodynamic correlate of BS may be consistent despite the various factors that have led to that neurological state. However, as is apparent from figures 5.3.5-8, the spatial distribution of the haemodynamic response to EEG bursts is highly variable across infants. Furthermore, the dominant features of the representative responses shown in Fig. 5.3.4 are not necessarily at their most pronounced in the same cortical area; while the initial dip of one infant may be most pronounced at the bilateral temporal-parietal boundaries (see Fig. 5.3.5), the peak increase in HbT in the same infant can be most pronounced in the prefrontal cortex (see Fig. 5.3.6).

These results constitute evidence that electro-cortical burst activity in HIE infants invoke variable haemodynamic responses in different cortical regions. Whether this

reflects localized neuronal activity, which otherwise is grossly seen as BS on scalp EEG must be explored further. So far, there is limited scientific evidence to show that the phenomenon of BS can be dependent on local dynamics rather than a global state (263). Future studies on animal models of neonatal asphyxia combining cortical EEG and DOT measures could elucidate this further.

It is also of striking interest that the MRI of patient 19 (see Fig. 5.3.9) revealed swelling of the bilateral medial temporal cortices and a possible haemorrhagic lesion over the right parietal lobe. These findings, to some extent, appear to correlate with the distribution of the peak HbT changes shown in figure 5.3.7. The largest response is apparent in the temporal lobes, while a distinct absence of a response can be noted in the right parietal region.

With this work, the haemodynamic correlate of electro-cortical burst activity in the burst-suppressed and discontinuous EEG traces of human infants with HIE was identified. These responses exhibit a consistent morphology but highly variable spatial distributions across different infants. This observation is consistent with the emerging picture of BS as a representation of a complex and variable functional brain state, rather than simply an indication of globally suppressed neuronal activity. DOT-EEG approaches are likely to play a significant part in future investigations of the neurophysiological and clinical implications of burst-suppressed and discontinuous EEG states.

Chapter 6: Diffuse Optical Tomography in the Early Detection of Perinatal Stroke

6.1. Background on functional imaging of perinatal stroke

This part of the thesis focuses on perinatal arterial ischaemic stroke (PAIS). The majority of perinatal stroke is arterial and ischaemic in origin (as also mentioned in section 1.1.3), which affects 1 in 2,300 infants (61) not including cases of PAIS recognised outside the neonatal period. PAIS, is associated with hemiplegia, epilepsy, cognitive impairment, and lifelong disability (419).

At present, there is no definitive treatment, other than a symptomatic and supportive one, unlike large vessel stroke in the adult population. Although PAIS is defined as occurring anytime between the second trimester of pregnancy and the first 28 days of life (60), the exact timing of injury for those of acute onset in the immediate postnatal period, is often not clear. The first clinical signs, usually being focal seizures, tend to present in the first few days of life but may go unnoticed. The current diagnostic tools are summarised in section 1.4 of chapter 1. A neuro-investigative tool facilitating early diagnosis of PAIS would aid in the study and application of early treatment strategies, such as therapeutic hypothermia (TH) (420).

Continuous wave NIR-DOT is a safe, portable, non-invasive brain-imaging tool, which allows long-term monitoring of critically ill infants. Various research groups have recorded changes in oxygenation during stroke using different NIR methodologies. Wolf et al. used NIRS to demonstrate a decrease in the concentration of HbO_2 and increase in the concentration of HHb during focal cerebral ischaemia in rats (421), with similar results obtained by Stankovic et al. in piglets (422). Analogous results were obtained in humans by Calderon-Arnulphi et al., who studied patients undergoing neurovascular surgery with quantitative frequency-domain (FD) NIRS and demonstrated a decrease in HbO_2 and HbT, accompanied by an increase in HHb in all patients who suffered an ischaemic event (423). Culver et al. used a simultaneous FD-DOI and diffuse correlation spectroscopy (DCS) device following MCA occlusion in rats. They demonstrated little changes in relative cerebral blood volume (rCBV) and HbT, but oxygen saturation (StO_2) decreased by 11%, once again agreeing with a decrease in HbO_2 concentration, and increase in HHb concentration the initial phases of MCA stroke (424).

In the examples mentioned, most NIR recordings were obtained after the stroke has occurred, as the precise timing of injury is unknown. Consequently, it becomes impossible to record an in vivo "baseline" chromophore state before MCA occlusion.

Therefore, alternative approaches, such as investigating transient non-physiological phenomena (such as burst suppression activity), measuring quantitative markers such as StO_2, or comparing the frequency content of the affected and healthy hemispheres have been employed. Cooper et al. used a simultaneous CW-DOI and EEG system to identify transient haemodynamic phenomena in a term infant with extensive unilateral stroke (366). This study reported successive distinct changes in both HbT and HbO2 that were significantly different between the healthy and stroke-affected brain region (see Fig. 6.1.1). Earlier, Vernieri et al. demonstrated discrepancies between hemispheres in adult stroke patients by using NIRS and transcranial doppler (TCD) to study the effects of hypercapnia on CBV. Amongst the subjects studied there were two with unilateral MCA stroke, in which the increased CBV expected following hypercapnia was only detected over the healthy hemisphere (425). More recently, Moreau et al. published a FD-NIRS study of brain oxygenation in adults with stroke, which found that all affected patients had an area of reduced StO_2 in the stroke-affected hemisphere (426). Whilst these studies provide valuable insight, transient haemodynamic changes are not always observed, and it is not possible to subject stroke-affected infants to hypercapnia. Additionally, commercial NIR technologies that can measure quantitative variables (such as FD-NIRS) tend to be expensive and bulky.
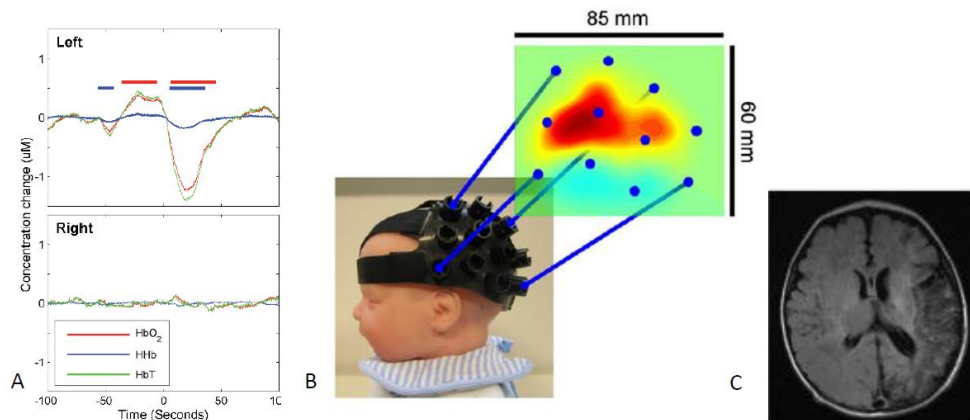
Figure 6.1.1: Cortical haemodynamic changes in an infant affected by left sided MCA infarct: (A) spectroscopic analysis of the optical signal showing a spontaneous significant decrease in both total and oxy-haemoglobin on the site of injury, whereas the changes on the right side are minimal, (B) reconstruced haemodynamic change according to the array used for the study of the infant as depicted on the head of the model, (C) T2 weighted image of the patinet's MRI showing an extensive left sided MCA infarct. Adapted from reference (366).

Another method for detecting stroke is to look at the disturbance of normal brain physiology. Spontaneous low frequency oscillations (LFOs) of cortical vasculature occur in the healthy brain, and their clinical significance remains under debate. They are believed to be associated with myogenic (427), metabolic (428) and neurogenic stimuli (429), sympathetic tone (430), and cerebral autoregulation (CA) (387, 431). Dynamic cerebral autoregulation maintains a constant cerebral blood flow (CBF) in the face of changing cerebral perfusion pressure; this protects the brain from rapid increase or decrease in CBF during fluctuations of the arterial blood pressure. Numerous studies support the idea that CA is altered in cases of brain injury, such as ischaemic stroke (432-436).

The LFO band can be subdivided into very low (VL) frequency oscillations from 0.004 to 0.009 Hz (385, 386), RS frequency oscillations from 0.01 to 0.08 Hz (355, 356), and Mayer waves from 0.09 to 0.4 Hz (437, 438). Very low frequency oscillations were originally detected in 1960 as spontaneous fluctuations in the intraventricular pressure of patients with intracranial disease (439). They have been observed physiologically in healthy adults by measuring intracranial pressure (440), flow velocity in the MCA (441), and MR imaging of intraventricular CSF and CBF (442), thus suggesting a link to a vascular myogenic mechanisms, possibly associated with the smooth muscle cells of the vessel bed. Resting state oscillations that display a synchronous, symmetrical pattern across homologous brain regions between hemispheres were initially detected with BOLD fMRI and are believed to possibly be a precursor to the default mode network (359). These same RS oscillations have also been observed in neonates using NIR imaging systems (443-445). More recently, both VL and RS oscillations have been explored as an indirect marker of CA in adult stroke patients receiving thrombolytic therapy; showing that stroke severity positively correlated with the degree of altered CA which was less impaired in the treated group (446). The functional significance of Mayer waves is a topic of continuing investigation and debate. Mayer waves have been detected in several species at different inherent frequencies, at 0.1 Hz in humans (458, 459), 0.1 Hz in cats (460, 461), 0.3 Hz in rabbits (462) and 0.4 Hz in rats (463). Some studies have suggested that Mayer waves are global oscillations in arterial blood pressure correlating with sympathetic neuronal activity (437), others that they trigger the release of endothelial-derived nitric oxide during vascular stress (464), or that they are part of normal vascular baroreflex mechanisms and of no particular function (465).

Diffuse optical imaging allows a novel method for the detection and further investigation of LFOs in PAIS patients. To date, few DOI based studies exist focussing on the role of LFOs in stroke, and only one of these had a neonatal application. In 2012, White et al. used CW-DOI to study RS networks in the occipital cortices of healthy term and preterm infants, demonstrating the absence of inter-hemispheric connectivity in one neonatal case with mono-hemispheric occipital stroke (see Fig. 6.1.2) (355).
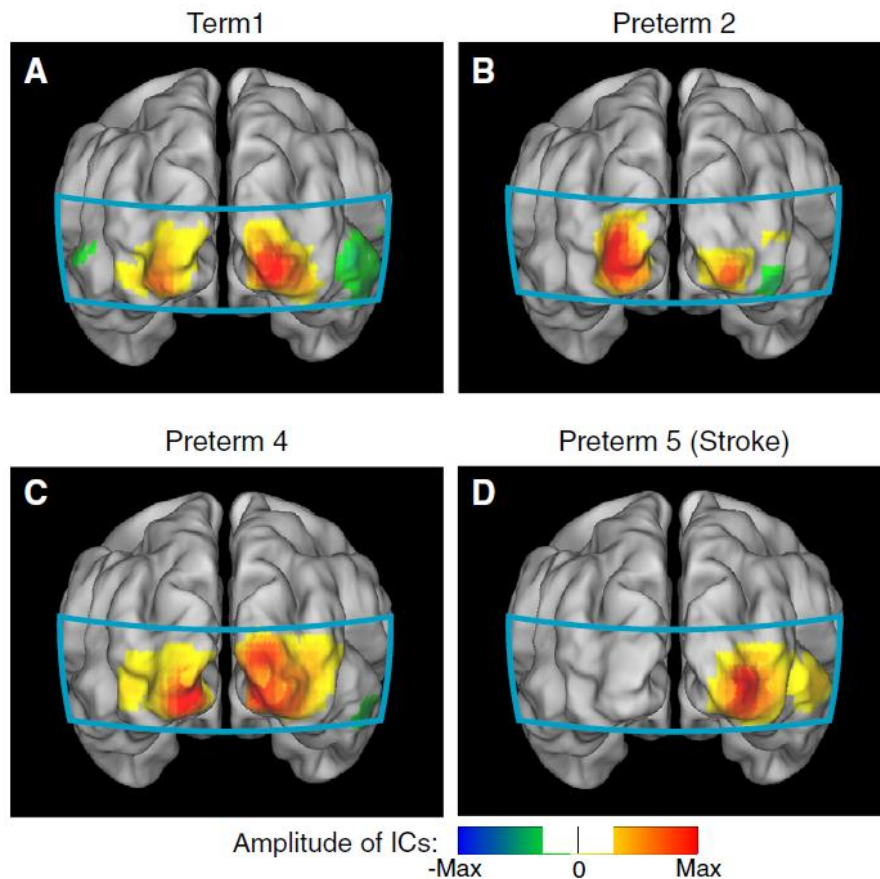
Figure 6.1.2: Diffuse optical images of functional connectivity; using independent component analysis to demonstrate occipital resting state functional connectivity in different subsets; (A) healthy term infant, (B) healthy preterm infant with no significant anatomical brain injury, (C) preterm infant with a complicated clinical course, and (D) a preterm infant with unilateral occipital stroke. Note the absence of interhemispheric connectivity in subset D. Adapted from reference (355).

Given the ability of CW diffuse optical systems to quickly obtain cerebral haemodynamic information early in the life of an infant, and the potential to meaningfully analyse post-injury data, a further investigation of LFOs of the optical signal in PAIS-affected infants was warranted. As previously described, spontaneous LFOs potentially derive from normal neuronal, myogenic, and other brain functions, which are likely

affected in cases of brain injury. Therefore, the hypothesis of this part of the study was that uni-hemispheric stroke would lead to a detectable difference in spontaneous LFOs between stroke-affected and healthy brain regions. A secondary objective of this study was to investigate how the results from the DOT data would differ depending on whether MRI-guided stroke location was encountered in the analysis.

6.2 Patients and Methods

6.2.1 Patients and Data Acquisition

Out of the cohort of infants studied in this project, 5 were selected for this part of the analysis. This was a retrospective investigation and patients were selected based on the detection of an arterial stroke on the MRI. The MRIs were performed as part of standard clinical care. Each infant was studied with the DOT-EEG device (as described in chapter 3) for a duration varying from 30 to 120 minutes whilst receiving intensive care on the NICU.

To support the hypothesis of interhemispheric difference for the LFO bands in perinatal stroke, the same methodology was applied to control subjects. Out of the cohort of healthy controls, 4 were selected based on the quality of their continuous DOT data. The control subjects were healthy newborn infants and most of them were scanned in the first week of life (except for one, Preterm_1).

Infants presenting with seizures and suspected stroke were scanned within 3 days from birth. The incidence and location of stroke was later confirmed by MRI between 7 to 10 days of life. Subjects presenting with seizures but no evidence of stroke on MRI as well as subjects with MRI confirmed bilateral stroke were excluded from the study. All infants were scanned at the cot-side in the NICU whilst receiving intensive clinical care.

6.2.2 EEG Analysis

Alongside the DOT recordings there was simultaneous video-EEG monitoring. The spectral analysis of the EEG traces was performed prior to the known diagnosis and MRI findings. The EEG traces were also reviewed and reported by the Clinical Neurophysiologist, Dr Andrew Michell (AWM). The key elements which would lead to suspicion of stroke would be lateralised signal attenuation of background activity, unilateral loss of certain frequencies within the electrical activity, detection of seizures consistently across a specific hemispheric brain region.

A further computational analysis of the raw EEG data was applied using the EEGLAB toolbox within MATLAB. The aim of this was to plot the channel spectra and cortical maps to identify whether there were any broad discrepancies between the two hemispheres for different frequencies of the EEG signal. For the purposes of this, each dataset was bandpass filtered (hpf 0.5 Hz, lpf 40 Hz) and visually inspected. For each dataset, artefact-free epochs were used for the calculation of the power spectra for certain frequencies between 2 and 25 Hz. An example of the power plots can be seen in figure 6.2.1. Using a spherical dipfit model within the EEGLAB toolbox which recognises the registration of EEG electrodes across the array used in the study, the spectral power for these frequencies was plotted and presented as cortical spectra maps. This is a simple approach to establish differences in the spectral power for certain frequencies of the EEG signal across different parts of the scalp.
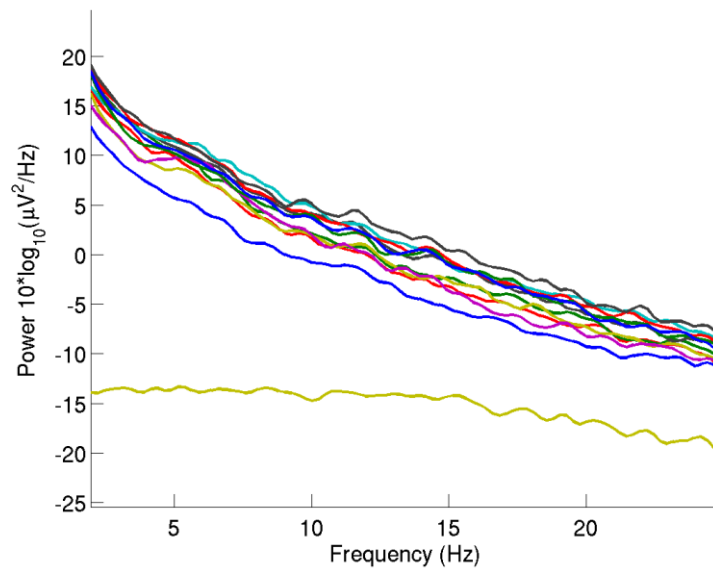
Figure 6.2.1: Example of power spectra plot of an EEG dataset for frequencies between 2 and 25 Hz. This is a plot of spectral power (in μV^2/Hz) on the y axis over frequency (in Hz) on the x axis. The different colours represent different channels and the isolated yellow line is the ECG. This shows a very similar distribution of power over frequency for all the different channels with no clear spectral features.

6.2.3 DOT analysis

The initial study design and analysis, described in this section, was devised, and performed by me. It was refined and expanded by RJC and LAD using bespoke scripts and MATLAB functions.

Pre-processing of the optical data

The initial pre-processing steps were followed as described in section 3.2.3 in chapter 3. For the selection of 'healthy channels', an arbitrary mean threshold of optical intensity was used (10e-4). If the mean measured optical intensity was found to be below this threshold the channels were excluded from the analysis. The motion related artefacts were removed manually (see Fig. 6.2.2). The remaining artefact-free epochs were concatenated thus producing continuous epochs of a minimum 20-minute duration of optical data per infant. The concatenation takes the non-motion sections and sandwiches them together. As part of this process, the mean intensity value of each non-motion segment is adjusted to match that of the previous segment, thus producing a continuous signal. The set minimum epochs of continuous DOT data required to capture and detect LFOs was 20 minutes. The length of every optical dataset, used in the analysis, satisfied the Nyquist criterion for the slowest investigated frequency (0.0055 Hz).

The intensity data were converted to optical density. Based on the modified Beer-Lambert Law the optical density data were converted to HbO_2, HHb, and HbT using a DPF of 4 for both wavelengths (447). The Hb oscillation data were bandpass filtered into the following low frequency bands: a) the VL, between 0.0055 and 0.0095 Hz, b) the RS, between 0.01 and 0.08 Hz, and c) the Mayer wave band, between 0.09 and 0.3 Hz. This process was guided by review of the literature as mentioned in section 6.1 as well as careful inspection of the spectral power of the data (for example see Fig. 6.2.6).
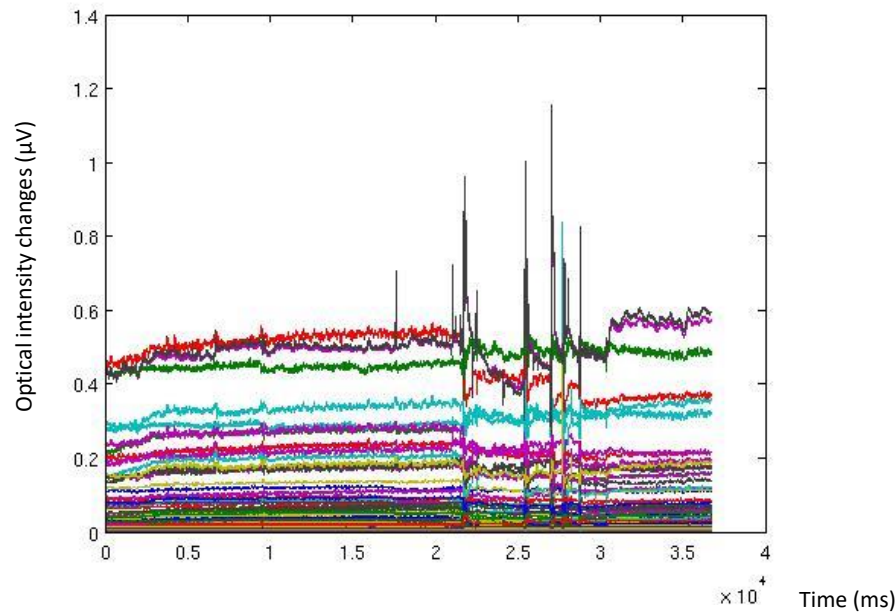
Figure 6.2.2: Raw optical signal of patient 25. This image depicts the raw optical signal; changes of optical density over time, as acquired by the DOT device. The y axis represents the changes in optical density and the different colours reflect separate optical channels. The x axis represents time in milliseconds. Note the sudden change of the trace of the signal from the baseline between 2.2 and 2.8 $x10^4$ milliseconds which reflects motion related artefact and would be rejected in the pre-processing phase of the analysis.

The main trajectory of the analysis was to compare interhemispheric difference in a channel-wise manner between the healthy and stroke affected brain regions. The distribution of the stroke in the MCA territory guided the initial channel selection. These channels were labelled 'blind channels' as their selection was an approximation based on the array and the MCA territory. Therefore, a more specific approach was attempted using the MRIs, as described below.

MRI processing, mesh manipulation, and ROI specification

The quality of the patients' MRIs was adequate to detect anatomical structures and the stroke affected brain regions. The MRIs were inspected in FSL (FMRIB Software Library, Oxford: functional MRI of the brain Software Library), which is a library of methodological tools for functional, structural and diffusion MRI brain data (448, 449)). The anatomical landmarks of nasion, inion, Ar, Al, and Cz were measured and recorded in mm, in each patient's MRI.

The next challenge in the analysis was to certify that the optical data coordinates were in alignment with each patient's MRI. This required that the optical atlas mesh was transformed to match the individual patient's anatomy. For each patient, an age-matched

neonatal head atlas (404) was chosen. This was based on each patient's GA at birth. This atlas was then affine transformed to the patient's individual head coordinates, as defined by the 5 anatomical landmarks on the MRI. The produced mesh contained all separate layers of the extra-cerebral tissues, CSF, grey matter, and white matter and its nodes were connected to these volumetric elements respectively. To each one of these volumetric elements, different optical properties were attributed, based on the type of tissue they originated from.

TA inspected the MRIs and marked the stroke-affected brain region across all layers, thus creating a 3D volumetric stroke mask. This was then utilised to detect the mesh nodes that overlapped with the stroke-affected region. In most cases, the sequence used to identify the stroke areas, was typically T2-weighted Fast Spin Echo (T2-FSE).

The following step was to identify which channels of the existing array were more sensitive to the stroke-affected region. This was accomplished by creating a simulation of light propagation by using the finite element method (FEM) and TOAST++ (351). The patient-based mesh was used as the finite element mesh. The 10-5 positions (370) of the 58 fibres in the cap provided the 3D locations on the mesh. Based on this, a model of how photons travel through tissue was calculated, otherwise known as the sensitivity matrix (for further details see section 2.2.5 in chapter 2, and previously published (365, 408)). This led to the photon measurement density function (PMDF) between a source and detector. This function generally explains how sensitive the detected optical signal is to the underlying mesh elements.

A channel was then deemed sensitive if all the nodes were 10% or greater of the maximum absolute sensitivity of the PMDF for that channel. The stroke related nodes were matched to the sensitive PMDF nodes. The ones overlapping were determined as the region of interest (ROI) channels. As previously mentioned when the ROI channels were not considered, they were referred to as blind channels. Only blind channels were used for the assessment of the control infants.
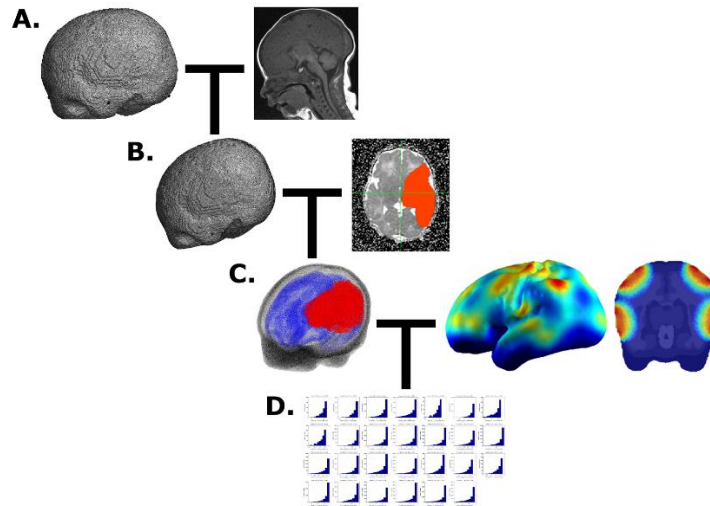
Figure 6.2.3: Flowchart of the MRI and mesh processing: A) the anatomical head atlas is affine transformed to the patient's head coordinates, B) creation of a stroke-specific mask in FSL, which is combined with the patient's mesh to determine which nodes in the mesh contain the stroke (the ROI nodes), C) a mesh with the labelled stroke region combined with light simulation (i.e. PMDFs) to determine D) which channels overlap by least 10% with the stroke area.

Frequency analysis

Power spectral density (PSD) was calculated for the HbO_2 and HHb signals and integrated within the three LFO bands (VL, RS, and Mayer wave).

Statistical analysis

The Wilcoxon signed-rank test was used to assess any difference in spectral power between the controls and the stroke-affected patients. The threshold for statistical significance was Bonferroni-corrected by the number of LFO bands to $p\alpha=0.01/3=0.0033$.

Pearson's R between every homotopic channel pair were calculated in relation to the HbO_2 and HHb signals in the three LFO bands. To assess the interhemispheric correlation difference between the control and PAIS-affected patient groups, the controls' 95% confidence interval (CI) of the correlation R values for 6 different conditions was calculated. This included the calculation of 95% CI of all the control R values for the HbO_2 oscillations in the VL, RS, and Mayer wave frequencies and the HHb oscillations in the VL, RS, and Mayer wave frequencies. This was then compared against the mean correlation R values in the PAIS blind and PAIS ROI groups to estimate the number of patients that lied within the CI values for each separate condition.

6.3 Results

6.3.1 Clinical Details

Within the cohort of infants studied, 5 had a large stroke detected by conventional MRI. Those were patients 16, 18, 20, 25 and 29. Patients 16, 25 and 29 had an isolated diagnosis of cerebral infarction, whereas patients 18 and 20 had a diagnosis of both HIE and cerebral infarction. Patient 20 was excluded from the analysis due to poor data quality. The clinical details of each patient, including the MRI findings can be seen in tables 6.1 and 6.2.

Within the cohort of infants studied with no identified or reported brain injury, controls 4, 8, 10, and preterm 1, were included in the stroke analysis. For the clinical details of the controls please refer to tables 3.2 and 3.3 in section 3.1.3, chapter 3.

Patients 18 and 20 presented with suspected HIE and seizures, fulfilling both criteria A and B as per TOBY cooling criteria for therapeutic hypothermia (43). However, in patient 20 therapeutic hypothermia was discontinued within the first 24 hours as it was determined that her primary diagnosis was not HIE but septicaemia/meningitis. The rest of the patients were admitted due to initial presentation with clinical seizures or a strong suspicion of seizures in the first 12 hours of life.

There are several clinical entities associated with the presentation of neonatal stroke which could possibly play a causative role (see section 1.1.3). The identified predisposing maternal factors in this cohort were gestational diabetes, prolonged rupture of membranes, and chorioamnionitis. The identified predisposing neonatal factors were suspected or confirmed infection/sepsis, HIE, profound anaemia, and persistent pulmonary hypertension of the newborn (PPHN).

Infant	GA	BW	Maternal Factors	Birth	Presentation	Neonatal Course	Outcome at Discharge
Patient 16	38^{+4}	3470	None	SVD, No resus.	Apnoeic episodes.	SVIA, received Phenobarbitone, Suspected sepsis, CSF clear.	Discharged home on Phenobarbitone maintenance. Breast feeding on demand. Normal neurology.
Patient 18	37^{+2}	3150	GDM modulated by diet and Metformin	EmLSCS for suspicious CTG, Profound anaemia (Hb of 2.5), Intubated.	Hypotonia, episodes of decerebrate posturing associated with desaturations.	Ventilated for 3 days, oxygen therapy till day 10 of life. PPHN, Anaemia, multiple transfusions, received Phenobarbitone.	Discharged back to local unit. NGT feeds. Some reduced tone on upper limbs compared to lower.
Patient 20	41^{+3}	3580	Chorioamnionitis, PROM	SVD, Meconium, Intubated.	Back arching, generalised clonic, cycling movements of lower limbs, eye flickering.	Ventilated for 3 days, SVIA since, received Phenobarbitone, Phenytoin and Midazolam, GBS sepsis and meningitis.	Discharged back to local unit. Breast feeding on demand. Normal neurology.
Patient 25	40	3500	PROM	Vaginal forceps, Stimulation and facial mask O$_2$, fast recovery.	Generalised clonic movements.	Ventilated for 1 day, SVIA since, received Phenobarbitone Phenytoin, and Clonazepam.	Discharged back to local unit. IV fluids and NGT feeds. Normal neurology.
Patient 29	41	3688	Chorioamnionitis, Maternal CRP: 181, PROM	EmLSCS for pathological CTG. No resus.	Apnoeic episodes and Rt sided clonic movements.	SVIA, received Phenobarbitone and Phenytoin, suspected sepsis, CSF clear.	Discharged home. Breast feeding on demand. Normal neurology.

Table 6.1: Clinical details of the patients diagnosed with PAIS. The information was gathered from the clinical notes, discharge summary and the clinical staff looking after the patients. The maternal factors refer to events prior to the infant's delivery. (GA: gestational age at birth in weeks /40 weeks of expected normal pregnancy duration, BW: birth weight in grams, GDM: gestational diabetes mellitus, PROM: prolonged rupture of membranes >24 hours prior to delivery, CRP: c-reactive protein (normal when <1), SVD: spontaneous vaginal delivery, no resus: no resuscitation required at birth, EmLSCS: emergency low segment Caesarean section. CTG: cardiotocogram, Hb: haemoglobin, SVIA: self-ventilating in air, CSF: cerebro-spinal fluid, PPHN: persistent pulmonary hypertension of the newborn, GBS: group B streptococcus, NGT: nasogastric tube, IV: intravenous).

Infant	GA	CGA	CrUS	Single-channel aEEG	Clinical EEG	MRI findings
Patient 16	38^{+4}	38^{+6}	Lt temporal lobe lesion suggestive of infarction	Seizures detected, normal background	Normal	Large haemorrhagic lesion in the Lt temporal lobe associated with overlying subdural haemorrhage; secondary to venous infarction related to the subdural or bled from a pre-existing vascular anomaly such as deep venous anomaly.
Patient 18	37^{+2}	37^{+2}	Normal	Seizures detected, discontinuous background	Mildly discontinuous. No evidence of seizures.	Abnormal signal intensities within the territory of the Lt middle cerebral artery consistent with infarction. Involvement of the basal ganglia, thalami and PLIC on the Lt with abnormal diffusion in the Lt cerebral peduncle.
Patient 20	41^{+3}	41^{+3}	Possible cerebral oedema	Seizures detected, discontinuous background	Discontinuous, no evidence of seizures.	Bilateral infarct of both posterior parietal, temporal, occipital white matter, and cortex (some sparing of the Lt visual cortex but involvement of both optic radiations).
Patient 25	40	40^{+3}	Normal	Seizures detected, normal background	Asymmetry with attenuation over the Rt hemisphere. Sharpened theta discharges over the Rt temporal region. No evidence of seizures.	Large infarct over the Rt hemisphere, involving the temporal, parietal, and occipital lobe.
Patient 29	41	41^{+3}	Normal	Seizures detected, normal background	Low amplitude activity over the Lt anterior region and runs of sharp waves maximal over the Lt temporal region. No evidence of seizures.	Abnormal signal intensity within white matter, cortex, and basal ganglia within the territory of the Lt middle cerebral artery consistent with infarction.

Table 6.2: Results of investigations of the patients diagnosed with PAIS. The cranial ultrasound results refer to the findings of scans performed by the clinical team (neonatologists) on admission and on day 3 of life. All patients had 72 hours' continuous single channel aEEG monitoring, and the results refer to the activity noted in the first 24 hours' post admission. The EEG results refer to routine 20 minute 21-lead video EEG performed as per standard clinical investigation of any infant presenting with seizures or seizure-like activity. The MRI findings refer to structural MRI, T1 and T2 weighted images obtained after day 7 of life as per standard clinical care (GA: gestational age at birth, CGA: corrected GA at time of study, both expressed in weeks /40 weeks of normal pregnancy duration, CrUS: cranial ultrasound scan, aEEG: amplitude integrated EEG, Rt: right, Lt: left).

As per standard clinical care all patients had 72 hours' continuous single channel aEEG monitoring. Serial cranial ultrasonography was performed on admission and day 3 of life as standard practice by the clinical team for identification of any obvious structural abnormality, haemorrhage or other. Within the first 48 hours of admission to the unit a

20-minute 21-lead video EEG was performed for exploration of the background activity and any ongoing seizure activity. All infants had received some form of anticonvulsant treatment prior to this EEG. Depending on presentation, clinical suspicion, matter of urgency and scan availability, the patients had a structural MRI within the first 10 days of life. The results of all the investigations performed can be seen in table 6.2. A representative sample of MR images per patient can be seen in figure 6.3.1 and a specific one to the patients included in the analysis in figure 6.3.2.
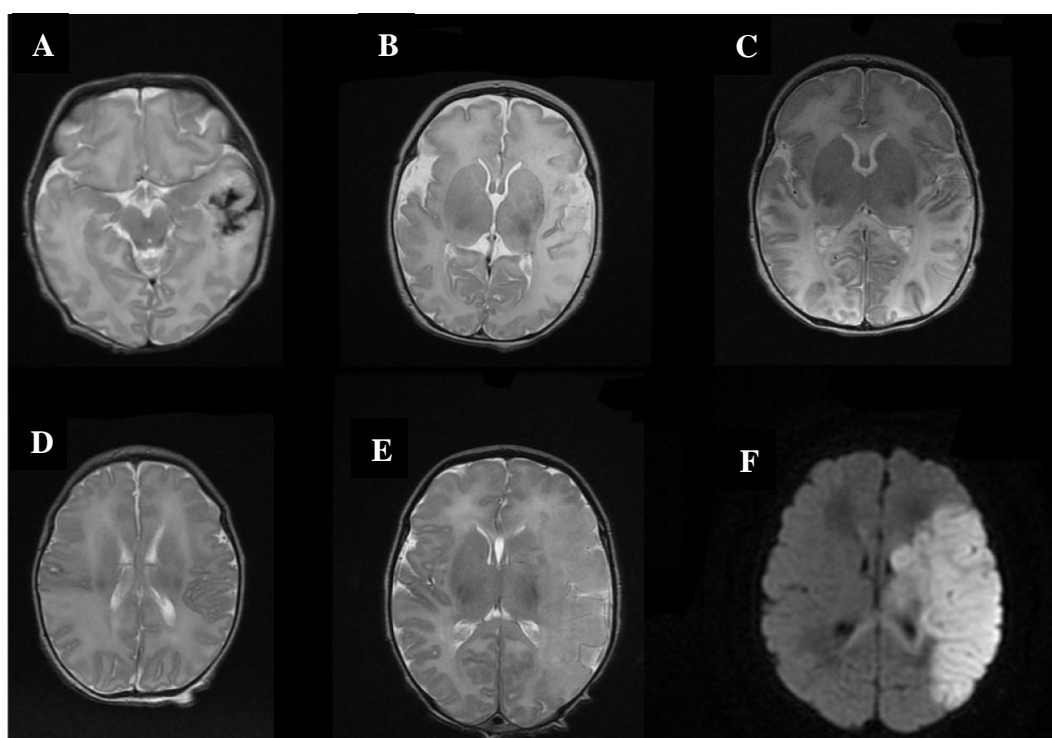
Figure 6.3.1: MR images for each of the stroke-affected patients. (A) T2-weighted image of patient 16 showing a large haemorrhagic lesion in the left temporal lobe associated with overlying subdural haemorrhage secondary to venous infarction, (B) T2-weighted image of patient 18 showing a left-sided MCA infarct with left-sided involvement of the basal ganglia, thalami and PLIC, (C) T2-weighted image of patient 20 showing global infarction of both hemispheres with some sparing of the left occipital lobe, (D) T2-weighted image of patient 25 showing a right-sided MCA infarct, (E) T2-weighted image of patient 29 showing a large left-sided MCA infarct, (F) Diffusion-weighted image of the same patient 29. (PLIC: posterior limb of the internal capsule).
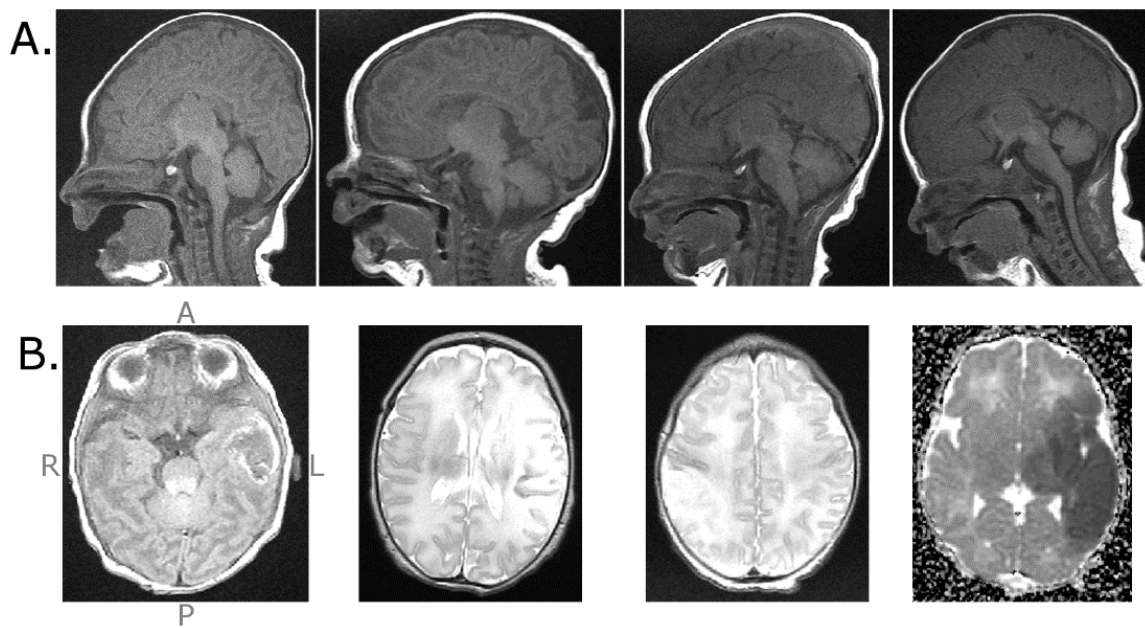
Figure 6.3.2: Anatomical MR images for the subjects in the PAIS group. A) Sagittal T1-weighted images of each stroke-affected patient (patient 16, 18, 25 and 29 from left to right respectively), B) Axial views showing abnormal signal in the stroke location (patient 16, 18, 25 and 29 from left to right respectively). From left to right, the MR sequences depicted here were T1 SE (Spin Echo), T2 FSE (Fast Spin Echo), T2 FSE, and ADC (Apparent Diffusion Coefficient). (A: anterior, P: posterior, R: right, L: left).

6.3.2 EEG Results

The results of the spectral analysis of the EEG, as reported by AWM were the following:

Patient 16: EEG recording of good quality, with no lateralisation or asymmetry. Overall background activity of low amplitude with apparent variation between sleep and wakefulness. No seizure activity detected.

Patient 18: EEG recording of moderate quality, with discontinuous background trace but not burst suppressed. No asymmetry identified. Seizure activity over the anterior midline seizure activity between 176 to 338s, 1,788 to 2,019s, 2,109 to 2,427s, 2,689 to 2,749s, 3,000 to 3,526s).

Patient 25: EEG recording of good quality, with no lateralisation or asymmetry. Overall normal background activity with variation between sleep and wakefulness. Sharpened theta discharges over the right temporal region No seizure activity detected.

Patient 29: EEG recording of good quality. Continuous background activity with low amplitude activity over the Lt anterior region and runs of sharp waves maximal over the Lt temporal region. No seizure activity detected.

Further information was obtained from the extraction of the power spectra of the EEG signal. The spectral maps are presented in figures 6.3.3-6.3.5.
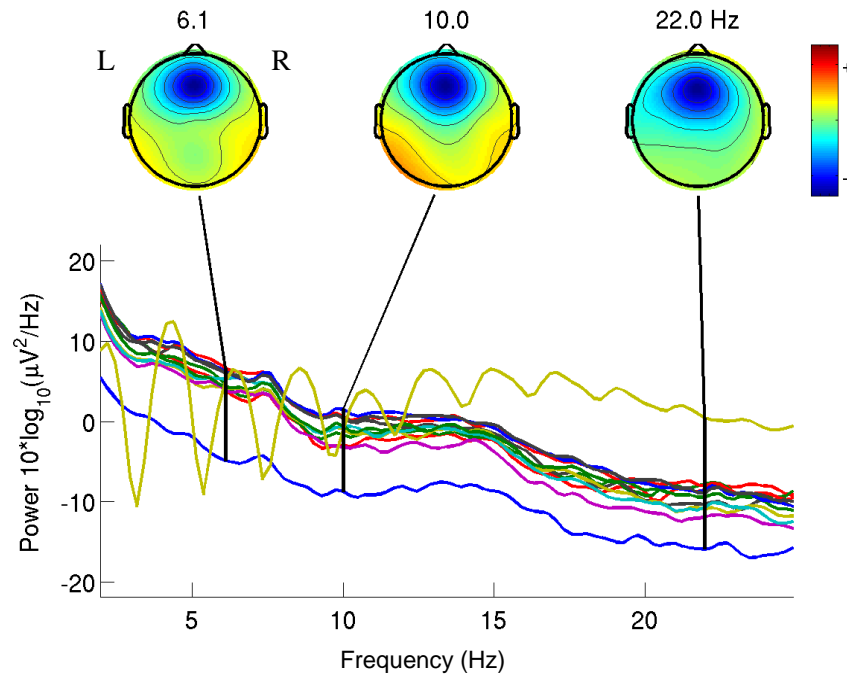
Figure 6.3.3: Power spectra plots with cortical maps in patient 16. These were calculated based on frequencies 6, 10 and 22 Hz of an artefact-free segment of EEG data. The plot depicts the power spectra (μV^2/Hz), on the y axis, over different frequencies (Hz) on the x axis. The different colours represent different EEG channels. The separated lime green line represents the ECG signal, whose power spectra is consistent throughout with few fluctuations.

For patient 16, there was lower spectral power at 6 Hz over the left hemisphere, and much lower at higher frequencies of 22 Hz with an overall paucity in the frontal and anterior parietal regions (see Fig. 6.3.3). For patient 25, it appears that overall there was increased power spectra over the right for all frequencies, which could be attributed to the occasional sharps of varied frequency content arising from the right temporal region (see Fig.6.3.4). For patient 29, there was overall paucity of power spectra for all frequencies on the left hemisphere compared to the contralateral one (see Fig. 6.3.5).
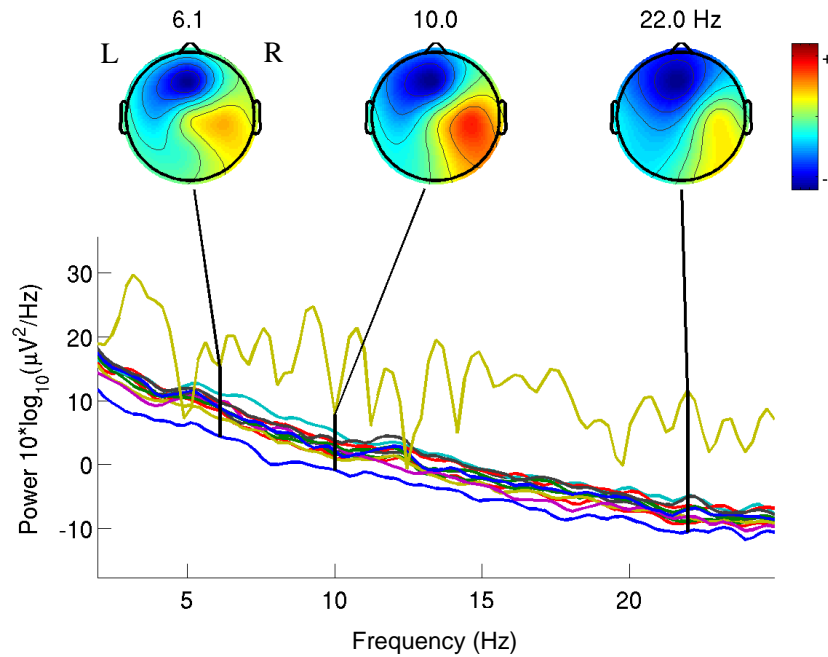
Figure 6.3.4: Power spectra plots with cortical maps in patient 25. These were calculated based on frequencies 6, 10 and 22 Hz of an artefact -free segment in patient 25. The plot depicts the power spectra (µV²/Hz), on the y axis, over different frequencies (Hz) on the x axis. The different colours represent different EEG channels. The separated lime green line represents the ECG signal, whose power spectra is consistent throughout with some fluctuations.

The quality of the EEG recording for patient 18 was suboptimal and no meaningful spectral map could be obtained as there was increased artefact interference. Excessive processing of the artefact would interfere with the frequencies under investigation for these spectral maps and hence was not performed.
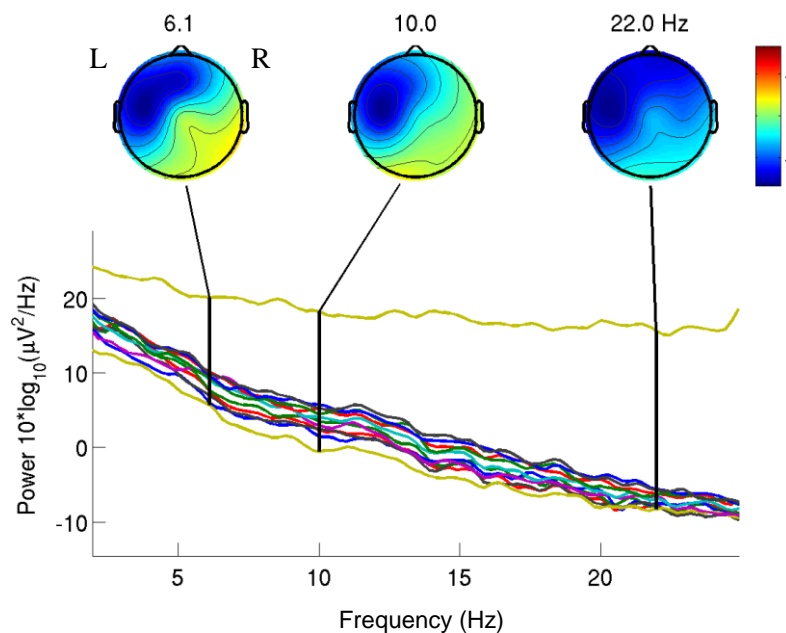
Figure 6.3.5: Power spectra plots with cortical maps in patient 29. These were calculated based on frequencies 6, 10 and 22 Hz of an artefact -free segment in patient 29. The plot depicts the power spectra (μV^2/Hz), on the y axis, over different frequencies (Hz) on the x axis. The different colours represent different EEG channels. The separated lime green line represents the ECG signal, whose power spectra is consistent throughout with few fluctuations.

6.3.3 DOT Results

Optical data quality

The quality of the optical signal from the stroke-affected patients was good, with roughly 83% of channels included in the analysis. An example of the data quality can be seen in figure 6.3.6A, which represents the continuous concatenated optical intensity signal for the selected channels per hemisphere. The selection of the channels as guided by the sensitive PMDFs for the same patient, are depicted in figure 6.3.6C. For each ROI channel, its homotopic partner was selected. In the spectral power graph (see Fig. 6.3.6B), one may notice a clear signal power from the cardiac and respiratory cycles at approximately 1.9 Hz and 0.6 Hz, respectively. Most of the power spectral density across the different datasets was located below 0.3 Hz. The length of each stroke-affected patient's data was on average 27.04 ± 9.21 min (mean $\pm$ standard deviation). The length of each control patient's data was on average 12.77 ± 5.89 min.

Spectral power content

There was no significant interhemispheric difference in any of the control infants. In the stroke-affected population, only patient 18 showed a significant interhemispheric difference, with the spectral power of the HbO_2, HHb, and HbT being significantly less in the healthy hemisphere compared to the stroke-affected hemisphere in all three frequency bands.
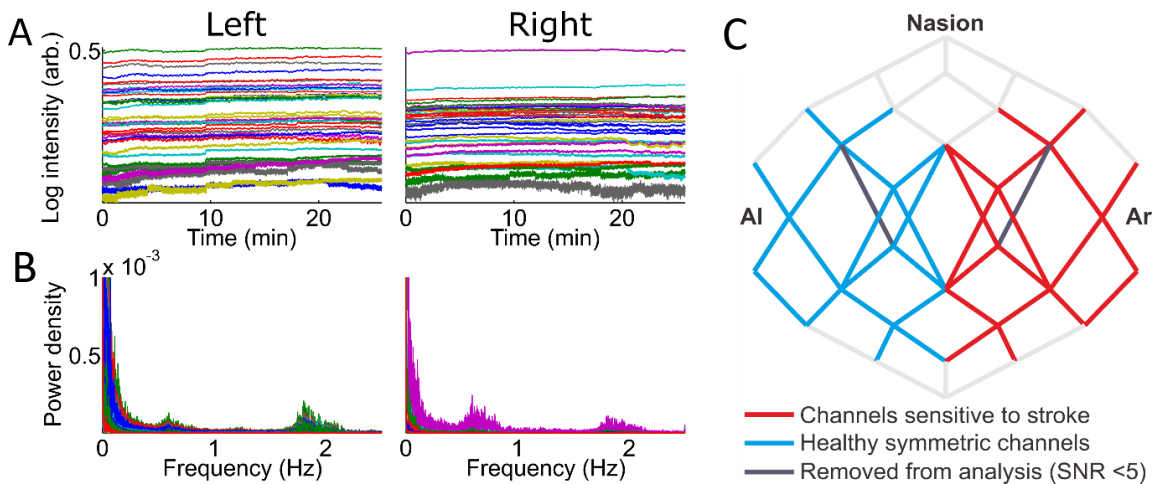
Figure 6.3.6: Processed optical data from patient 25. A) Raw concatenated intensity data from all channels with SNR >5. B) Power spectral density of the channels in (B). C) DOI channels sensitive to the stroke (red) and the healthy homotopic channels (blue). One channel from the ROI had insufficient signal to noise ratio (SNR) (grey) and neither that or its homotopic one was used in the analysis.

Correlation results

As mentioned above in the optical data quality section, the optical signal from the stroke-affected patients was good, with roughly 83% of channels included in the analysis. The selection of the channels as guided by the sensitive PMDFs (ROI group) was narrowed based on whether the channels were sampling the area of the stroke. In the ROI group, 2 pairs of channels were deemed to be sampling the area of the stroke for patient 16, 16 pairs for patient 18, 9 pairs for patient 25, and 18 pairs for patient 29.

The mean interhemispheric correlation values for patients 18, 25 and 29 lied outside the 95% CI of the controls for the HbO_2 and HHb oscillations in all three frequency bands. This was consistently noted in both the blind and ROI group. The mean interhemispheric correlation values of the ROI channels tested in patient 16 for the HbO_2 oscillations in the resting state frequency fell within the 95% CI of the controls, 0.656 (95% CI: 0.635 - 0.713). The rest of the mean interhemispheric correlation values of the ROI channels tested in patient 16 (as seen below in Table 6.3) lied outside the 95% CI of the controls. Similarly, the mean interhemispheric correlation values of the blind channels tested in patient 16 (as seen below in Table 6.3) lied outside the 95% CI of the controls.

The absolute mean values per patient in each condition were either similar or marginally lower in the ROI group compared to the blind group except for patient 16, where the mean values of the blind group were the lower ones. The absolute mean values of patient 16, in both the ROI and blind groups, were much higher compared the ones of the rest of the patients. This was consistently seen across the different frequency bands. The mean correlation values of patient 18, 25, and 29 were significantly and consistently low regardless of MRI-guided channel selection (with values ranging from 0.109 to 0.598 across the ROI and blind groups, see Table 6.3).

ROI		P16	P18	P25	P29	95% CI
HbO₂	VL	0.823	0.289	0.357	0.510	0.693 - 0.792
	RS	0.656	0.348	0.214	0.498	0.635 - 0.713
	Mayer	0.736	0.485	0.226	0.319	0.432 - 0.542
HHb	VL	0.833	0.235	0.117	0.377	0.581 - 0.724
	RS	0.764	0.177	0.205	0.248	0.624 - 0.704
	Mayer	0.653	0.281	0.109	0.119	0.341 - 0.441
Blind		P16	P18	P25	P29	95% CI
HbO₂	VL	0.639	0.315	0.464	0.598	0.693 - 0.792
	RS	0.618	0.352	0.365	0.561	0.639 - 0.712
	Mayer	0.621	0.484	0.300	0.379	0.432 - 0.542
HHb	VL	0.581	0.197	0.316	0.436	0.582 - 0.724
	RS	0.509	0.174	0.333	0.357	0.624 - 0.704
	Mayer	0.471	0.266	0.204	0.182	0.339 - 0.441

Table 6.3: Mean interhemispheric correlation values of patients 16, 18, 25, and 29 for HbO₂ and HHb oscillations in the VL, RS, and Mayer wave frequency bands compared against the 95% CI of all the controls in each condition. The table is referring to the two study groups the ROI group (top half of the table) where channels were selected based on MRI-guided stroke localisation and the blind group where channels were selected without imaging-guidance. Note that the given 95% CI values are the same for both the ROI and blond group. For the controls only one standard channel election was performed, which was not MRI informed, as there were no neurological concerns or lateralised clinical findings.

6.4 Discussion and Conclusions

The results of this part of the thesis are in keeping with some evidence of disrupted lateralised and inter-hemispheric brain function in stroke-affected subjects. No difference in the LFO spectral power of either hemisphere was identified in either of the controls or patients, apart from patient 18. There was a difference in interhemispheric correlation between controls and PAIS-affected patients in HbO_2 and HHb oscillations for all three frequency bands, with deviation from the relevant 95% CIs of the controls. It was only the mean interhemispheric correlation value of the ROI channels in HbO_2 resting state oscillations of patient 16, which lied within the 95% CI of the controls in the same frequency band.

The EEG recordings during the study were similar to the expected results from other studies (148, 150). In two of the patients, patient 18 and 20, electrographic seizure activity with focal onset was detected, thus aiding the diagnosis. The EEG can be a reliable tool for detection of features characteristic or suggestive of stroke. However, if the lesion is not extensive enough, it does not always appear to cause attenuation or sharp-like waveform activity (150). In the absence of long, multi-channel recordings it is much less informative. If no seizures are captured during the EEG recording, it is difficult to establish the presence of a focal point of their origin or suspect stroke in the first instance. Administration of medication (such as phenobarbitone) for cessation of seizure activity, may alter the background activity and mask potential peri-ictal elements suggestive of perinatal stroke. A pathological EEG does aid the diagnosis but a completely normal one does not exclude the final diagnosis of perinatal stroke. In the EEG power spectra results there was some suggestion of lower frequency content over the affected side for patients 16 and 29 (see Figures 6.3.3 and 6.35) and higher frequency content over the right side for patient 25 where sharp wave activity was ongoing in keeping with lateralisation of stroke (see Fig. 6.3.4). However, the source analysis performed here was limited by the small number of EEG electrodes used in the study, thus limiting the use of this tool and its interpretation.

The MRIs performed, invariably between day 4 to 10 of life, ultimately establish the diagnosis of perinatal stroke. The cranial ultrasound scans were not diagnostic apart from patient 16, where the one performed within 24 hours from clinical presentation,

accurately detected an echogenic lesion in the left temporal region later confirmed on MRI.

The optical power spectra content in the different low frequency bands did not return any significant results for any of the control or PAIS-affected patients, apart from patient 18. The presumption was that stroke-affected regions would have altered vascular tone and abnormal circulation patterns which would be represented in the frequency content of the optical signal. A possible explanation could be that PAIS patients were scanned with DOT before bulk tissue necrosis had occurred; meaning any change to the frequency power content of underlying circulation patterns was undetectable. There is ongoing research to improve the understanding of recovery mechanisms following stroke not only looking at the infarcted region but also the peri-infarct zone (450-452). In contrast to our results, Li et al. studied spontaneous cerebral oscillations amongst healthy adults and patients at risk for atherosclerotic stroke by performing a wavelet transform analysis on a single left prefrontal NIRS signal in five frequency bands subdivided between 0.005-2.0 Hz. They found significantly lower oscillation power for HbT and HbO_2 in the group of patients at risk of stroke versus the controls (453). Perhaps the primarily different origin (haemorrhagic as opposed to ischaemic) and pathophysiological cascade in adult compared to perinatal stroke may help explain why no interhemispheric differences in spectral frequency band power were noticed.

The interhemispheric difference in spectral power content was detected only in patient 18, who had lower spectral power of the HbO_2, HHb, and HbT in the healthy hemisphere compared to the stroke-affected hemisphere in all three frequency bands. This could be attributed to the ongoing electrographic seizure activity noted on the simultaneous continuous EEG recording (five discrete episodes of epileptiform activity were noted, see Table 4.3). This activity was originating from the left hemisphere (stroke-affected side), spreading across the cortex within seconds of onset. Further studies are warranted to investigate how the LFO spectral power content of the optical signal could be used as a method of seizure-detection in the NICU.

The mean interhemispheric correlation values of all patients deviated from the 95% CIs of the controls. This was noted for both HbO_2 and HHb oscillations in all three frequency bands consistently in the blind and ROI groups. The exception was patient 16, where there was deviation for one of the conditions tested. More specifically, the mean

correlation value of the ROI channels for HbO_2 resting state oscillations in patient 16 was the one found to lie within the 95% CI of the controls (0.656, 95% CI: 0.635 - 0.713). Overall these results (see Table 6.3) demonstrated a significant difference in interhemispheric correlation in cases of stroke-affected patients. Additionally, the absolute mean values of patients 18, 25 and 29 were much lower in both the blind and ROI groups, thus supporting low interhemispheric correlation in stroke-affected patients. This interhemispheric correlation difference was noted consistently regardless of MRI-informed channel selection. This potentially supports that having the patient's MRI is not necessarily a prerequisite for extracting some early diagnostic information from the optical data prior to definitive imaging. However, this was only tested on four patients.

The absolute mean values of patient 16 were much higher than the ones of patients 18, 25, and 29. This was a consistent observation regardless of MRI-informed channel selection, although the values were noted to be lower in the blind-channel assessment. This would suggest a higher interhemispheric correlation between homotopic channels in patient 16 as opposed to the rest of the patients. This difference noted could be attributed to the fact that the lesion in patient 16 was significantly smaller, only occupying a small region of the left temporal lobe, whereas the lesions in all other patients were significantly larger (see Figures 6.3.1 and 6.3.2). It was observed that the correlation values for patient 16 were lower in the blind-channel group compared to the ROI-channel assessment. It is worth noting here that the ROI channels sampling the stroke lesion in patient 16 were only two homotopic pairs compared to a fair number of channels assessing the stroke regions in the rest of the patients. The relatively sparse array over the temporal lobe and small stroke lesion per se would have this effect upon the MRI-guided channel selection and assessment of interhemispheric correlation. In the blind-channel assessment, however, the interhemispheric values for patient 16 were lower and still outside the 95% CI of the controls.

This indirectly could suggest that interhemispheric correlation appears lower in the event of larger lesions, something which also appears in the EEG literature regarding perinatal stroke; the larger the lesion, the more pronounced the attenuation of the signal on the stroke-affected side (150). These results also highlight the importance of using a dense array over the areas of interest and is explained in further detail later in the discussion.

In a similar fashion, White et al. observed inter-hemispheric Pearson's R values of approximately 0.8 for HbO_2 and 0.65 HHb in healthy term patients, whereas the patient with occipital stroke had markedly decreased correlation of approximately 0.2 for HbO_2 and -0.15 for HHb (355). White et al., however, demonstrated this only on one patient at a later stage (at 10 weeks of life) using a high density (HD) DOI device with 106 channels covering the occipital cortex only. No follow up studies have been presented by the group.

Certain research groups have also explored Hb oscillations in the respiratory and heart rate frequency bands. Muehlschlegel et al. used bi-hemispheric CW-NIRS to investigate inter-hemispheric correlation coefficients for the respiratory and cardiac oscillations amongst nine healthy adults and twelve stroke-affected patients, identifying that the latter had a lower inter-hemispheric correlation coefficient for both the cardiac and respiratory frequency bands (454). In this thesis, the respiratory and heart rate frequencies were not included in the analysis due to the absence of continuous monitoring of these physiological parameters. There is, however, ongoing work on recording and integrating this information into the analysis for future studies. Similarly, arterial blood pressure (ABP) was not recorded, due to no consistently existing continuous invasive blood pressure monitoring across all the subjects.

Other groups have investigated the interhemispheric phase shift between the ABP in relation to the flow velocity across the MCA (as measured by transcranial Doppler (TCD)) and the low frequency HbO_2 oscillations using NIRS in both healthy and stroke-affected adults (446, 455). It was demonstrated that HbO_2 inter-hemispheric phase shift was significantly less in subjects undergoing thrombolytic therapy compared to untreated stroke adults (446). Han et al. investigated inter-hemispheric phase synchronisation of HbO_2 oscillations in the prefrontal area of stroke-affected elderly patients (21 patients with cerebral infarction and 21 controls). The group looked at low frequencies (0.021-0.052 Hz and 0.052-0.145 Hz) and higher frequencies (0.145-0.6 Hz and 0.6-2 Hz), finding significantly lower phase coherence within the lower frequency bands in hypertensive patients with cerebral infarction (456). Although this study was a single channel NIRS experiment on elderly patients, it still demonstrated the disruption of inter-hemispheric coherence due to stroke primarily within the VL and RS frequency bands. In healthy adult volunteers, Kuo et al. identified high coherence between the spontaneous oscillations of the MCA blood flow velocity (as measured by TCD) and ABP only within

low frequencies above 0.04 Hz, but not for very low frequencies (0.016 to 0.04 Hz) (431). Further analysis in their study showed that the phase angle between ABP and the MCA flow velocity was particularly dependent upon frequencies in the RS band (431). Both studies add credence to the idea that physical injury to the MCA would most directly affect VL and RS oscillations, and that these frequency bands should be a primary target of investigation for stroke detection as presented in this thesis.

The sample of the patients is small, but the consistency of the results suggests an interhemispheric difference deviating from the expected interhemispheric correlation seen in controls. Additionally, the results appear to be consistent and independent to MRI-informed stroke localisation. This supports further research and development of this technology in early assessment and cortico-vascular monitoring in the first few days of life until more definitive imaging such as MRI is available or applicable depending on the patient's overall clinical condition.

With currently available commercial DOI systems there is insufficient channel count to densely cover the entire head with sources and detectors; consequently, the only way to sample the entire cortex was to create a sparse array. As the most likely site of PAIS injury is the MCA, the richest data generally came from channels sampling the frontal and parietal cortical regions. A custom-made array to sample the MCA territory could have been designed. However, the repercussion of this approach is that stroke located in other brain regions, will be insufficiently sampled. This would decrease the possibility of providing information on an individual patient basis. There is ongoing research in the field of high-density DOI systems (see section 7.2 of chapter 7 for further details).

This part of the thesis is one of very few evaluating PAIS using DOT in the acute phase of the perinatal stroke, and to current knowledge, it is the first to assess inter-hemispheric connectivity in stroke-affected infants using a multichannel, whole-head DOT-EEG system. However, this project is limited by the small number of subjects, sparse channel arrangement, and lack of access to peripheral physiology data. However, the inter-hemispheric correlation results, warrant further investigations to develop definite conclusions regarding the potential for early monitoring and detection of PAIS. These findings could serve as the basis of a larger study in establishing DOT as an early

diagnostic tool of PAIS at the cot-side, one which would complement the existing neuro-monitoring and neuro-imaging tools to inform clinical management and prognosis.

Chapter 7: Conclusions and Future Directions

7.1 Summary of Conclusions

This thesis has presented certain encouraging results in the field of simultaneous DOT and EEG investigation of neonatal term brain injury with a focus on HIE and PAIS. The results have hopefully contributed to a better understanding of these clinical entities and associated neurophysiological phenomena such as seizures and burst suppression.

This project demonstrated the feasibility of studying critically ill infants in their first few days of life by the cot side, without interfering with acute clinical care or causing any adverse reactions. The methodology of combined EEG and multi-channel continuous wave DOT application proved to be safe, non-invasive, available out of hours, and portable to the cot side.

As shown, in the case study published by our group (365), DOT and EEG can be used to capture neonatal seizures and investigate the associated cortico-vascular fluctuations of HbO_2, HHb and HbT. This was an encouraging first step in recognising some of the haemodynamic changes occurring during a seizure on an infant's cortex. However, there was little reproducibility of this data in the later part of this project as described in my thesis in chapter 4. Although it was incredibly challenging to time and capture seizure activity in an infant at risk, in 1 to 4-hour recordings, such data were collected from 4 patients. During these recordings, some changes in the concentration of mainly HbO_2, HbT and less of HHb were noted. Some of the features of these changes were unlike the typical functional stimulation response seen in infants (457, 458). On the contrary they were of an amplitude greater than the typically observed in healthy infants (305, 316). However, the recordings were overall heavily corrupted with artefact, thus minimising their contribution to substantial analysis and reproducibility of the original data seen in the case study (365). The artefacts noted were not always patient-related or seizure related as one would expect (as this was the case for patient 24). In one recording there was a harmonic oscillation which could be attributed to electrical interference (in patient 15). In two other recordings, there was a slower superimposing artefact which seemed to be synchronised with the periodic inflation of the cooling mattress the patient was wrapped in (patient 18 and 20). These events coincided with either seizure onset or offset, thus making the extraction of the haemodynamic response challenging.

The first ever images of the cortical haemodynamic changes associated with burst suppression in the clinical background of neonatal HIE were published during this

research project (408). A significant increase in the HbO_2, HbT, and HHb concentrations was noted in response to burst activity. This again did not follow the expected functional stimulation response in infants. The observed changes could potentially be attributed to either insufficient supply to meet the metabolic demand of the injured tissue or part of the developmental processes occurring in the neonatal period. The increased spatial resolution of multichannel DOT, revealed spatiotemporal characteristics of the haemodynamic changes across the neonatal cortex which in a retrospective analysis, appeared to be associated with pathological findings in the patient's own MRI. However, there is still the requirement for methodological development in establishing image-based statistical approaches comparable to the ones used in other means of functional neuro-imaging.

In the investigation of PAIS, there was a consistent deviation of the stroke-affected patients' mean interhemispheric correlation from the 95% CI of the interhemispheric correlation values of all controls in HbO2 and HHb low frequency oscillations. These results were consistent and somewhat independent to MRI-guided stroke localisation as the results were similar in both the ROI-channel and blind-channel selection groups. A variation in the mean interhemispheric correlation values amongst the patients suggested that the interhemispheric correlation is much lower in cases of large unilateral lesions. However, one must err on the side of caution as the total number of patients was only 4 in total. The results indeed originated from a very small number of patients, principally because of the relative scarcity of PAIS patients. This could still be an initial step towards further research in the development of a DOT-based methodology that can complement the existing diagnostic methods in the early detection of perinatal stroke. The small number of patients in combination with a relatively sparse whole head array were the main challenging factors in this part of the thesis.

The key issues and challenges identified in this thesis are described in section 7.2 alongside suggestions on how to improve the methodological approach and reproducibility of this research.

7.2 Challenges and Methodology Development

The key challenges during the conduction of this research and different aspects of this study were the following: motion artefact, physiological parameters that may affect or contaminate the optical signal, design and density of the array, lack of image-based statistical approach to the methodology and number of patients. This section attempts to address some of these key issues.

One of the most significant issues in acquiring DOT data is the impact of motion in signal quality. As one may imagine, and as shown in the previous chapters, this is even more challenging when performing infant studies. Even subtle movement between the optical fibre and the scalp can cause changes of high amplitude in the optical signal that only cease as the movement stops. Slight variation in the force applied upon an optical fibre against the skin affects the intensity measurements significantly, and the same applies to the presence of hair. As described in the methodology there are ways to overcome motion artefacts. One way to avoid or minimise the occurrence of motion, is to make sure the infant is in a comfortable position, ideally in the postprandial phase (especially in the case of a healthy term infant), asleep or quiet. Prior to the beginning of the recording, it is also important to arrange the headgear and optical fibres in an optimal position to avoid their movement during the study. In the pre-processing phase one may proceed to careful visual inspection and manual rejection of artefact-corrupted periods. A last option is to apply post-processing methods for filtering artefacts (374). Most DOT-based studies use all the above-mentioned ways to identify artefact-free epochs whilst there are ongoing advances in motion artefact rejection (459, 460).

However, there are occasions where movement is inevitable, for instance if the infant is seizing (as seen in chapter 4). As described previously, clinical seizures in infants are often subtle, and most frequently detected retrospectively by video-EEG. A possible way of addressing this would be to include an accelerometer (or other motion sensor) into the existing DOT headgear. All the above notions could be maintained in minimising motion with the added advantage of being able to separately capture any movement of the head whilst acquiring the data. This would allow fully automated detection of motion-related events and thus aid the artefact filtering processing.

A different type of artefact identified in the group of patients with seizures during the recordings raised different questions as to what the potential effect on surrounding

factors to data acquisition and the optical signal is. In chapter 4, a re-occurring slow wave in the optical signal was observed. This was noted in two patients (patient 18 and 20) who were undergoing hypothermia at the same time. This artefact coincided with the inflation and deflation of the cooling mattress that the patients had wrapped around them (see Figures 4.3.8, and 4.3.10-11). The patients' torso upper and lower limbs were wrapped within the mattress, whereas the head was exposed as the elastic headgear was applied. The head part of the cooling mattress was still lying underneath the patients head with the headgear applied on. There was increase of the optical signal from the baseline with the inflation of the mattress and decrease relevant to the baseline with the deflation of the mattress. These changes coincided with either the onset or offset of seizure events making the extraction of the haemodynamic response to seizure activity challenging. One theory that could explain this, is that as the mattress was inflating there was slight head movement. However, the observed morphology of this change in the optical signal was slower than the one expected to be associated with a motion-related artefact (see Figures 4.3.8, and 4.3.10-11). Another theory that could explain this phenomenon is that the inflation and deflation of the mattress causes arterial blood pressure changes observed as cortico-vascular changes in a hypoxic encephalopathic patient with presumed altered cerebral autoregulation.

To explore the above-mentioned theory there are a lot of questions that remain unanswered and require further development of the technology for any justifiable conclusions to be reached. The assessment of any movement of the head could be addressed with the use of an accelerometer applied onto the headgear as described previously. The assessment of any peripheral changes such as changes in arterial blood pressure or heart rate is challenging if there is no simultaneous ongoing monitoring of these parameters during data acquisition. For future projects, continuous monitoring of physiological parameters such as heart rate, respiratory rate, SaO_2 and arterial blood pressure should be considered as a requirement. It improves the understanding of cortico-vascular changes observed and informs the analysis. And finally, is it possible that the observed changes are not reflective of cortical changes but more superficial tissue changes?

A frequent issue in DOT data acquisition and analysis is the contamination of the signal by vascular activity in the layers of extracerebral tissue. Light must penetrate

several layers of tissue before reaching the brain, including the skin and skull. Physiological changes, such as those due to heart rate, blood pressure or respiration, occurring within these superficial tissues may contaminate the signal. Recent work shows that the use of short source-detector NIRS channels (<15 mm), (which are used to measure haemodynamics of the scalp alone rather than cortical signal) can be used to improve the brain-specificity of NIRS and DOT measures (see Fig. 2.2.10). Further analytical methods such as signal regression (346, 461, 462), independent component analysis (ICA) (463) or principal component analysis (PCA) (464, 465) can be utilised to calculate and hence eliminate the cortico-vascular changes attributed to superficial layers of the head. The process of DOT image reconstruction (as mentioned in chapter 2 and 3) includes the separation of signals arising from the separate superficial structures over the brain tissue (351). Therefore, the presence of short separation channels onto the head array during data acquisition would further inform signal analysis and should be considered in further developing this DOT-EEG technique. Furthermore, in situations like the presumed "artefact" seen secondary to the cooling mattress, the presence of short separation channels would clarify whether this could be a response to changes in superficial vasculature.

The whole-head array used in the project was designed to capture seizure activity arising from different areas of the cortex. The arrangement of the sources and detectors was chosen to maximise head coverage and provide good quality signal without the optical fibres being arranged too sparsely. DOT requires the use of relatively large source-detector separations to provide sensitivity to deeper regions of the tissue. This sparsity affects the spatial resolution of the final DOT images. However, denser arrays with source-detector separations down to <15 mm have been described in the literature (466). It is anticipated that the limiting trade-off between channel count and cortical coverage will disappear in the next few years as HD-DOI systems become more widely available. Indeed, the first diffuse optical images of cortical activation that parallel the spatial resolution and accuracy of BOLD fMRI have recently been reported (467).

A denser array could have been achieved with the system employed in this thesis. For instance, if the cortical target is well known, one may increase the density of the optical fibres by sacrificing a wider field-of-view. In the case of perinatal stroke, a denser array could be designed, thus addressing the primary areas of interest. As the most

frequent location of perinatal stroke is the MCA territory, one could target high density coverage of these cortical regions. However, targeting very specific brain regions would increase the risk of missing stroke in the ACA territory or in the posterior fossa. On the other hand, the possibility of using a HD-DOT system would maximise the coverage of the stroke region whilst sampling the whole head.

Continuous wave DOT systems are simple, portable, inexpensive, and able to provide images with a good spatiotemporal resolution. One of the challenges in data acquisition, is the large number of optical fibres between head gear and device. This inevitably is accountable for movement and friction between the fibres and the scalp, thus that any minimal movement of the infant's head may introduce artefact. Having discussed various ways of extracting motion related artefacts, it is worthwhile mentioning at this point that different groups, , including the UCL BORL group, are in the process of creating wireless, wearable fNIRS systems, with the first HD-DOT images from adult functional studies recently published (468, 469). This offers the potential of advanced fNIRS systems to be used in cognitive tasks performed in normal daily life (331). This widens the research horizons allowing longer continuous recordings both on healthy controls and critically ill subjects.

Diffuse optical tomography allows image reconstruction of the human cortex. The accuracy of the images reproduced significantly relies on the head model used. The model applied in this thesis for image reconstruction, is based on a 4D neonatal head atlas (http://www.ucl.ac.uk/medphys/4dneonatalmodel) (404). This was developed by the UCL BORL. It consists of an infant anatomical brain atlas based on an MRI image database of 324 infants between 29 to 40 weeks of gestational age. This indeed offers a good basis for group analysis. However, when it comes to looking at spatial characteristics of the cortico-vascular changes at rest or in pathological situations, on an individual basis, there is a certain degree of approximation of the calculations and reproduced images. Obtaining the subject's individual MRI would optimize the representation of spatial characteristics of the cortico-vascular changes (355, 365).

Another significant challenge in DOT is that the methodological approaches used for image-based analysis require further development. Due to fundamentally different characteristics and signal to noise ratio between the two technologies, immediate application of the statistical methods used in fMRI can be inappropriate. However, in this

thesis a general linear model (GLM) approach was used to extract the haemodynamic response to EEG bursts. As in fMRI statistical analysis, there are statistical parametric mapping (SPM) tools using a GLM approach to yield statistical maps. These have similarly been used in fNIRS for image reconstruction (470). However, there is still the need for ongoing assessment and refinement of these techniques to account for certain noise characteristics of DOT data prior to their full integration to DOT image reconstruction (471).

Additionally, to the above-mentioned challenges in DOT data the, there remains the limitation of absolute quantification of HbO_2 and HHb concentrations. Without additional information regarding the optical properties of the interrogated tissues, CW-DOT devices can only provide relative measurements of the observed cortico-vascular changes, rather than absolute measurements of the chromophore concentration. More advanced optical systems can provide both quantitative measurements and a better understanding of the optical properties of the investigated tissue such as time domain fNIRS systems (for details see section 2.2.4 of chapter 2) (350, 472-474). However, compared to CW-DOT systems, they remain expensive. Although they are portable, they are often physically large, which makes them less suitable for neuro-imaging in the neonatal intensive care unit. They are sensitive to movement and stability of their laser alignment making them less easy to use. With the development of relatively low cost single photon avalanche detectors (SPADS), the cost and size of time-domain devices will likely be minimised, allowing these technologies to also become wireless and wearable in the coming years (475).

Finally, one of the main issues in this study has been the numbers of patients studied. Given the frequency and nature of some of the conditions investigated, for instance perinatal stroke, the recruited numbers are expected to be low. However, ways to improve this in the future is to consider communication of research studies to satellite referring units to facilitate the consenting process. Another possibility is to consider seeking ethics approval for consenting over the telephone. This would improve the recruitment in the acute phase when targeting acute admissions of infants presenting with seizures. Most of the infants presenting with seizures that were recruited in this study, were referred from other units and transferred in frequently without their parents being present in the first hours or days of admission to the unit. This attempt will require careful

consideration, but it would potentially improve the consenting and recruiting process. Another possibility would be to consider running such studies on a multi-centre basis.

7.3 Future Directions

As this project comes to its end, it is natural to contemplate how it has contributed to research and what the next step would be in its further evolution. Overall, this project has shown DOT-EEG to be a safe, cot-side method to study critically ill infants, without interference in their clinical care and any adverse events during its conduction. It has shown the potential of CW-DOT in exploring the neurovascular coupling of seizures, and burst suppression, and investigating perinatal stroke in relation to physiological, low frequency, haemodynamic oscillations. This has broadened the horizons of infant optical neuro-imaging studies and provided new knowledge regarding brain injury in the neonatal term population. It has also highlighted certain challenges in the investigation of the above-mentioned patient groups and clinical entities which were summarised above, in section 7.2, alongside suggestion for further development of the technology, recruitment, data acquisition, and analysis.

Following the results and challenges identified in this thesis, there is scope for ongoing investigation in the field of neonatal seizures, neurophysiological phenomena, and perinatal stroke. The key areas of future investigations identified are described in the following paragraphs.

The notion of cortical spreading depression or depolarisation (CSD) is one that is better defined in adults and considered to be associated with brain injury (397), head trauma (476), stroke (477), migraine with aura (478), and seizures (479). CSD is described as a wave of electrical hyperactivity followed by relative inactivity across the neurons and glial cells, occurring at a speed of 2 to 9 mm/min across the cortex (480, 481). Santos et al., more recently published images of the CSD phenomenon in male swine models under deep anaesthesia with intrinsic optical imaging demonstrating waves of spreading depolarisation varying according to the surface of the gyri, sulci and pial vessels (482). The observed prolonged decrease in HbO_2 and HbT lasting for a few minutes after the excitation, in this instance of seizure activity (365) mimics the morphology of CSD. Based on this theory and as to whether the observed cortico-vascular response to seizure activity in infants could be secondary to CSD, the methodology of DOT-EEG could be applied on an animal model. This would allow a controlled prolonged observation of neurovascular coupling of induced seizure activity.

Elevation of the baseline optical signal suggesting increase in HbT, observed in patients undergoing TH, and coinciding with the periodic inflation of the cooling mattress, suggested a potential impact of the restraining of limbs to arterial blood pressure and subsequently cortical vasculature in situations of impaired CA. The fact that this was observed in very few patients amongst the group undergoing TH further supports the above-mentioned notion. However, further refinement of the technique is required and more specifically the addition of short separation channels (as described in section 7.2) to elucidate potential corruption of the signal from superficial layers. This in combination with the synchronous acquisition of physiological parameters such as heart and ABP could facilitate the understanding of the impact of therapeutic hypothermia in the cortical vasculature.

As described in chapter 6, refinement of the methodological approach and image-based analysis are the main two areas towards improving the investigation of perinatal stroke. With HD-DOT systems becoming more widely available in the years to come, a denser array could be developed for the exploration of stroke in the neonatal period. Such an evolution of the technology could potentially lead to reproduction of the presented data in this thesis on a limited number of patients and lead to a multicentre study on perinatal stroke. At present, TH remains the principal neuroprotective treatment of neonatal brain injury following HIE with significant reduction in lifelong neuro-disability (43, 44), with a recent systematic review showing its benefits on patients and reduction of mortality without increasing the risk of disability (483). Therefore, it has been debated in the literature as to whether its beneficial effects, such as reduced metabolic demand and reduced free radical and reactive oxygen species (ROS) formation, can be translated in other forms of ischaemic injury such as perinatal stroke (85, 86) (for review see reference (484)). The evolution of DOT and its potential future as a cot-side, neuro-imaging tool in the NICU, could facilitate clinical trials in perinatal stroke.

The fundamental techniques employed in this project are directly transferable to the preterm neonatal population. This could form the basis of a study in preterm infants in the future. There are two main trajectories which could be investigated with simultaneous DOT-EEG in preterm infants: an investigation of the haemodynamic correlates of developmental changes in their EEG and an investigation of seizures in the pre-term neonatal population.

As described in chapter 2 (see section 2.1.4), the neonatal EEG differs between different gestational ages at birth and similarly matures as the infant reaches term equivalent age. Studies of neonatal EEGs have provided the research community with wealth of knowledge regarding the behaviour and phenomenology of neonatal brain activity (179, 190, 203, 485). One of the main characteristics of preterm neonatal EEG is its discontinuity, which resembles the appearance of burst suppression with alternating periods of inactivity and burst like activity. As the infant matures from prematurity to term, the periods of inactivity shorten, and the EEG progressively becomes continuous. Most of the emerging features of EEG maturation are noted in active sleep, rather than quiet sleep, with the latter remaining a period of relative inactivity up to 34-36 weeks of postconceptional age (trace alternant-for further details see section 2.1.4). Similarly, to the investigation of burst suppression (see chapter 4), combined DOT-EEG could be applied in the study of neurovascular coupling of discontinuous neonatal EEG. Coupling to this burst-like activity of preterm EEG has been shown before using NIRS (363). However, the methodology described in this thesis could provide further spatiotemporal information regarding preterm neuronal activity and lead to image reconstruction of the associated haemodynamic changes. Additionally, longitudinal follow-up with scans of extreme preterm infants (born below 28 weeks of gestation) could help identify any maturational process in the cortico-vascular activity in line with the described and well established evolution of the electrical brain activity (203). Considering distinct occipital characteristics in the neonatal EEG as well as the excess of motion artefact when studying well preterm infants, a denser array and ideally wireless technology would facilitate such as a project. The basis of the technology, and analysis would be similar with the advantage of a wireless, HD-DOT system.

Finally, simultaneous DOT-EEG could be applied in the study of seizures amongst preterm infants at risk. There is debate as to the frequency of seizure occurrence in the preterm population with certain studies showing a low incidence using continuous EEG monitoring (486) as opposed to a high incidence using aEEG (487). Nevertheless, there is great variation in such studies based on the population selection, investigating tools, access to expertise in neonatal neurophysiology and level of neonatal care (regional, tertiary as opposed to smaller, lower intensity units). Single centre studies have shown an incidence of up to 48% in low birth weight infants (birth weight of less than 1,500 grams) (488-490). A recent multicentre study considered the incidence and characteristics of

seizures in preterm infants as well as in comparison to term infants. Amongst 611 infants being diagnosed with seizures, 92 were preterm (born with a GA of less than 37 weeks), with main aetiological factors being HIE and intracranial haemorrhage. The incidence of subclinical seizures and the overall mortality were significantly higher in the preterm versus the term population (24% versus 14% and 35% versus 15%, respectively) (491). This highlights the importance of monitoring, but also the significance of further investigation of underlying physiology and mechanisms with the help of simultaneous DOT-EEG. The fact that the haemodynamic signal in response to seizures in the HIE infant appeared of high amplitude was easily observed within the raw optical trace (365), also poses the potential of DOT aiding in the primary identification of seizures.

Most importantly though, in all the above suggested potential future projects, there is the requirement of correlating the observed phenomena or results to long term neuro-developmental follow up at 2 years of age and ideally at 5 years of age. This study works as a basis of observed phenomena which could be reproduced in future projects and explain as to what they may mean with regards to the future neurological status and cognitive function of the patient. The presence of outcome data could help justify further development of the DOT-EEG technology as a neuro-monitoring tool in the NICU.

In conclusion, this study has demonstrated the feasibility of DOT-EEG to be used at the cot side, revealing novel physiological information and potentially contributing as an early detection tool. More importantly, though, it has highlighted the main challenges and key areas to be addressed towards the use of this methodology for future studies.

References

1.   Nelson KB, Leviton A. How much of neonatal encephalopathy is due to birth asphyxia? Am J Dis Child. 1991;145(11):1325-31.

2.   Ronen GM, Penney S, Andrews W. The epidemiology of clinical neonatal seizures in Newfoundland: a population-based study. J Pediatr. 1999;134(1):71-5.

3.   Jensen FE. Neonatal seizures: an update on mechanisms and management. Clin Perinatol. 2009;36(4):881-900, vii.

4.   Berg A. J, P., Preux, P. . Handbook of Clinical Neurology. Pediatric Neurology, Part 1: The epidemiology of seizure disorders in infancy and childhood: definitions and

classifications. . al. IODe, editor. Amsterdam, Netherlands: Elsevier; 2013.

5.   Silverstein FS, Jensen FE. Neonatal seizures. Ann Neurol. 2007;62(2):112-20.

6.   Lagercrantz H, Hanson, M.A., Ment, L.R., Peebles, D.M. The Newbornn Brain, Neuroscience and Clinical Applications. 2nd ed. New York: Cambridge University Press; 2010. 216-8 p.

7.   Greisen G, Hellstrom-Westas L, Lou H, Rosen I, Svenningsen NW. EEG depression and germinal layer haemorrhage in the newborn. Acta Paediatr Scand. 1987;76(3):519-25.

8.   Hellstrom-Westas L, Rosen I, Svenningsen NW. Cerebral function monitoring during the first week of life in extremely small low birthweight (ESLBW) infants. Neuropediatrics. 1991;22(1):27-32.

9.   Scher MS, Aso K, Beggarly ME, Hamid MY, Steppe DA, Painter MJ. Electrographic seizures in preterm and full-term neonates: clinical correlates, associated brain lesions, and risk for neurologic sequelae. Pediatrics. 1993;91(1):128-34.

10.   Biagioni E, Ferrari F, Boldrini A, Roversi MF, Cioni G. Electroclinical correlation in neonatal seizures. Eur J Paediatr Neurol. 1998;2(3):117-25.

11.   Tekgul H, Gauvreau K, Soul J, Murphy L, Robertson R, Stewart J, et al. The current etiologic profile and neurodevelopmental outcome of seizures in term newborn infants. Pediatrics. 2006;117(4):1270-80.

12.   Nagarajan L. Neonatal Seizures. Current management and future challenges. 1st ed. Ohuonu U, editor. London: Man Keith Press; 2016. 114-27 p.

13.   Mastrangelo M, Van Lierde A, Bray M, Pastorino G, Marini A, Mosca F. Epileptic seizures, epilepsy and epileptic syndromes in newborns: a nosological approach to 94 new cases by the 2001 proposed diagnostic scheme for people with epileptic seizures and with epilepsy. Seizure. 2005;14(5):304-11.

14.   Loman AM, ter Horst HJ, Lambrechtsen FA, Lunsing RJ. Neonatal seizures: aetiology by means of a standardized work-up. Eur J Paediatr Neurol. 2014;18(3):360-7.

15.   Levene M. The clinical conundrum of neonatal seizures. Arch Dis Child Fetal Neonatal Ed. 2002;86(2):F75-7.

16.   Holmes GL. The long-term effects of neonatal seizures. Clin Perinatol. 2009;36(4):901-14, vii-viii.

17.   Nagarajan L, Palumbo L, Ghosh S. Neurodevelopmental outcomes in neonates with seizures: a numerical score of background encephalography to help prognosticate. J Child Neurol. 2010;25(8):961-8.

18.   Glass HC, Nash KB, Bonifacio SL, Barkovich AJ, Ferriero DM, Sullivan JE, et al. Seizures and magnetic resonance imaging-detected brain injury in newborns cooled for hypoxic-ischemic encephalopathy. J Pediatr. 2011;159(5):731-5 e1.

19.   Shah DK, Wusthoff CJ, Clarke P, Wyatt JS, Ramaiah SM, Dias RJ, et al. Electrographic seizures are associated with brain injury in newborns undergoing therapeutic hypothermia. Arch Dis Child Fetal Neonatal Ed. 2014;99(3):F219-24.

20.   Volpe JJ. Neurology of the Newborn. 'Hypoxic-ischaemic encephalopathy: neuropathology and pathogenesis'. Philadelphia: PA: W. B. Saunders; 2008. 347-99 p.

21.   Rennie JM. Rennie & Roberton's Textbook of Neonatology. Neurological Problems in the Newborn. 5th ed. London: Churchill Livingstone, Elsevier Limited; 2012. 1114-5 p.

22.   Badawi N, Kurinczuk JJ, Keogh JM, Alessandri LM, O'Sullivan F, Burton PR, et al. Intrapartum risk factors for newborn encephalopathy: the Western Australian case-control study. BMJ. 1998;317(7172):1554-8.

23.   Smith J, Wells L, Dodd K. The continuing fall in incidence of hypoxic-ischaemic encephalopathy in term infants. BJOG. 2000;107(4):461-6.

24.   Lawn J, Shibuya K, Stein C. No cry at birth: global estimates of intrapartum stillbirths and intrapartum-related neonatal deaths. Bull World Health Organ. 2005;83(6):409-17.

25.   Marlow N, Rose AS, Rands CE, Draper ES. Neuropsychological and educational problems at school age associated with neonatal encephalopathy. Arch Dis Child Fetal Neonatal Ed. 2005;90(5):F380-7.

26.   Gonzalez FF, Miller SP. Does perinatal asphyxia impair cognitive function without cerebral palsy? Arch Dis Child Fetal Neonatal Ed. 2006;91(6):F454-9.

27.   Bonifacio SL, Glass HC, Peloquin S, Ferriero DM. A new neurological focus in neonatal intensive care. Nat Rev Neurol. 2011;7(9):485-94.

28.   Peeters LL, Sheldon RE, Jones MD, Jr., Makowski EL, Meschia G. Blood flow to fetal organs as a function of arterial oxygen content. Am J Obstet Gynecol. 1979;135(5):637-46.

29.   Lange S. Peptidylarginine Deiminases as Drug Targets in Neonatal Hypoxic-Ischemic Encephalopathy. Front Neurol. 2016;7:22.

30.   Silbereis JC, Huang EJ, Back SA, Rowitch DH. Towards improved animal models of neonatal white matter injury associated with cerebral palsy. Dis Model Mech. 2010;3(11-12):678-88.

31.   Martinez-Biarge M, Diez-Sebastian J, Rutherford MA, Cowan FM. Outcomes after central grey matter injury in term perinatal hypoxic-ischaemic encephalopathy. Early Hum Dev. 2010;86(11):675-82.

32.   Cowan FM, de Vries LS. The internal capsule in neonatal imaging. Semin Fetal Neonatal Med. 2005;10(5):461-74.

33.   Forbes KP, Pipe JG, Bird R. Neonatal hypoxic-ischemic encephalopathy: detection with diffusion-weighted MR imaging. AJNR Am J Neuroradiol. 2000;21(8):1490-6.

34.   Sarnat HB, Sarnat MS. Neonatal encephalopathy following fetal distress. A clinical and electroencephalographic study. Arch Neurol. 1976;33(10):696-705.

35.   Thompson CM, Puterman AS, Linley LL, Hann FM, van der Elst CW, Molteno CD, et al. The value of a scoring system for hypoxic ischaemic encephalopathy in predicting neurodevelopmental outcome. Acta Paediatr. 1997;86(7):757-61.

36.   Shah P, Riphagen S, Beyene J, Perlman M. Multiorgan dysfunction in infants with post-asphyxial hypoxic-ischaemic encephalopathy. Arch Dis Child Fetal Neonatal Ed. 2004;89(2):F152-5.

37.   Ergenekon E. Therapeutic Hypothermia in neonatal intensive care unit: Challenges and practical points. Journal of Clinical Neonatology. 2016;5(1):8-17.

38.   Azzopardi D, Strohm B, Edwards AD, Halliday H, Juszczak E, Levene M, et al. Treatment of asphyxiated newborns with moderate hypothermia in routine clinical practice: how cooling is managed in the UK outside a clinical trial. Arch Dis Child Fetal Neonatal Ed. 2009;94(4):F260-4.

39.   Kapetanakis A, Azzopardi D, Wyatt J, Robertson NJ. Therapeutic hypothermia for neonatal encephalopathy: a UK survey of opinion, practice and neuro-investigation at the end of 2007. Acta Paediatr. 2009;98(4):631-5.

40.   Gluckman PD, Wyatt JS, Azzopardi D, Ballard R, Edwards AD, Ferriero DM, et al. Selective head cooling with mild systemic hypothermia after neonatal encephalopathy: multicentre randomised trial. Lancet. 2005;365(9460):663-70.

41.   Shankaran S, Laptook AR, Ehrenkranz RA, Tyson JE, McDonald SA, Donovan EF, et al. Whole-body hypothermia for neonates with hypoxic-ischemic encephalopathy. N Engl J Med. 2005;353(15):1574-84.

42.   Simbruner G, Mittal RA, Rohlmann F, Muche R, neo.n EnTP. Systemic hypothermia after neonatal encephalopathy: outcomes of neo.nEURO.network RCT. Pediatrics. 2010;126(4):e771-8.

43.   Edwards AD, Brocklehurst P, Gunn AJ, Halliday H, Juszczak E, Levene M, et al. Neurological outcomes at 18 months of age after moderate hypothermia for perinatal hypoxic ischaemic encephalopathy: synthesis and meta-analysis of trial data. BMJ. 2010;340:c363.

44.   Azzopardi DV, Strohm B, Edwards AD, Dyet L, Halliday HL, Juszczak E, et al. Moderate hypothermia to treat perinatal asphyxial encephalopathy. N Engl J Med. 2009;361(14):1349-58.

45.   Azzopardi D, Robertson NJ, Bainbridge A, Cady E, Charles-Edwards G, Deierl A, et al. Moderate hypothermia within 6 h of birth plus inhaled xenon versus moderate hypothermia alone after birth asphyxia (TOBY-Xe): a proof-of-concept, open-label, randomised controlled trial. Lancet Neurol. 2015.

46.   Hobbs C, Thoresen M, Tucker A, Aquilina K, Chakkarapani E, Dingley J. Xenon and hypothermia combine additively, offering long-term functional and histopathologic neuroprotection after neonatal hypoxia/ischemia. Stroke. 2008;39(4):1307-13.

47.   Chakkarapani E, Dingley J, Liu X, Hoque N, Aquilina K, Porter H, et al. Xenon enhances hypothermic neuroprotection in asphyxiated newborn pigs. Ann Neurol. 2010;68(3):330-41.

48.   Alonso-Alconada D, Alvarez A, Arteaga O, Martinez-Ibarguen A, Hilario E. Neuroprotective effect of melatonin: a novel therapy against perinatal hypoxia-ischemia. Int J Mol Sci. 2013;14(5):9379-95.

49.   Tutunculer F, Eskiocak S, Basaran UN, Ekuklu G, Ayvaz S, Vatansever U. The protective role of melatonin in experimental hypoxic brain damage. Pediatr Int. 2005;47(4):434-9.

50.   Gitto E, Reiter RJ, Cordaro SP, La Rosa M, Chiurazzi P, Trimarchi G, et al. Oxidative and inflammatory parameters in respiratory distress syndrome of preterm newborns: beneficial effects of melatonin. Am J Perinatol. 2004;21(4):209-16.

51.   Buonocore G, Groenendaal F. Anti-oxidant strategies. Semin Fetal Neonatal Med. 2007;12(4):287-95.

52.   Robertson NJ, Faulkner S, Fleiss B, Bainbridge A, Andorka C, Price D, et al. Melatonin augments hypothermic neuroprotection in a perinatal asphyxia model. Brain. 2013;136(Pt 1):90-105.

53.   Liu R, Suzuki A, Guo Z, Mizuno Y, Urabe T. Intrinsic and extrinsic erythropoietin enhances neuroprotection against ischemia and reperfusion injury in vitro. J Neurochem. 2006;96(4):1101-10.

54.   Wu YW, Bauer LA, Ballard RA, Ferriero DM, Glidden DV, Mayock DE, et al. Erythropoietin for neuroprotection in neonatal encephalopathy: safety and pharmacokinetics. Pediatrics. 2012;130(4):683-91.

55.   Fang AY, Gonzalez FF, Sheldon RA, Ferriero DM. Effects of combination therapy using hypothermia and erythropoietin in a rat model of neonatal hypoxia-ischemia. Pediatr Res. 2013;73(1):12-7.

56.   Fan X, van Bel F, van der Kooij MA, Heijnen CJ, Groenendaal F. Hypothermia and erythropoietin for neuroprotection after neonatal brain damage. Pediatr Res. 2013;73(1):18-23.

57.   Zhu C, Kang W, Xu F, Cheng X, Zhang Z, Jia L, et al. Erythropoietin improved neurologic outcomes in newborns with hypoxic-ischemic encephalopathy. Pediatrics. 2009;124(2):e218-26.

58.   Wu YW, Mathur AM, Chang T, McKinstry RC, Mulkey SB, Mayock DE, et al. High-Dose Erythropoietin and Hypothermia for Hypoxic-Ischemic Encephalopathy: A Phase II Trial. Pediatrics. 2016;137(6).

59.   Raju TN, Nelson KB, Ferriero D, Lynch JK, Participants N-NPSW. Ischemic perinatal stroke: summary of a workshop sponsored by the National Institute of Child Health and Human Development and the National Institute of Neurological Disorders and Stroke. Pediatrics. 2007;120(3):609-16.

60.   Lynch JK, Nelson KB. Epidemiology of perinatal stroke. Curr Opin Pediatr. 2001;13(6):499-505.

61.   Wu YW, Lynch JK, Nelson KB. Perinatal arterial stroke: understanding mechanisms and outcomes. Semin Neurol. 2005;25(4):424-34.

62.   Volpe JJ. Neurology of the Newborn: Hypoxic Ischaemic Encephalopathy: Neuropathology and Pathogenesis. 5th ed. Philadelphia: Saunders Esevier; 2008. 379-88 p.

63.   Fitzgerald KC, Golomb MR. Neonatal arterial ischemic stroke and sinovenous thrombosis associated with meningitis. J Child Neurol. 2007;22(7):818-22.

64.   Chen J, Zimmerman RA, Jarvik GP, Nord AS, Clancy RR, Wernovsky G, et al. Perioperative stroke in infants undergoing open heart operations for congenital heart disease. Ann Thorac Surg. 2009;88(3):823-9.

65.   Ramaswamy V, Miller SP, Barkovich AJ, Partridge JC, Ferriero DM. Perinatal stroke in term infants with neonatal encephalopathy. Neurology. 2004;62(11):2088-91.

66.   Cheong JL, Cowan FM. Neonatal arterial ischaemic stroke: obstetric issues. Semin Fetal Neonatal Med. 2009;14(5):267-71.

67.   Gupta M, Dinakaran S, Chan TK. Congenital horner syndrome and hemiplegia secondary to carotid dissection. J Pediatr Ophthalmol Strabismus. 2005;42(2):122-4.

68.   Rennie JM. Rennie & Roberton's Textbook of Neonatology. Neurological Problems in the Newborn. 5th ed. London: Churchill Livingstone, Elsevier Limited; 2012. 1107-13 p.

69.   Lee J, Croen LA, Backstrand KH, Yoshida CK, Henning LH, Lindan C, et al. Maternal and infant characteristics associated with perinatal arterial stroke in the infant. JAMA. 2005;293(6):723-9.

70.   Nelson KB. Perinatal ischemic stroke. Stroke. 2007;38(2 Suppl):742-5.

71.   Barmada MA, Moossy J, Shuman RM. Cerebral infarcts with arterial occlusion in neonates. Ann Neurol. 1979;6(6):495-502.

72.   Benders MJ, Groenendaal F, Uiterwaal CS, Nikkels PG, Bruinse HW, Nievelstein RA, et al. Maternal and infant characteristics associated with perinatal arterial stroke in the preterm infant. Stroke. 2007;38(6):1759-65.

73.   Benders MJ, Groenendaal F, Uiterwaal CS, de Vries LS. Perinatal arterial stroke in the preterm infant. Semin Perinatol. 2008;32(5):344-9.

74.   Yager JY, Ashwal S. Animal models of perinatal hypoxic-ischemic brain damage. Pediatr Neurol. 2009;40(3):156-67.

75.   Rice JE, 3rd, Vannucci RC, Brierley JB. The influence of immaturity on hypoxic-ischemic brain damage in the rat. Ann Neurol. 1981;9(2):131-41.

76.   Derugin N, Ferriero DM, Vexler ZS. Neonatal reversible focal cerebral ischemia: a new model. Neurosci Res. 1998;32(4):349-53.

77.   Mu D, Jiang X, Sheldon RA, Fox CK, Hamrick SE, Vexler ZS, et al. Regulation of hypoxia-inducible factor 1alpha and induction of vascular endothelial growth factor in a rat neonatal stroke model. Neurobiol Dis. 2003;14(3):524-34.

78.   Woo MS, Wang X, Faustino JV, Derugin N, Wendland MF, Zhou P, et al. Genetic deletion of CD36 enhances injury after acute neonatal stroke. Ann Neurol. 2012;72(6):961-70.

79.   Renolleau S, Aggoun-Zouaoui D, Ben-Ari Y, Charriaut-Marlangue C. A model of transient unilateral focal ischemia with reperfusion in the P7 neonatal rat: morphological changes indicative of apoptosis. Stroke. 1998;29(7):1454-60; discussion 61.

80.   d'Orey MC, Melo MJ, Ramos I, Guimaraes H, Alves AR, Silva JS, et al. [Cerebral ischemic infarction in newborn infants. Diagnosis using pulsed and color Doppler imaging]. Arch Pediatr. 1999;6(4):457-9.

81.   Govaert P, de Vries, L.S. An Atlas of Neonatal Brain Sonography. 2nd ed. London: Mac Keith Press; 2010. 295-312 p.

82.   Cnossen MH, van Ommen CH, Appel IM. Etiology and treatment of perinatal stroke; a role for prothrombotic coagulation factors? Semin Fetal Neonatal Med. 2009;14(5):311-7.

83.   Kollmar R, Staykov D, Dorfler A, Schellinger PD, Schwab S, Bardutzky J. Hypothermia reduces perihemorrhagic edema after intracerebral hemorrhage. Stroke. 2010;41(8):1684-9.

84.   van der Worp HB, Sena ES, Donnan GA, Howells DW, Macleod MR. Hypothermia in animal models of acute ischaemic stroke: a systematic review and meta-analysis. Brain. 2007;130(Pt 12):3063-74.

85.   Krieger DW, De Georgia MA, Abou-Chebl A, Andrefsky JC, Sila CA, Katzan IL, et al. Cooling for acute ischemic brain damage (cool aid): an open pilot study of induced hypothermia in acute ischemic stroke. Stroke. 2001;32(8):1847-54.

86.   Lyden PD, Allgren RL, Ng K, Akins P, Meyer B, Al-Sanani F, et al. Intravascular Cooling in the Treatment of Stroke (ICTuS): early clinical experience. J Stroke Cerebrovasc Dis. 2005;14(3):107-14.

87.   De Georgia MA, Krieger DW, Abou-Chebl A, Devlin TG, Jauss M, Davis SM, et al. Cooling for Acute Ischemic Brain Damage (COOL AID): a feasibility trial of endovascular cooling. Neurology. 2004;63(2):312-7.

88.   Harbert MJ, Tam EW, Glass HC, Bonifacio SL, Haeusslein LA, Barkovich AJ, et al. Hypothermia is correlated with seizure absence in perinatal stroke. J Child Neurol. 2011;26(9):1126-30.

89.   Ricci D, Mercuri E, Barnett A, Rathbone R, Cota F, Haataja L, et al. Cognitive outcome at early school age in term-born children with perinatally acquired middle cerebral artery territory infarction. Stroke. 2008;39(2):403-10.

90.   Lee J, Croen LA, Lindan C, Nash KB, Yoshida CK, Ferriero DM, et al. Predictors of outcome in perinatal arterial stroke: a population-based study. Ann Neurol. 2005;58(2):303-8.

91.   Boardman JP, Ganesan V, Rutherford MA, Saunders DE, Mercuri E, Cowan F. Magnetic resonance image correlates of hemiparesis after neonatal and childhood middle cerebral artery stroke. Pediatrics. 2005;115(2):321-6.

92.   Nelson KB, Lynch JK. Stroke in newborn infants. Lancet Neurol. 2004;3(3):150-8.

93.   Ramenghi LA, Govaert P, Fumagalli M, Bassi L, Mosca F. Neonatal cerebral sinovenous thrombosis. Semin Fetal Neonatal Med. 2009;14(5):278-83.

94.   deVeber G, Andrew M, Adams C, Bjornson B, Booth F, Buckley DJ, et al. Cerebral sinovenous thrombosis in children. N Engl J Med. 2001;345(6):417-23.

95.   Dlamini N, Billinghurst L, Kirkham FJ. Cerebral venous sinus (sinovenous) thrombosis in children. Neurosurg Clin N Am. 2010;21(3):511-27.

96.   Berfelo FJ, Kersbergen KJ, van Ommen CH, Govaert P, van Straaten HL, Poll-The BT, et al. Neonatal cerebral sinovenous thrombosis from symptom to outcome. Stroke. 2010;41(7):1382-8.

97.   Simons B, Nijeholt, G.L., Smithuis, R. Neuroradiology: Cerebral Venous Thrombosis Netherlands [Educational site of the Radiological Society of the Netherlands].

98.   Kirton A, deVeber G. Cerebral palsy secondary to perinatal ischemic stroke. Clin Perinatol. 2006;33(2):367-86.

99. Fitzgerald KC, Williams LS, Garg BP, Carvalho KS, Golomb MR. Cerebral sinovenous thrombosis in the neonate. Arch Neurol. 2006;63(3):405-9.

100. Moharir MD, Shroff M, Pontigon AM, Askalan R, Yau I, Macgregor D, et al. A prospective outcome study of neonatal cerebral sinovenous thrombosis. J Child Neurol. 2011;26(9):1137-44.

101. Wanigasinghe J, Reid SM, Mackay MT, Reddihough DS, Harvey AS, Freeman JL. Epilepsy in hemiplegic cerebral palsy due to perinatal arterial ischaemic stroke. Dev Med Child Neurol. 2010;52(11):1021-7.

102. Wasay M, Dai AI, Ansari M, Shaikh Z, Roach ES. Cerebral venous sinus thrombosis in children: a multicenter cohort from the United States. J Child Neurol. 2008;23(1):26-31.

103. Kersbergen KJ, de Vries LS, van Straaten HL, Benders MJ, Nievelstein RA, Groenendaal F. Anticoagulation therapy and imaging in neonates with a unilateral thalamic hemorrhage due to cerebral sinovenous thrombosis. Stroke. 2009;40(8):2754-60.

104. Kersbergen KJ, de Vries LS, Leijten FS, Braun KP, Nievelstein RA, Groenendaal F, et al. Neonatal thalamic hemorrhage is strongly associated with electrical status epilepticus in slow wave sleep. Epilepsia. 2013;54(4):733-40.

105. Mercuri E, Anker S, Guzzetta A, Barnett A, Haataja L, Rutherford M, et al. Neonatal cerebral infarction and visual function at school age. Arch Dis Child Fetal Neonatal Ed. 2003;88(6):F487-91.

106. Ballantyne AO, Spilkin AM, Hesselink J, Trauner DA. Plasticity in the developing brain: intellectual, language and academic functions in children with ischaemic perinatal stroke. Brain. 2008;131(Pt 11):2975-85.

107. Westmacott R, MacGregor D, Askalan R, deVeber G. Late emergence of cognitive deficits after unilateral neonatal stroke. Stroke. 2009;40(6):2012-9.

108. van Buuren LM, van der Aa NE, Dekker HC, Vermeulen RJ, van Nieuwenhuizen O, van Schooneveld MM, et al. Cognitive outcome in childhood after unilateral perinatal brain injury. Dev Med Child Neurol. 2013;55(10):934-40.

109. Kersbergen KJ, Groenendaal F, Benders MJ, van Straaten HL, Niwa T, Nievelstein RA, et al. The spectrum of associated brain lesions in cerebral sinovenous thrombosis: relation to gestational age and outcome. Arch Dis Child Fetal Neonatal Ed. 2011;96(6):F404-9.

110. Grunt S, Wingeier K, Wehrli E, Boltshauser E, Capone A, Fluss J, et al. Cerebral sinus venous thrombosis in Swiss children. Dev Med Child Neurol. 2010;52(12):1145-50.

111. Hellstrom-Westas L, Rosen I, Svenningsen NW. Predictive value of early continuous amplitude integrated EEG recordings on outcome after severe birth asphyxia in full term infants. Arch Dis Child Fetal Neonatal Ed. 1995;72(1):F34-8.

112. Hellstrom-Westas L, Rosen I. Continuous brain-function monitoring: state of the art in clinical practice. Semin Fetal Neonatal Med. 2006;11(6):503-11.

113. van Rooij LG, Toet MC, Osredkar D, van Huffelen AC, Groenendaal F, de Vries LS. Recovery of amplitude integrated electroencephalographic background patterns within 24 hours of perinatal asphyxia. Arch Dis Child Fetal Neonatal Ed. 2005;90(3):F245-51.

114. Toet MC, Hellstrom-Westas L, Groenendaal F, Eken P, de Vries LS. Amplitude integrated EEG 3 and 6 hours after birth in full term neonates with hypoxic-ischaemic encephalopathy. Arch Dis Child Fetal Neonatal Ed. 1999;81(1):F19-23.

115.   Toet MC, van Rooij LG, de Vries LS. The use of amplitude integrated electroencephalography for assessing neonatal neurologic injury. Clin Perinatol. 2008;35(4):665-78, v.

116.   Govaert P, de Vries, L.S. An Atlas of Neontal Brain Sonography. 2nd ed. Hart HM, editor. London: Mac Keith Press; 2010. 265-92 p.

117.   Rutherford MA, Pennock JM, Dubowitz LM. Cranial ultrasound and magnetic resonance imaging in hypoxic-ischaemic encephalopathy: a comparison with outcome. Dev Med Child Neurol. 1994;36(9):813-25.

118.   Archer LN, Levene MI, Evans DH. Cerebral artery Doppler ultrasonography for prediction of outcome after perinatal asphyxia. Lancet. 1986;2(8516):1116-8.

119.   Elstad M, Whitelaw A, Thoresen M. Cerebral Resistance Index is less predictive in hypothermic encephalopathic newborns. Acta Paediatr. 2011;100(10):1344-9.

120.   Rutherford M, Malamateniou C, McGuinness A, Allsop J, Biarge MM, Counsell S. Magnetic resonance imaging in hypoxic-ischaemic encephalopathy. Early Hum Dev. 2010;86(6):351-60.

121.   Rutherford M, Ramenghi LA, Edwards AD, Brocklehurst P, Halliday H, Levene M, et al. Assessment of brain tissue injury after moderate hypothermia in neonates with hypoxic-ischaemic encephalopathy: a nested substudy of a randomised controlled trial. Lancet Neurol. 2010;9(1):39-45.

122.   McKinstry RC, Miller JH, Snyder AZ, Mathur A, Schefft GL, Almli CR, et al. A prospective, longitudinal diffusion tensor imaging study of brain injury in newborns. Neurology. 2002;59(6):824-33.

123.   Barkovich AJ, Hajnal BL, Vigneron D, Sola A, Partridge JC, Allen F, et al. Prediction of neuromotor outcome in perinatal asphyxia: evaluation of MR scoring systems. AJNR Am J Neuroradiol. 1998;19(1):143-9.

124. Martinez-Biarge M, Diez-Sebastian J, Kapellou O, Gindner D, Allsop JM, Rutherford MA, et al. Predicting motor outcome and death in term hypoxic-ischemic encephalopathy. Neurology. 2011;76(24):2055-61.

125. Martinez-Biarge M, Bregant T, Wusthoff CJ, Chew AT, Diez-Sebastian J, Rutherford MA, et al. White matter and cortical injury in hypoxic-ischemic encephalopathy: antecedent factors and 2-year outcome. J Pediatr. 2012;161(5):799-807.

126. Goergen SK, Ang H, Wong F, Carse EA, Charlton M, Evans R, et al. Early MRI in term infants with perinatal hypoxic-ischaemic brain injury: interobserver agreement and MRI predictors of outcome at 2 years. Clin Radiol. 2014;69(1):72-81.

127. Bonifacio SL, Miller, S.P. Neonatal seizures and brain imaging. Journal of Pediatric Neurology. 2009;7(1):61-7.

128. Osmond E, Billetop A, Jary S, Likeman M, Thoresen M, Luyt K. Neonatal seizures: magnetic resonance imaging adds value in the diagnosis and prediction of neurodisability. Acta Paediatr. 2014;103(8):820-6.

129. De Vis JB, Alderliesten T, Hendrikse J, Petersen ET, Benders MJ. Magnetic resonance imaging based noninvasive measurements of brain hemodynamics in neonates: a review. Pediatr Res. 2016;80(5):641-50.

130. Benders MJ, Hendrikse J, De Vries LS, Van Bel F, Groenendaal F. Phase-contrast magnetic resonance angiography measurements of global cerebral blood flow in the neonate. Pediatr Res. 2011;69(6):544-7.

131. Varela M, Groves AM, Arichi T, Hajnal JV. Mean cerebral blood flow measurements using phase contrast MRI in the first year of life. NMR Biomed. 2012;25(9):1063-72.

132. De Vis JB, Petersen ET, de Vries LS, Groenendaal F, Kersbergen KJ, Alderliesten T, et al. Regional changes in brain perfusion during brain maturation measured non-

invasively with Arterial Spin Labeling MRI in neonates. Eur J Radiol. 2013;82(3):538-43.

133.   De Vis JB, Hendrikse J, Petersen ET, de Vries LS, van Bel F, Alderliesten T, et al. Arterial spin-labelling perfusion MRI and outcome in neonates with hypoxic-ischemic encephalopathy. Eur Radiol. 2015;25(1):113-21.

134.   Shi H, Song D, Zhang YX, Qi M, Li HS, Tan ZS, et al. [Analysis of arterial spin labeling in 33 patients with hypoxic ischemic encephalopathy]. Zhonghua Er Ke Za Zhi. 2012;50(2):131-5.

135.   Roth SC, Baudin J, Cady E, Johal K, Townsend JP, Wyatt JS, et al. Relation of deranged neonatal cerebral oxidative metabolism with neurodevelopmental outcome and head circumference at 4 years. Dev Med Child Neurol. 1997;39(11):718-25.

136.   Wintermark P, Moessinger AC, Gudinchet F, Meuli R. Temporal evolution of MR perfusion in neonatal hypoxic-ischemic encephalopathy. J Magn Reson Imaging. 2008;27(6):1229-34.

137.   Cheong JL, Cady EB, Penrice J, Wyatt JS, Cox IJ, Robertson NJ. Proton MR spectroscopy in neonates with perinatal cerebral hypoxic-ischemic injury: metabolite peak-area ratios, relaxation times, and absolute concentrations. AJNR Am J Neuroradiol. 2006;27(7):1546-54.

138.   Thayyil S, Chandrasekaran M, Taylor A, Bainbridge A, Cady EB, Chong WK, et al. Cerebral magnetic resonance biomarkers in neonatal encephalopathy: a meta-analysis. Pediatrics. 2010;125(2):e382-95.

139.   Azzopardi D, Wyatt JS, Cady EB, Delpy DT, Baudin J, Stewart AL, et al. Prognosis of newborn infants with hypoxic-ischemic brain injury assessed by phosphorus magnetic resonance spectroscopy. Pediatr Res. 1989;25(5):445-51.

140. Robertson NJ, Cox IJ, Cowan FM, Counsell SJ, Azzopardi D, Edwards AD. Cerebral intracellular lactic alkalosis persisting months after neonatal encephalopathy measured by magnetic resonance spectroscopy. Pediatr Res. 1999;46(3):287-96.

141. Penrice J, Cady EB, Lorek A, Wylezinska M, Amess PN, Aldridge RF, et al. Proton magnetic resonance spectroscopy of the brain in normal preterm and term infants, and early changes after perinatal hypoxia-ischemia. Pediatr Res. 1996;40(1):6-14.

142. Penrice J, Lorek A, Cady EB, Amess PN, Wylezinska M, Cooper CE, et al. Proton magnetic resonance spectroscopy of the brain during acute hypoxia-ischemia and delayed cerebral energy failure in the newborn piglet. Pediatr Res. 1997;41(6):795-802.

143. Lei H, Peeling J. Effect of temperature on the kinetics of lactate production and clearance in a rat model of forebrain ischemia. Biochem Cell Biol. 1998;76(2-3):503-9.

144. Rothman DL, Howseman AM, Graham GD, Petroff OA, Lantos G, Fayad PB, et al. Localized proton NMR observation of [3-13C]lactate in stroke after [1-13C]glucose infusion. Magn Reson Med. 1991;21(2):302-7.

145. Groenendaal F, Veenhoven RH, van der Grond J, Jansen GH, Witkamp TD, de Vries LS. Cerebral lactate and N-acetyl-aspartate/choline ratios in asphyxiated full-term neonates demonstrated in vivo using proton magnetic resonance spectroscopy. Pediatr Res. 1994;35(2):148-51.

146. Barkovich AJ, Baranski K, Vigneron D, Partridge JC, Hallam DK, Hajnal BL, et al. Proton MR spectroscopy for the evaluation of brain injury in asphyxiated, term neonates. AJNR Am J Neuroradiol. 1999;20(8):1399-405.

147. Zarifi MK, Astrakas LG, Poussaint TY, Plessis Ad A, Zurakowski D, Tzika AA. Prediction of adverse outcome with cerebral lactate level and apparent diffusion coefficient in infants with perinatal asphyxia. Radiology. 2002;225(3):859-70.

148. Mercuri E. Early diagnostic and prognostic indicators in full term infants with neonatal cerebral infarction: an integrated clinical, neuroradiological and EEG approach. Minerva Pediatr. 2001;53(4):305-11.

149. Rafay MF, Cortez MA, de Veber GA, Tan-Dy C, Al-Futaisi A, Yoon W, et al. Predictive value of clinical and EEG features in the diagnosis of stroke and hypoxic ischemic encephalopathy in neonates with seizures. Stroke. 2009;40(7):2402-7.

150. Low E, Mathieson SR, Stevenson NJ, Livingstone V, Ryan CA, Bogue CO, et al. Early postnatal EEG features of perinatal arterial ischaemic stroke with seizures. PLoS One. 2014;9(7):e100973.

151. de Vries LS, Groenendaal F, Eken P, van Haastert IC, Rademaker KJ, Meiners LC. Infarcts in the vascular distribution of the middle cerebral artery in preterm and fullterm infants. Neuropediatrics. 1997;28(2):88-96.

152. Govaert P, Matthys E, Zecic A, Roelens F, Oostra A, Vanzieleghem B. Perinatal cortical infarction within middle cerebral artery trunks. Arch Dis Child Fetal Neonatal Ed. 2000;82(1):F59-63.

153. Cowan F, Mercuri E, Groenendaal F, Bassi L, Ricci D, Rutherford M, et al. Does cranial ultrasound imaging identify arterial cerebral infarction in term neonates? Arch Dis Child Fetal Neonatal Ed. 2005;90(3):F252-6.

154. Golomb MR, Dick PT, MacGregor DL, Armstrong DC, DeVeber GA. Cranial ultrasonography has a low sensitivity for detecting arterial ischemic stroke in term neonates. J Child Neurol. 2003;18(2):98-103.

155. Donaldson B. Real time ultrasound, arterial pulsation and neonatal cerebral infarction. Postgrad Med J. 1987;63(738):263-5.

156. Steventon DM, John PR. Power Doppler ultrasound appearances of neonatal ischaemic brain injury. Pediatr Radiol. 1997;27(2):147-9.

157. Lequin MH, Dudink J, Tong KA, Obenaus A. Magnetic resonance imaging in neonatal stroke. Semin Fetal Neonatal Med. 2009;14(5):299-310.

158. Dudink J, Mercuri E, Al-Nakib L, Govaert P, Counsell SJ, Rutherford MA, et al. Evolution of unilateral perinatal arterial ischemic stroke on conventional and diffusion-weighted MR imaging. AJNR Am J Neuroradiol. 2009;30(5):998-1004.

159. Wintermark P, Warfield SK. New insights in perinatal arterial ischemic stroke by assessing brain perfusion. Transl Stroke Res. 2012;3(2):255-62.

160. van der Aa NE, Porsius ED, Hendrikse J, van Kooij BJ, Benders MJ, de Vries LS, et al. Changes in carotid blood flow after unilateral perinatal arterial ischemic stroke. Pediatr Res. 2012;72(1):50-6.

161. De Vis JB, Petersen ET, Kersbergen KJ, Alderliesten T, de Vries LS, van Bel F, et al. Evaluation of perinatal arterial ischemic stroke using noninvasive arterial spin labeling perfusion MRI. Pediatr Res. 2013;74(3):307-13.

162. Wyatt JS. Near-infrared spectroscopy in asphyxial brain injury. Clin Perinatol. 1993;20(2):369-78.

163. Meek JH, Elwell CE, McCormick DC, Edwards AD, Townsend JP, Stewart AL, et al. Abnormal cerebral haemodynamics in perinatally asphyxiated neonates related to outcome. Arch Dis Child Fetal Neonatal Ed. 1999;81(2):F110-5.

164. Marin T, Moore J. Understanding near-infrared spectroscopy. Adv Neonatal Care. 2011;11(6):382-8.

165. Caton R. The electric currents of the brain. British Medical Journal. 1875;2:278.

166. Fritsch G HE. Ueber die elektrishe Erregarkeit des Grosshims. The Cerebral Cortex Thomas, Springfield. 1870(101):73-96.

167. Beck A CN. Further research on the electrical phenomena of the cerebral cortex in monkeys and dogs. Rozpr Akad Um Wydz Mat-Przyr Ser. 1891;11(32):369-75.

168. Cybulski N. Action currents of the cerebral cortex (in Polish). Bull Int Acad Cracovie. 1914:776.

169. Berger H. Über das Elektrenkephalogramm des Menschen. Archiv für Psychiatrie und Nervenkrankheiten. 1929;87(1):527-70.

170. Tao JX, Ray A, Hawes-Ebersole S, Ebersole JS. Intracranial EEG substrates of scalp EEG interictal spikes. Epilepsia. 2005;46(5):669-76.

171. Bear MF, Connors, B.W., Paradiso, M.A. Neuroscience: Exploring the Brain. 4th Edition ed: Wolters Kluwer; 2016.

172. Niedermeyer E. The electrocerebellogram. Clin EEG Neurosci. 2004;35(2):112-5.

173. Schaul N. The fundamental neural mechanisms of electroencephalography. Electroencephalogr Clin Neurophysiol. 1998;106(2):101-7.

174. Gloor P. Neuronal generators and the problem of localization in electroencephalography: application of volume conductor theory to electroencephalography. J Clin Neurophysiol. 1985;2(4):327-54.

175. Gloor P, editor Electroencephalography and the role of intracerebral depth electrode recordings in the selection of patients for surgical treatment of epilepsy. Advances in Epileptology XVth Epikepsy International Symposium; 1984; New York: Raven Press.

176. Report of the Committee on Methods of Clinical Examination in Electroencephalography. Electroencephalogr Clin Neurophysiol. 1958;10:370-75.

177. Kellaway P, Crawley, J.W. A primer of electroencephalography of infants, sections I & II: methodology and criteria of nomrality. Houston: Baylor University College of Medicine; 1964. 47 p.

178.   Tekgul H, Bourgeois BF, Gauvreau K, Bergin AM. Electroencephalography in neonatal seizures: comparison of a reduced and a full 10/20 montage. Pediatr Neurol. 2005;32(3):155-61.

179.   Mizrahi EM, Hrachovy, R.A., Kellaway, P. Atlas of Neonatal Encephalography. 3rd ed. Philadelphia: Lippincott Williams & Wilkins; 2004.

180.   Pressler RM, Binnie, C.D., Cooper, R., Robinson, R. . Neonatal and Paediatric Clinical Neurophysiology, 1e. Philadelphia: Churchill Livingstone; 2007. 59-60, 190-1 p.

181.   Shellhaas RA, Chang T, Tsuchida T, Scher MS, Riviello JJ, Abend NS, et al. The American Clinical Neurophysiology Society's Guideline on Continuous Electroencephalography Monitoring in Neonates. J Clin Neurophysiol. 2011;28(6):611-7.

182.   Maynard DE. EEG analysis using an analogue frequency analyser and a digital computer. Electroencephalogr Clin Neurophysiol. 1967;23(5):487.

183.   Maynard D, Prior PF, Scott DF. Device for continuous monitoring of cerebral activity in resuscitated patients. Br Med J. 1969;4(5682):545-6.

184.   Maynard D, Prior PF, Scott DF. A continuous monitoring device for cerebral activity. Electroencephalogr Clin Neurophysiol. 1969;27(7):672-3.

185.   Hellstrom-Westas L, de Vries, L.S., Rosen, I. Atlas of AMPLITUDE-INTEGRATED EEGs in the NEWBORN. 2nd ed. London: Informa Healthcare; 2008.

186.   Burdjalov VF, Baumgart S, Spitzer AR. Cerebral function monitoring: a new scoring system for the evaluation of brain maturation in neonates. Pediatrics. 2003;112(4):855-61.

187.	al Naqeeb N, Edwards AD, Cowan FM, Azzopardi D. Assessment of neonatal encephalopathy by amplitude-integrated electroencephalography. Pediatrics. 1999;103(6 Pt 1):1263-71.

188.	Dreyfus-Brisac C. Ontogenesis of brain bioelectrical activity and sleep organisation in neonates and infants1979.

189.	Dreyfus-Brisac C. Neurophysiological studies in human premature and full-term newborns. Biol Psychiatry. 1975;10(5):485-96.

190.	Andre M, Lamblin MD, d'Allest AM, Curzi-Dascalova L, Moussalli-Salefranque F, T SNT, et al. Electroencephalography in premature and full-term infants. Developmental features and glossary. Neurophysiol Clin. 2010;40(2):59-124.

191.	Torres F, Anderson C. The normal EEG of the human newborn. J Clin Neurophysiol. 1985;2(2):89-103.

192.	Lamblin MD, Andre M, Challamel MJ, Curzi-Dascalova L, d'Allest AM, De Giovanni E, et al. [Electroencephalography of the premature and term newborn. Maturational aspects and glossary]. Neurophysiol Clin. 1999;29(2):123-219.

193.	Prechtl HF. The behavioural states of the newborn infant (a review). Brain Res. 1974;76(2):185-212.

194.	Anders T ER, Parmelee A. . A manual of standardized terminology, techniques and criteria for scoring of states of sleep and wakefulness in newborn infants: Los Angeles: UCLA Brain Information Service/BRI Publications Office; 1971.

195.	Monod N, Curzi-Dascalova L. [Transitional sleep states in the neonate at term]. Rev Electroencephalogr Neurophysiol Clin. 1973;3(1):87-96.

196.	Curzi-Dascalova L, Figueroa JM, Eiselt M, Christova E, Virassamy A, d'Allest AM, et al. Sleep state organization in premature infants of less than 35 weeks' gestational age. Pediatr Res. 1993;34(5):624-8.

197.   Dreyfus-Brisac C. The electroencephalogram of the premature infant. World Neurol. 1962;3:5-15.

198.   Laoprasert P. Atlas of Pediatric EEG: Mac Graw Hill Companies, Inc.; 2011.

199.   Vecchierini MF, d'Allest AM, Verpillat P. EEG patterns in 10 extreme premature neonates with normal neurological outcome: qualitative and quantitative data. Brain Dev. 2003;25(5):330-7.

200.   Hahn JS, Monyer H, Tharp BR. Interburst interval measurements in the EEGs of premature infants with normal neurological outcome. Electroencephalogr Clin Neurophysiol. 1989;73(5):410-8.

201.   Selton D, Andre M, Hascoet JM. Normal EEG in very premature infants: reference criteria. Clin Neurophysiol. 2000;111(12):2116-24.

202.   Blanc C, Dreyfus-Brisac C. Electroencephalogramme et maturation cerebrale. Encephale. 1956;45(3):205-41.

203.   Vanhatalo S, Kaila K. Development of neonatal EEG activity: from phenomenology to physiology. Semin Fetal Neonatal Med. 2006;11(6):471-8.

204.   Marmor MF, Holder GE, Seeliger MW, Yamamoto S, International Society for Clinical Electrophysiology of V. Standard for clinical electroretinography (2004 update). Doc Ophthalmol. 2004;108(2):107-14.

205.   Young GB, da Silva OP. Effects of morphine on the electroencephalograms of neonates: a prospective, observational study. Clin Neurophysiol. 2000;111(11):1955-60.

206.   Selton D, Andre M. Prognosis of hypoxic-ischaemic encephalopathy in full-term newborns--value of neonatal electroencephalography. Neuropediatrics. 1997;28(5):276-80.

207.   Glass HC, Wusthoff CJ, Shellhaas RA, Tsuchida TN, Bonifacio SL, Cordeiro M, et al. Risk factors for EEG seizures in neonates treated with hypothermia: a multicenter cohort study. Neurology. 2014;82(14):1239-44.

208.   Boylan GB, Kharoshankaya L, Wusthoff CJ. Seizures and hypothermia: importance of electroencephalographic monitoring and considerations for treatment. Semin Fetal Neonatal Med. 2015;20(2):103-8.

209.   Amzica F. What does burst suppression really mean? Epilepsy Behav. 2015;49:234-7.

210.   Gibbs FA, Gibbs, E.L. Atlas of electroencephalography. Cambridge: Addison-Wesley; 1952.

211.   Demyer W, White PT. Eeg in Holoprosencephaly (Arhinencephaly). Arch Neurol. 1964;11:507-20.

212.   Bokisa AE, Bonachea EM, Jadcherla SR. Death by neurologic criteria in a neonate: Implications for organ donation. J Neonatal Perinatal Med. 2015;8(3):263-7.

213.   Mizrahi EM, Tharp BR. A characteristic EEG pattern in neonatal herpes simplex encephalitis. Neurology. 1982;32(11):1215-20.

214.   Mikati MA, Feraru E, Krishnamoorthy K, Lombroso CT. Neonatal herpes simplex meningoencephalitis: EEG investigations and clinical correlates. Neurology. 1990;40(9):1433-7.

215.   Blume WT, Dreyfus-Brisac C. Positive rolandic sharp waves in neonatal EEG; types and significance. Electroencephalogr Clin Neurophysiol. 1982;53(3):277-82.

216.   Kidokoro H, Okumura A, Hayakawa F, Kato T, Maruyama K, Kubota T, et al. Chronologic changes in neonatal EEG findings in periventricular leukomalacia. Pediatrics. 2009;124(3):e468-75.

217.   Novotny EJ, Jr., Tharp BR, Coen RW, Bejar R, Enzmann D, Vaucher YE. Positive rolandic sharp waves in the EEG of the premature infant. Neurology. 1987;37(9):1481-6.

218.   Freeman JM, Lietman PS. A basic approach to the understanding of seizures and the mechanism of action and metabolism of anticonvulsants. Adv Pediatr. 1973;20(0):291-321.

219.   Moshe SL. Epileptogenesis and the immature brain. Epilepsia. 1987;28 Suppl 1:S3-15.

220.   Lothman EW. Pathophysiology of seizures and epilepsy in the mature and immature brain: Cells, synapses and circuits. New York: Demos Publications; 1993.

221.   Clancy RR, Legido A. The exact ictal and interictal duration of electroencephalographic neonatal seizures. Epilepsia. 1987;28(5):537-41.

222.   Volpe JJ. Neurology of the Newborn: Neonatal Seizures. 5th ed. Philadelphia: Saunders Esevier; 2008. 203 p.

223.   Volpe JJ. Neurology of the Newborn: Neonatal Seizures. 5th ed. Philadelphia: Saunders Elsevier; 2008. 203-41 p.

224.   Ronen GM, Buckley D, Penney S, Streiner DL. Long-term prognosis in children with neonatal seizures: a population-based study. Neurology. 2007;69(19):1816-22.

225.   Uria-Avellanal C, Marlow N, Rennie JM. Outcome following neonatal seizures. Semin Fetal Neonatal Med. 2013;18(4):224-32.

226.   Malone A, Ryan CA, Fitzgerald A, Burgoyne L, Connolly S, Boylan GB. Interobserver agreement in neonatal seizure identification. Epilepsia. 2009;50(9):2097-101.

227.   Dreyfus-Brisac C, Monod, N. Electroclinical studies of status epilepticus and convulsions in the newborn. In Kellaway P, Petterson, S., editor. New York: Grune & Stratton; 1964.

228.   Radvanyi-Bouvet MF, Vallecalle MH, Morel-Kahn F, Relier JP, Dreyfus-Brisac C. Seizures and electrical discharges in premature infants. Neuropediatrics. 1985;16(3):143-8.

229.   Mizrahi EM, Kellaway P. Characterization and classification of neonatal seizures. Neurology. 1987;37(12):1837-44.

230.   Mizrahi EM, Kellaway, P. Diagnosis and Management of Neonatal Seizures. Philadelphia: Lippincott-Raven; 1998.

231.   Rennie JM. Rennie & Roberton's Textbook of Neonatology. Neurological Problemss in the Newborn. 5th ed. London: Churchill Livingstone, Elsevier Limited; 2012. 1080-98 p.

232.   Pisani F, Cerminara C, Fusco C, Sisti L. Neonatal status epilepticus vs recurrent neonatal seizures: clinical findings and outcome. Neurology. 2007;69(23):2177-85.

233.   Scher MS, Hamid MY, Steppe DA, Beggarly ME, Painter MJ. Ictal and interictal electrographic seizure durations in preterm and term neonates. Epilepsia. 1993;34(2):284-8.

234.   Shellhaas RA, Clancy RR. Characterization of neonatal seizures by conventional EEG and single-channel EEG. Clin Neurophysiol. 2007;118(10):2156-61.

235.   Lynch NE, Stevenson NJ, Livingstone V, Murphy BP, Rennie JM, Boylan GB. The temporal evolution of electrographic seizure burden in neonatal hypoxic ischemic encephalopathy. Epilepsia. 2012;53(3):549-57.

236.   Low E, Boylan GB, Mathieson SR, Murray DM, Korotchikova I, Stevenson NJ, et al. Cooling and seizure burden in term neonates: an observational study. Arch Dis Child Fetal Neonatal Ed. 2012;97(4):F267-72.

237.   McBride MC, Laroia N, Guillet R. Electrographic seizures in neonates correlate with poor neurodevelopmental outcome. Neurology. 2000;55(4):506-13.

238.   Abend NS, Wusthoff CJ. Neonatal seizures and status epilepticus. J Clin Neurophysiol. 2012;29(5):441-8.

239.   Shah DK, Boylan GB, Rennie JM. Monitoring of seizures in the newborn. Arch Dis Child Fetal Neonatal Ed. 2012;97(1):F65-9.

240.   Clancy RR. The contribution of EEG to the understanding of neonatal seizures. Epilepsia. 1996;37 Suppl 1:S52-9.

241.   Okumura A, Hayakawa F, Kato T, Itomi K, Maruyama K, Kubota T, et al. Ictal electroencephalographic findings of neonatal seizures in preterm infants. Brain Dev. 2008;30(4):261-8.

242.   Wusthoff CJ. Diagnosing neonatal seizures and status epilepticus. J Clin Neurophysiol. 2013;30(2):115-21.

243.   Patrizi S, Holmes GL, Orzalesi M, Allemand F. Neonatal seizures: characteristics of EEG ictal activity in preterm and fullterm infants. Brain Dev. 2003;25(6):427-37.

244.   Scher MS, Painter MJ, Bergman I, Barmada MA, Brunberg J. EEG diagnoses of neonatal seizures: clinical correlations and outcome. Pediatr Neurol. 1989;5(1):17-24.

245.   Lombroso CT. Neonatal seizures: a clinician's overview. Brain Dev. 1996;18(1):1-28.

246.   Mizrahi EM. Neonatal seizures: problems in diagnosis and classification. Epilepsia. 1987;28 Suppl 1:S46-55.

247.   Clayton GH, Owens GC, Wolff JS, Smith RL. Ontogeny of cation-Cl-cotransporter expression in rat neocortex. Brain Res Dev Brain Res. 1998;109(2):281-92.

248.   Rivera C, Voipio J, Payne JA, Ruusuvuori E, Lahtinen H, Lamsa K, et al. The K+/Cl- co-transporter KCC2 renders GABA hyperpolarizing during neuronal maturation. Nature. 1999;397(6716):251-5.

249.   Yamada J, Okabe A, Toyoda H, Kilb W, Luhmann HJ, Fukuda A. Cl- uptake promoting depolarizing GABA actions in immature rat neocortical neurones is mediated by NKCC1. J Physiol. 2004;557(Pt 3):829-41.

250.   McCoy B, Sharma R, Ochi A, Go C, Otsubo H, Hutchison JS, et al. Predictors of nonconvulsive seizures among critically ill children. Epilepsia. 2011;52(11):1973-8.

251.   Abend NS, Gutierrez-Colina AM, Topjian AA, Zhao H, Guo R, Donnelly M, et al. Nonconvulsive seizures are common in critically ill children. Neurology. 2011;76(12):1071-7.

252.   Abend NS, Arndt DH, Carpenter JL, Chapman KE, Cornett KM, Gallentine WB, et al. Electrographic seizures in pediatric ICU patients: cohort study of risk factors and mortality. Neurology. 2013;81(4):383-91.

253.   Kwon JM, Guillet R, Shankaran S, Laptook AR, McDonald SA, Ehrenkranz RA, et al. Clinical seizures in neonatal hypoxic-ischemic encephalopathy have no independent impact on neurodevelopmental outcome: secondary analyses of data from the neonatal research network hypothermia trial. J Child Neurol. 2011;26(3):322-8.

254.   Jensen FE, Applegate CD, Holtzman D, Belin TR, Burchfiel JL. Epileptogenic effect of hypoxia in the immature rodent brain. Ann Neurol. 1991;29(6):629-37.

255.   Lowenstein DH, Shimosaka S, So YT, Simon RP. The relationship between electrographic seizure activity and neuronal injury. Epilepsy Res. 1991;10(1):49-54.

256.   Wasterlain CG, Shirasaka Y. Seizures, brain damage and brain development. Brain Dev. 1994;16(4):279-95.

257.   Sanchez RM, Koh S, Rio C, Wang C, Lamperti ED, Sharma D, et al. Decreased glutamate receptor 2 expression and enhanced epileptogenesis in immature rat hippocampus after perinatal hypoxia-induced seizures. J Neurosci. 2001;21(20):8154-63.

258.   Meldrum B. Excitotoxicity and epileptic brain damage. Epilepsy Res. 1991;10(1):55-61.

259.   Holmes GL. Effects of seizures on brain development: lessons from the laboratory. Pediatr Neurol. 2005;33(1):1-11.

260.   Nagarajan L, Ghosh S, Palumbo L. Ictal electroencephalograms in neonatal seizures: characteristics and associations. Pediatr Neurol. 2011;45(1):11-6.

261.   Jain P, Sharma S, Tripathi M. Diagnosis and management of epileptic encephalopathies in children. Epilepsy Res Treat. 2013;2013:501981.

262.   Pinto LC, Giliberti P. Neonatal seizures: background EEG activity and the electroclinical correlation in full-term neonates with hypoxic-ischemic encephalopathy. Analysis by computer-synchronized long-term polygraphic video-EEG monitoring. Epileptic Disord. 2001;3(3):125-32.

263.   Lewis LD, Ching S, Weiner VS, Peterfreund RA, Eskandar EN, Cash SS, et al. Local cortical dynamics of burst suppression in the anaesthetized brain. Brain. 2013;136(Pt 9):2727-37.

264.   Menache CC, Bourgeois BF, Volpe JJ. Prognostic value of neonatal discontinuous EEG. Pediatr Neurol. 2002;27(2):93-101.

265.   Monod N, Pajot, N. and Guidasci, S. The neonatal EEG: statistical studies and prognostic value in full-term and pre-term babies. Electroencephalogr Clin Neurophysiol. 1972;32(5):529-44.

266.   Eken P, Toet MC, Groenendaal F, de Vries LS. Predictive value of early neuroimaging, pulsed Doppler and neurophysiology in full term infants with hypoxic-ischaemic encephalopathy. Arch Dis Child Fetal Neonatal Ed. 1995;73(2):F75-80.

267.   Iyer KK, Roberts JA, Metsaranta M, Finnigan S, Breakspear M, Vanhatalo S. Novel features of early burst suppression predict outcome after birth asphyxia. Ann Clin Transl Neurol. 2014;1(3):209-14.

268.   Japaridze N, Muthuraman M, Reinicke C, Moeller F, Anwar AR, Mideksa KG, et al. Neuronal Networks during Burst Suppression as Revealed by Source Analysis. PLoS One. 2015;10(4):e0123807.

269.   Young GB. The EEG in coma. J Clin Neurophysiol. 2000;17(5):473-85.

270.   Ohtahara S, Yamatogi Y. Epileptic encephalopathies in early infancy with suppression-burst. J Clin Neurophysiol. 2003;20(6):398-407.

271.   Akrawi WP, Drummond JC, Kalkman CJ, Patel PM. A comparison of the electrophysiologic characteristics of EEG burst-suppression as produced by isoflurane, thiopental, etomidate, and propofol. J Neurosurg Anesthesiol. 1996;8(1):40-6.

272.   Stecker MM, Cheung AT, Pochettino A, Kent GP, Patterson T, Weiss SJ, et al. Deep hypothermic circulatory arrest: II. Changes in electroencephalogram and evoked potentials during rewarming. Ann Thorac Surg. 2001;71(1):22-8.

273.   Thoresen M, Hellstrom-Westas L, Liu X, de Vries LS. Effect of hypothermia on amplitude-integrated electroencephalogram in infants with asphyxia. Pediatrics. 2010;126(1):e131-9.

274.   Wertheim D, Mercuri E, Faundez JC, Rutherford M, Acolet D, Dubowitz L. Prognostic value of continuous electroencephalographic recording in full term infants with hypoxic ischaemic encephalopathy. Arch Dis Child. 1994;71(2):F97-102.

275.   Jobsis FF. Non-invasive, infra-red monitoring of cerebral O2 sufficiency, bloodvolume, HbO2-Hb shifts and bloodflow. Acta Neurol Scand Suppl. 1977;64:452-3.

276.   Bouguer P. *Essai d'optique sur la gradation de la lumiere* Paris, France: Claude Jombert; 1729. 16-22 p.

277. Lambert JH. *Photometria sive de mensura et gradibus luminis, colorum et umbrae:* Photometry, or On the measure and gradiations of light, colours, and shade. Germany: Eberhardt Klett; 1760.

278. Beer A. *Bestimmung der Absorption des rothen Lichts in fabrigen Flussigkeiten:* Determination of the absorption of red light in coloured liquids. Annalen der Physik und Chemie. 1852;86:78-88.

279. Woodard HQ, White DR. The composition of body tissues. Br J Radiol. 1986;59(708):1209-18.

280. Matcher SJ, Elwell CE, Cooper CE, Cope M, Delpy DT. Performance comparison of several published tissue near-infrared spectroscopy algorithms. Anal Biochem. 1995;227(1):54-68.

281. Gervain J, Mehler J, Werker JF, Nelson CA, Csibra G, Lloyd-Fox S, et al. Near-infrared spectroscopy: a report from the McDonnell infant methodology consortium. Dev Cogn Neurosci. 2011;1(1):22-46.

282. Tisdall MM, Tachtsidis I, Leung TS, Elwell CE, Smith M. Near-infrared spectroscopic quantification of changes in the concentration of oxidized cytochrome c oxidase in the healthy human brain during hypoxemia. J Biomed Opt. 2007;12(2):024002.

283. Delpy DT, Cope M, van der Zee P, Arridge S, Wray S, Wyatt J. Estimation of optical pathlength through tissue from direct time of flight measurement. Phys Med Biol. 1988;33(12):1433-42.

284. Arridge SR, Cope M, Delpy DT. The theoretical basis for the determination of optical pathlengths in tissue: temporal and frequency analysis. Phys Med Biol. 1992;37(7):1531-60.

285. van der Zee P, Cope M, Arridge SR, Essenpreis M, Potter LA, Edwards AD, et al. Experimentally measured optical pathlengths for the adult head, calf and forearm and

the head of the newborn infant as a function of inter optode spacing. Adv Exp Med Biol. 1992;316:143-53.

286. Gordon GR, Mulligan SJ, MacVicar BA. Astrocyte control of the cerebrovasculature. Glia. 2007;55(12):1214-21.

287. Buxton RB, Wong EC, Frank LR. Dynamics of blood flow and oxygenation changes during brain activation: the balloon model. Magn Reson Med. 1998;39(6):855-64.

288. Iadecola C. Neurovascular regulation in the normal brain and in Alzheimer's disease. Nat Rev Neurosci. 2004;5(5):347-60.

289. Liao LD, Tsytsarev V, Delgado-Martinez I, Li ML, Erzurumlu R, Vipin A, et al. Neurovascular coupling: in vivo optical techniques for functional brain imaging. Biomed Eng Online. 2013;12:38.

290. Magistretti PJ, Pellerin L, Rothman DL, Shulman RG. Energy on demand. Science. 1999;283(5401):496-7.

291. Iadecola C, Nedergaard M. Glial regulation of the cerebral microvasculature. Nat Neurosci. 2007;10(11):1369-76.

292. Attwell D, Buchan AM, Charpak S, Lauritzen M, Macvicar BA, Newman EA. Glial and neuronal control of brain blood flow. Nature. 2010;468(7321):232-43.

293. Orozco-Cabal L, Pollandt S, Liu J, Shinnick-Gallagher P, Gallagher JP. Regulation of synaptic transmission by CRF receptors. Rev Neurosci. 2006;17(3):279-307.

294. Rossi DJ. Another BOLD role for astrocytes: coupling blood flow to neural activity. Nat Neurosci. 2006;9(2):159-61.

295.   Fox PT, Raichle ME. Focal physiological uncoupling of cerebral blood flow and oxidative metabolism during somatosensory stimulation in human subjects. Proc Natl Acad Sci U S A. 1986;83(4):1140-4.

296.   Boas DA, Strangman G, Culver JP, Hoge RD, Jasdzewski G, Poldrack RA, et al. Can the cerebral metabolic rate of oxygen be estimated with near-infrared spectroscopy? Phys Med Biol. 2003;48(15):2405-18.

297.   Tak S, Jang J, Lee K, Ye JC. Quantification of CMRO(2) without hypercapnia using simultaneous near-infrared spectroscopy and fMRI measurements. Phys Med Biol. 2010;55(11):3249-69.

298.   Hock C, Muller-Spahn F, Schuh-Hofer S, Hofmann M, Dirnagl U, Villringer A. Age dependency of changes in cerebral hemoglobin oxygenation during brain activation: a near-infrared spectroscopy study. J Cereb Blood Flow Metab. 1995;15(6):1103-8.

299.   Hock C, Villringer K, Muller-Spahn F, Wenzel R, Heekeren H, Schuh-Hofer S, et al. Decrease in parietal cerebral hemoglobin oxygenation during performance of a verbal fluency task in patients with Alzheimer's disease monitored by means of near-infrared spectroscopy (NIRS)--correlation with simultaneous rCBF-PET measurements. Brain Res. 1997;755(2):293-303.

300.   Hoshi Y, Tamura M. Dynamic multichannel near-infrared optical imaging of human brain activity. J Appl Physiol (1985). 1993;75(4):1842-6.

301.   Hoshi Y, Tamura M. Detection of dynamic changes in cerebral oxygenation coupled to neuronal function during mental work in man. Neurosci Lett. 1993;150(1):5-8.

302.   Sakatani K, Xie Y, Lichty W, Li S, Zuo H. Language-activated cerebral blood oxygenation and hemodynamic changes of the left prefrontal cortex in poststroke aphasic patients: a near-infrared spectroscopy study. Stroke. 1998;29(7):1299-304.

303.   Villringer K, Minoshima S, Hock C, Obrig H, Ziegler S, Dirnagl U, et al. Assessment of local brain activation. A simultaneous PET and near-infrared spectroscopy study. Adv Exp Med Biol. 1997;413:149-53.

304.   Obrig H, Villringer A. Beyond the visible--imaging the human brain with light. J Cereb Blood Flow Metab. 2003;23(1):1-18.

305.   Lloyd-Fox S, Blasi A, Elwell CE. Illuminating the developing brain: the past, present and future of functional near infrared spectroscopy. Neurosci Biobehav Rev. 2010;34(3):269-84.

306.   Kwong KK, Belliveau JW, Chesler DA, Goldberg IE, Weisskoff RM, Poncelet BP, et al. Dynamic magnetic resonance imaging of human brain activity during primary sensory stimulation. Proc Natl Acad Sci U S A. 1992;89(12):5675-9.

307.   Ogawa S, Tank DW, Menon R, Ellermann JM, Kim SG, Merkle H, et al. Intrinsic signal changes accompanying sensory stimulation: functional brain mapping with magnetic resonance imaging. Proc Natl Acad Sci U S A. 1992;89(13):5951-5.

308.   Toronov V, Webb A, Choi JH, Wolf M, Michalos A, Gratton E, et al. Investigation of human brain hemodynamics by simultaneous near-infrared spectroscopy and functional magnetic resonance imaging. Med Phys. 2001;28(4):521-7.

309.   Toronov V, Walker S, Gupta R, Choi JH, Gratton E, Hueber D, et al. The roles of changes in deoxyhemoglobin concentration and regional cerebral blood volume in the fMRI BOLD signal. Neuroimage. 2003;19(4):1521-31.

310.   MacIntosh BJ, Klassen LM, Menon RS. Transient hemodynamics during a breath hold challenge in a two part functional imaging study with simultaneous near-infrared spectroscopy in adult humans. Neuroimage. 2003;20(2):1246-52.

311.   Kleinschmidt A, Obrig H, Requardt M, Merboldt KD, Dirnagl U, Villringer A, et al. Simultaneous recording of cerebral blood oxygenation changes during human brain

activation by magnetic resonance imaging and near-infrared spectroscopy. J Cereb Blood Flow Metab. 1996;16(5):817-26.

312.   Yamamoto T, Kato T. Paradoxical correlation between signal in functional magnetic resonance imaging and deoxygenated haemoglobin content in capillaries: a new theoretical explanation. Phys Med Biol. 2002;47(7):1121-41.

313.   Strangman G, Culver JP, Thompson JH, Boas DA. A quantitative comparison of simultaneous BOLD fMRI and NIRS recordings during functional brain activation. Neuroimage. 2002;17(2):719-31.

314.   Punwani S, Ordidge RJ, Cooper CE, Amess P, Clemence M. MRI measurements of cerebral deoxyhaemoglobin concentration [dHb]--correlation with near infrared spectroscopy (NIRS). NMR Biomed. 1998;11(6):281-9.

315.   Chen Y, Tailor DR, Intes X, Chance B. Correlation between near-infrared spectroscopy and magnetic resonance imaging of rat brain oxygenation modulation. Phys Med Biol. 2003;48(4):417-27.

316.   Huppert TJ, Hoge RD, Diamond SG, Franceschini MA, Boas DA. A temporal comparison of BOLD, ASL, and NIRS hemodynamic responses to motor stimuli in adult humans. Neuroimage. 2006;29(2):368-82.

317.   Coutts LV, Cooper CE, Elwell CE, Wilkins AJ. Time course of the haemodynamic response to visual stimulation in migraine, measured using near-infrared spectroscopy. Cephalalgia. 2012;32(8):621-9.

318.   Baird AA, Kagan J, Gaudette T, Walz KA, Hershlag N, Boas DA. Frontal lobe activation during object permanence: data from near-infrared spectroscopy. Neuroimage. 2002;16(4):1120-5.

319.   Hoshi Y, Kohri S, Matsumoto Y, Cho K, Matsuda T, Okajima S, et al. Hemodynamic responses to photic stimulation in neonates. Pediatr Neurol. 2000;23(4):323-7.

320.   Meek JH, Firbank M, Elwell CE, Atkinson J, Braddick O, Wyatt JS. Regional hemodynamic responses to visual stimulation in awake infants. Pediatr Res. 1998;43(6):840-3.

321.   Sakatani K, Chen S, Lichty W, Zuo H, Wang YP. Cerebral blood oxygenation changes induced by auditory stimulation in newborn infants measured by near infrared spectroscopy. Early Hum Dev. 1999;55(3):229-36.

322.   Wilcox T, Bortfeld H, Woods R, Wruck E, Boas DA. Using near-infrared spectroscopy to assess neural activation during object processing in infants. J Biomed Opt. 2005;10(1):11010.

323.   Zaramella P, Freato F, Amigoni A, Salvadori S, Marangoni P, Suppiej A, et al. Brain auditory activation measured by near-infrared spectroscopy (NIRS) in neonates. Pediatr Res. 2001;49(2):213-9.

324.   Martin E, Joeri P, Loenneker T, Ekatodramis D, Vitacco D, Hennig J, et al. Visual processing in infants and children studied using functional MRI. Pediatr Res. 1999;46(2):135-40.

325.   Marcar VL, Strassle AE, Loenneker T, Schwarz U, Martin E. The influence of cortical maturation on the BOLD response: an fMRI study of visual cortex in children. Pediatr Res. 2004;56(6):967-74.

326.   Marcar VL, Schwarz U, Martin E, Loenneker T. How depth of anesthesia influences the blood oxygenation level-dependent signal from the visual cortex of children. AJNR Am J Neuroradiol. 2006;27(4):799-805.

327.   Wilcox T, Bortfeld H, Woods R, Wruck E, Boas DA. Hemodynamic response to featural changes in the occipital and inferior temporal cortex in infants: a preliminary methodological exploration. Dev Sci. 2008;11(3):361-70.

328.   Arichi T, Fagiolo G, Varela M, Melendez-Calderon A, Allievi A, Merchant N, et al. Development of BOLD signal hemodynamic responses in the human brain. Neuroimage. 2012;63(2):663-73.

329.   Scholkmann F, Kleiser S, Metz AJ, Zimmermann R, Mata Pavia J, Wolf U, et al. A review on continuous wave functional near-infrared spectroscopy and imaging instrumentation and methodology. Neuroimage. 2014;85 Pt 1:6-27.

330.   Irani F, Platek SM, Bunce S, Ruocco AC, Chute D. Functional near infrared spectroscopy (fNIRS): an emerging neuroimaging technology with important applications for the study of brain disorders. Clin Neuropsychol. 2007;21(1):9-37.

331.   Ferrari M, Quaresima V. A brief review on the history of human functional near-infrared spectroscopy (fNIRS) development and fields of application. Neuroimage. 2012;63(2):921-35.

332.   Gibson AP, Hebden JC, Arridge SR. Recent advances in diffuse optical imaging. Phys Med Biol. 2005;50(4):R1-43.

333.   Franceschini MA, Toronov V, Filiaci M, Gratton E, Fantini S. On-line optical imaging of the human brain with 160-ms temporal resolution. Opt Express. 2000;6(3):49-57.

334.   Sato H, Takeuchi T, Sakai KL. Temporal cortex activation during speech recognition: an optical topography study. Cognition. 1999;73(3):B55-66.

335.   Taga G, Asakawa K, Maki A, Konishi Y, Koizumi H. Brain imaging in awake infants by near-infrared optical topography. Proc Natl Acad Sci U S A. 2003;100(19):10722-7.

336.   Gervain J, Macagno F, Cogoi S, Pena M, Mehler J. The neonate brain detects speech structure. Proc Natl Acad Sci U S A. 2008;105(37):14222-7.

337.   Lloyd-Fox S, Blasi A, Volein A, Everdell N, Elwell CE, Johnson MH. Social perception in infancy: a near infrared spectroscopy study. Child Dev. 2009;80(4):986-99.

338.   Lloyd-Fox S, Blasi A, Mercure E, Elwell CE, Johnson MH. The emergence of cerebral specialization for the human voice over the first months of life. Soc Neurosci. 2012;7(3):317-30.

339.   Minagawa-Kawai Y, van der Lely H, Ramus F, Sato Y, Mazuka R, Dupoux E. Optical brain imaging reveals general auditory and language-specific processing in early infant development. Cereb Cortex. 2011;21(2):254-61.

340.   Sato H, Hirabayashi Y, Tsubokura H, Kanai M, Ashida T, Konishi I, et al. Cerebral hemodynamics in newborn infants exposed to speech sounds: a whole-head optical topography study. Hum Brain Mapp. 2012;33(9):2092-103.

341.   Arridge SR, Dehghani H, Schweiger M, Okada E. The finite element model for the propagation of light in scattering media: a direct method for domains with nonscattering regions. Med Phys. 2000;27(1):252-64.

342.   Culver JP, Ntziachristos V, Holboke MJ, Yodh AG. Optimization of optode arrangements for diffuse optical tomography: A singular-value analysis. Opt Lett. 2001;26(10):701-3.

343.   Boas DA, Dale AM, Franceschini MA. Diffuse optical imaging of brain activation: approaches to optimizing image sensitivity, resolution, and accuracy. Neuroimage. 2004;23 Suppl 1:S275-88.

344.   Joseph DK, Huppert TJ, Franceschini MA, Boas DA. Diffuse optical tomography system to image brain activation with improved spatial resolution and validation with functional magnetic resonance imaging. Appl Opt. 2006;45(31):8142-51.

345. Fukui Y, Ajichi Y, Okada E. Monte Carlo prediction of near-infrared light propagation in realistic adult and neonatal head models. Appl Opt. 2003;42(16):2881-7.

346. Liao SM, Ferradal SL, White BR, Gregg N, Inder TE, Culver JP. High-density diffuse optical tomography of term infant visual cortex in the nursery. J Biomed Opt. 2012;17(8):081414.

347. Chance B, Anday E, Nioka S, Zhou S, Hong L, Worden K, et al. A novel method for fast imaging of brain function, non-invasively, with light. Opt Express. 1998;2(10):411-23.

348. Culver JP, Choe R, Holboke MJ, Zubkov L, Durduran T, Slemp A, et al. Three-dimensional diffuse optical tomography in the parallel plane transmission geometry: evaluation of a hybrid frequency domain/continuous wave clinical system for breast imaging. Med Phys. 2003;30(2):235-47.

349. Hebden JC, Delpy DT. Enhanced time-resolved imaging with a diffusion model of photon transport. Opt Lett. 1994;19(5):311-3.

350. Austin T, Gibson AP, Branco G, Yusof RM, Arridge SR, Meek JH, et al. Three dimensional optical imaging of blood volume and oxygenation in the neonatal brain. Neuroimage. 2006;31(4):1426-33.

351. Schweiger M, Arridge S. The Toast++ software suite for forward and inverse modeling in optical tomography. J Biomed Opt. 2014;19(4):040801.

352. Chance B, Zhuang Z, UnAh C, Alter C, Lipton L. Cognition-activated low-frequency modulation of light absorption in human brain. Proc Natl Acad Sci U S A. 1993;90(8):3770-4.

353. Kato T, Kamei A, Takashima S, Ozaki T. Human visual cortical function during photic stimulation monitoring by means of near-infrared spectroscopy. J Cereb Blood Flow Metab. 1993;13(3):516-20.

354. Villringer A, Planck J, Hock C, Schleinkofer L, Dirnagl U. Near infrared spectroscopy (NIRS): a new tool to study hemodynamic changes during activation of brain function in human adults. Neurosci Lett. 1993;154(1-2):101-4.

355. White BR, Liao SM, Ferradal SL, Inder TE, Culver JP. Bedside optical imaging of occipital resting-state functional connectivity in neonates. Neuroimage. 2012;59(3):2529-38.

356. Biswal BB, Van Kylen J, Hyde JS. Simultaneous assessment of flow and BOLD signals in resting-state functional connectivity maps. NMR Biomed. 1997;10(4-5):165-70.

357. Fransson P, Skiold B, Engstrom M, Hallberg B, Mosskin M, Aden U, et al. Spontaneous brain activity in the newborn brain during natural sleep--an fMRI study in infants born at full term. Pediatr Res. 2009;66(3):301-5.

358. Doria V, Beckmann CF, Arichi T, Merchant N, Groppo M, Turkheimer FE, et al. Emergence of resting state networks in the preterm human brain. Proc Natl Acad Sci U S A. 2010;107(46):20015-20.

359. Smyser CD, Inder TE, Shimony JS, Hill JE, Degnan AJ, Snyder AZ, et al. Longitudinal analysis of neural network development in preterm infants. Cereb Cortex. 2010;20(12):2852-62.

360. Nunez PL, Silberstein RB, Cadusch PJ, Wijesinghe RS, Westdorp AF, Srinivasan R. A theoretical and experimental study of high resolution EEG based on surface Laplacians and cortical imaging. Electroencephalogr Clin Neurophysiol. 1994;90(1):40-57.

361. Srinivasan R, Nunez PL, Tucker DM, Silberstein RB, Cadusch PJ. Spatial sampling and filtering of EEG with spline laplacians to estimate cortical potentials. Brain Topogr. 1996;8(4):355-66.

362.   Makeig S, Bell, A., Jung, T.-P., Sejnowski, T. . Independent component analysis of electroencephalographic data Touretzky D, Mozer, M., Hasselmo, M., editor. Cambridge1996. 145–51 p.

363.   Roche-Labarbe N, Wallois F, Ponchel E, Kongolo G, Grebe R. Coupled oxygenation oscillation measured by NIRS and intermittent cerebral activation on EEG in premature infants. Neuroimage. 2007;36(3):718-27.

364.   Franceschini MA, Fantini S, Thompson JH, Culver JP, Boas DA. Hemodynamic evoked response of the sensorimotor cortex measured noninvasively with near-infrared optical imaging. Psychophysiology. 2003;40(4):548-60.

365.   Singh H, Cooper RJ, Wai Lee C, Dempsey L, Edwards A, Brigadoi S, et al. Mapping cortical haemodynamics during neonatal seizures using diffuse optical tomography: a case study. Neuroimage Clin. 2014;5:256-65.

366.   Cooper RJ, Hebden JC, O'Reilly H, Mitra S, Michell AW, Everdell NL, et al. Transient haemodynamic events in neurologically compromised infants: a simultaneous EEG and diffuse optical imaging study. Neuroimage. 2011;55(4):1610-6.

367.   World Medical A. World Medical Association Declaration of Helsinki: ethical principles for medical research involving human subjects. JAMA. 2013;310(20):2191-4.

368.   National Institute for Health and Care of Excellence N. Therapeutic hypothermia with intracorporeal temperature monitoring for hypoxic perinatal brain injury. IPG347. UK2010.

369.   Everdell NL, Gibson, A.P., Tullis, I.D., Vaithianathan, T., Hebden, J.C., Delpy, D.T. A frequency multiplexed near-infrared topography system for imaging functional activation in the brain. Review of Scientific Instruments. 2005;76(9).

370.   Oostenveld R, Praamstra P. The five percent electrode system for high-resolution EEG and ERP measurements. Clin Neurophysiol. 2001;112(4):713-9.

371.   Arridge SR. Photon-measurement density functions. Part I: Analytical forms. Appl Opt. 1995;34(31):7395-409.

372.   Brunner C, Delorme A, Makeig S. Eeglab - an Open Source Matlab Toolbox for Electrophysiological Research. Biomed Tech (Berl). 2013.

373.   Huppert TJ, Diamond SG, Franceschini MA, Boas DA. HomER: a review of time-series analysis methods for near-infrared spectroscopy of the brain. Appl Opt. 2009;48(10):D280-98.

374.   Cooper RJ, Selb J, Gagnon L, Phillip D, Schytz HW, Iversen HK, et al. A systematic comparison of motion artifact correction techniques for functional near-infrared spectroscopy. Front Neurosci. 2012;6:147.

375.   Girouard H, Iadecola C. Neurovascular coupling in the normal brain and in hypertension, stroke, and Alzheimer disease. J Appl Physiol (1985). 2006;100(1):328-35.

376.   Steinhoff BJ, Herrendorf G, Kurth C. Ictal near infrared spectroscopy in temporal lobe epilepsy: a pilot study. Seizure. 1996;5(2):97-101.

377.   Sokol DK, Markand ON, Daly EC, Luerssen TG, Malkoff MD. Near infrared spectroscopy (NIRS) distinguishes seizure types. Seizure. 2000;9(5):323-7.

378.   Zhao M, Suh M, Ma H, Perry C, Geneslaw A, Schwartz TH. Focal increases in perfusion and decreases in hemoglobin oxygenation precede seizure onset in spontaneous human epilepsy. Epilepsia. 2007;48(11):2059-67.

379.   van Bel F, Dorrepaal CA, Benders MJ, Zeeuwe PE, van de Bor M, Berger HM. Changes in cerebral hemodynamics and oxygenation in the first 24 hours after birth asphyxia. Pediatrics. 1993;92(3):365-72.

380.   Wallois F, Patil A, Kongolo G, Goudjil S, Grebe R. Haemodynamic changes during seizure-like activity in a neonate: a simultaneous AC EEG-SPIR and high-resolution DC EEG recording. Neurophysiol Clin. 2009;39(4-5):217-27.

381. Suh M, Bahar S, Mehta AD, Schwartz TH. Temporal dependence in uncoupling of blood volume and oxygenation during interictal epileptiform events in rat neocortex. J Neurosci. 2005;25(1):68-77.

382. Scholkmann F, Wolf M. General equation for the differential pathlength factor of the frontal human head depending on wavelength and age. J Biomed Opt. 2013;18(10):105004.

383. Wusthoff CJ, Dlugos DJ, Gutierrez-Colina A, Wang A, Cook N, Donnelly M, et al. Electrographic seizures during therapeutic hypothermia for neonatal hypoxic-ischemic encephalopathy. J Child Neurol. 2011;26(6):724-8.

384. Srinivasakumar P, Zempel J, Wallendorf M, Lawrence R, Inder T, Mathur A. Therapeutic hypothermia in neonatal hypoxic ischemic encephalopathy: electrographic seizures and magnetic resonance imaging evidence of injury. J Pediatr. 2013;163(2):465-70.

385. Schroeter ML, Schmiedel O, von Cramon DY. Spontaneous low-frequency oscillations decline in the aging brain. J Cereb Blood Flow Metab. 2004;24(10):1183-91.

386. Obrig H, Neufang M, Wenzel R, Kohl M, Steinbrink J, Einhäupl K, et al. Spontaneous Low Frequency Oscillations of Cerebral Hemodynamics and Metabolism in Human Adults. NeuroImage. 2000;12(6):623-39.

387. Schytz HW, Hansson A, Phillip D, Selb J, Boas DA, Iversen HK, et al. Spontaneous low-frequency oscillations in cerebral vessels: applications in carotid artery disease and ischemic stroke. J Stroke Cerebrovasc Dis. 2010;19(6):465-74.

388. Laptook AR, Corbett RJ. The effects of temperature on hypoxic-ischemic brain injury. Clin Perinatol. 2002;29(4):623-49, vi.

389. Polderman KH. Induced hypothermia and fever control for prevention and treatment of neurological injuries. Lancet. 2008;371(9628):1955-69.

390.	Wintermark P, Hansen A, Gregas MC, Soul J, Labrecque M, Robertson RL, et al. Brain perfusion in asphyxiated newborns treated with therapeutic hypothermia. AJNR Am J Neuroradiol. 2011;32(11):2023-9.

391.	Wintermark P, Hansen A, Warfield SK, Dukhovny D, Soul JS. Near-infrared spectroscopy versus magnetic resonance imaging to study brain perfusion in newborns with hypoxic-ischemic encephalopathy treated with hypothermia. Neuroimage. 2014;85 Pt 1:287-93.

392.	Zhao M, Nguyen J, Ma H, Nishimura N, Schaffer CB, Schwartz TH. Preictal and ictal neurovascular and metabolic coupling surrounding a seizure focus. J Neurosci. 2011;31(37):13292-300.

393.	Ma H, Zhao M, Schwartz TH. Dynamic neurovascular coupling and uncoupling during ictal onset, propagation, and termination revealed by simultaneous in vivo optical imaging of neural activity and local blood volume. Cereb Cortex. 2013;23(4):885-99.

394.	Kramer DR, Fujii T, Ohiorhenuan I, Liu CY. Interplay between Cortical Spreading Depolarization and Seizures. Stereotact Funct Neurosurg. 2017;95(1):1-5.

395.	Leao AAP. Spreading depression of activity in the cerebral cortex. Journal of Neurophysiology. 1944;7(6):359-90.

396.	Dreier JP. The role of spreading depression, spreading depolarization and spreading ischemia in neurological disease. Nat Med. 2011;17(4):439-47.

397.	Somjen GG. Mechanisms of spreading depression and hypoxic spreading depression-like depolarization. Physiol Rev. 2001;81(3):1065-96.

398.	Franceschini MA, Radhakrishnan H, Thakur K, Wu W, Ruvinskaya S, Carp S, et al. The effect of different anesthetics on neurovascular coupling. Neuroimage. 2010;51(4):1367-77.

399.   Makiranta MJ, Jauhiainen JP, Oikarinen JT, Suominen K, Tervonen O, Alahuhta S, et al. Functional magnetic resonance imaging of swine brain during change in thiopental anesthesia into EEG burst-suppression level--a preliminary study. MAGMA. 2002;15(1-3):27-35.

400.   Makiranta M, Ruohonen J, Suominen K, Niinimaki J, Sonkajarvi E, Kiviniemi V, et al. BOLD signal increase preceeds EEG spike activity--a dynamic penicillin induced focal epilepsy in deep anesthesia. Neuroimage. 2005;27(4):715-24.

401.   Liu X, Zhu XH, Zhang Y, Chen W. Neural origin of spontaneous hemodynamic fluctuations in rats under burst-suppression anesthesia condition. Cereb Cortex. 2011;21(2):374-84.

402.   Vincent JL, Patel GH, Fox MD, Snyder AZ, Baker JT, Van Essen DC, et al. Intrinsic functional architecture in the anaesthetized monkey brain. Nature. 2007;447(7140):83-6.

403.   Sutin JC, C., Boas, D., Brown, E., Franceschini, M.A. , editor Diffuse Optical Spectroscopy Measurement Of Cerebral Hemodynamics And Oxygen Metabolism During Anesthesia-Induced Burst Suppression In Rats. Biomedical Optics 2014; USA.

404.   Brigadoi S, Aljabar P, Kuklisova-Murgasova M, Arridge SR, Cooper RJ. A 4D neonatal head model for diffuse optical imaging of pre-term to term infants. Neuroimage. 2014;100:385-94.

405.   Hall R, Murdoch J. Brain protection: physiological and pharmacological considerations. Part II: The pharmacology of brain protection. Can J Anaesth. 1990;37(7):762-77.

406.   Claassen J, Hirsch LJ, Emerson RG, Mayer SA. Treatment of refractory status epilepticus with pentobarbital, propofol, or midazolam: a systematic review. Epilepsia. 2002;43(2):146-53.

407. Kroeger D, Florea B, Amzica F. Human brain activity patterns beyond the isoelectric line of extreme deep coma. PLoS One. 2013;8(9):e75257.

408. Chalia M, Lee CW, Dempsey LA, Edwards AD, Singh H, Michell AW, et al. Hemodynamic response to burst-suppressed and discontinuous electroencephalography activity in infants with hypoxic ischemic encephalopathy. Neurophotonics. 2016;3(3):031408.

409. Mackert BM, Wubbeler G, Leistner S, Uludag K, Obrig H, Villringer A, et al. Neurovascular coupling analyzed non-invasively in the human brain. Neuroreport. 2004;15(1):63-6.

410. Roche-Labarbe N, Carp SA, Surova A, Patel M, Boas DA, Grant PE, et al. Noninvasive optical measures of CBV, StO(2), CBF index, and rCMRO(2) in human premature neonates' brains in the first six weeks of life. Hum Brain Mapp. 2010;31(3):341-52.

411. Kozberg MG, Chen BR, DeLeo SE, Bouchard MB, Hillman EM. Resolving the transition from negative to positive blood oxygen level-dependent responses in the developing brain. Proc Natl Acad Sci U S A. 2013;110(11):4380-5.

412. Hagberg H, Andersson P, Kjellmer I, Thiringer K, Thordstein M. Extracellular overflow of glutamate, aspartate, GABA and taurine in the cortex and basal ganglia of fetal lambs during hypoxia-ischemia. Neurosci Lett. 1987;78(3):311-7.

413. Stein DT, Vannucci RC. Calcium accumulation during the evolution of hypoxic-ischemic brain damage in the immature rat. J Cereb Blood Flow Metab. 1988;8(6):834-42.

414. Szaflarski J, Burtrum D, Silverstein FS. Cerebral hypoxia-ischemia stimulates cytokine gene expression in perinatal rats. Stroke. 1995;26(6):1093-100.

415. Bell AH, Greisen G, Pryds O. Comparison of the effects of phenobarbitone and morphine administration on EEG activity in preterm babies. Acta Paediatr. 1993;82(1):35-9.

416. Lagercrantz H, Hanson, M.A., Ment, L.R., Peebles, D.M. . The Newborn Brain, Neuroscience and Clinical Applications. 2nd ed. New York City, USA: Cambridge University Press; 2010. 220-1 p.

417. Shany E, Benzaquen O, Friger M, Richardson J, Golan A. Influence of antiepileptic drugs on amplitude-integrated electroencephalography. Pediatr Neurol. 2008;39(6):387-91.

418. Dehaes M, Aggarwal A, Lin PY, Rosa Fortuno C, Fenoglio A, Roche-Labarbe N, et al. Cerebral oxygen metabolism in neonatal hypoxic ischemic encephalopathy during and after therapeutic hypothermia. J Cereb Blood Flow Metab. 2014;34(1):87-94.

419. Golomb MR. Outcomes of perinatal arterial ischemic stroke and cerebral sinovenous thrombosis. Semin Fetal Neonatal Med. 2009;14(5):318-22.

420. Wu TC, Grotta JC. Hypothermia for acute ischaemic stroke. Lancet Neurol. 2013;12(3):275-84.

421. Wolf T, Lindauer U, Reuter U, Back T, Villringer A, Einhaupl K, et al. Noninvasive near infrared spectroscopy monitoring of regional cerebral blood oxygenation changes during peri-infarct depolarizations in focal cerebral ischemia in the rat. J Cereb Blood Flow Metab. 1997;17(9):950-4.

422. Stankovic MR, Maulik D, Rosenfeld W, Stubblefield PG, Kofinas AD, Drexler S, et al. Real-time optical imaging of experimental brain ischemia and hemorrhage in neonatal piglets. J Perinat Med. 1999;27(4):279-86.

423. Calderon-Arnulphi M, Alaraj A, Amin-Hanjani S, Mantulin WW, Polzonetti CM, Gratton E, et al. Detection of cerebral ischemia in neurovascular surgery using

quantitative frequency-domain near-infrared spectroscopy. J Neurosurg. 2007;106(2):283-90.

424.   Culver JP, Durduran T, Furuya D, Cheung C, Greenberg JH, Yodh AG. Diffuse optical tomography of cerebral blood flow, oxygenation, and metabolism in rat during focal ischemia. J Cereb Blood Flow Metab. 2003;23(8):911-24.

425.   Vernieri F, Rosato N, Pauri F, Tibuzzi F, Passarelli F, Rossini PM. Near infrared spectroscopy and transcranial Doppler in monohemispheric stroke. Eur Neurol. 1999;41(3):159-62.

426.   Moreau F, Yang R, Nambiar V, Demchuk AM, Dunn JF. Near-infrared measurements of brain oxygenation in stroke. Neurophotonics. 2016;3(3):031403.

427.   Auer LM, Gallhofer B. Rhythmic activity of cat pial vessels in vivo. Eur Neurol. 1981;20(6):448-68.

428.   Hudetz AG, Smith JJ, Lee JG, Bosnjak ZJ, Kampine JP. Modification of cerebral laser-Doppler flow oscillations by halothane, PCO2, and nitric oxide synthase blockade. Am J Physiol. 1995;269(1 Pt 2):H114-20.

429.   Mayhew JE, Askew S, Zheng Y, Porrill J, Westby GW, Redgrave P, et al. Cerebral vasomotion: a 0.1-Hz oscillation in reflected light imaging of neural activity. Neuroimage. 1996;4(3 Pt 1):183-93.

430.   Tachtsidis I, Elwell CE, Leung TS, Lee CW, Smith M, Delpy DT. Investigation of cerebral haemodynamics by near-infrared spectroscopy in young healthy volunteers reveals posture-dependent spontaneous oscillations. Physiol Meas. 2004;25(2):437-45.

431.   Kuo TB, Chern CM, Sheng WY, Wong WJ, Hu HH. Frequency domain analysis of cerebral blood flow velocity and its correlation with arterial blood pressure. J Cereb Blood Flow Metab. 1998;18(3):311-8.

432. Diehl RR, Linden D, Lucke D, Berlit P. Spontaneous blood pressure oscillations and cerebral autoregulation. Clin Auton Res. 1998;8(1):7-12.

433. Hu HH, Kuo TB, Wong WJ, Luk YO, Chern CM, Hsu LC, et al. Transfer function analysis of cerebral hemodynamics in patients with carotid stenosis. J Cereb Blood Flow Metab. 1999;19(4):460-5.

434. Reinhard M, Roth M, Muller T, Czosnyka M, Timmer J, Hetzel A. Cerebral autoregulation in carotid artery occlusive disease assessed from spontaneous blood pressure fluctuations by the correlation coefficient index. Stroke. 2003;34(9):2138-44.

435. Immink RV, van Montfrans GA, Stam J, Karemaker JM, Diamant M, van Lieshout JJ. Dynamic cerebral autoregulation in acute lacunar and middle cerebral artery territory ischemic stroke. Stroke. 2005;36(12):2595-600.

436. Dawson SL, Panerai RB, Potter JF. Serial changes in static and dynamic cerebral autoregulation after acute ischaemic stroke. Cerebrovasc Dis. 2003;16(1):69-75.

437. Julien C. The enigma of Mayer waves: Facts and models. Cardiovasc Res. 2006;70(1):12-21.

438. Bumstead JR, Bauer AQ, Wright PW, Culver JP. Cerebral functional connectivity and Mayer waves in mice: Phenomena and separability. J Cereb Blood Flow Metab. 2017;37(2):471-84.

439. Lundberg N. Continuous recording and control of ventricular fluid pressure in neurosurgical practice. Acta Psychiatr Scand Suppl. 1960;36(149):1-193.

440. Newell DW, Aaslid R, Stooss R, Reulen HJ. The relationship of blood flow velocity fluctuations to intracranial pressure B waves. J Neurosurg. 1992;76(3):415-21.

441. Lang EW, Diehl RR, Timmermann L, Baron R, Deuschl G, Mehdorn HM, et al. Spontaneous oscillations of arterial blood pressure, cerebral and peripheral blood flow in healthy and comatose subjects. Neurol Res. 1999;21(7):665-9.

442.   Strik C, Klose U, Kiefer C, Grodd W. Slow rhythmic oscillations in intracranial CSF and blood flow: registered by MRI. Acta Neurochir Suppl. 2002;81:139-42.

443.   White BR, Snyder AZ, Cohen AL, Petersen SE, Raichle ME, Schlaggar BL, et al. Resting-state functional connectivity in the human brain revealed with diffuse optical tomography. Neuroimage. 2009;47(1):148-56.

444.   Homae F, Watanabe H, Otobe T, Nakano T, Go T, Konishi Y, et al. Development of global cortical networks in early infancy. J Neurosci. 2010;30(14):4877-82.

445.   Lu CM, Zhang YJ, Biswal BB, Zang YF, Peng DL, Zhu CZ. Use of fNIRS to assess resting state functional connectivity. J Neurosci Methods. 2010;186(2):242-9.

446.   Phillip D, Schytz, H.W., Iversen, H.K., Selb, J., Boas, D.A., Ashina, M. Spontaneous Low Frequency Oscillations in Acute Ischemic Stroke – A Near Infrared Spectroscopy (NIRS) Study. Journal of Neurology and Neurophysiology. 2014;5(6):1000241.

447.   Arri SJ, Muehlemann T, Biallas M, Bucher HU, Wolf M. Precision of cerebral oxygenation and hemoglobin concentration measurements in neonates measured by near-infrared spectroscopy. J Biomed Opt. 2011;16(4):047005.

448.   Smith SM, Jenkinson M, Woolrich MW, Beckmann CF, Behrens TE, Johansen-Berg H, et al. Advances in functional and structural MR image analysis and implementation as FSL. Neuroimage. 2004;23 Suppl 1:S208-19.

449.   Jenkinson M, Beckmann CF, Behrens TE, Woolrich MW, Smith SM. Fsl. Neuroimage. 2012;62(2):782-90.

450.   Katsman D, Zheng J, Spinelli K, Carmichael ST. Tissue microenvironments within functional cortical subdivisions adjacent to focal stroke. J Cereb Blood Flow Metab. 2003;23(9):997-1009.

451.   Carmichael ST. Rodent models of focal stroke: size, mechanism, and purpose. NeuroRx. 2005;2(3):396-409.

452.   Caine S, Hackett MJ, Hou H, Kumar S, Maley J, Ivanishvili Z, et al. A novel multi-modal platform to image molecular and elemental alterations in ischemic stroke. Neurobiol Dis. 2016;91:132-42.

453.   Li Z, Zhang M, Xin Q, Chen G, Liu F, Li J. Spectral analysis of near-infrared spectroscopy signals measured from prefrontal lobe in subjects at risk for stroke. Med Phys. 2012;39(4):2179-85.

454.   Muehlschlegel S, Selb J, Patel M, Diamond SG, Franceschini MA, Sorensen AG, et al. Feasibility of NIRS in the neurointensive care unit: a pilot study in stroke using physiological oscillations. Neurocrit Care. 2009;11(2):288-95.

455.   Phillip D, Schytz HW, Selb J, Payne S, Iversen HK, Skovgaard LT, et al. Low frequency oscillations in cephalic vessels assessed by near infrared spectroscopy. Eur J Clin Invest. 2012;42(11):1180-8.

456.   Han Q, Li Z, Gao Y, Li W, Xin Q, Tan Q, et al. Phase synchronization analysis of prefrontal tissue oxyhemoglobin oscillations in elderly subjects with cerebral infarction. Med Phys. 2014;41(10):102702.

457.   Gibson AP, Austin T, Everdell NL, Schweiger M, Arridge SR, Meek JH, et al. Three-dimensional whole-head optical tomography of passive motor evoked responses in the neonate. Neuroimage. 2006;30(2):521-8.

458.   Roche-Labarbe N, Fenoglio A, Radhakrishnan H, Kocienski-Filip M, Carp SA, Dubb J, et al. Somatosensory evoked changes in cerebral oxygen consumption measured non-invasively in premature neonates. Neuroimage. 2014;85 Pt 1:279-86.

459. Barker JW, Rosso AL, Sparto PJ, Huppert TJ. Correction of motion artifacts and serial correlations for real-time functional near-infrared spectroscopy. Neurophotonics. 2016;3(3):031410.

460. Gu Y, Han J, Liang Z, Yan J, Li Z, Li X. Empirical mode decomposition-based motion artifact correction method for functional near-infrared spectroscopy. J Biomed Opt. 2016;21(1):15002.

461. Saager R, Berger A. Measurement of layer-like hemodynamic trends in scalp and cortex: implications for physiological baseline suppression in functional near-infrared spectroscopy. J Biomed Opt. 2008;13(3):034017.

462. Gregg NM, White BR, Zeff BW, Berger AJ, Culver JP. Brain specificity of diffuse optical imaging: improvements from superficial signal regression and tomography. Front Neuroenergetics. 2010;2.

463. Zhang H, Zhang YJ, Lu CM, Ma SY, Zang YF, Zhu CZ. Functional connectivity as revealed by independent component analysis of resting-state fNIRS measurements. Neuroimage. 2010;51(3):1150-61.

464. Franceschini MA, Joseph DK, Huppert TJ, Diamond SG, Boas DA. Diffuse optical imaging of the whole head. J Biomed Opt. 2006;11(5):054007.

465. Zhang Y, Brooks DH, Franceschini MA, Boas DA. Eigenvector-based spatial filtering for reduction of physiological interference in diffuse optical imaging. J Biomed Opt. 2005;10(1):11014.

466. Ferradal SL, Liao SM, Eggebrecht AT, Shimony JS, Inder TE, Culver JP, et al. Functional Imaging of the Developing Brain at the Bedside Using Diffuse Optical Tomography. Cereb Cortex. 2016;26(4):1558-68.

467.   Eggebrecht AT, Ferradal SL, Robichaux-Viehoever A, Hassanpour MS, Dehghani H, Snyder AZ, et al. Mapping distributed brain function and networks with diffuse optical tomography. Nat Photonics. 2014;8(6):448-54.

468.   Chitnis D, Airantzis D, Highton D, Williams R, Phan P, Giagka V, et al. Towards a wearable near infrared spectroscopic probe for monitoring concentrations of multiple chromophores in biological tissue in vivo. Rev Sci Instrum. 2016;87(6):065112.

469.   Chitnis D, Cooper RJ, Dempsey L, Powell S, Quaggia S, Highton D, et al. Functional imaging of the human brain using a modular, fibre-less, high-density diffuse optical tomography system. Biomed Opt Express. 2016;7(10):4275-88.

470.   Tak S, Ye JC. Statistical analysis of fNIRS data: a comprehensive review. Neuroimage. 2014;85 Pt 1:72-91.

471.   Huppert TJ. Commentary on the statistical properties of noise and its implication on general linear models in functional near-infrared spectroscopy. Neurophotonics. 2016;3(1):010401.

472.   Hintz SR, Benaron DA, van Houten JP, Duckworth JL, Liu FW, Spilman SD, et al. Stationary headband for clinical time-of-flight optical imaging at the bedside. Photochem Photobiol. 1998;68(3):361-9.

473.   Hebden JC, Gibson A, Yusof RM, Everdell N, Hillman EM, Delpy DT, et al. Three-dimensional optical tomography of the premature infant brain. Phys Med Biol. 2002;47(23):4155-66.

474.   Torricelli A, Contini D, Pifferi A, Caffini M, Re R, Zucchelli L, et al. Time domain functional NIRS imaging for human brain mapping. Neuroimage. 2014;85 Pt 1:28-50.

475.   Lee CW, Cooper RJ, Austin T. Diffuse optical tomography to investigate the newborn brain. Pediatr Res. 2017.

476.   Hartings JA, Bullock MR, Okonkwo DO, Murray LS, Murray GD, Fabricius M, et al. Spreading depolarisations and outcome after traumatic brain injury: a prospective observational study. Lancet Neurol. 2011;10(12):1058-64.

477.   Dohmen C, Sakowitz OW, Fabricius M, Bosche B, Reithmeier T, Ernestus RI, et al. Spreading depolarizations occur in human ischemic stroke with high incidence. Ann Neurol. 2008;63(6):720-8.

478.   Lauritzen M, Dreier JP, Fabricius M, Hartings JA, Graf R, Strong AJ. Clinical relevance of cortical spreading depression in neurological disorders: migraine, malignant stroke, subarachnoid and intracranial hemorrhage, and traumatic brain injury. J Cereb Blood Flow Metab. 2011;31(1):17-35.

479.   Fabricius M, Fuhr S, Willumsen L, Dreier JP, Bhatia R, Boutelle MG, et al. Association of seizures with cortical spreading depression and peri-infarct depolarisations in the acutely injured human brain. Clin Neurophysiol. 2008;119(9):1973-84.

480.   Strong AJ, Anderson PJ, Watts HR, Virley DJ, Lloyd A, Irving EA, et al. Peri-infarct depolarizations lead to loss of perfusion in ischaemic gyrencephalic cerebral cortex. Brain. 2007;130(Pt 4):995-1008.

481.   Woitzik J, Hecht N, Pinczolits A, Sandow N, Major S, Winkler MK, et al. Propagation of cortical spreading depolarization in the human cortex after malignant stroke. Neurology. 2013;80(12):1095-102.

482.   Santos E, Scholl M, Sanchez-Porras R, Dahlem MA, Silos H, Unterberg A, et al. Radial, spiral and reverberating waves of spreading depolarization occur in the gyrencephalic brain. Neuroimage. 2014;99:244-55.

483.   Jacobs SE, Berg M, Hunt R, Tarnow-Mordi WO, Inder TE, Davis PG. Cooling for newborns with hypoxic ischaemic encephalopathy. Cochrane Database Syst Rev. 2013(1):CD003311.

484. Titomanlio L, Fernandez-Lopez D, Manganozzi L, Moretti R, Vexler ZS, Gressens P. Pathophysiology and neuroprotection of global and focal perinatal brain injury: lessons from animal models. Pediatr Neurol. 2015;52(6):566-84.

485. Vanhatalo S, Palva JM, Andersson S, Rivera C, Voipio J, Kaila K. Slow endogenous activity transients and developmental expression of K+-Cl- cotransporter 2 in the immature human cortex. Eur J Neurosci. 2005;22(11):2799-804.

486. Lloyd RO, O'Toole JM, Pavlidis E, Filan PM, Boylan GB. Electrographic Seizures during the Early Postnatal Period in Preterm Infants. J Pediatr. 2017;187:18-25 e2.

487. Evans E, Koh S, Lerner J, Sankar R, Garg M. Accuracy of amplitude integrated EEG in a neonatal cohort. Arch Dis Child Fetal Neonatal Ed. 2010;95(3):F169-73.

488. Sheth RD, Hobbs GR, Mullett M. Neonatal seizures: incidence, onset, and etiology by gestational age. J Perinatol. 1999;19(1):40-3.

489. Shah DK, Zempel J, Barton T, Lukas K, Inder TE. Electrographic seizures in preterm infants during the first week of life are associated with cerebral injury. Pediatr Res. 2010;67(1):102-6.

490. Vesoulis ZA, Inder TE, Woodward LJ, Buse B, Vavasseur C, Mathur AM. Early electrographic seizures, brain injury, and neurodevelopmental risk in the very preterm infant. Pediatr Res. 2014;75(4):564-9.

491. Glass HC, Shellhaas RA, Tsuchida TN, Chang T, Wusthoff CJ, Chu CJ, et al. Seizures in Preterm Neonates: A Multicenter Observational Cohort Study. Pediatr Neurol. 2017;72:19-24.

Index of Abbreviations

2D: two-dimensional

3D: three-dimensional

AA: arachidonic acid

ACA: anterior cerebral artery

ADC: Apparent Diffusion Coefficient

aEEG: amplitude integrated EEG

AS: active sleep

ASL: arterial spinning labelling

ATP: adenosine triphosphate

AW: active wakefulness

BGT: basal ganglia and thalamus

BOLD fMRI: blood oxygen level dependent functional magnetic resonance imaging

BORL: Biomedical Optics Research Lab

BP: blood pressure

BW: birth weight

Ca^{++}: calcium

CA: cerebral autoregulation

CBF: cerebral blood flow

CBV: cerebral blood volume

CCA: common carotid artery

CFM: cerebral function monitor

CGA: corrected gestational age

$CMRO_2$: cerebral metabolic rate of oxygen

CNS: central nervous system

COOL-AID: cooling for acute ischaemic brain damage

CP: cerebral palsy

CPAP: continuous positive airway pressure

CRP: c-reactive protein (normal when <1)

CrUS: cranial ultrasonography

CSD: cortical spreading depression

CSF: cerebro-spinal fluid

CSVT: cerebral sinus venous thrombosis

CTG: cardiotocogram (foetal heart rate monitoring device)

CT: computed tomography

CtO$_x$: cytochrome c oxidase

CUH: Cambridge University Hospitals

CW: continuous wavelength

DoH: Declaration of Helsinki

DOI: diffuse optical imaging

DOT: diffuse optical tomography

DPF: differential pathlength factor

DQ: developmental quotient

DWI: diffusion weighted imaging

ECG: electro-cardiogram

ECMO: extracorporeal membrane oxygenation

EEG: electro-encephalogram

EMG: electro-myogram

EmLSCS: emergency low segment Caesarean section

EOG: electro-oculogram

EPIC: Evelyn Perinatal Imaging Centre

EPSP: excitatory post-synaptic potential

FEM: finite element method

FFT: fast Fourier transform

fMRI: functional magnetic resonance

fNIRS: functional near-infrared spectroscopy

FSE: Fast Spin Echo

FSL: FMRIB Software Library

GA: gestational age at birth in weeks /40 weeks of expected normal pregnancy duration

GABA: γ-aminobutyric acid

GBS: group B streptococcus (Streptococcus agalactiae)

GDM: gestational diabetes mellitus

GLM: general linear model

Hb: haemoglobin

HbO_2: oxy-haemoglobin

HHb: deoxy-haemoglobin

HbT: total haemoglobin

Hb_{vol}: volume haemoglobin

HFNC: high frequency nasal cannula

HFOV: high frequency oscillatory ventilation

HIE: hypoxic ischaemic encephalopathy

hpf: high pass filter

HPI: haemorrhagic parenchymal infarct

HR: heart rate

HRF: haemodynamic response function

IBI: inter-burst interval

ICA: independent component analysis

ICTus: intravascular cooling in the treatment of stroke

iNO: inhaled nitric oxide

IOL: induction of labour

IPSP: inhibitory post-synaptic potential

IQR: interquartile range

IUGR: intrauterine growth restriction

IV: intravenous

IVH: intraventricular haemorrhage

K^+: potassium

LEOG: left electro-oculogram

LFOs: low frequency oscillations

LMWH: low molecular weight heparin

lpf: low pass filter

MABP: mean arterial blood pressure

MCA: middle cerebral artery

MRA: magnetic resonance angiography

MRI: magnetic resonance imaging

MRS: magnetic resonance spectroscopy

Na$^+$: sodium

NAA: N-acetyl-asparate

NE: neonatal encephalopathy

NGT: nasogastric tube

NICU: neonatal intensive care unit

NIR: near infrared

NIRS: near infrared spectroscopy

NMDA: N-methyl-D-asparate

NO: nitric oxide

No resus: no resuscitation required at birth

OEF: oxygen extraction fraction

PAIS: perinatal arterial ischaemic stroke

PASL: pulsed arterial spinning labelling

PCA: posterior cerebral artery

PCA: principal component analysis

PCr: phosphor-creatinine

PC-MRA: phase contrast magnetic resonance angiography

PET: positron emission tomography

PLIC: posterior limb of the internal capsule

PMDF: photon measurement density function

PPHN: persistent pulmonary hypertension of the newborn

PROM: prolonged rupture of membranes >24 hours prior to delivery

PSP: post-synaptic potential

PVL: periventricular leukomalacia

QS: quiet sleep

QW: quiet wakefulness

rCBV: regional cerebral blood volume

REM: rapid eye movement

REOG: right electro-oculogram

RI: resistance index

ROI: region of interest

ROS: reactive oxygen species

RR: respiratory rate

RS: resting state

RSFN: resting state function network

rSO_2: regional cerebral oxygen saturation

SaO_2: oxygen saturation

SAT: spontaneous activity transient

SE: Spin Echo

SIMV: synchronized intermittent mandatory ventilation

SNR: signal to noise ratio

SVD: spontaneous vaginal delivery

SVIA: self-ventilating in air

TA: tracé alternant

TCD: transcranial doppler

TD: trace discontinu

T2-FSE: T2-weighted fast spin echo

TH: therapeutic hypothermia

TOAST++: time-resolved optical absorption and scatter tomography

TOBY: TOtal BodY therapeutic hypothermia for perinatal asphyxia

TOI: tissue oxygenation index

TPSF: temporal point spread function

TTTS: twin to twin transfusion syndrome

UCL: University College London

Vg: volume guarantee

VL: very low

VLFOs: very low frequency oscillations

WMA: world medical association

Xe: xenon